Addis Ababa University
Addis Ababa Institute of Technology
School of Graduate Studies
School of Mechanical & Industrial Engineering

Structural Optimization, Crashworthiness and Strength Analysis of Midi – Bus Structure in Static and Rollover Condition

By:
Hailemichael Solomon Addisu
Advisor: Dr. Ermias Gebrekidan Koricho (Assistance Professor)

A Thesis Submitted for the partial fulfillment of the requirements for the Degree of Master of Science(M.Sc) in Mechanical Engineering (Mechanical Design) to the School of Mechanical and Industrial Engineering, Addis Ababa Institute of Technology, Addis Ababa University

October 2021
Addis Ababa, Ethiopia

Declaration

This is to confirm that the thesis presented by H/Michael Solomon Addisu, entitled "***Structural Optimization, Crashworthiness and Strength Analysis of Midi-Bus Structure in Static and Rollover Condition***," has been approved under university requirements.

Declared by:

Hailemichael Solomon Addisu _____ _____

Name Signature Date

This thesis has been submitted and verified as a university advisor by:

Dr. Erimias Gebrekidan Koricho _____ _____

Advisor Signature Date

Addis Ababa University

Addis Ababa Institute of Technology

School of Mechanical and Industrial Engineering(SMIE)

Structural Optimization, Crashworthiness and Strength Analysis of Midi – Bus Structure in Static and Rollover Condition

By

Hailemichael Solomon Addisu

Approved by Board of Examiners:

1.	Dr. Erimas Gebrekidan Koricho	_____	_____
	Advisor	Signature	Date
2.	Dr. Mulugeta Habtemariam	_____	_____
	Internal Examiner	Signature	Date
3.	Dr. Samuel Tesfaye	_____	_____
	External Examiner	Signature	Date
4.	Dr. Areya Abera	_____	_____
	Mechanical Design Chair	Signature	Date
5.	Dr. Yilma Tadesse	_____	_____
	SMIE Dean	Signature	Date
6.	Dr. Ermias Tesfaye	_____	_____
	Post-Graduate Program Director	Signature	Date

Acknowledgments

I wish to express my heartfelt gratitude to the almighty God for giving me the power and strength to accomplish this thesis. Furthermore, I want to share my thankfulness and appreciation to Dr. Ermias G. Koricho for their continuous encouragement, guidance, and generous support to complete this thesis in a timely and professional manner.

The local bodybuilders located in Addis Ababa were an essential resource for this research. Especially, SIMEX bus builder (Garage) is highly appreciated for their continuous supports and comments. Lastly, I want to extend my gratitude to individuals who help me by giving their helpful idea and information regarding my work.

I want to thank the following persons for supporting me from the data collection up to finding the solution to the problem:

Mr. Semeneh(bus bodybuilder owner & expert)

Mr. Elias(welder & technician)

Mr. Kibru(Oromia Transport Minster)

Those mentioned above have helped with their skills and knowledge through the development of this thesis paper. Last but not least, I would also like to express thankfulness to Mr. Hairedin M. (Ph.D. Candidate) and all the staff and classmates at the School of Mechanical & Industrial Engineering (SMIE) for their continuous support and cooperation.

Abstract

Midi-buses are a valuable vehicle to transport services and goods in Ethiopia's rural and urban areas. However, midi-bus are indirectly regulated through inspecting the end product (finished bus) during licensing for the public transport business in Ethiopia. Because of the lack of engineering analysis and testing procedures, the reliability and crashworthiness of a midi-bus are compromised and ultimately costing human lives and the overweight of the bus. Moreover, the weld formation and their types have been done without scientific reasons. Consequently, this method leads to a catastrophic structural failure during accidents.

This research aimed to analyze the original midi-bus structure based on the static strength and rollover analysis using United Nations Regulation 66 via numerical investigation (ANSYS & LS-DYNA). Moreover, four design optimizations of the midi-bus structure were conducted: reinforcement design (model-I); numerical optimization (Response Surface Optimization (RSO) in ANSYS DesignXplorer for static case (model – II_{stat}); Successive Response Surface Method (SRSM) in LS-OPT for rollover case (model – II_{roll})); and combined design approach (model - III) by merging of the static and rollover optimized models. Furthermore, the effect of full and spot arc welding on the quasi-static analysis of floor-wall and roof-wall connections was evaluated.

The result shows that the maximum deformation in static and tare-weight rollover cases occurs at the baseline structure's roof section and pillar A and bays from one to three, respectively. The bending stiffness of the reinforced design (model – I), model – $II_{stat,}$ and model – III (combined) was increased by 41.65 % (1911.4 N/m), 55.8 % (2,563.1 N/m), and 58.1 % (2,667 N/m), as compared to the baseline structure. Moreover, compared to the baseline model, the structure's weights of the reinforced model (model – I), model – II_{stat}, and model – III (combined) were effectively reduced by 5.23 %, 7.73 %, and 2.33 %, respectively. In addition, model – II_{roll} exhibited the weight of the reinforced model by 5.6 % in the rollover case. During structural connection, full and spot arc welding are formed at the edges and corners of the frames. Accordingly, these types of welds highly affect the energy absorbing capacity of the floor-wall and roof-wall connections. Generally, this research gives vital information on the midi-bus structure weight, stiffness, and crashworthiness capability from slight to severe loading cases for both static and rollover conditions. Moreover, this research suggests the new optimized bus structure and better weld type while welding the structural connections.

Keywords: Crashworthiness; Deformation; Finite Element Methods; Midi-Bus; Reinforcement, Response Surface Optimization; Rollover; Static Strength; and Structural Optimization

Table of Contents

List of Figures

List of Tables

Abbreviations

AIS	Automotive Industry Standards
CAD	Computer-Aided Design
CAE	Computer-Aided Engineering
CG	Center of Gravity
CS	Conventional Structural
DI	Deformation Index
DRTWBs	Dual Rectangular Thin-Walled Beams
EMA	Experimental Modal Analysis
FEA	Finite Element Analysis
FEM	Finite Element Method
FMVSS	Federal Motor Vehicle Safety Standards
FW	Floor-Wall
GA	Genetic Algorithm
GFRP	Glass Fiber Reinforced Plastic
GVW	Gross Vehicle Weight
HM-CFRP	High Modulus Carbon Fiber Reinforced Plastics
MO	Multi-Objective
NHTSA	National Highway Traffic Safety Administration
PRA	Protectable Rollover Accidents
R66	Regulation 66
RHS	Rectangular-Hollow Section
RTWBs	Rectangular Thin-Walled Beams
RW	Roof-Wall
SAE	Society of American Engineer
SHS	Square-Hollow Section
SM-CFRP	Standard Modulus Carbon Fiber Reinforced Plastics
SME	Small and Medium Enterprises
SRSM	Successive Respond Surface Method
SSF	Static Stability Factor
SPR	Side Pull Ratio
TTR	Tilt Table Ratio
UNECE	United Nations Economy Commission for Europe
VLCP	Vertical Longitudinal Center Plane

List of Symbols

A_{j0}	Angular position vector form
${}_j\omega_{0j}$	Angular velocity
${}_j\dot{\omega}_{0j}$	Angular acceleration
${}_j r_{S_j}$	Linear position vector
${}_j v_{S_j}$	Linear velocity
${}_j a_{S_j}$	Linear acceleration
M	Mass matrix
g	Vector form of generalized Coriolis forces
q_e	External torques
ϕ	Angle between the mass of the vehicle and road plane
r	Radius measured from the CG to pivot point O
L_{cr}	Angular momentum,
W_{jmax}	Maximum length of a bay
m_j	Mass attributed to the j^{th} bay
s	Number of bays
M_k	Unladen kerb mass of the vehicle(M),
L_2	Distance between CG and rear Axle center
Δl_2	Changes in distance between CG and unladen mass
α	Tilting angle of the vehicle
ΔM	Change in mass between the rear and front of the vehicle
l_1	Longitudinal distance
t	Transverse distance
h_o	Height of the Center of gravity
L_f	Track Width
θ	Critical angle
Δh_{CG}	Vertical distance of the Center of gravity during rollover impact
W	Overall vehicle's width
H_f	Height between floor and occupant compartment
h_d	Depth between the horizontal plane of the ditch and tilting platform plane
ρ	Density
σ_y	Yield Strength
σ_{ut}	Ultimate Tensile Strength

E	Young's Modulus
v	Poisson's Ratio
σ_t	True stress
ε_t	True plastic strain
σ_{eng}	Engineering stress
ε_{eng}	Engineering strain
T_m	Total moment(torque)
K_T	Torsional stiffness or rigidity
L_a	Distance between the two sides of frontal wheel supports
δy	Deflection of the structure
g	Gravitational constant ($9.81\ m^2/s$)
E_i	Energy absorbed by the "i^{th}"bay
m_i	Mass of the "i^{th}" bay
E_{min}	Minimum energy absorbed by the bus sections
$E_{st,a}$	Energy absorbed by the bus sections
θ_3	Angle between wall & floor
θ_2	Angle of waist rails
θ_1	Angle between roof & wall
DI_θ	Angular Deformation Index
$\Delta\theta_3$	Angle changes between wall & floor
$\Delta\theta_2$	Angle changes of waist rails
l	Distance from floor to waist rails

Chapter One

Introduction

1.1 Introduction

Midi-Buses are used in rural and urban areas of Ethiopia for transportation purposes. It has a seating capacity of between 23 – 34 passengers reported by AIS Standards [1]. Nowadays, Midi-buses are widely helpful in high populated countries, especially in Asia and Africa. Likewise, rollover crashes frequently happen due to the reasons of being rolled down into a cliff, collision with vehicles, and rotates sideways by obstacles (ditch, kerb, or objects)[2]–[4]. Most rollover crashes happened on the road of curved(tangent) sections due to the pedestrian's priority and fast-moving(high speed) crashes[5]. Moreover, bus rollover accidents occurred under the circumstance of dropping down into a cliff in this country, leading to 50 % fatalities and 50 % passengers' injuries in 2004[6]. Mainly, the bus rollover accidents obtained serious structural deformation and severe injuries & fatalities to the passengers[2], [3]. The public transport vehicles(buses) involved high numbers of deaths and injuries during crashes. In Ethiopia, the fatal crashes by buses involved nearly 35.42 % (1,324 road traffic deaths) in 2018. (UN ECE 2020) reported that the crash tendency increased averagely by 9 % in Ethiopia in 2010 – 2018[7].

Most bus manufacturers in the world follow the requirements of the standards and regulations to visualize and test the crashworthiness behavior of bus structures in rollover conditions. However, most of the bus bodies in Ethiopia are locally built on truck chassis Isuzu N-Series (NPR (71H, 71K, and 66L), NQR,) and FSR using locally available materials without considering the standards and regulations. In addition, the strength of the midi-bus structure and occupant safety in static and rollover crash cases are not stated and measured scientifically using experimental or numerical approaches. Accordingly, this research aims to analyze and optimize the midi-bus structure in static structural and rollover crash conditions according to UN ECE R66.

In this research, the bus structure's static, quasi-static, and rollover crashes analyses are conducted through FE Methods (ANSYS/LS – DYNA). However, the static structural and quasi-static analysis are pre-request tasks used to identify the strength of the structural parts against rollover accident [5], [6]. Based on the standards' specifications, the bus structures are analyzed to decrease the limit of injuries, fatalities, and damages on both occupants and the bus frame. Then the bus structure weight, strength, and crashworthiness capability were determined and optimized through reinforcement design, numerical optimization (ANSYS DesignXplorer and LS-OPT), and

combined design for both analysis cases. Moreover, the effects of welding types on the quasi-static FE Analysis of connection were carried out. Finally, the midi-buses rollover crashes scenarios in the loading capacities (tare-weight, full-loading, and overloading) were also analyzed. The comparison of design alternatives solution was presented based on the parameters of angular deformation index and absorbed energy.

1.1.1 Background and Justification of the study

Crashworthiness is the ability to absorb vehicle crashes and protect the occupants in survival space [8], [9]. In most previous works, A numerical and Experimental investigation of full-scale bus section were conducted to analyze the quasi-static and rollover tests using the UNECE R66 procedure [10]–[12]. Computer-Aided Engineering(CAE) method is very well arranged and developed to assess and evaluate the scenarios of bus rollover crashes [13]. The plot of energy, displacement of the structure was determined [11], [14]. The optimization process may be achieved by the calculation or trial and error method or the automated optimization method [15].

The bus superstructure's static structural analysis was conducted via FE Method on the load cases of the bus, such as bending and torsion, breaking, and steering conditions[16]–[19]. Moreover, The experimental and numerical analysis of bus structure strength and structural design optimization was discussed[20]. A Genetic Algorithm (GA) is a well-matched optimization approach to reduce the weight and torsional stiffness in very complex problems [21], [22]. A Response Surface Optimization (RSO) method gives a better optimal design in the static structural analysis[23]. Consequently, the mass of paratransit bus structure optimizes using Multi-Objective(MO) Optimization by Sobol's indices and linear ANOVA method in the rollover crash [24]. On the other hand, improving the intermediate structural rings' geometric property increases the bus's mechanical resistance with lower weight [25].

The FE Model of weld formation at the connection of the bus structure was developed as spotweld, a solid element with tiebreak contact, shell element (Shell 63), and rigid element spring element with tied contact [12], [26]–[32]. Moreover, the local manufacturer and above researchers mostly use both full and spot arc welds to join the bus structure. However, both local manufacturers and the above scholars are not addressed the effects of weld types on the energy absorbing capacity of the structural connection. Hence, the effects of weld techniques (full and spot arc weld) on the structural connection strength could be analyzed by quasi-static simulation of connections.

The rollover crashes consist of 17.34 % fatalities and 17.17 % injuries within six years (2005 – 2011) in Ethiopia [5]. Also, the severity of occupant's fatalities and injuries happened in rollover

accidents, as shown in Figure 1.1(right). The super-structure members have a low stiffness and energy capacity during rollover accidents in Ethiopia, as shown in Figure 1.1(left).

Figure 1.1: Damaged midi-buses structure, fatalities, and injuries during rollover accidents

(Source: Ethiopian Insurance Corporation in 2017(left) and field photo, Geregera town in 2019(right))

The main motives for doing this research are the severity of conditions in bus rollover accidents. Moreover, the locally modified midi-bus were not analyzed and tested according to standards after they were manufactured. Therefore, for most midi-bus manufacturers globally, the bus's experimental and numerical simulation in rollover conditions is costly and challenging. This challenge leads to conducting this research using numerical investigation.

The local buses (modified midi-buses) and public transport vehicles in Ethiopia are frequently used. Most bus body-builders ' design and manufacturing standards are indirectly regulated by inspecting the end product (finished bus) during licensing for the public transport business. To be approved, conformity with set parameters are expected, usually spatial (length, width, and height), seating, and weight measurement. It implies that the midi-buses are not designed and manufactured for the passenger safety and strength of the bus in static and dynamic conditions.

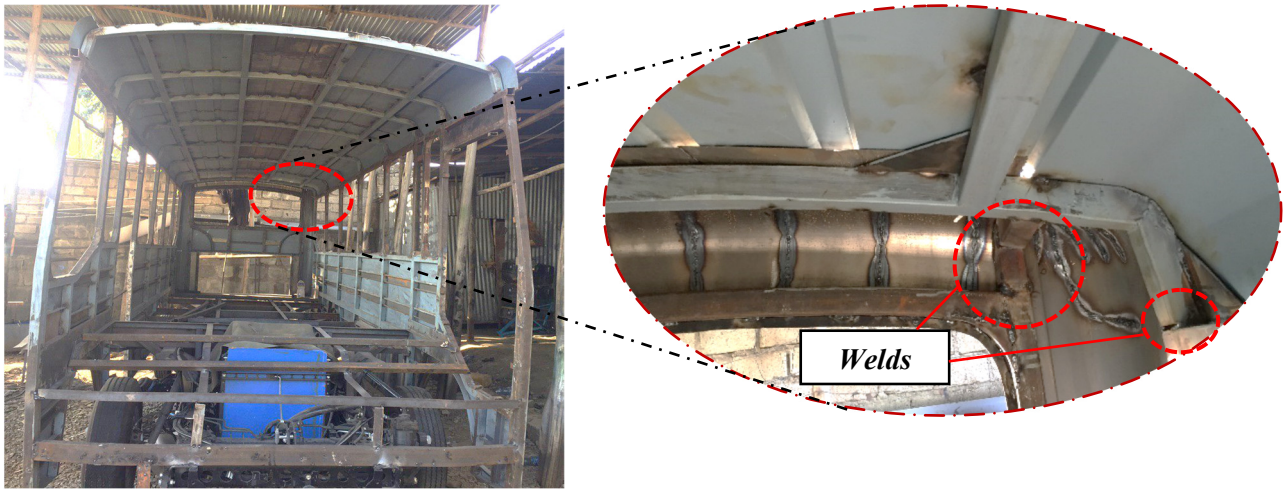

Figure 1.2: Midi-bus structure with cross-sections and welding types during manufacturing

(source: Simex midi-bus body-builder workshop, Kality, Addis Ababa)

Moreover, the local manufacturer does not consider the cross-section, the center of gravity, joining(welding) quality, arrangement, and bus weight during manufacturing. Figure 1.2 displays the construction of the midi-bus structure located in Ethiopia. Due to the above factors, this research facilitates a detailed analysis of midi-bus structure during static and dynamic conditions and studies the effects of welds on the structure quasi-static connections analysis. Moreover, structural optimization was carried out because of the damaged structure in static strength and dynamic crashes.

1.1.2 Important Terminologies and Overview of vehicle loading conditions

a) Vehicle

A specific illustration of a vehicle type (a bus or coach) used for passengers' transportation is called a vehicle [33].

b) Bay (Ring)

A bay(ring) is a unit of structure that forms a closed-loop among perpendicular to the planes of the vertical longitudinal Center (VLCP) of the vehicle [34],[35].

c) Residual space (occupant restraint)

In a rollover accident, a space preserved by passengers', drivers, and crew to deliver possibilities of survival is defined as residual(occupant) space [33], [35].

d) Structural Crashworthiness

Structural crashworthiness is concerned with designing a vehicle's structural system and components, which requires absorbing the dynamic energies and loads and energies in dynamic case (collision(impact) occasion) [34],[33].

In this research work, the following load conditions are considered and applied on the vehicle structure in a principal regular running and worst scenario to axis directions (see Figure 1.3).

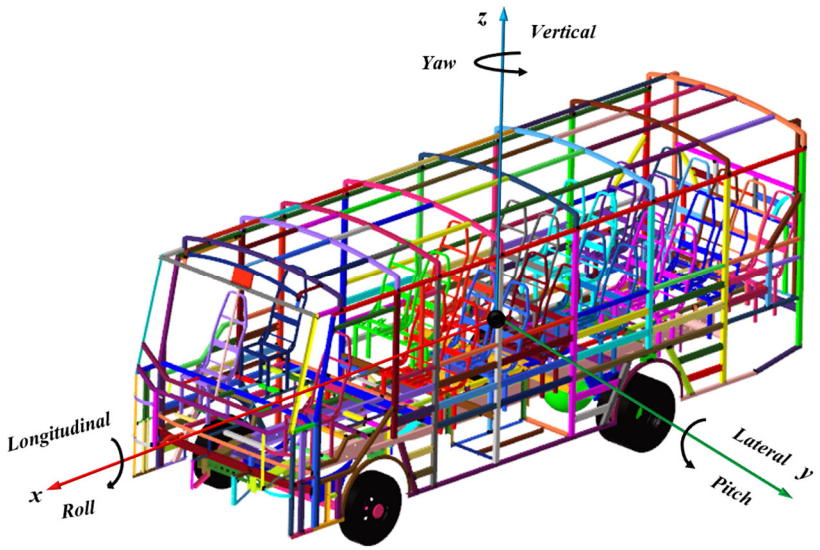

Figure 1.3: Axis system of the midi-bus structure

The following loading cases describes as follows:

I. Pure Bending case (Vertical Bending load)
II. Pure torsion case (Vertical Asymmetric torsion load)
III. Emergency Braking (Longitudinal load) case
IV. Emergency Steering (Lateral Bending/cornering) case and
V. Rollover crash (impact load) case

1.2 Statement of the problem

As mentioned earlier, occupant fatalities and injuries due to midi-bus rollover accidents frequently happen in Ethiopia. Moreover, the midi-bus structure compromises easily deformed structure members with overweight and ultimately costs a human life due to a lack of engineering analysis and tests.

During manufacturing of midi-bus by small and medium enterprises (SME) in Ethiopia, the center of gravity (CG), length of the bay, mass distribution, and weld types of the midi-bus structure have not been considered. Moreover, a midi-bus is indirectly regulated and inspected the ended bus to license the public transport business instead of implementing the standards and regulation. This challenge was due to the absence of standards and regulations to evaluate the structural design and manufacturing method. Furthermore, the structural components of the midi-bus need to study the structure's strength in static and dynamic conditions before prototyping and launching to the community.

In addition, the weld formation and their types have been done without scientific reasons by a local manufacturer, and this method leads the structure to fail during accidents. The overloading of passenger vehicles significantly increases the danger of crashes due to driver behavior and low traffic capacity in Ethiopia. However, Recent research and local manufacturers do not entirely address the study on the effects of welds type on the strength of quasi-static structural connection and the risks of overloading passengers with their luggage in rollover crashes of bus structures. Significantly, this research surveys the input data, concepts, and procedures from local manufacturers and legislator bodies, standards and regulations, and other previous research to study the above gaps using analytical and numerical methods.

1.3 Objectives

1.3.1 General Objective

The main objective of this research is to analyze and optimize the midi-bus structure in static and rollover conditions based on the UNECE R66 Standard.

1.3.2 Specific Objectives

Significantly, this research has the following sub-objectives:

- Analyze the static strength, quasi-static, and rollover crashworthiness behavior of the midi-bus structure
- Study effects of loading capacities (tare-weight, full-load, and over-load) and seats frame on the strength of the midi-bus structure during rollover impact
- Determine the deformation, reaction force, bending moment, absorbed energy, stress, and angular deformation index for all FE analyses
- Optimize the structure of a midi-bus to minimize the weight and increase the structural strength via reinforcement, numerical optimization (RSO/SRSM), and combined design in static and rollover cases
- Investigate the effect of welding types on the quasi-static simulation of structural connections

1.4 Scope & Limitation

The full-vehicle rollover simulation needs a high-performance computer processor and extra modeling techniques. However, this simulation was conducted only by modeling the rigid chassis, deformable structure, seat frame, and lumped mass of passengers and luggage using LS-DYNA R11 by ECE R66. In addition, the structural optimization tasks were taken only for specific parts and iterations due to the high computational resource with the time required during numerical optimization (LS-OPT 5.2). Furthermore, static analysis was taken into consideration to estimate the strength of the structure using ANSYS 19.2. Moreover, the optimization tasks minimize the mass within a stiffed structure by using the response surface method in Design Explorer. Lastly, only the effects of welding on structural strength develop by the quasi-static simulation of connections due to randomly joining the structure.

1.5 Significance

This research feeds vital information on the crashworthiness capability of the midi-bus structure and its components from slight to serious rollover crashes. Moreover, this research also encouraged applying the regulations of ECE R66(rollover test) and Florida standards (welds behavior on the connection tests) through experimental investigation by the manufacturer and legislator bodies. The determination of the center of gravity, mass distribution, and length of the bay of the midi-bus develops analytically to ensure the static stability of the bus. Overall, this research also gives the new optimized structure design that is better than the existing one.

Generally speaking, this research suggests the preferable weld type while joining (welding) the structure through the quasi-static simulation of roof-wall and floor-wall connection.

1.6 Methodology

Figure 1.4 illustrates the general materials and methods to fulfill the objectives of this research. The research methodology is grouped into four methodologies: data collection and literature reviews, Geometrical analysis and Modeling, numerical investigation, and structural optimization.

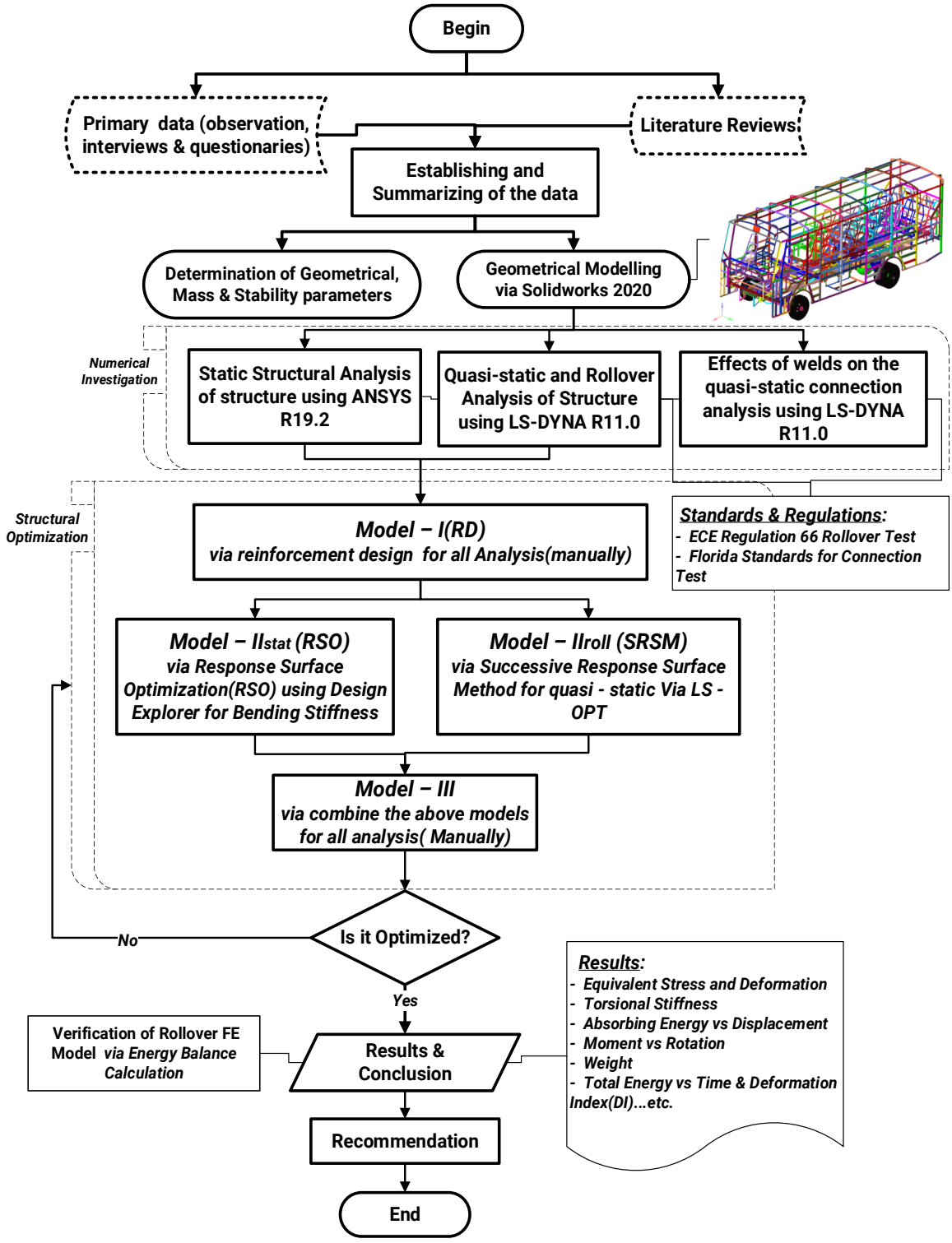

Figure 1.4: Flow chart of the overall methodology of the research works

1.7 Organization of the thesis

In this research, the six chapters are organized as follows:

Chapter one

The first chapter comprises an introduction, problem statement, objectives, scope & limitation, and thesis methodology. This chapter also defines the terminology & overview of bus structural components, a summary of the thesis, and the loading conditions of the vehicle.

Chapter two

The second chapter discusses the current standards and regulations on the rollover testing procedures with their applications. This chapter reviews previously researched static, quasi-static, and rollover analysis with optimization of the bus via experimental and numerical methods. It summarizes the weld formation in the bus structural components executed by other scholars.

Chapter three

The third chapter presents the finite element model development in static, quasi-static, and rollover conditions. It shows the mathematical modeling for roll plane motion and the determination of the length of the bay, mass distribution, and center of gravity of a bus. The third chapter contains the mesh convergence study for all FE models. Finally, it shows the concept of the deformation index for rollover crashes and analyzes the effects of the weld on the connection quasi-static simulation.

Chapter four

Chapter four presents the bus structure's modified design and structural optimization process for static and rollover analysis using reinforced design, numerical optimization, and combined approach. This chapter also analyzes which parts of the baseline structure influence strength and weight of the locally built midi–bus structure.

Chapter five

Chapter five shows the results of the research based on the analysis types via figures and tables. In addition, this chapter also expresses the discussion and comparison of baseline and alternative solutions on their results.

Chapter six

In chapter six, the thesis's conclusions, recommendations, and future works are gathered and discussed.

Chapter Two

Literature Review

2.1 Standards and Regulations Review

2.1.1 Standards and Regulations for Quasi-static and Rollover Analysis

(Trans, 2006) [35] states that during bus rollover crashworthiness tests, 4(four) equivalent and 1(one) basic methods were implemented and considered. School bus tests were approved by (Federal Motor Vehicle Safety Standards) FMVSS 220 [36]. FMVSS 220 standard used most commonly for the bus requires applying quasi-static loading tests to assess the roof static structural response.

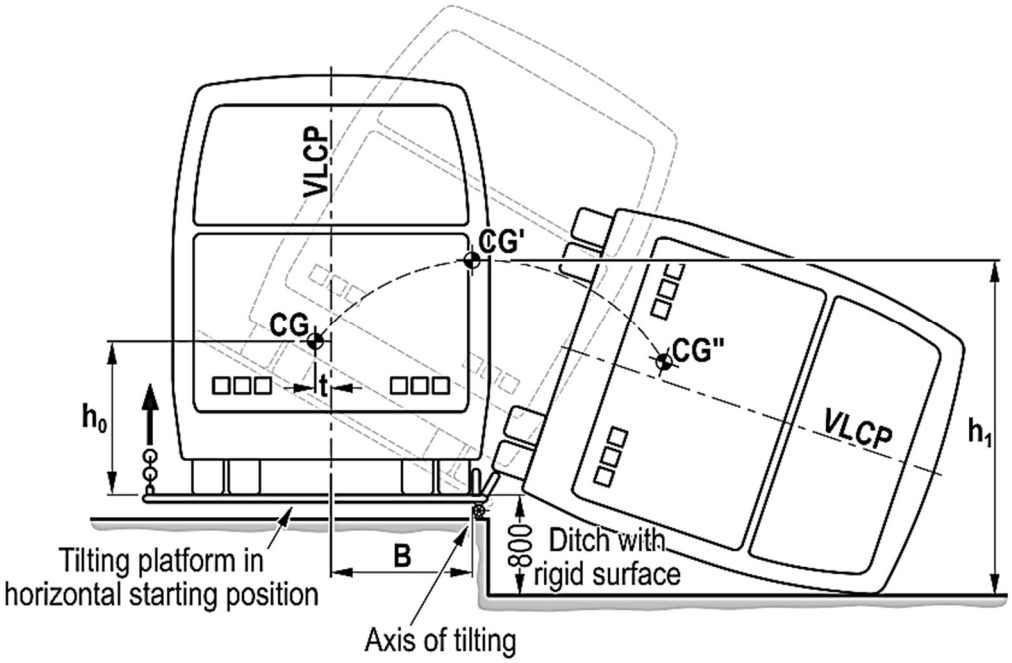

Figure 2.1: Rollover test setup according to ECE R66 [35]

As shown in Figure 2.1, the UNECE R66 Regulation mentions a setup of bus rollover tests before and after impact. This regulation stays used to confirm a sufficient structural strength and the occupant space, as shown in Figure 2.2(left). The full vehicle rotated with short time intervals on one side. If the bus starts dropping because of gravity, the Center of gravity (CG) reaches the critical point(highest). The ditch remains positioned in the depth of 800 mm from the horizontal ground surface. The tilt table or bus rotates by the initial angular velocity of 5 deg/s (0.0875 rad/s).

The test setup procedure and the residual space dimension are illustrated schematically in Figures 2.1 and 2.2, respectively.

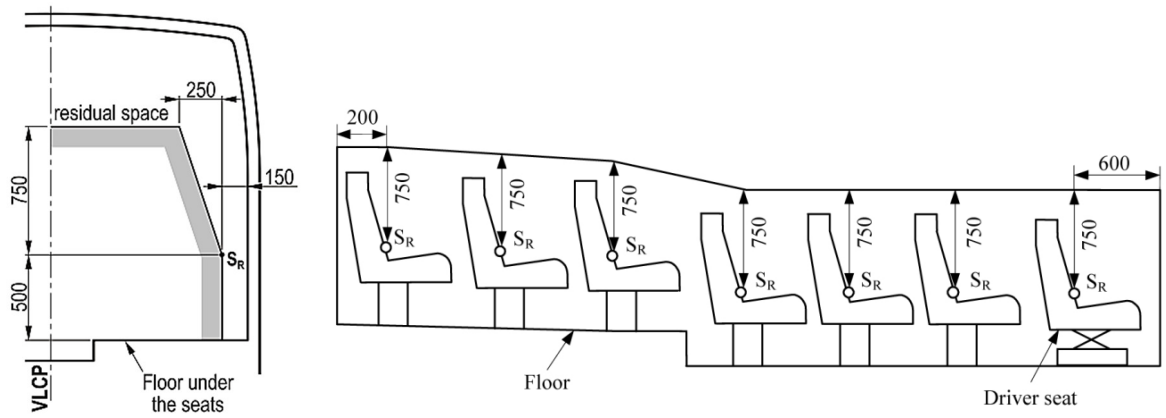

Figure 2.2: Residual space in lateral (left) & longitudinal (right) configuration [35]

Besides, UNECE R66 Standard states that the body section's quasi-static test is an equivalent method to measure the bus body section's energy absorbing capacity by applying incremental quasi-static load at the cant rail of the body section, as shown in Figure 2.3.

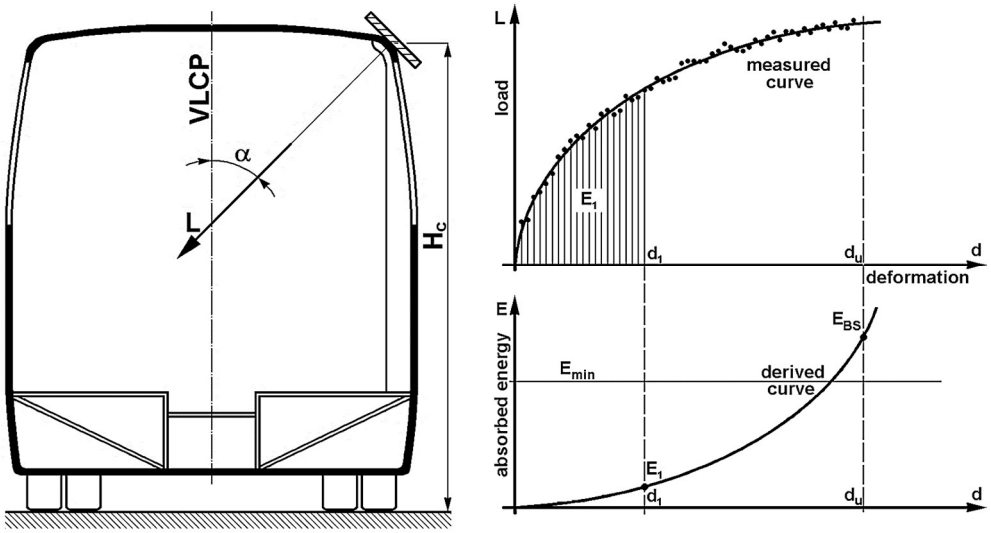

Figure 2.3: Illustration of quasi-static load applying to cant rail body section(left) and energy absorbing capacity for the body section from the load-deformation curve(right) [35]

(Motors et al., 1973) [37] FMVSS 216 aims to facilitate the fatalities and injuries rates, and the roof crushes into the occupant's space in rollover crashes. It introduces a quasi-static test procedure where force equal to 1.5 times its Gross Vehicle Weight (GVW) applies through an inclined rectangular plate to the A-pillar area that cannot deflect by more than 12.7 cm (5 in).

As stated by Florida Standard for a rollover accident, the bus structure's crashworthiness depends on the roof to wall and floor to wall connection. Therefore, in this quasi-static analysis of the components' connection, the loading conditions and boundary conditions are mentioned, such as

the roof or floor panel, fixed while the wall panel is loaded horizontally inwards. Table 2.1 displays the United Nations (UNECE) and the United States (US) Standards in rollover accidents. However, this research follows the standards of Florida and UN ECE R66 to analyze the rollover crashworthiness and the connection tests of the structure, respectively.

Table 2.1: Standard of U.N. (UNECE) & US in Rollover and Connection Test

Standards/Reg.	***Procedures***	***Criteria(pass/failure)***	***Application***
ECE Regulation 66 "***Uniform provisions concerning large passenger vehicles –The strength of their superstructure.***" [35]	A rollover test on a complete vehicle (primary method)	During and after the rollover test, occupant space on a whole vehicle will be uninjured by intrusions of bus elements.	More than 22 passenger's vehicles
	A rollover test using body sections	Similar to Criteria I.	
	A quasi-static loading test of the body section	Energy absorbed by the bus section will be greater than the minimum value of potential energy fraction dependent on the section's mass.	
	A quasi-static calculation based on testing of components	Energy absorbed by plastic hinges & plastic zones needed to deform structure to intrude residual space shall be more significant than specified total potential energy.	
	A computer simulation of rollover test on complete vehicle	Similar to Criteria I.	
United States of America FMVSS 220 "***School bus rollover protection"*** [36]	A quasi-static loading test on a complete vehicle	The load should not cause deflection more significant than 13.02 cm (5-1/8 in)	School buses

*Federal Motor Vehicle Safety Standard (FMVSS) 216 "**Roof crush resistance**"* [37]	- A quasi-static loading test on complete vehicle:	The load should not cause deflection greater than 127 mm (5 in).	Less than 6000 lbs. (2722 kg) GVWR of passenger cars and vehicles (trucks & buses)
Florida Standard **"*Crash and safety testing standard for paratransit buses acquired by the state of Florida*"** [38], [39]	- full-scale rollover test - computer rollover crashworthiness simulations -Validation and Verification Tests (energy, a center of gravity, wheels reactions, material characterization, and quasi-static connection tests)	Same as ECE R66 Regulation	Same as ECE R66 regulation

2.2 Previous Works

Some scientific papers are organized and reflected in bus structure optimization and crashworthiness analysis in rollover accidents using different techniques in this stage. Likewise, literature on the static and quasi-static structural analysis of the bus structure is reviewed and discussed. Moreover, this section presents the weld formation in the bus structural crashworthiness analysis.

2.2.1 Previous studies on Static Analysis of bus structure

(Agostinis & Vincenzi, 2011) [16] focused on a static analysis of an articulated bus via Numerical simulation. These researchers also analyze and validate the four different loading conditions, such as the gravitational acceleration (bending only), the torsion loading, the cornering maneuvers, and the braking using sensitivity analysis. However, according to (Lapapong et al., 2013) [40], the three loading conditions (braking, speed-bump crossing, and double-lane change) for strength analysis of bus superstructure are conducted via Field testing and FEM Simulation(ANSYS). Moreover, (Lan et al., 2004) [20] discussed the experimental and numerical analysis of bus structure strength with the sensitivity study and structural design optimization to reduce the bus bodyweight via cross-sectional parameters and wall thickness.

(Rooppakhun & Wichairahad, 2018) [17], the bus superstructure's static structural analysis conducts via FE Method(ANSYS) on the load cases of the bus, such as bending, longitudinal, torsion, and lateral conditions. Besides, (Z. Yang et al., 2018) [41] focuses on the static analysis of the electric bus frame via a finite element analysis (FEA). Moreover, the bending (the assembly parts, passenger weight, and self-weight), torsional (the front left wheel off the ground), braking (0.7g longitudinal deceleration), and steering (0.4g lateral acceleration) loading conditions conducts for strength analysis. The bus's weight reduces by changing the frame of a bus structure for a lightweight design. However, according to (Reyes-ruiz et al., 2013; H. Wang et al., 2018) [18], [19], only torsion and bending load conditions are considered to study the static strength of the bus structure by the FE Approach(ANSYS). The overall research works show that the strength parameters of the bus superstructure and structural optimization for lightweight design are crucial during experimental and numerical studies.

2.2.2 Previous studies on Quasi-static and Rollover Crash

In a quasi-static analysis, (Micu et al., n.d.) [42] presents a study of quasi-static loading test on bus body sections by regulation of UNECE R66 via both FEM simulation(ANSYS) and experimental test. Furthermore, the deformations results using FEM (ANSYS) compares with a physical model, and the absorbed energy and necessary mass of the structure is analyzed and computed. Likewise, (Nurhadi et al., 2010) [43] discussed that the incremental quasi-static loads and boundary conditions(fixed restraints) are applied at the cant rail of the body section and ladder frame of the bus body section, respectively. Additionally, according to ECE R66 requirements, the load-deflection curve and the structure's energy absorbing capacity are analyzed and evaluated using FE Analysis (ANSYS Explicit Dynamic Analysis). Furthermore, (Nor & Baharin, 2014) [44] studied that A quasi-static simulation test was also accomplished by ANSYS Explicit Dynamic Analysis using the standard of UN ECE R66.

According to (Bai, Meng, & Zuo, 2019) [2], rollover of a bus frame analyzes by the experimental method and detailed FEM method (Carframe, LS-DYNA & Hyperworks) using rectangular & dual_rectangular_thin-walled beams. Moreover, some sizes of bus frames are selected and optimized to reduce the angle of deformation and total mass, and the frame model of bus structure is better for computational cost and time than the detailed model, as shown in Figure 2.4. (Zhou, Kuznectov, Wu, & Telichev, 2019) [12] a comparative analysis of a motor-coach structure's energy absorption and rollover resistance by experimental and numerical methods through two test conditions(zero and entire passenger mass). Moreover, these researchers found that plastic deformation obtains at the joints of the beam in the rollover test.

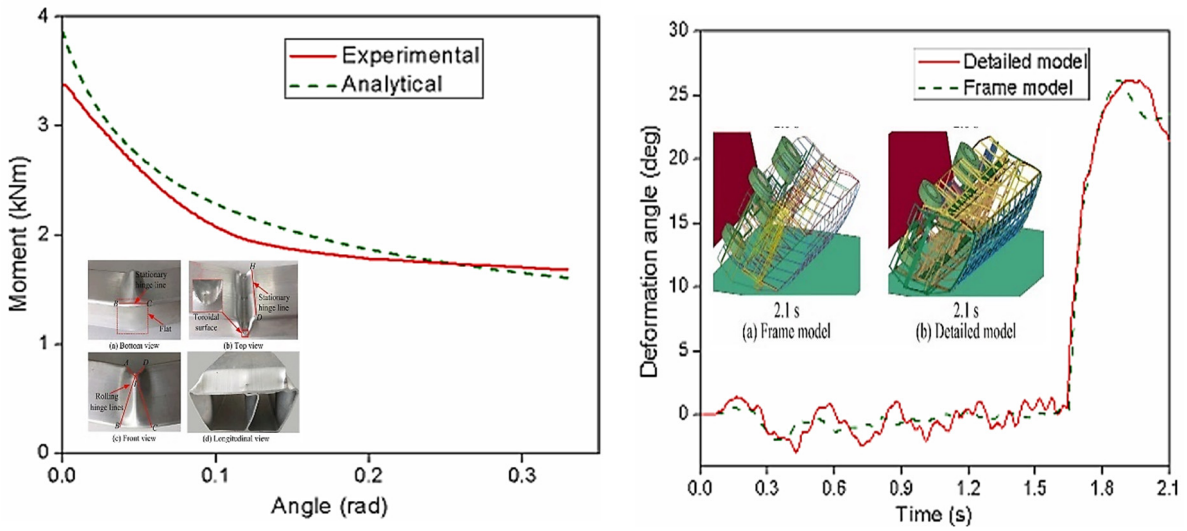

Figure 2.4: Bending collapse characteristic of DRTWB (left) and Comparison of deformation angle(right) [2]

(VD. Phadatare, 2017) [45] discussed that bus structure of roll-bar for rollover analysis are validated and optimized by experimental tests, and numerical model with FEM(LS-DYNA) Using three-point bending of bus components and new roll-bar. These researchers obtained a newly designed roll-bar structure with a stiffener with more crash energy absorption capacity than the old model. Also, (Thosare & Patil, 2017) [46] designed and analyzed the deformation of pillars of bus sections by adding C brackets to roof bars and simulating the new and original design by using LS-DYNA to obtain positions of the supports and their deformations. Thus, the deformation of the supports decreases during a rollover.

The study (Rogov Petr Sergeevich & Orlov Lev Nikolaevich, 2015) [47] verifies and analyzes the bus body structure components in rollover tests by experimental and numerical crashworthiness investigations. First, the rollover numerical simulation establishes to study the deformation of the structure and the amounts of absorbed energy of top, right side and left sidewalls of the passenger vehicle using LS-DYNA software based on regulation ECE R66 (see in Figure 2.5). Moreover, the number of contact points, deformation, kinetic energy, friction coefficient, velocity, and acceleration of the bus sections are determined. In this finding, the change in distance(deformation) of the test's number of control points is smaller than the calculation. Furthermore, (Wang, Pan, Zhang, & Cui, 2015) [32] discussed and analyzed the system's energy dissipation and the effects of energy-absorbing of the main structure in the rollover crash process using experiment tests and FE model.

Moreover, the column's deformation successively decreases from top to bottom and the front to the back. Again, (Yang & Deng, 2015) [48] analyzed and studied the structural optimization and lightweight of the bus body skeleton using the numerical model by Hyperworks. Then, the bus

body section optimizes by varying the beams' thicknesses in the gussets and the end corner radius of the roof cross rails. The bus section's maximum stress of the cross-rail end corner beam under various thicknesses decreases as the thickness and the larger arc transitions increases.

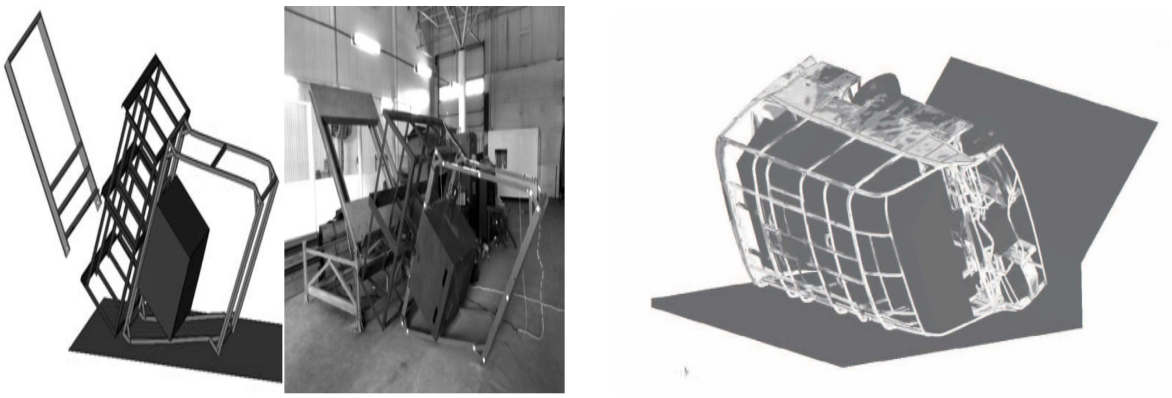

Figure 2.5: Deformed conditions of the model & real body section construction(left) [47] and vehicle deformation (right) [49]

According to (Na, Wang, & Xu, 2014) [50], the bus section using three methods is developed and analyzed by experimental setup for the rollover test of bus middle section and numerical model with FEM by LS-DYNA strain theory. Furthermore, these researchers study an algorithm to obtain pillar deformation, gauging points, energy, time, and stress. (M. K. Mohd Nor & M. Z. Dol Baharin, 2014) [44] studied the numerical simulation(ANSYS) of a heavy vehicle bus structure according to FMVSS 220 & ECE R66 for quasi-static and rollover analysis. During a quasi-static load test, the maximum deformation & maximum stress occur on the front compartment's side-impact and around the middle of the bus frame, respectively. Moreover, the right side of the bus body section deforms towards the (concrete) ground surface, the left-side bend towards the point of impact, the roof structure deforms outwards, away from the bus occupant. Lastly, (Karliński et al., 2014) [4] focused on the strength of the Volkswagen LT vans bus structure according to ECE R66 using numerical model & simulation using FEM. These researchers imply that the bus structure subjects to plastification partially, the most extensive deformation observed at the front part of the structure.

Consequently, (Korta & Uhl, 2013) [51] studies and analyzes the multi-material optimization of bus structure using Genetic Algorithm (GA) optimization and numerical simulation for different materials. The following parameters, such as torsional stiffness and rollover resistance, are obtained from FE Analysis using multi-materials (Standard_Modulus_Carbon_Fiber_Reinforced Plastics (SM-CFRP) and High_Modulus_Carbon_Fiber_Reinforced_Plastics (HM-CFRP), GFRP (Glass_Fiber_Reinforced_Plastic), aluminum, and steel). Consequently, the rollover deflection and torsional stiffness parameters are safe when using the composition of SM-CFRP, HM-CFRP, and steel materials. Similarly, (Reyes-ruiz et al., 2013) [18] discovered on optimized and analyzed

the passenger bus frame by using the design concept, numerical analysis, and simulation for different materials with FE Method on the parameters of strength (torsion, bending), dynamics (vibration response) constants and the thickness of bus frame structure. Hence, the torsion and bending constants for the optimized bus frame decreases by optimizing the mass reduction of the beam's thickness. Lastly, (Yusof & Afripin, 2013) [52] studied that bus superstructure and effect of beam profile size undergo rollover event through experimental tests with a high-speed video camera and numerical simulation with FEM by considering cant-rail and roof structure profile size. Moreover, these researchers study the von mises stress, deformation, size, strain, and time parameters. These researchers found only a slight improvement when using a larger profile size than the beam of bus structure standard.

In the study of (Hu, Yang, & Wang, 2012) [32], a numerical(Finite Element) Model of a welded transit bus structure is developed and validated using numerical simulation with FEM and Experimental Modal Analysis (EMA). Thus, these researchers achieved good correlations of natural frequencies and mode shapes between FEA and EMA. Correspondingly, (Li et al., 2012) [53] studied and analyzed that the coach body section under rollover via experimental tests (local collapse behaviors and coupon test for materials) and numerical model, analysis with FEM(LS-DYNA) on the parameters such as dynamic deformation and impact acceleration, energy, stress, strain and time.

Furthermore, the simulation results agree with the experimental tests for the maximum deformation and give an error of 4.71 %. Lastly, (Yusof et al., 2012) [3] discovered the bus frame and validated it through a single box model experiment and FE analysis for the masses effects and bus structure strength. According to (Su, Gui, & Fan, 2011) [54], it focuses on minimizing the weight and maximizing the torsional stiffness of the bus frame under rollover protection. These researchers ensure via experimental investigation and optimization techniques ('NSGA-II' (nondominated sorting genetic algorithm-II) & 'AMISS-MOP' (Adaptive_Multi-Island Search_Strategy for Multi-Objective Optimization Problem) algorithms). Lastly, they found that the weight of 2,783 kg, stiffness 40.18 KN.m/deg, maximum stress 313(MPa), and maximum intrusion of 23.8 mm significantly optimize the bus's performance.

Consequently, (C. Bojanowski & R. F. Kulak, 2011) [24] studied the paratransit bus structure for sensitivity and Multi-Objective(MO) Optimization using numerical simulation with FEM by LS-DYNA and Sobol's indices and linear ANOVA method. The mass objective increased by ∼9% from sensitivity analysis. On the other hand, the Deformation Index (DI) and Intrusion max scaled decreased by ∼2% & ∼26%, respectively. On the other hand, (Tech & Iturrioz, 2009) [25] discussed that the bus structure in rollover conditions optimizes & analyzes via experimental and

numerical methods with optimization methodology using super-beam elements by plastic hinge lateral-base union of two samples. Hence, improving the intermediate structural rings' geometric property is the best option to increase the bus's mechanical resistance with lower gins of its weight.

(Mahajan et al., 2003) [55] studied the bus structure resistance of rollover by experimental setup for the rollover test of bus section and numerical model with FEM (LS-DYNA solver). The study parameters are thickness, energy (absorbed, internal and kinetic), time, intrusion inside residual space, and deformation. As a result, the bus section's Simulation results were within 11 % of the experimental work, and the superstructure intruded in the residual area. Also, (Matolcsy 1997) [56] focuses on severe conditions and parameters in rollover accidents of bus structures through statistical and qualitative data analysis by using standards and general principles of testing methods with study parameters(Intrusion, causality fatality rates, complete and partial ejection, projection and Protectable Rollover Accidents (PRA). Thus, the surroundings strongly influence the role of the rollover accident, intrusion considered to enhance passenger safety in the rollover, and all casualty rates are 3-4 times lower, the fatality rate is lower with one order (10 times) PRA.

(R. P. Sergeevich & O. L. Nikolaevich, 2015) [47] focused on verifying and analyzing the bus body structure components in the rollover test by experimental and numerical crashworthiness investigations of bus structure for each element. The researchers have also studied the parameters such as the number of contact points, deformation, kinetic energy, friction coefficient, velocity, & acceleration of the bus section. According to (Friedman et al., 2006) [57], the composite roof structures in transit buses are implemented and analyzed. A new material(composite) only for roof structure is used for numerical model and simulation by LS-DYNA. Lastly, the numerical results are a decrease in roof deformation and practical design.

In the study of (Lin & Nian, 2006) [58], the design and analysis of the bus body section develops by experimental investigation, design optimization (changing the thickness), and numerical simulation(LS-DYNA & HYPERSTUDY). Thus, the body section's deformation can be reduced by 50% while only increasing by 2% of the weight. (Lan et al., 2004) [20] discovered the experimental tests of strength and numerical model, analysis & simulation (ANSYS), and optimization (Geometric parameters) conducted on a lightweight bus side structure. These researchers found the frame torsional stiffness, weight body, and frequency reduction by 11 %, 5.7 %, and 3.5 %. Moreover, the other researchers (Cho Chung Liang & Le, 2009) [15] studied lightweight bus frame structure during a rollover by numerical analysis and simulation(LS-DYNA) bus structure sections and optimized through successive_respond_surface_method (SRSM) using LS-OPT. They obtained an enhancement displacement of 56.42 % and 39.28 % for the lower bus frame, respectively, with a 1.53% reduction in the vehicle. (Rahman, 2011) [11]

designs and analyzes the numerical modeling and analysis of the middle section of the bus structure. Moreover, these researchers identify the critical to structural frame components' rigidity and most stresses upon impact structural joints.

(Park et al., 2006) [59] discusses the beam's analytical and numerical model and non-linear spring elements of the bus structure in a rollover. These researchers concluded that a spring element with characteristics was estimated structural stiffness correctly and improved reaction forces and internal energy. (Tech et al., 2007) [8] studied experimental and theoretical predictions of the collapse of basic bus structure with FEM(LS-DYNA) for plastic hinge by a super-beam element of bus section in a rollover. The deformed configuration results of the experimental test & those obtained through simulation have presented a perfect correlation.

(C. C. Liang & Nam, 2010) [10] studied bus rollover protection using the numerical model, analysis & simulation using FEM (ANSYS) according to ECE R66 & FMVSS 220. With 57.16% total absorbed energy, the sidewall section is the highest requirement, following ECE R66. However, with 50.01% of the total absorbed energy, the roof section is the highest requirement following FMVSS 220. (Subic & He, 1997) [60] discussed on the experimental and analytical modal analysis of the bus roll-cage structure by an Alternative Research Approach. And also, the bus frame natural frequencies in the low-frequency range of up to 40 Hz. The difference between the experimental & analytical natural frequencies is lower than 10% for the first ten modes.

(Bojanowski et al., 2011) [61] studied the experimental setup and numerical model of a paratransit bus for roof crush and rollover by LS-DYNA. These researchers study the multi-objective optimization by minimizing Deformation Index (DI) in rollover using sheet steel, strip & tubing, stainless steel & galvanized steel. (Valladares et al., 2010) [62] numerical simulation by ABAQUS Explicit using three models (beam elements, structural beams with shell elements, and sandwich structure detail of bus body sections in the case of a rollover. These researchers obtained that the addition of sandwich structures improves the actual structural behavior significantly.

2.2.3 Weld Formation during bus structural crashworthiness analysis

(Kwa et al., 2011; Li et al., 2018), [26], [27] developed the rollover FE Models of the bus structural connection using spotweld (rigid) links between the nodes. Similarly, (Cezary Bojanowski, 2009), [28] discussed the importance of spotweld (Constrained_spotweld) as compared to a layer of solid element and TIEBREAK contact between structural parts during modeling of welds using LS-DYNA. Moreover, (Mertcan Kaptanoğlu, 2015), [29] welds are modeled as a rigid element (RBE2) using Hypermesh. Moreover, (Sidhu, 2012; S. Kumar, 2012), [30], [31] also studied that the connection of welds constructs as the spring elements with tied contact using RADIOSS.

However, According to (Zhou et al., 2019), [12] the welds are constructed as a solid part and tied to the beams (structure element) in the quasi-static test of the structural components(pillar). Moreover, these researchers present and compare the results of force vs. displacement from the experimental test and numerical methods. (Hu et al., 2012), [32] welds are modeled as a shell element (Shell 63) and assigned the tensile test data.

2.3 Research Potential

The above researchers' literature review has discussed the experimental investigation and numerical modeling, optimization techniques, and crashworthiness analysis of the buses and body section during static, quasi-static, and rollover conditions. However, the optimization methods using response surface optimization (RSO) and ANSYS DesignXplorer are not included in the static analysis to minimize the weight at the sufficient stiffed structure. Moreover, the above researchers did not address the consequences of overloading the passengers and luggage on the bus structural deformation and the severity of accidents during rollover crashes. Moreover, the effects of welding techniques (weld types) during welding of the bus structure are not considered.

As mentioned earlier, the bus bodies are manufactured by small and medium enterprises (SME) in Ethiopia, guided by their experience and thumb rules. Therefore, this study targets the problem specified in the locally modified bus and the above research gaps.

Chapter Three

Methodology

3.1 Mathematical modeling for rollover analysis

3.1.1 Coordinate system and equation of motion in a multi-body system

Coordinate systems are used to define the vehicle's equation of motion, and they are vital for modeling a mathematical equation of the rollover motion. Figure 3.1(a) explains a coordinate system in the right-hand rule. Roll, pitch, and yaw are defined as rotations around the x, y, and z axes, respectively [63].

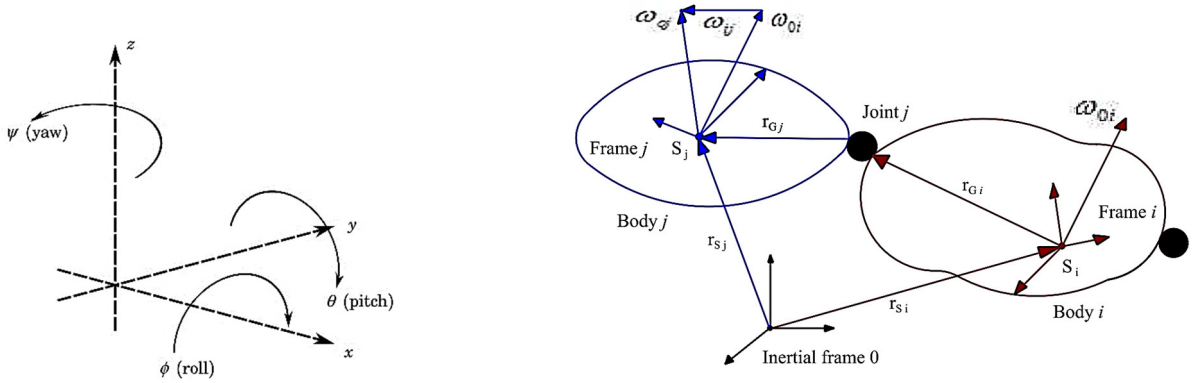

(a) (b)

Figure 3.1: a) The coordinate axes and rotations around axes and b) a loop-free connected bodies in a multi-body system [64]

The roll & yaw plane motions of the vehicle are factors to the root cause of vehicle rollover. Most researchers describe the vehicle's rollover motion only in roll plane with or without damping coefficient & spring stiffness [47], [64]–[67]. Some researchers also analyze rollover motion detection in the roll and yaw motion together [63], [65].

For a simple model, the roll plane motion is the factor to study vehicle rollover. A loop-free connected bodies in a multi-body system see (Figure 3.1(b)), the kinematics (position, velocity, and acceleration) formulation are given by [64]:

The vector form, A_{j0}

$$A_{j0} = A_{ji} A_{i0} \tag{3.1}$$

The angular velocity, ${}_j\omega_{0j}$

$${}_j\omega_{0j} = {}_j\omega_{ij} + A_{jii}\omega_{0i} \tag{3.2}$$

The angular acceleration, ${}_j\dot{\omega}_{0j}$

$$ {}_j\dot{\omega}_{0j} = {}_j\dot{\omega}_{ij} + A_{jii}\dot{\omega}_{0i} + {}_j\tilde{\omega}_{ij}A_{jii}\omega_{0i} \tag{3.3} $$

The linear position vector, ${}_jr_{S_j}$

$$ {}_jr_{S_j} = {}_jr_{G_j} + A_{ji}({}_ir_{S_i} + {}_ir_{G_i}) \tag{3.4} $$

The linear velocity, ${}_jv_{S_j}$

$$ {}_jv_{S_j} = A_{ji}({}_iv_{S_i} + {}_i\tilde{\omega}_{0i} \cdot {}_ir_{G_i} + {}_i\dot{r}_{G_i}) + {}_j\tilde{\omega}_{ij} \cdot {}_jr_{G_j} + {}_j\dot{r}_{G_j} \tag{3.5} $$

The linear acceleration, ${}_ja_{S_j}$

$$ {}_ja_{S_j} = A_{ji}({}_ia_{S_i} + {}_i\dot{\tilde{\omega}}_{0i} \cdot {}_ir_{G_i} + {}_i\dot{r}_{G_i}) + {}_i\tilde{\omega}_{0i} \cdot {}_i\tilde{\omega}_{0i} \cdot {}_ir_{G_i} + 2{}_i\tilde{\omega}_{0i} \cdot {}_ir_{G_i} + {}_i\ddot{r}_{G_i}) $$
$$ +2{}_j\tilde{\omega}_{ij} \cdot {}_j\dot{r}_{G_j} + {}_j\ddot{r}_{G_j} + {}_j\tilde{\omega}_{ij} \cdot {}_jr_{G_j} + {}_j\tilde{\omega}_{ij} \cdot {}_j\tilde{\omega}_{ij} \cdot {}_jr_{G_j} \tag{3.6} $$

By D'Alembert's principle is used to derive the motion equation. Thus, the equations of motion of the system are derived in the following manner:

$$ M(q)\ddot{q} + g(q,\dot{q}) = q_e(q,\dot{q}) \tag{3.7} $$

Where: ***M***- the mass matrix, ***g*** **-** the vector form of generalized Coriolis forces, and $\boldsymbol{q_e}$ – the external torques and forces and generalized coordinates, ***q,*** and Jacobians, ***J***

The equation of the mass matrix is collected by

$$ M(q) = \sum_{i=1}^{n}\left[J_{R_i}^T I_{s\,i} J_{R_i} + J_{T_i}^T m_i J_{T_i} \right] $$

And also, the generalized Coriolis forces, ***g,*** & the external torques and forces, $\boldsymbol{q_e}$ are

$$ g(q,\dot{q}) = \sum_{i=1}^{n}\left[J_{R_i}^T (I_{s_i} J_{R_i}\dot{q} + \tilde{\omega}_i I_{s_i}\omega_i) + J_{T_i}^T m_i \dot{J}_{T_i}\dot{q} \right] $$

$$ q_e(q,\dot{q}) = \sum_{i=1}^{n}\left[J_{R_i}^T l_i^e + J_{T_i}^T f_i^e \right] $$

3.1.2 Development of mathematical modeling for roll plane motion

The two approaches to developing the rollover system equation are based on the conservation of energy theorem and conservation of momentum(Newton's 2nd law) [64]. Thus, the bus's roll plane motion mathematical model is demonstrated in this section based on the Newton-Euler 2nd law of motion.

The planar bus motion is located at a random roll angle ($\phi < \theta$) shown in Figure 3.2. The frictional and normal forces act at the pivot point O. However, the damping and spring forces are neglected

to derivate the motion equation. Nevertheless, an inertial coordinate system with the origin is well-defined.

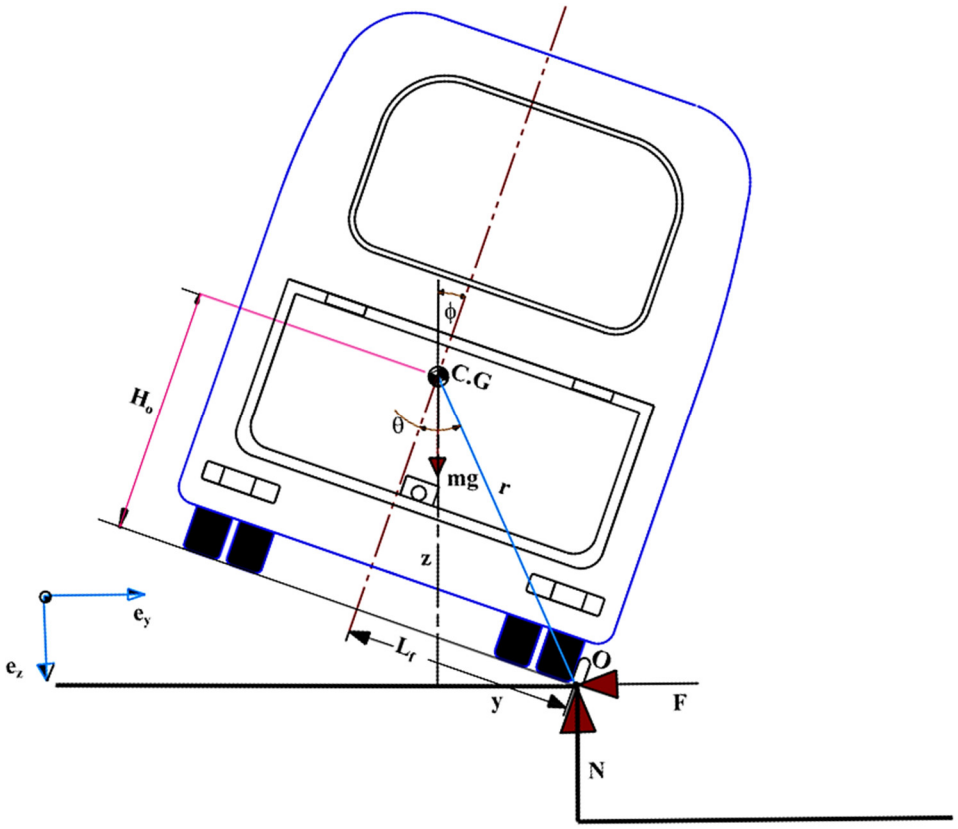

Figure 3.2: illustrates the roll plane motion of the bus model before rollover, *[0 ≤ t ≤ t_{cr}]*

The equations of position coordinates (*y, z*) of the center of gravity (CG) by

$$y = -r\sin(\theta - \phi); \qquad z = -r\cos(\theta - \phi) \tag{3.8}$$

Where:

ϕ - an angle between the mass of the vehicle and road plane

r – radius measured from the CG to pivot point O and θ - critical angle, by second integration of the eq. 3.8, the equivalent accelerations ($\ddot{y}, \ddot{z}$) are

$$\ddot{y} = r\sin(\theta - \phi)\dot{\phi}^2 + r\cos(\theta - \phi)\ddot{\phi}$$

$$\ddot{z} = r\cos(\theta - \phi)\dot{\phi}^2 - r\sin(\theta - \phi)\ddot{\phi} \tag{3.9}$$

Applying the summation of forces and moments,

$$m\ddot{z} = mg - N \tag{3.10}$$

$$m\ddot{y} = -F \tag{3.11}$$

$$I_x\ddot{\phi} = F|z| - N|y| \tag{3.12}$$

(Chen & Guenther, 1993), [64] derived that the sequence of rollover interval is split between *[0 ≤ t ≤ t_{cr}]* and *[t_{cr} < t < T]*.

Foremost, the bus angular momentum, L_{cr}, is developed through external forces (N and F), causing a potential rollover in the first interval, as shown in Figure 3.2. Lastly, assuming that the forces are an act to support the rollover until a critical time, t_{cr}. Thus, the rolling motion slows down, and only the normal force, N, leaves, when $t = T$ or $\phi = \theta$ (static tip angle) is reached (see Figure 3.3).

$$L_{cr} = \int_0^{t_{cr}} F(t)\left|z(t)\right| - N(t)\left|y(t)\right| dt \qquad \text{for} \quad (0 \le t \le t_{cr}) \tag{3.13}$$

$$L_1 = \int_{t_{cr}}^{T} -N(t)\left|y(t)\right| dt \qquad \text{for} \quad (t_{cr} < t < T) \tag{3.14}$$

The rollover of the bus occurs when the angular momentum remains positive $\phi = \theta$. The rollover condition is sure to occur after critical time, t_{cr}, with no lateral supporting forces, F, occurs by applying eq. (3.13) and (3.14)

$$L_{cr} + L_1 > 0 \tag{3.15}$$

The stability boundary condition is the $\omega = \dot{\phi}(t) \le 0$ for $\phi = \theta$

And applying eq. (3.12) to a static boundary, the angular acceleration $\ddot{\phi}$ is

$$I_x \ddot{\phi} = -N\left|y\right| = m\ddot{z} \cdot y - mg \cdot y \tag{3.16}$$

$$\ddot{\phi} = \frac{\left[\frac{m}{2} r^2 \sin 2(\theta - \phi)\right]\dot{\phi} - mgr\sin(\theta - \phi)}{I_x + mr^2 \sin^2(\theta - \phi)} \qquad \text{for} \quad t \ge t_{cr} \tag{3.17}$$

a representation to find a trajectory in the (ϕ, ω)-plane

$$\omega = f(\phi)$$

$$\ddot{\phi} = f'(\phi) f(\phi) \tag{3.18}$$

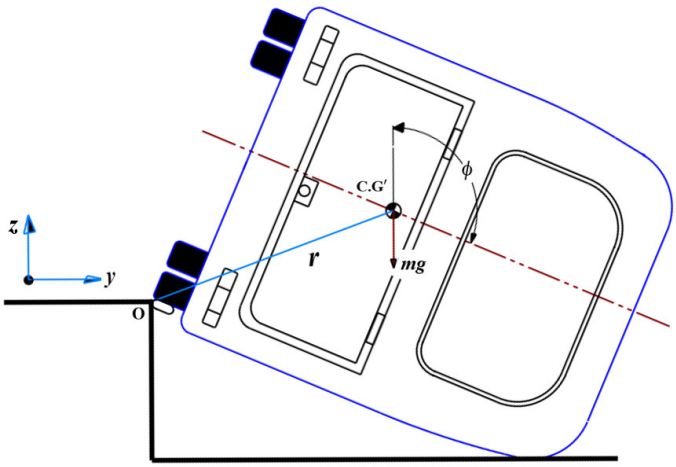

Figure 3.3: Illustrates the settlement of the bus model in touch to the ground, *[$t_{cr} < t < T$]*

by applying the eq. (3.18) into Eq. (3.17), the Bernoulli-type differential equation is found

$$f' = g(\phi)\cdot f - h(\phi)\cdot f^{\alpha} \text{ with } \alpha = -1 \tag{3.19}$$

Substituting the above relations & writing in the form of Linear Differential Equation (LDE) for z

$$z(\phi) = f(\phi)^2 \text{ such that } f(\phi) = \sqrt{z(\phi)} \tag{3.20}$$

$$z' = 2\cdot f\cdot f' \rightarrow z' = 2g(\phi)\cdot z - h(\phi) = A(t) + B(t) \tag{3.21}$$

and solving the above LDE equation, the general solution $z(\phi)$ is

$$z(\phi) = 2z_0\left|\frac{I_x + mr^2\sin^2(\theta-\phi_0)}{I_x + mr^2\sin^2(\theta-\phi)}\right| + \frac{2mgr\left[\cos(\theta-\phi_0)-\cos(\theta-\phi)\right]}{I_x + mr^2\sin^2(\theta-\phi)} \tag{3.22}$$

Now, the angular velocity of the vehicle is given by

$$\omega = f(\phi) = \sqrt{z(\phi)}$$

$$\omega = \omega_0 + \sqrt{2z_0\left|\frac{I_x + mr^2 sin^2(\theta-\phi_0)}{I_x + mr^2 sin^2(\theta-\phi)}\right| + \frac{2mgr\left[cos(\theta-\phi_0)-cos(\theta-\phi)\right]}{I_x + mr^2 sin^2(\theta-\phi)}} \tag{3.23}$$

Therefore, in this study, the equation of the rolling motion of the bus is significant to verify the result obtained by finite element simulation of the rollover.

3.2 Length of bays, Mass Distribution and Center of Gravity

3.2.1 Location and Length of Bay

The number and location of the bays(rings)(B1-B8) of the structures, the neglections and reduction of bay in-plane (increase the safety), and the connecting elements of the bodywork are arranged in the horizontal direction Figure 3.4.

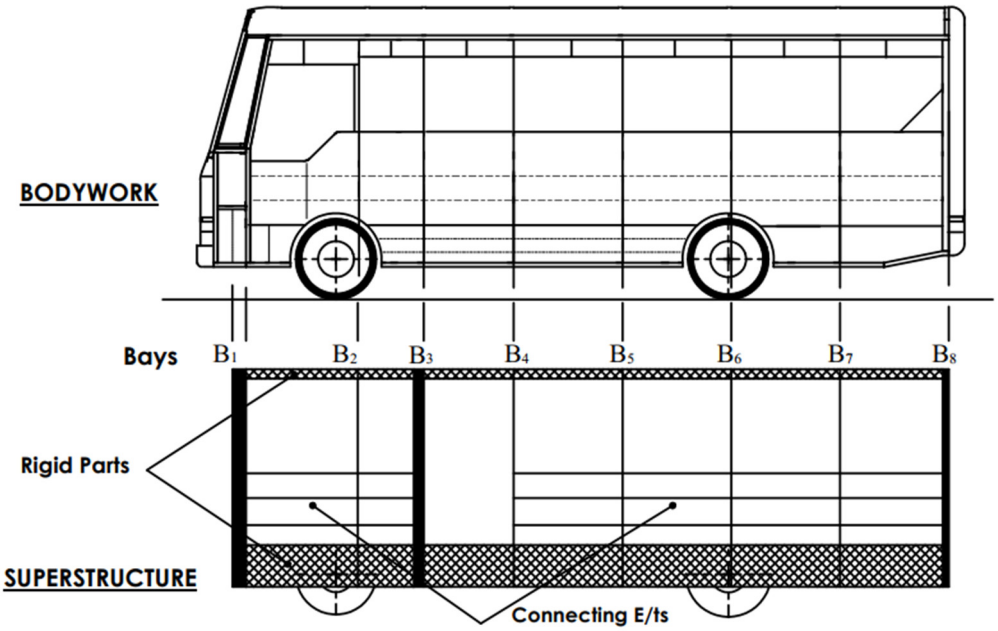

Figure 3.4: The superstructure from the bus body[35]

In the direction of the vehicle's longitudinal axis, the maximum length of a bay is well-defined and determined by the window (door) frames the length of the pillar, as shown in Figure 3.5.

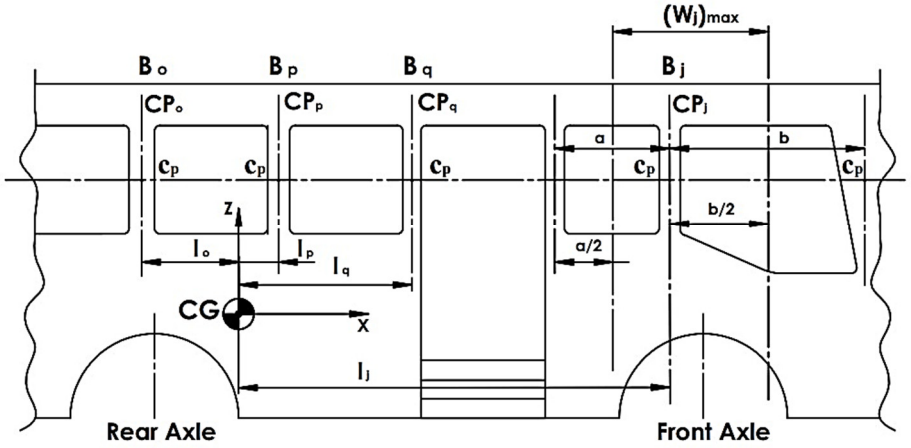

a)

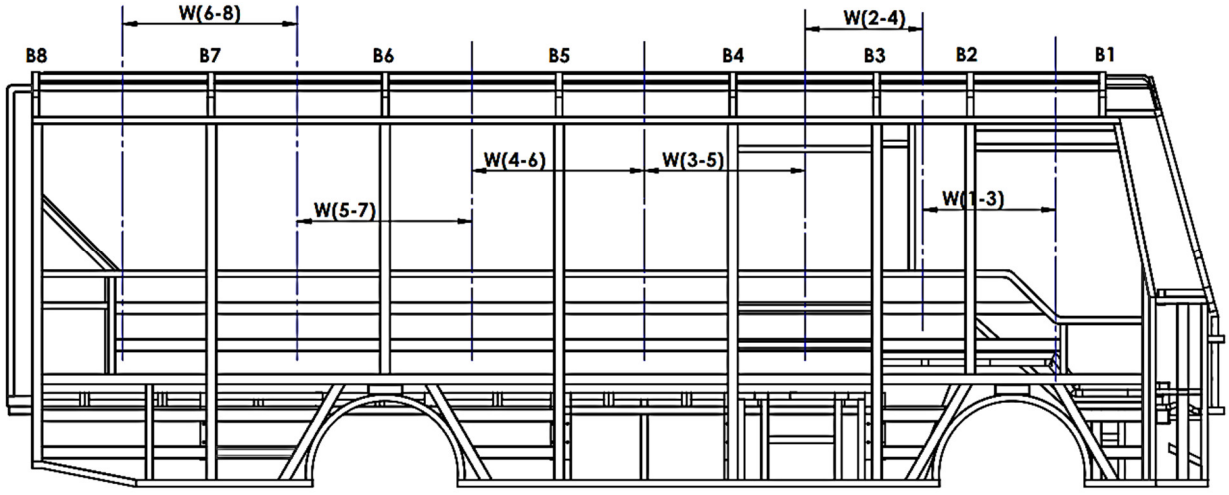

b)

Figure 3.5: Illustration of Length of bays; Length of bays from the door view of the vehicle [35] and b) Location of the length of bays (Wj)

The maximum length of a bay is given by:

$$(W_j)_{max} = \frac{1}{2}(a + b) \qquad 3.24$$

Where, a - window frame length behind the j^{th} pillar, and

b - window frame length in front of the j^{th} pillar

Consequently, there are six maximum bay lengths between eight numbers of the bay's center plane, as shown in Figure 3.5(b). As shown in Appendix A or (see Table A3.1), the bay's minimum length (695 mm) is located between the door frame and the most petite window frame length (W_{2-4}), and the bay's maximum lengths (1110 mm) are located between two window frame lengths (W_{4-6}, W_{5-7} & W_{6-8}).

3.2.2 Mass Distribution

The mass distribution expresses the energy-absorbing capability and load-bearing capacity of each bay ([34], [35]). The mass distribution of the bus is defined as:

$$\sum_{j=1}^{s} (m_j) \geq M \qquad 3.25$$

Where: m_j - the mass attributed to the j^{th} bay, s - the number of bays and

M - unladen kerb mass (M_k)

As shown in Figure 3.6, The equations used for the ring ($R_{i)}$ having four mass components is given by [34]

$$\begin{aligned} m_{i1} &= m_{iu} + m_{icm} + \frac{2}{3}(m_{ilwl} + m_{irwl}) \\ m_{i2} &= \frac{2}{3} m_{ilwu} + \frac{1}{3} m_{ilwl} \\ m_{i3} &= m_{ir} + \frac{1}{3}(m_{ilwu} + m_{irwu}) \\ m_{i4} &= \frac{2}{3} m_{irwu} + \frac{1}{3} m_{irwl} \end{aligned} \qquad 3.26$$

Where: m_r - the mass of the entire roof containing roof luggage structure and others,

m_{lwu} - mass of the left_upper wall, distributed consistently under the window rail,

m_{rwu} - mass of the right_side wall same as the left-upper wall,

m_{lwl} - mass of the left_lower wall, distributed consistently under the window rail,

m_{rwl} - mass of the right_side wall same as the left-lower wall,

m_u - mass of the underfloor structure comprising electrical and smaller components,

m_{cm} - mass of the main components (mass of individual > 100 kg).

Note that the rear wall (m_{rw}) and the front wall's mass (m_{fw}) are consistently distributed in the underframe structures.

In actual accidents and rollover tests, these glasses(windscreen) break frequently; it is challenging to analyze the theoretical approach to whether it fails or not [34]. As shown in Table A3.2, the summarized mass components of the bays are mentioned. From the mass distribution calculation, the sum of the four mass components leads to the result of the total mass of ring (R_i), and also the sum of the ring masses leads to giving the total empty mass of the bus (m_o) [34], [35] (see eq. 3.27). Thus, the mass of the bus's unladen kerb obtained by the manufacturers equals the calculated sum of the bay's masses (see Table A3.2).

$$\sum_{j}^{4} m_{ij} = m_{Ri} \text{ and } \sum_{j} m_{Ri} = m_o \quad 3.27$$

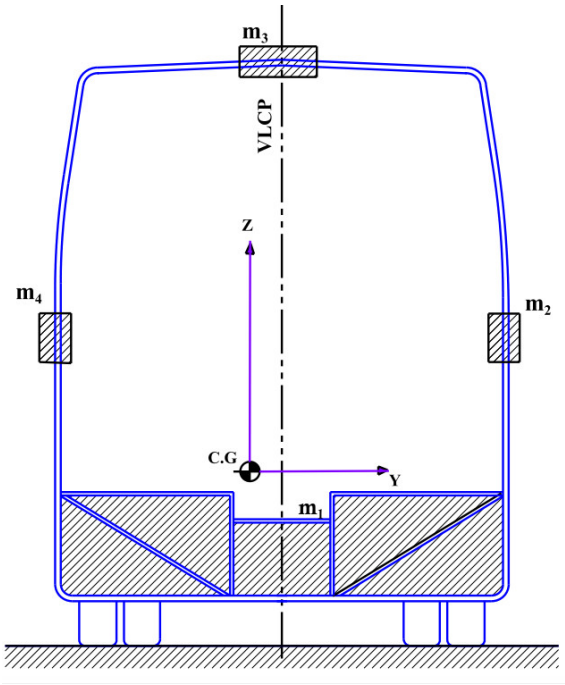

Figure 3.6: Illustrations of distributed masses in the bay(ring) [34], [35]

3.2.3 Centre of Gravity (CG)

The center of gravity is well-defined through three constraints (vertical height, transverse distance from the vertical longitudinal central plane of the vehicle, and longitudinal distance from the centerline of the front axle) above the surface of the horizontal ground if the tires are inflated position.

3.2.3.1 The longitudinal direction of the center of gravity(l_1)

Figure 3.7 shows the center of gravity's longitudinal direction relative to the center of the front wheels' contact point. Using summation of a moment at the center of gravity of the vehicle is given by,

$$M_r \times (L_{wb} - l_1) = M_f \times l_1$$

Where: M_r - the mass of the rear axle,

L_{wb} - length of the wheel-base, and

M_f - the mass of the front axle

Rearrange the above equation, the longitudinal direction of the center of gravity (l_1) will be

$$l_1 = \frac{M_r \times L_{wb}}{(M_f + M_r)} \quad 3.28$$

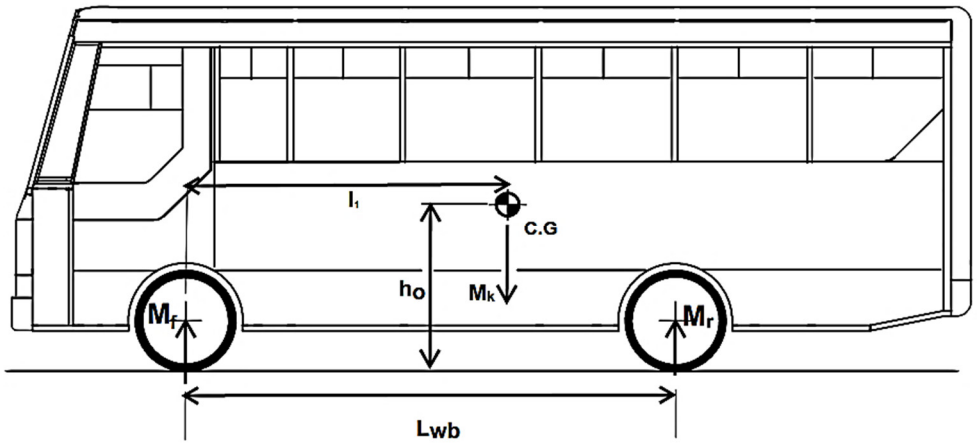

Figure 3.7: Longitudinal direction of the center of gravity

3.2.3.2 Transverse Direction of the Center of Gravity(t)

Figure 3.8 shows the transverse direction (t) of the vehicle's center of gravity relative to its longitudinal vertical center plane. Using summation of a moment at the center of gravity of the vehicle is given by

$$M_R \times (\frac{L_f}{2} - t) = M_L \times (\frac{L_f}{2} + t)$$

Where: M_R - right-side vehicle's mass,

L_f - distance between front tires (width) &

M_L - left-side vehicle's mass

Rearrange the above equation, the transverse direction of the center of gravity(t) will be

$$t = \left(\frac{M_R - M_L}{M_R + M_L} \right) \times \frac{L_f}{2} \qquad 3.29$$

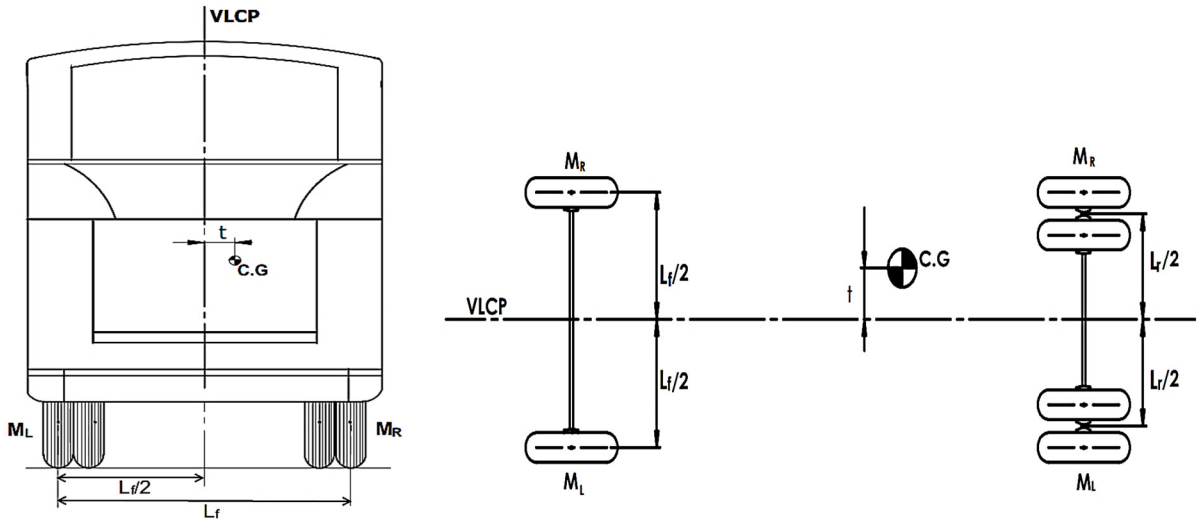

Figure 3.8: Transverse direction of the CG from rear-view (left) & top-view (right) [35]

3.2.3.3 Height of the Center of Gravity (h_o)

The height of the center of gravity (h_o) can be determined by tilting the vehicle longitudinally, as shown in Figure 3.9. By taking the summation of a moment at the rear wheels of an axle

$$M_k \times (l_2 + \Delta l_2) \times cos\alpha = (M_r + \Delta M) \times L_{wb} \times cos\alpha$$

Where:

M_k - Unladen kerb mass of the vehicle(M) L_2 - the distance between CG and rear Axle center

Δl_2 - the changes in distance between CG and unladen mass & α - tilting angle of the vehicle and

ΔM - change in mass between the rear and front of the vehicle, $\Delta M = \left| \frac{M_r - M_f}{2} \right|$

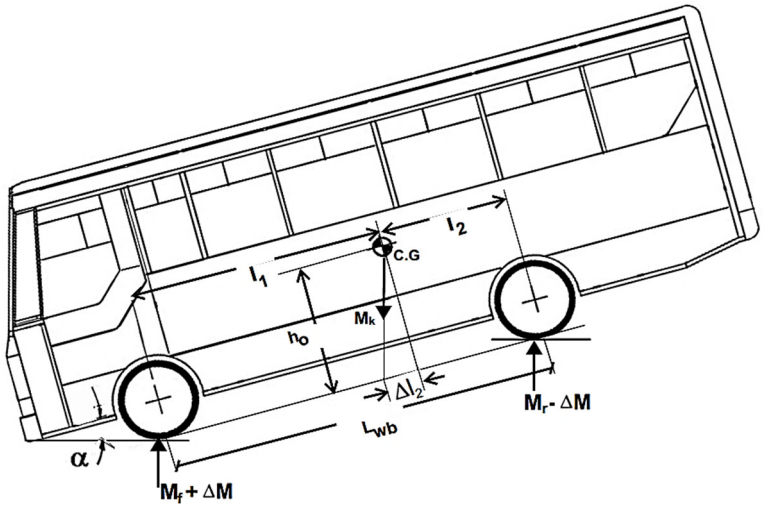

Figure 3.9: Determination of height of the center of gravity

Rearranging the above equation,

$$\Delta l_2 = \frac{(M_r + \Delta M) \times L_{wb}}{M_k} - l_2 \qquad 3.30$$

From the longitudinal position of the vehicle, by taking the summation moment at the rear wheels of an axle;

$$l_2 = \frac{M_r}{M_k} \times L_{wb} \qquad 3.31$$

Substituting eq. (3.4) into Eq. (3.3)

$$\Delta l_2 = \frac{\Delta M}{M_k} \times L_{wb} \qquad 3.32$$

The relationship between the height of the center of gravity (h_o) & angle inclination of the tilting vehicle (α) is defined by

$$tan\,\alpha = \frac{\Delta l_2}{h_o} \qquad 3.33$$

Thus, the height of the center of gravity (h_o) is given by

$$h_o = \frac{\Delta M \times L_{wb}}{M_k \times tan\alpha} \tag{3.34}$$

The vehicle's significant masses are taken from the local manual's mass distribution calculation and measured data (see Table A1.1). Besides, using geometrical modeling (Graphical Method), the vehicle is tilted at an angle of 35° to touch the vehicle's frontal nose, as shown in Figure 3.9. the results of the center of gravity of the vehicle are determined and described using the Eqs. 3.28, 3.29, and 3.34, as shown in Table 3.1.

Table 3.1: Summary of the center of gravity (CG) of the original bus

Constraints of Center of Gravity	
longitudinal distance (l_1), mm	2792
transverse distance (t), mm	48
height of the center of gravity (h_o), mm	1501

The inclination angle (α) for the vehicle should be greater than 20° to obtain the most accurate result in calculating the center of gravity[35]. Accordingly, the CG height (h_o) value depends on the vehicle's angle inclination, as shown in Figure 3.10.

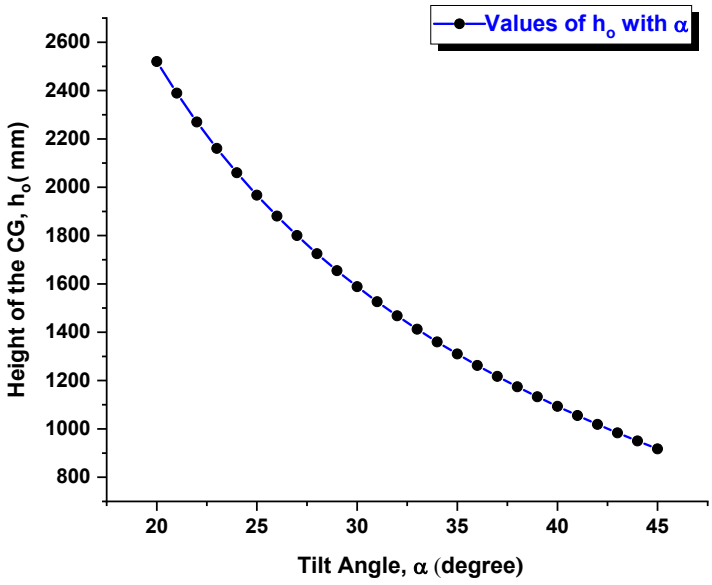

Figure 3.10: Illustrates the values of height of CG and the angle of inclination of the bus

3.2.4 Static Stability Factor (SSF) and Critical Angle (θ)

For vehicle rollover stability prevention, static matrices such as static stability factor (SSF), side pull ratio(SPR), and tilt table ratio (TTR) are the alternative approaches [60]. In this section, the

roll index of an untripped vehicle rollover, such as the static stability, is described to check the vehicle rollover stability, shown in Figure 3.11. A static stability factor is given by

$$SSF = \frac{L_f}{2H_o} \qquad 3.34$$

Where: H_o - Height of the center of gravity of the vehicle, and

L_f - Track Width (the distance between the right & left tires centers along the axle).

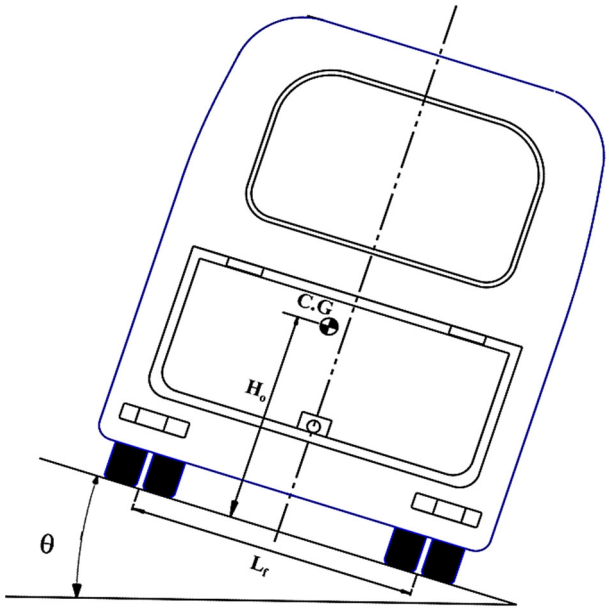

Figure 3.11: Illustrations of a static stability factor during untripped rollover

And the angle of tilt of the vehicle before rollover or critical angle (θ) is specified by

$$\theta = \tan^{-1}\left(\frac{L_f}{2H_o}\right) \qquad 3.35$$

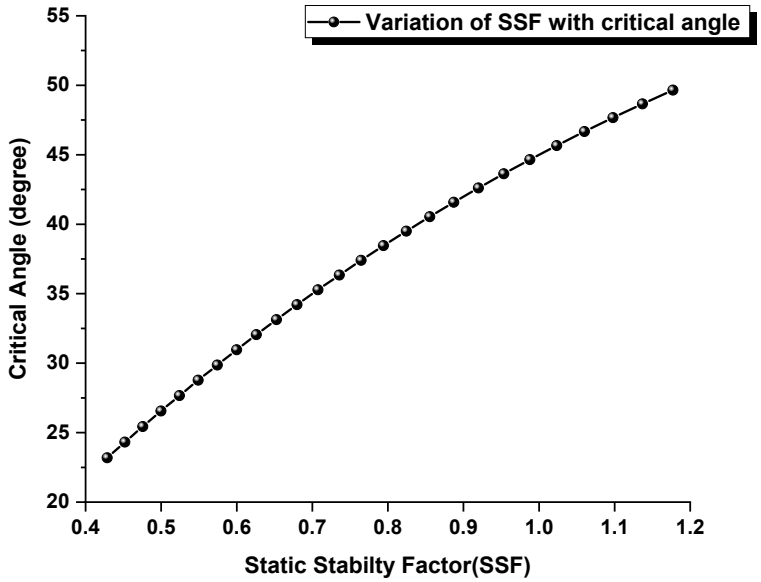

Figure 3.12: A variation of static stability factor (SSF) with a critical angle

Accordingly, (Jin et al., 2019) [65] stated that the variation of the critical title angle of the vehicle body is varied with SSF & the tire(road) friction that means the more significant the SSF value gives, the larger the tilt angle and this leads to the more negligible rollover effect and vice versa. Therefore, as predictable, the bus's tilt angle is varied with SSF, as shown in Figure 3.12.

3.2.5 The vertical distance of the center of gravity (Δh_{CG})

Figure 3.13 illustrates that the center of gravity (CG) of the bus does not change its location to the floor of the bus in rollover condition. However, in the case of a rollover crash, the rear ring section of the bus involves a vast amount of deformation. The values of the vertical distance of CG (Δh_{CG}) reduce during translation of the crashed wall. Thus, this value is compensated by a coefficient of the deformation ($\varsigma_{def} = 0.95$) [68]. The vertical distance of the center of gravity during rollover impact Δh_{CG} is calculated by

$$\Delta h_{CG} = \varsigma_{def} \Delta h_{CGo} \qquad 3.36$$

In this section, the vertical movement of the vehicle's CG in its starting, unstable equilibrium and at the moment when the residual space touches the ditch is defined as [68] (see Figure 3.13):

$$\Delta h_{CGo} = (H_{ref} - h_{CG_1}) + h_{CG_2} \qquad 3.37$$

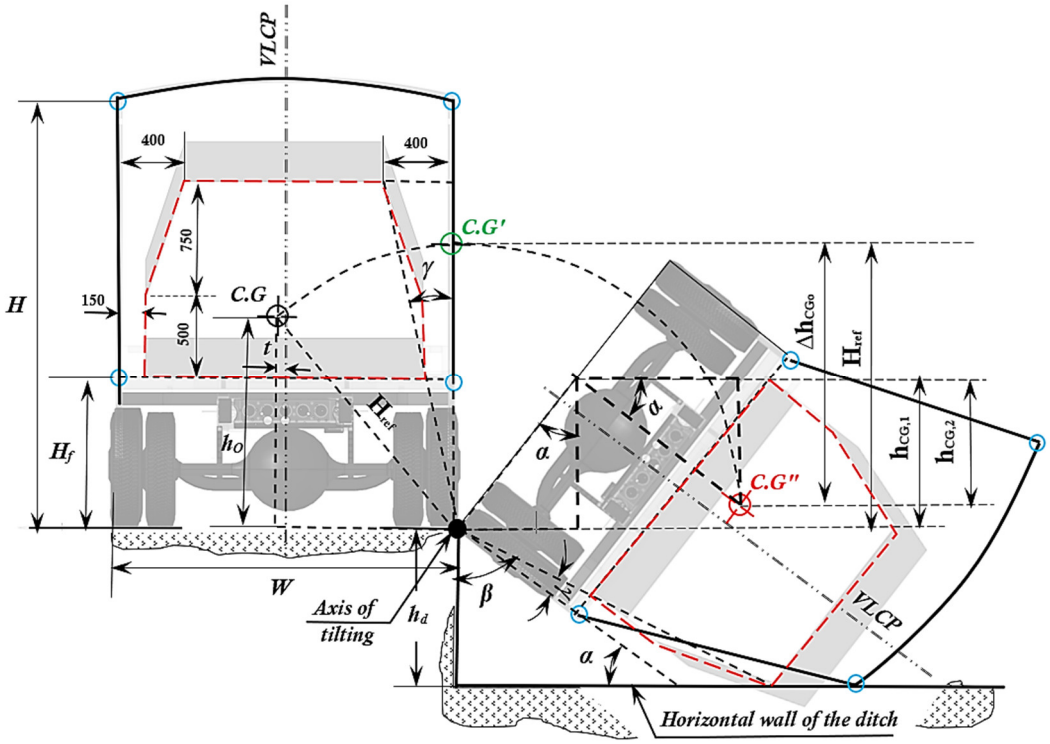

Figure 3.13: Locations of the vehicle CG in the rollover test

From the geometric relationships shown in Figure 3.13, the H_{ref}, h_{CG_1} & h_{CG_2} are

$$H_{ref} = \sqrt{\left(\frac{W}{2} + t\right)^2 + h_o{}^2} \quad 3.38$$

$$h_{CG,1} = \left(\frac{W}{2} + t\right).\cos(\alpha) \quad 3.39$$

$$h_{CG,2} = h_o.\sin(\alpha) \quad 3.40$$

$$\alpha = 90° - \beta + \gamma \quad 3.41$$

$$\beta = \cos^{-1}\left(\frac{h_d}{\sqrt{(H_f + 1250)^2 + (400)^2}}\right) \quad 3.42$$

$$\gamma = \tan^{-1}\left(\frac{400}{(H_f + 1250)}\right) \quad 3.43$$

Where:

W - the total width of the bus

H_f - the height among floor and occupant compartment

h_d - the depth between the horizontal plane of the ditch and tilting platform plane (800 mm)

h_o - the height of the center of gravity and

t - transverse distance of the center of gravity

3.3 Developments of FE Models for bus structure

The FE Model development consists of static strength analysis, quasi-static, and rollover crash analyses of the midi-bus structure. In static analysis, ANSYS software is preferable for implicit analysis than LS-DYNA to obtain a stable analysis for a high time increment. LS-DYNA is the best and most efficient for the explicit dynamic analysis because of uses a return mapping algorithm and the central difference method to avoid expensive numerical iteration and matrix inversion[69]. This study presents the analysis of the static structure strength during four loading conditions using ANSYS R19.2. Furthermore, the rollover crash FE analysis with the quasi-static FE analysis is developed using the explicit code of LS-DYNA R11.0 as stated by the standard of UNECE R66.

3.3.1 Components of midi-bus structure

The original local midi-bus structure has six parts: front, roof, rear, floor, left, and right frame, as shown in Figure 3.14. In this research, all geometrical bus sections are obtained by directly measuring the bus section's construction from local bus body-builders. Mainly, the body-builders used ISUZU trucks to build a midi-bus using diverse methods. First, the midi-bus structure is

constructed into six central components and then welded with chassis together. Next, the other way is welding every part of the structure from the chassis step by step.

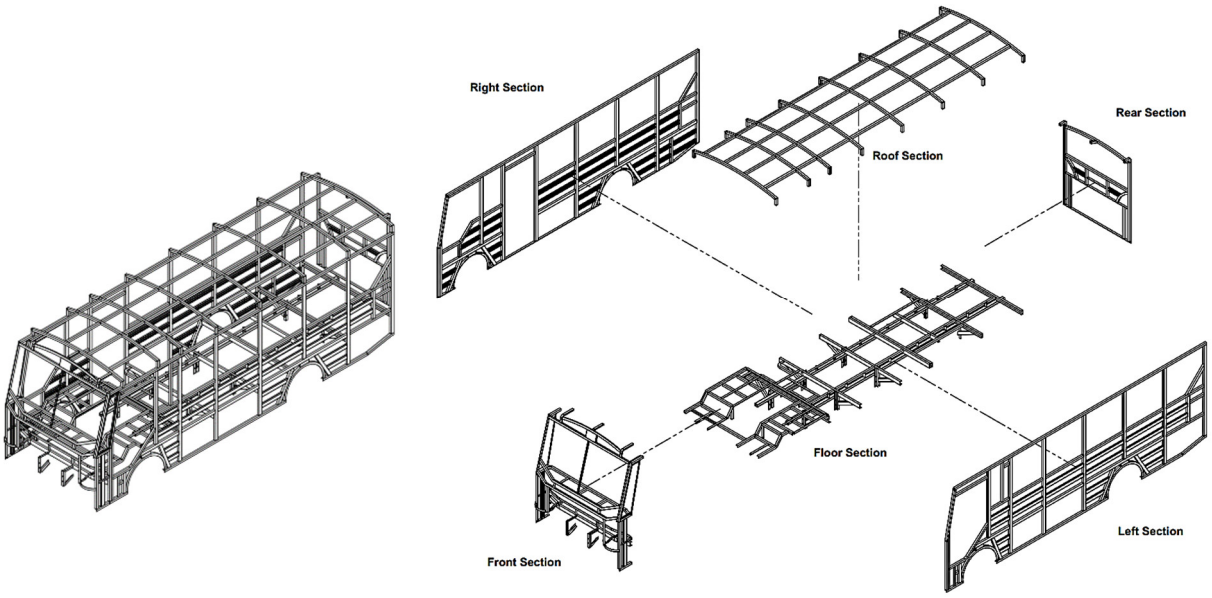

Figure 3.14: Main parts of the original midi-bus structure

3.3.1.1 General specification of the midi-bus

According to the local manufacturer & legislator body, the mass of the unladen kerb (M_k) & Gross Vehicle Weight (GVW) of the midi-buses having 28+1 passenger capacity measured 4400 $-$4700 kg and 7200$-$7400 kg, respectively. In table 3.2 describes the overall specification of the selected midi-bus model (ISUZU NPR 71K chassis).

Table 3.2: General specification of the midi-bus (NPR 71K chassis)

Overall Dimension			***Unladen Kerb Mass*** (M_k), *kg*	***Gross Vehicle Weight*** *(GVW), kg*
Length (l), *mm*	***Width*** (w), *mm*	***Height*** (h), *mm*		
7250	*2880*	*2580*	*4500*	*7350*

3.3.1.2 Cross-section of the frames

The frames of the structure are constructed and manufactured using the available materials, shapes, and cross-sections. Moreover, cross-sections of the midi-bus structure such as Rectangular Hollow Section (RHS), Square Hollow Section (SHS), L-Shape (Angle Steel), and U-shaped have clearly stated in Figure 3.15.

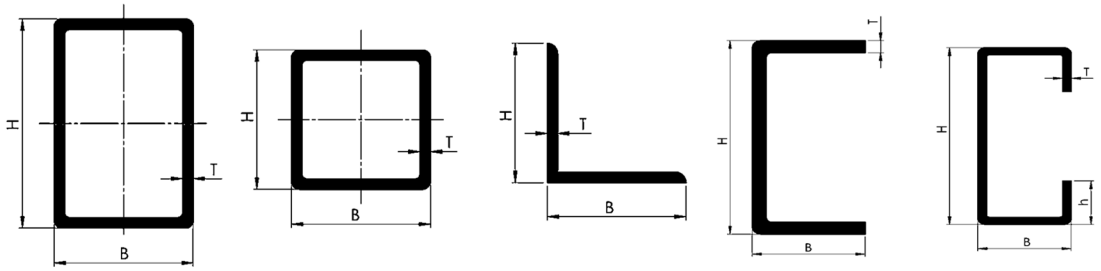

Figure 3.15: Geometrical configurations of cross-sections

As depicted in Table 3.3, the dimension (height(H), width(B), and thickness(T)) of cross-sections according to the cross-section type are mentioned.

Table 3.3: Sizes and types of cross-sections

***Types of* cross-sections with dimension**				
RHS Tubes (HxBxT) mm	**SHS Tubes** (HxBxT) mm	**L-Angle** (HxBxT) mm	**C-Shaped** (HxBxT) mm	**U-shaped** (HxBxTxh) mm
60x40x1.5	40x40x1.5	40x40x1.5	70x40x5	70x40x1.5x16.5
60x50x3	40x40x3	-	-	-

As discussed earlier, the two separate parts of the bus, such as the chassis and bus body section, are manufactured by ISUZU chassis manufacturers and local bus body-builders. Thus, all geometrical details of the midi-bus structure are developed by the specifications of the local body manufacturer and the ISUZU chassis specification manual using Solidworks. Some of the bus's structural components such as cant-rail, window rail, waist rail, Pillar A and B, vertical pillars, and skirt rail are described, shown in Figure 3.16. Moreover, the eight bays(B1-B8) of the structures are arranged.

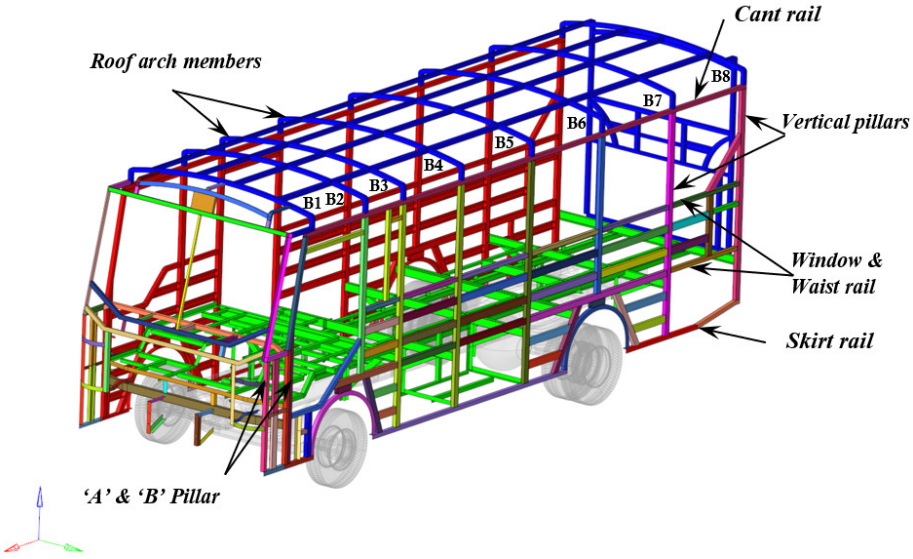

Figure 3.16: Components of original bus body structure

3.3.2 Material Properties of bus structure

As mentioned earlier, the midi-bus superstructure parts are constructed by the local bodybuilders. Consequently, most local bus bodybuilders are used imported and locally available steel for a bus's superstructure. However, the material properties of the structural steel were taken from the Akaki Kality Metal Industry (local metal manufacturer) for this research. Moreover, the material properties obtained from the tested tensile outcome are mentioned, as shown in Table 3.4.

Table 3.4: Material property of conventional structural (CS) steel

Property	***CS Steel***
Density ρ (kg / mm³)	*7850*
Yield Strength σ_y (MPa)	*260*
Ultimate Tensile Strength σ_{ut} (MPa)	*360*
Elongation (%)	*30*
Young's Modulus E (GPa)	*210*
Poisson's Ratio v	*0.3*

Figure 3.17 describes the effective stress & plastic strain curve of the bus structure steel drawn from the tested research output (engineering stress & strain).

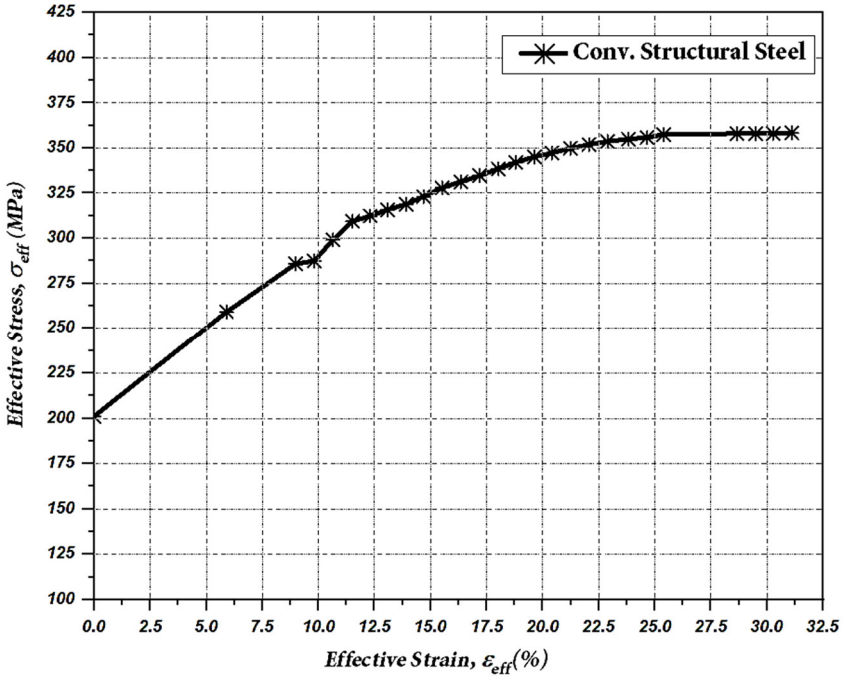

Figure 3.17: Effective stress vs. plastic strain curve for conventional structural steel

The material input data of the FE Simulation (ANSYS & LS-DYNA) needs the effective stress versus the effective plastic strain curve. The true stress σ_t and the true plastic strain, ε_t determined by:

$$\sigma_t = \sigma_{eng}(1+\varepsilon_{eng}) \quad 3.44$$

$$\varepsilon_t = ln[1+\varepsilon_{eng}] \quad 3.45$$

Where: σ_{eng} - the engineering stress and ε_{eng} - the engineering strain

3.3.3 Static Structural Strength Analysis of the structure

3.3.3.1 Procedures for static structural analysis

In this section, the static structural analysis includes the bending, torsional, steering (cornering), and breaking strength via FE Methods (ANSYS Software). Accordingly, the four load conditions are full pure bending, full pure torsion, longitudinal bending, and lateral load. Figure 3.18 presents the FE procedure to analyze the structure of a midi-bus using ANSYS 19.2. The bus structure's CAD model is developed in the Initial Graphics Exchange Specification (IGES) format as a surface and imported to ANSYS 19.2 Software.

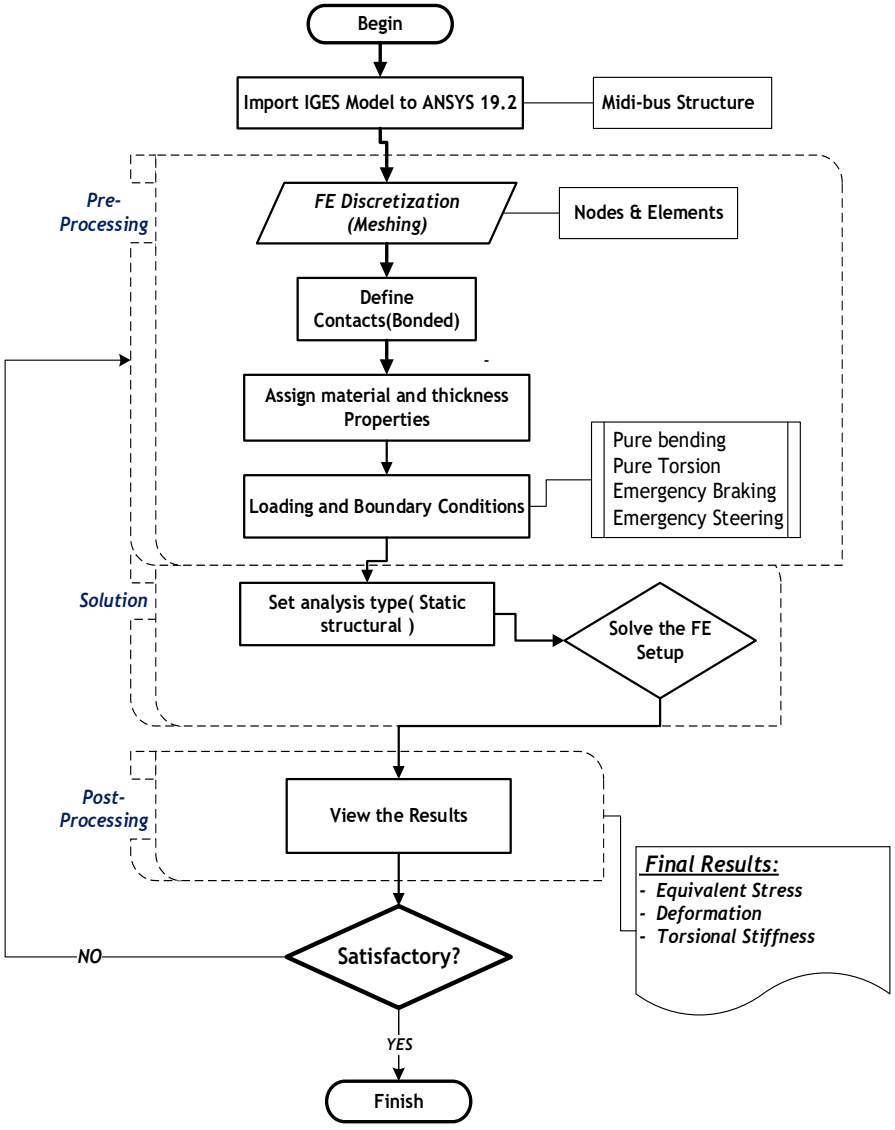

Figure 3.18: FE Procedure for static structural Analysis via ANSYS 19.2

The FE model of bus sections is constructed as a shell (shell_180) with mixed mesh (quadrilateral and triangular element), as shown in Figure 3.19. However, the body sections' maximum and minimum element sizes are 10 mm & 2.5 mm due to the small and large frame size.

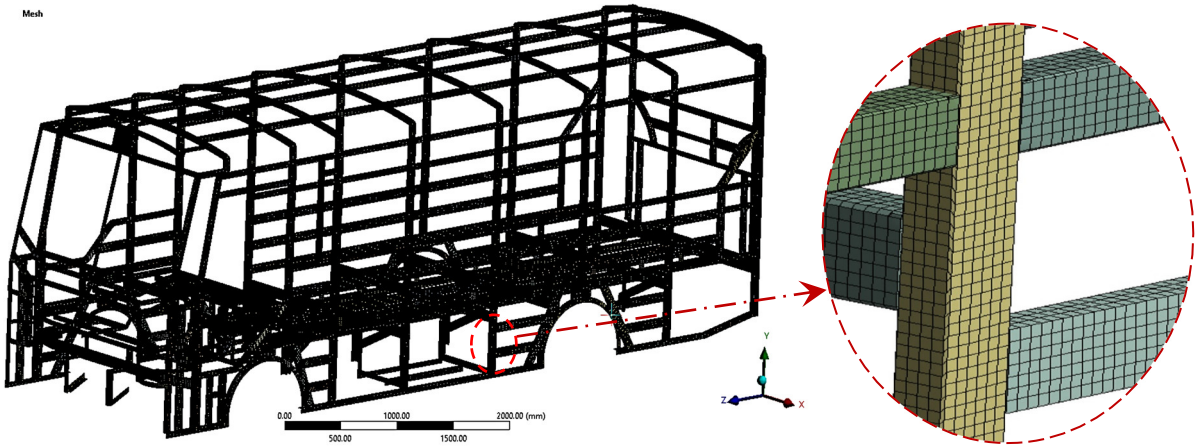

Figure 3.19: FE discretization of the structure

Table 3.5 describes the FE Model of the bus body section containing 553,040 elements and 572,578 nodes with 355 parts. Furthermore, the connection between frames (structural components) is considered as a bonded contact.

Table 3.5: Statistics of the original FE Model for static analysis

Description	**Bus structure**
Element type	*Shell_180*
Min. Element Size(mm)	2.5
Max. Element Size(mm)	10
Numbers of Parts	355
Number of Nodes	572,578
Number of Elements	553,040

3.3.3.2 Statical loading and boundary conditions

As discussed earlier, several types of loading are applied to the bus structure. First, the average values of the masses floor & roof luggage and chairs are taken per the local manufacturer standard (see Table 3.6). Then, the distributed masses of side & roof luggage, driver, passengers, and seats are loaded on the structural parts. This study takes the driver and passenger mass of 75 kg as stated by UNECE R66 and local manufacturer standards.

Table 3.6: Sum of masses applied on the bus structure

Categories	***Qty.***	***Total Mass(kg)***
Passengers with Driver (each 75 kg)	29+1	2250
Seat (each 8.5 kg)	29+1	255
Floor (side+ rear) luggage	-	200
Roof luggage	-	350

3.3.3.2.1 Pure Bending condition

In this loading case, The distributed masses of floor & roof luggage, driver, passengers, and seats are distributed on the structural parts with gravitational force [16], [17]. According to the original midi-bus structure model, the realistic boundary conditions are applied between the chassis (chassis axles and frames) and structural frames, as shown in Figure 3.20. The bending stiffness of the structure is the ratio of applied load and vertical deformation on a pure bending case[17]. The equation of bending stiffness (K_b) can be calculated by

$$K_b = \frac{W_b}{\delta y} \qquad 3.46$$

Where: W_b – the applied load in the pure bending, (N) and δy - linear deformation, (mm)

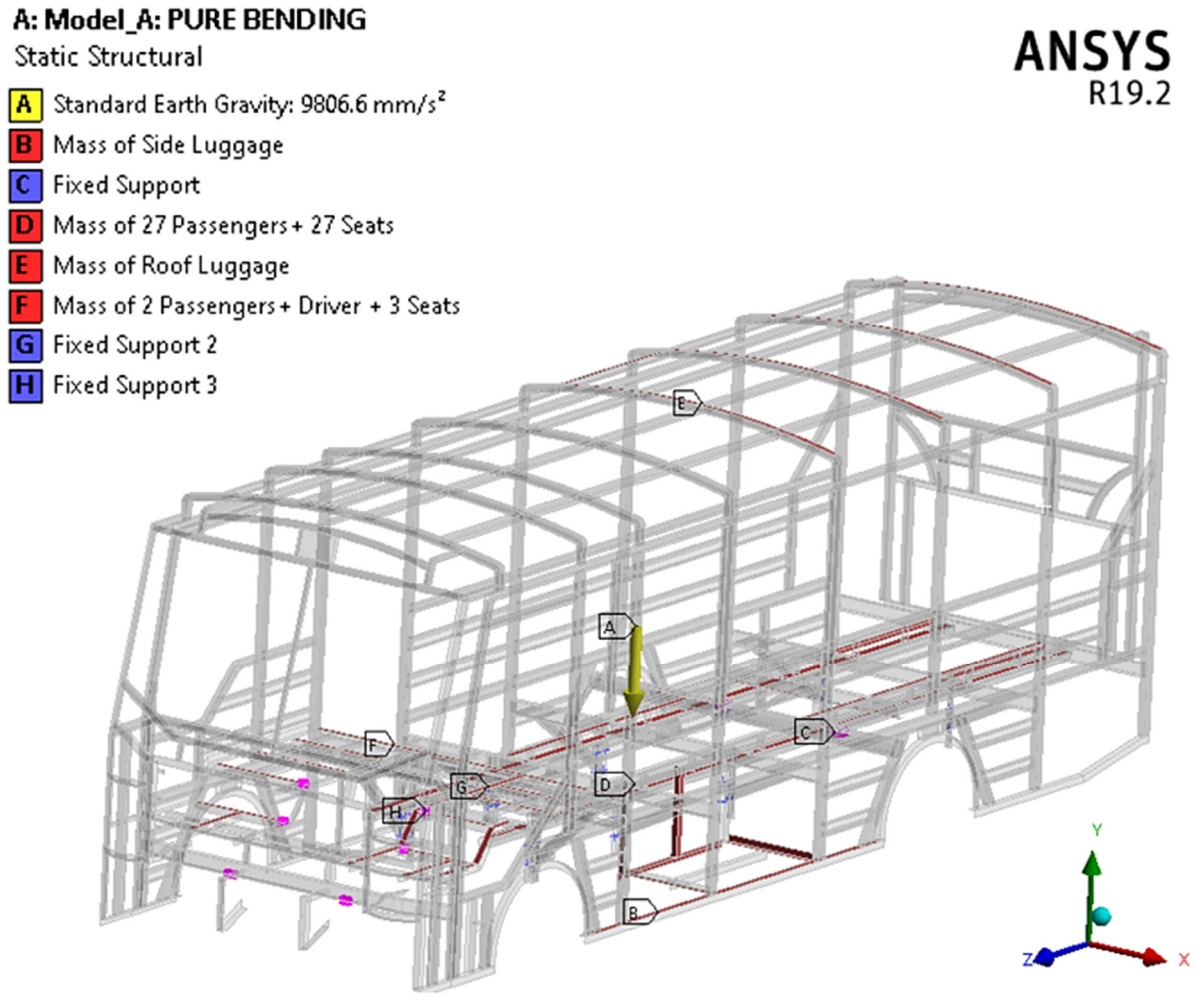

Figure 3.20: Pure bending load applied to the original midi-bus structure

This case's fixed constraints are significantly located at the rear axle & front c-channel(support C), the engine side support(support H), and L-angle steels with a hole(support G), shown in Figure 3.21.

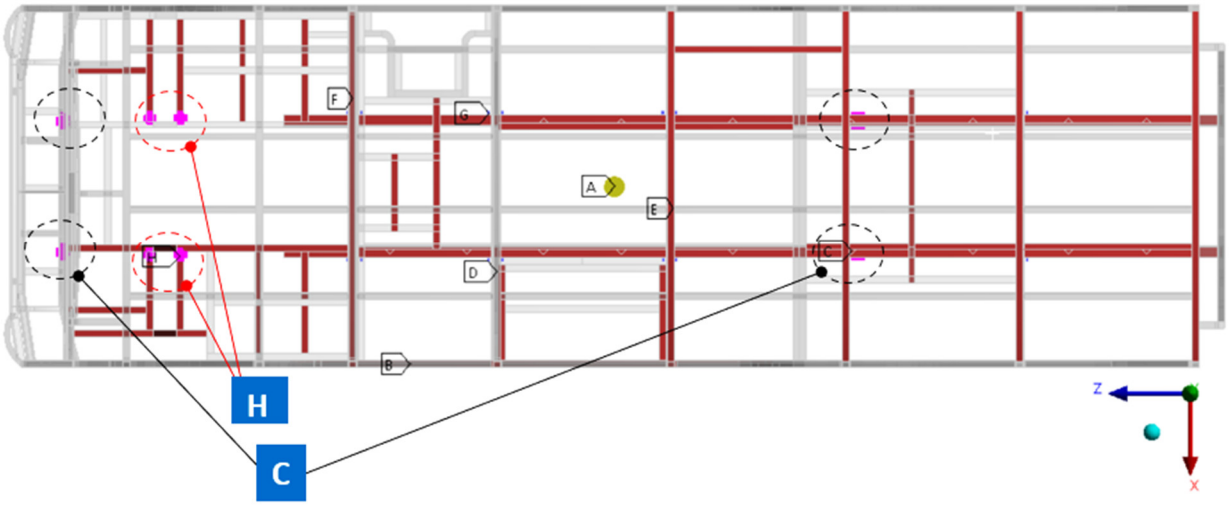

a)

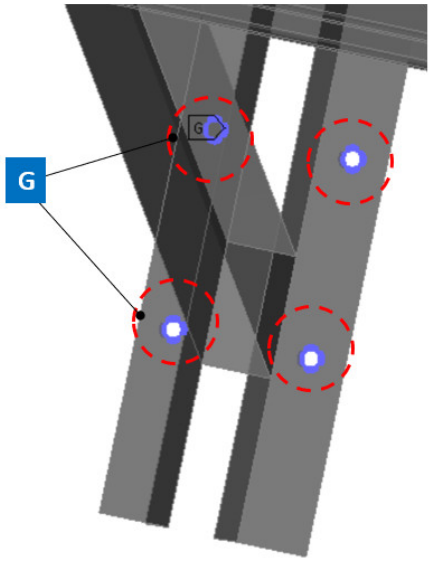

b)

Figure 3.21: Fixed constraints(boundary) through pure bending case: a) support C & H and b) support G

Table 3.7 describes the locations of the boundary conditions during the pure bending loading case.

Table 3.7: Description of the fixed boundary positions

connection among	***Location***
chassis and rear axle(two-side) & frontal C-Channel	At C
chassis and frames on the engine positions	At G
chassis and holed L-Angle plate (bolt connection)	At H

3.3.3.2.2 Pure torsion loading condition

In this study, the distributed masses are the same as the pure bending case, and torsional loads act on the structural parts with gravitational force [16], [19], [70]. However, the torsional loads are obtained from the total reaction forces (5,309.2 N) of the bending case's four-axle points. The torsional loads are applied for each frontal c-channel connected with nodes (Nodal forces G & H) as a value of 1,327.3 N, as shown in Figure 3.22.

The boundary conditions are applied at the rear axle (fixed support F), engine frames connected to chassis (fixed support J), and the l-shaped parts bolted with chassis (fixed support I). The moment(couple) acted on the hinges defines as the applied force multiplied by the perpendicular distance from the center of the lateral axis of the structure.

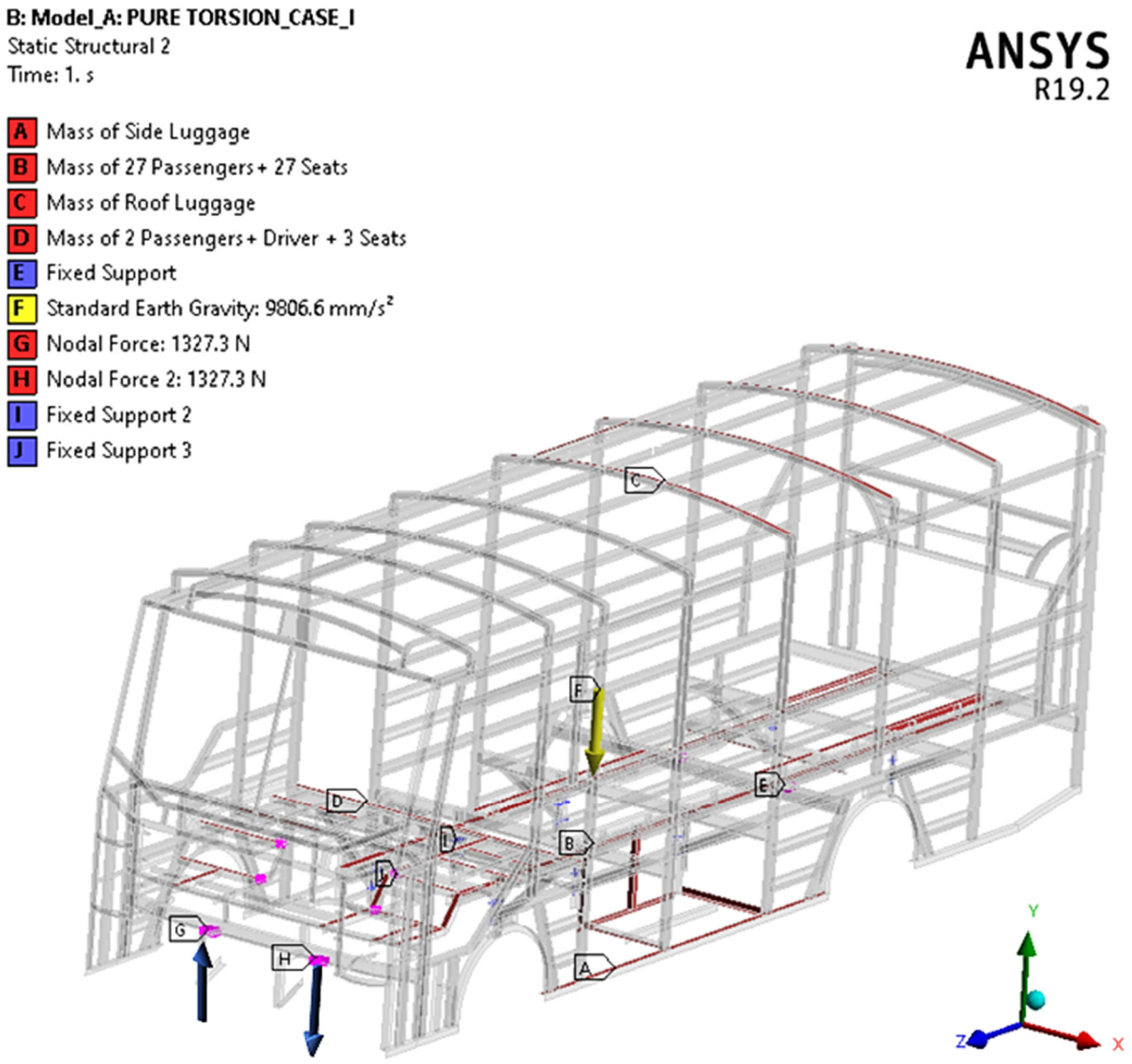

Figure 3.22: Pure torsion load applied to the original midi-bus structure

The moment acts in the two sides of the front (axle) steering system as a couple. Therefore, the total moment(torque), T_m becomes:

$$T_m = \text{Applied Force x L} \quad 3.47$$

The torsional stiffness or rigidity of the structure (K_t) is calculated by:

$$K_t = \frac{T_m}{\theta} \quad 3.48$$

$$\theta = \tan^{-1}\left(\frac{\delta y}{(L_a / 2)}\right) \quad 3.49$$

Where:

θ - the angle of rotation, degree

$L_a\,(L)$ - the distance between the two sides of frontal wheel supports (see Figure 3.23), mm

δy - the linear deformation, mm

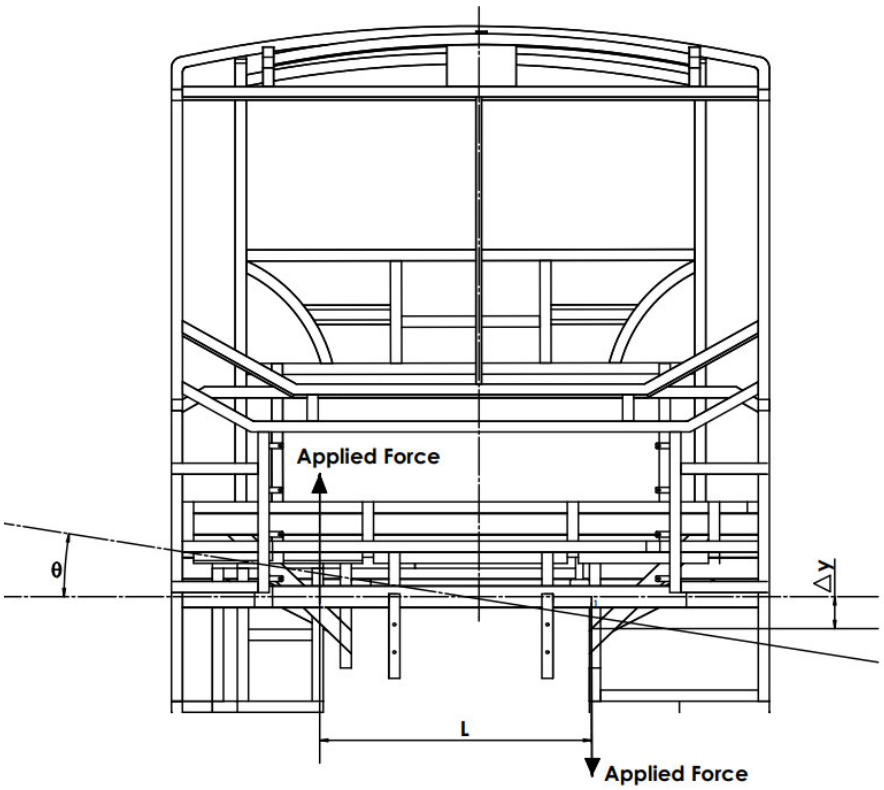

Figure 3.23: Torsional force applied to the midi-bus structure

3.3.3.2.3 Longitudinal (Breaking) loading condition

The loadings case for this case is the same as the bending condition. However, a 0.7g (6,864.6 mm/s^2) deceleration to the bus in the longitudinal direction is considered[16], [17], [41] (see Figure 3.24). Moreover, the constraints are similar to the bending condition.

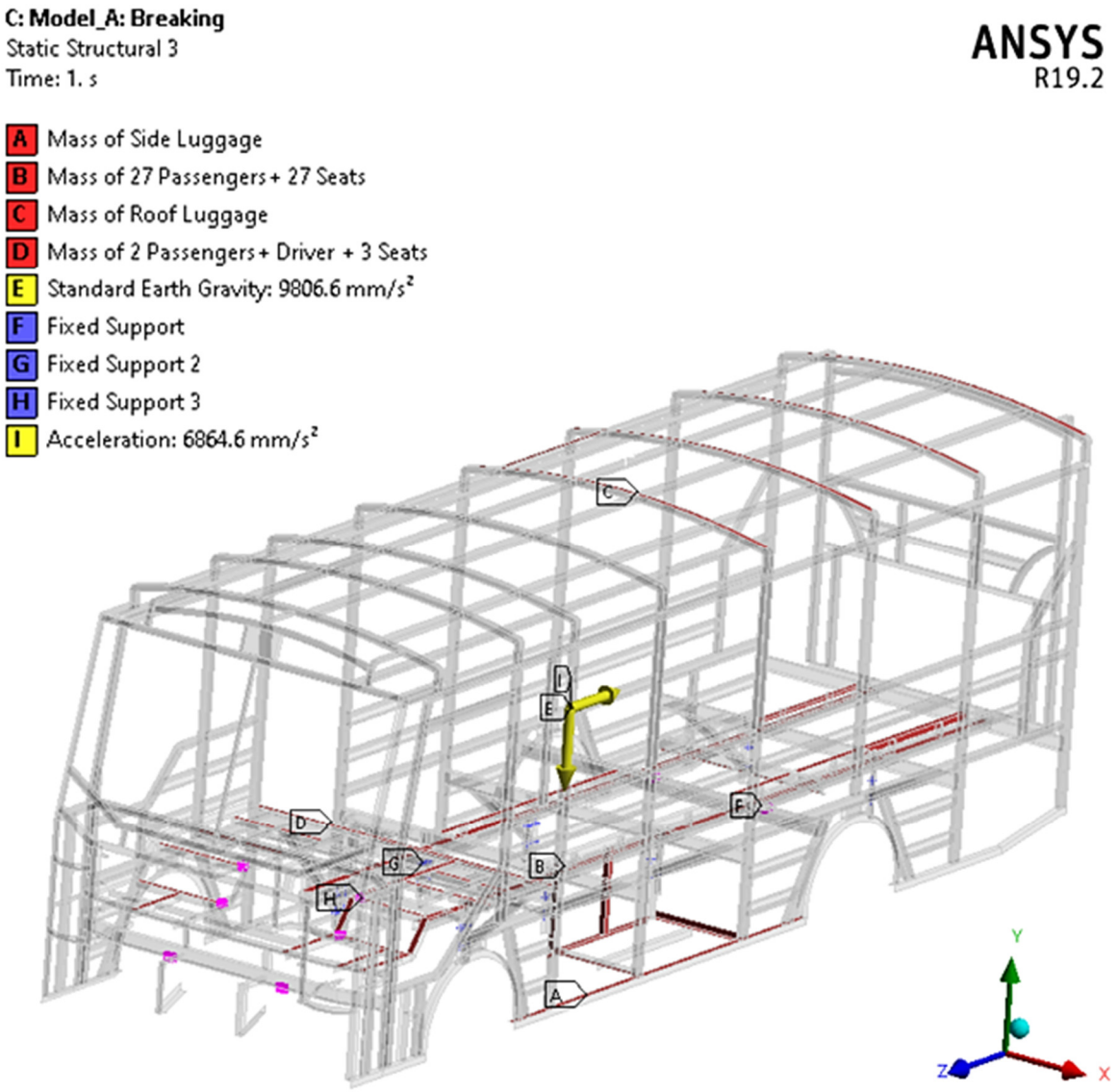

Figure 3.24: Longitudinal load applied to the original midi-bus structure

3.3.3.2.4 Lateral bending (cornering) loading condition

The loadings & constraints situations are the same as the bending condition. However, a lateral acceleration 0.4g(3,922.6 mm/s^2) is applied to the bus structure[17](see Figure 3.25).

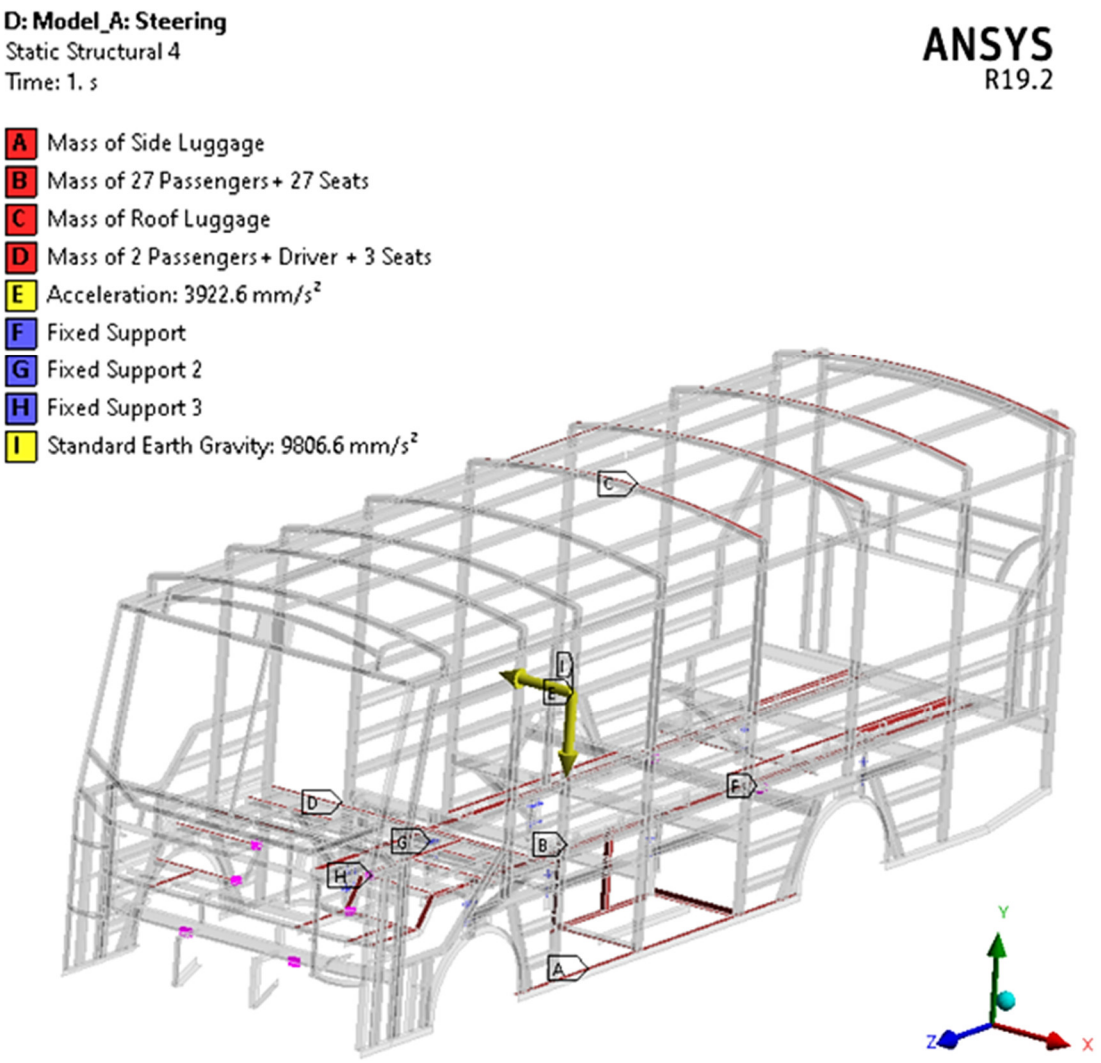

Figure 3.25: Lateral bending load applied to the original midi-bus structure

3.3.4 Quasi-static Analysis of the structure

3.3.4.1 Procedures for Quasi-static analysis of bus body structure

The quasi-static simulation uses to check whether the bus sections and their bays withstand the rollover crash or not[35], [68]. Hence, the body sections and their bays evaluate whether they failed or passed the quasi-static loading test. This paper develops the bus superstructure model as a shell element for fast and high computational simulation. The selected Belytschko-Lin-Tsay shell element is defaulted to calculate the shell element formulation in LS-DYNA R11.0. Moreover, this shell element has high computational efficiency [67], [68]. The simulation procedures have been done according to UNECE R66 using LS-DYNA Software to study and analyze the bus structure energy absorbing and load-deformation behavior, as shown in Figure 3.26.

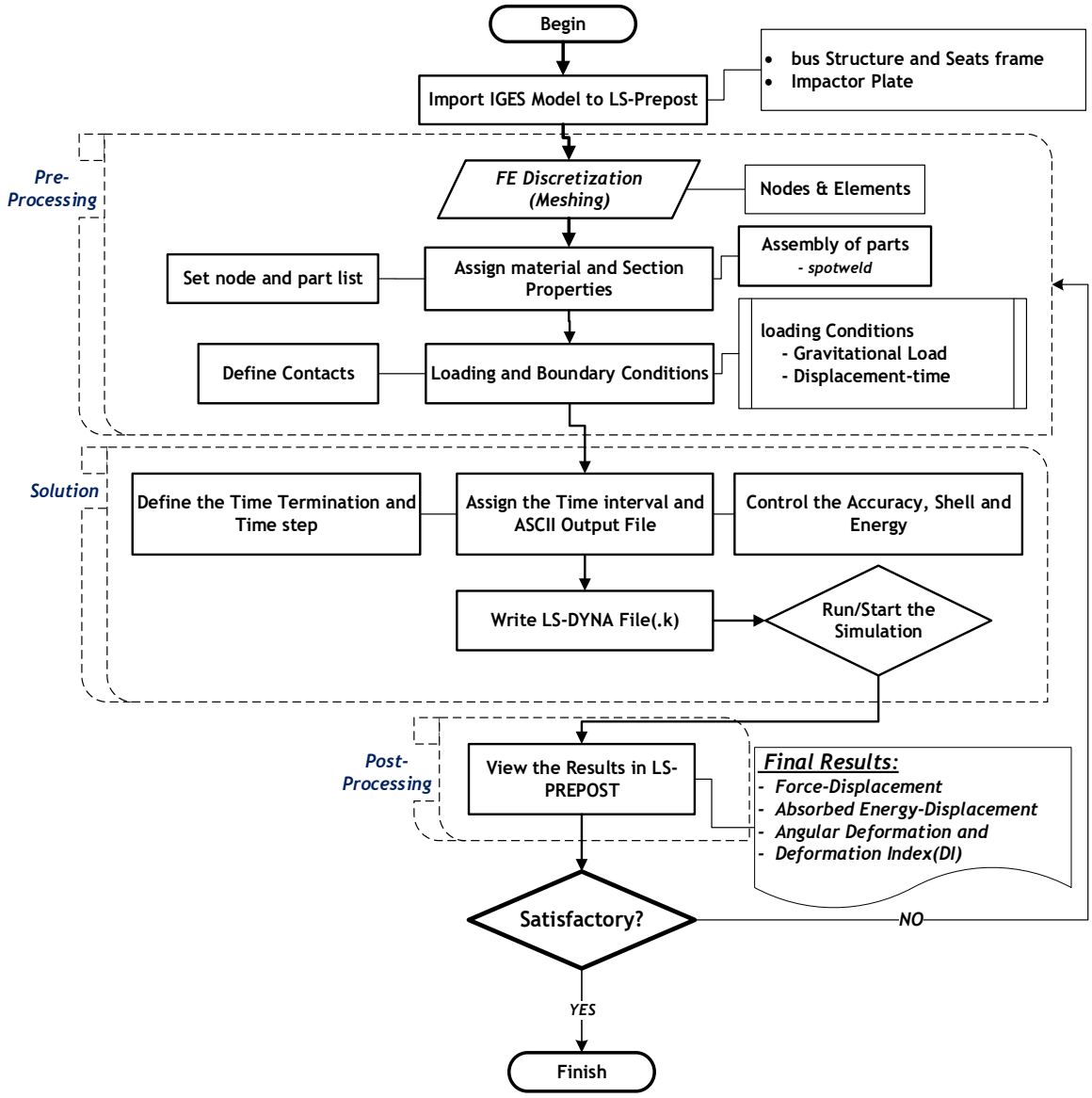

Figure 3.26: LS-DYNA Process for quasi-static simulation

In this section, the bus structure element size is constructed the same as the static analysis case. In addition, however, the residual space and rigid plate(impactor) model are developed for the quasi-static simulation. The entire quasi-static FE Model consisted of 885,722 shell elements with 885,722 nodes with an average element size of 15 mm (see Figure 3.27). Thus, the weld formulation between all frame parts is modeled as spot welds (rigid nodes) through the 'CONSTRAINED_SPOTWELD' card without defining the failure forces and coefficients [26]–[28], [68], [71], [72].

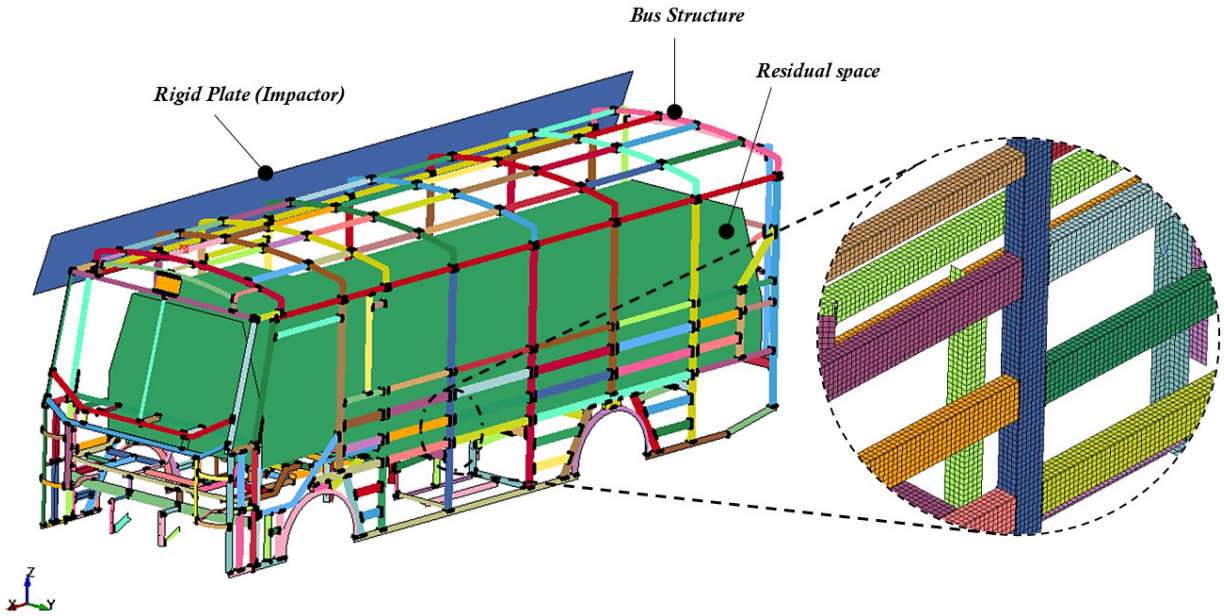

Figure 3.27: FE Model for quasi-static simulation

Table 3.8: Statistics of the original FE Model for the quasi-static Analysis

Description	***Bus structure***	***Residual Space & Impactor***	***Entire Model***
Material type	Pieces-wise Linear Plasticity (MAT_24)	Rigid (MAT_20) & Null (MAT_09)	-
Min. Element Size(mm)	2.5	-	2.5
Max. Element Size(mm)	10	15	15
Number of Parts	355	2	357
Number of Nodes	572,578	333,345	905,923
Number of Elements	553,040	332,682	885,722

The material used for all parts of bus sections (frame) is conventional structural steel. Experimental material properties of structural steel were executed into the FE models formulation. The PIECEWISE_LINEAR_PLASTICITY (MAT_24) material definition was implemented[68]. A rigid plate (the impactor) is developed by the material model of Rigid (MAT_20). A null (MAT_09) material is used to represent occupant space (see Table 3.8).

3.3.4.1.1 Loading and Boundary conditions

During the simulation, the rigid rectangular plate (impactor) touches the roof frames at an angle between the vehicle's longitudinal vertical center plane (VLCP) and the load direction[35]. A quasi-static load is distributed on the cant rail section with a rectangular plate(impactor). Thus, the quasi-static loading rate is applied quasi-equally for the 500 mm displacement with a short incremental time of 2.25 sec. However, the computational time of the simulation takes 1.75 sec to

reach the passenger compartment. The external load card 'LOAD_BODY_Z' is applied as the gravity of the bus structure.

The fixed supports are causing no effect on the structure's deformation. These supports are applied to the underfloor structure section (see Figure 3.28(right)). The angle between the load direction & the vehicle's longitudinal vertical center plane (VLCP), (α) is determined by

$$\alpha = \frac{\pi}{2} - \sin^{-1}\left(\frac{800}{H_c}\right) \qquad 3.50$$

Where: H_c - height of the vehicle's cant rail (in mm) from the horizontal plane (see Figure 3.28(left)

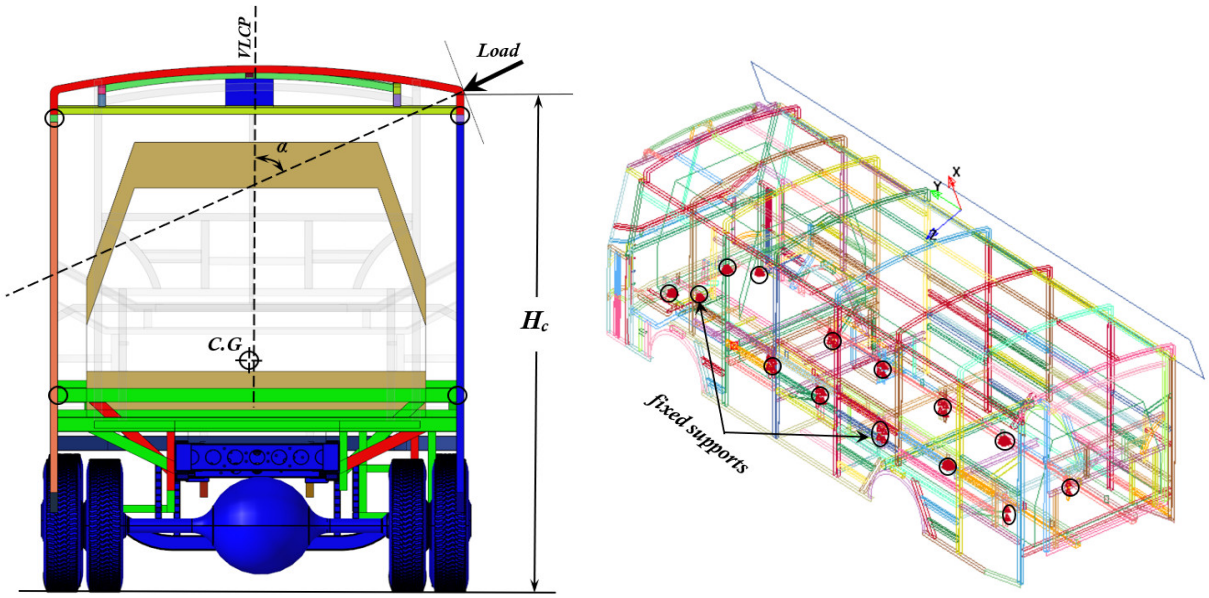

Figure 3.28: loading direction (left) and fixed supports(right) in the quasi-static simulation

3.3.4.1.2 Definition of contacts

The penalty-based contacts are contacts algorithms used in crash simulation[26]. The contact algorithm of 'AUTOMATIC_SINGLE_SURFACE' is appropriate for self-contacting cases. In this section, this contact type was used to state the contact between all bus section components. The contact 'AUTOMATIC_SURFACE_TO_SURFACE' is defined for the contact relationship between the bus section and a rigid plate(impactor). The static and dynamic friction coefficient for steel-to-steel contact is a value of 0.15 and default, respectively[73].

3.3.4.2 Evaluation criteria for quasi-static simulation result

According to the ECE R66 standard, the minimum energy absorbed by the structure (body sections) (E_{min}) is quals to the sum of the energy of the i^{th} bay and calculated by:

$$E_{min} = \sum_{i}^{s} E_i = E_T \frac{\sum_{i}^{s} m_i}{M} \quad 3.51$$

Then, the total absorbed Energy (E_T) by the vehicle is calculated by:

$$E_T = 0.75\, M\, g\, \Delta h \quad 3.52$$

Where:

$M(M_k)$ - the unladen kerb mass of the vehicle

g - the gravitational constant (9.81 m^2/s)

Δh - the vertical distance of the vehicle center of gravity in rollover test (equation 3.36)

E_i - the energy absorbed by the "i^{th}" bay and

m_i - the mass of the "i^{th}" bay

By substituting Eq. 3.51 into Eq. 3.52, the minimum energy absorbed by the structure (E_{min}) is determined by:

$$E_{min} = 0.75\, g\, \Delta h \sum_{i}^{s} m_i \quad 3.53$$

In the quasi-static loading test, the energy absorbed by the structure ($E_{st,a}$) passes, if:

$$E_{st,a} \geq E_{min} \quad 3.54$$

Otherwise, the structure fails the tests, even if only one of the bays is touched the residual space. Moreover, Energy absorption (E_{st}) and reaction force are indicators of the crashworthiness capability of the structure. The Energy absorption (E_{st}) of the structure can be determined by integration of the load-displacement curve. Furthermore, it can be formulated by:

$$E_{st,a} = \int_0^l P\, d\delta \quad 3.55$$

Where: P – applied load (reaction force), l – length of the crushed structure, and δ - displacement

3.3.5 Rollover Crash Analysis of the midi-bus structure

3.3.5.1 FEA Procedures for Rollover Analysis

According to the UNECE R66 standard, the rollover test of a vehicle is used to evaluate the crashworthiness capability and occupant safety during rollover crashes. The rollover crashworthiness via finite element analysis (FEA) is extensively done due to the experimental test's long time and extreme cost [2]. In the bus rollover crash, passenger safety is affected by structure, seats, and seat belt strength[74]. In this study, the bus structure and seat frames are the main components of the bus to study the strength and crashworthiness behavior. As mentioned

later, the gross vehicle weight of the locally built midi-bus (NPR 71K Chassis midi-bus) is 7350 kg (7.35 tons). Table 3.9 illustrates the quantities and masses of components in the case of full-weight.

Table 3.9: Components of the gross weight(full-load) vehicle

Items	***Qty.***	***Total Mass(kg)***
Passengers with driver (each 75 kg)	29+1	2250
Seat (each 8.5 kg)	29+1	255
Self-weight of the structure	-	577.35
Roof and floor luggage	-	550
Chassis body with fuel tank, engine, and battery, wheel, axle (NPR 71K)	-	3620
	Gross vehicle weight (GVW)	7350

In Ethiopia, some buses are overloaded by carrying extreme passengers and roof luggage than the permissible passenger numbers and weight, respectively[7]. Consequently, the average mass of ten (10) passengers (standing on the floor & sitting on the adjusted seats) and 350 kg roof luggage are added to the selected vehicle type. This loading case is considered as the over-weight scenario (scenario – III) shown in Table 3.10. However, passengers' overloading with their luggage is a factor that causes severe damages and structural deformation in real rollover cases [75]. Therefore, in this section, the three loading cases (tare weight, full-load, and over-load) are considered to study the effect of mass on the strength of the bus structure (see Table 3.10).

Table 3.10: Summary of load cases and its weight used for rollover case

Scenario	***Load case***	***Weight(kg)***
I	*Tare weight (Unladen Kerb mass)*	4500
II	*Full-load (Gross vehicle weight)*	7350
III	*Over-load (Gross vehicle weight with over-weighted passenger and roof luggage)*	8450

The chassis components are modeled using the ISUZU N-series body builder manual and guide[76]–[78]. However, the structure and seat are developed by directly measuring and observing the bus construction from the available local manufacturers(body-builders). Then, the bus structure, chassis, seat frame, tilt platform, and other assembled components were imported to the LS-Prepost as an Initial Graphics Exchange Specification (IGES) file format to develop a finite element mesh.

The entire rollover model is developed as a Belytschko-Lin-Tsay shell element to decrease the computational time of the simulation. However, the thickness of the shell element is defined by its section properties and its values. Figure 3.29 presents the FE procedure of rollover crashworthiness simulation using LS-DYNA R11.0. Hence, the weld connection between all structural parts with seats frame and rail is modeled as spot welds (rigid nodes) using a card 'CONSTRAINED_SPOTWELD' without defining the failure forces and coefficients [26]–[28], [68], [71], [72]. The keyword 'CONSTRAINED_RIGID_BODIES' defines the assembly between the rigid parts of the chassis by assigning one of them as a master part and merging the others[79].

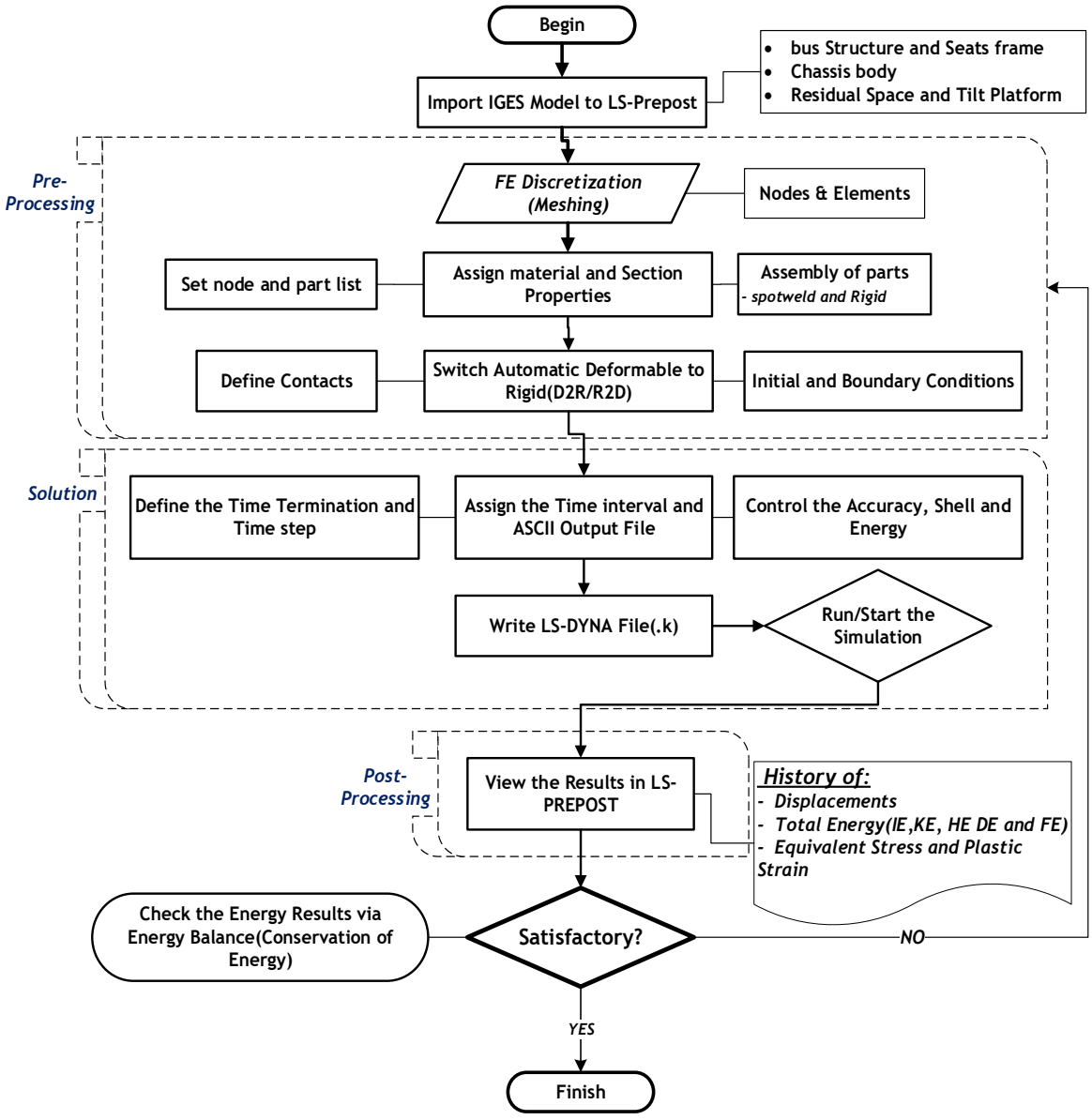

Figure 3.29: LS-DYNA Process for rollover simulation

The bus structure, chassis, seat frame, tilt table, ground (rigid platform), residual space, and element mass of other components of the vehicle model are considered for the full vehicle rollover simulation without bus skin and other deformable parts, as shown in Figure 3.30. However, in this

study, the bus skin, glasses, and other sensitive parts of the vehicle are not modeled due to the difficulty of modeling and simulation.

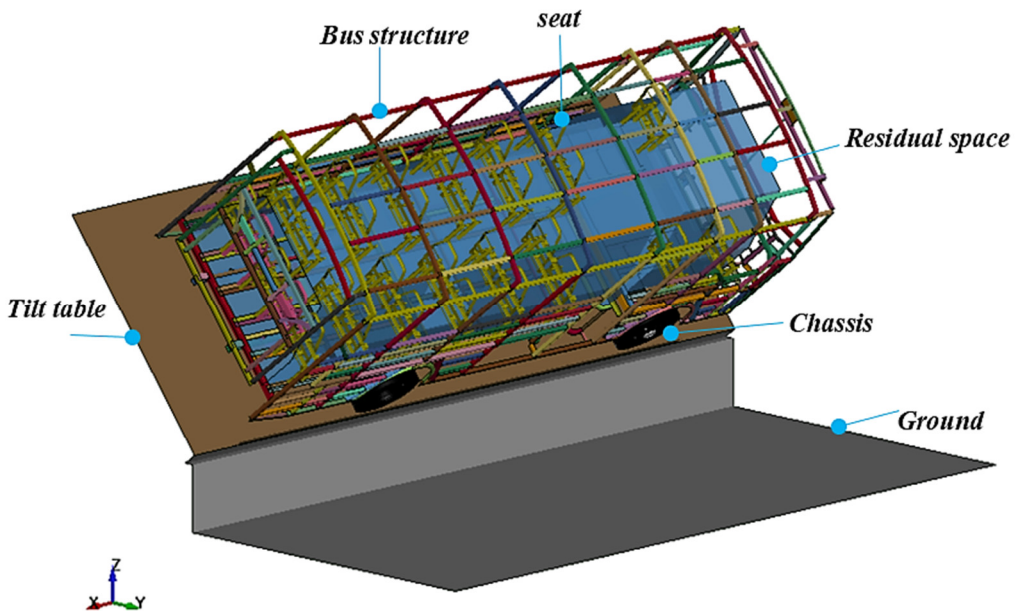

Figure 3.30: FE Model for rollover simulation

The entire rollover FE Model consisted of 1,771,305 shell elements with 1,790,729 nodes (see Table 3.11). the overall original tare weight FE Model contains 412 parts. Hourglass control type (type 4, 5) defines within ranges of coefficient between 0.03 to 0.05 for parts of the structure, which is used to reduce the response of non-physical stiffening [80]. The shell elements of FE models, such as fully integrated (type 16) and Belytschko-Tsay (type 2) elements, are the most accurate and high computational efficiency in crashworthiness simulation[28]. Thus, this study also conducts Belytschko-Tsay (default type) shell element and hourglass control type 4 with its coefficient of 0.05 for all FE models of rollover.

Table 3.11 mentions the mesh sizes according to the main components of the rollover FE model. The bus rollover mechanics' mass distribution of passengers and seats generates the additional inertia force and modified bending moment. It indicates that passengers and seat mass position may disturb the center of gravity (CG) and structural deformation of the bus[68]. In this section, the two cases that used to study the effects of seat frames in the rollover impact tests of bus structure are conducted:

- ***Case – a***: a tare-weight bus without seats and seat rail frames and mass elements representing the weight of seats attached to the floor,
- ***Case – b***: a tare-weight bus with seat frame and rail. Tare-weight bus with seat and seat rail frames and mass elements representing the weight of seats attached to the floor.

Table 3.11: Statistics of original tare weight FE model

Parameters	***Bus structure and seat frame***	***Tilt table, Residual Space & Ground***	***Chassis body***	***Entire Model***
Min. Element Size(mm)	2.5	-	-	2.5
Max. Element Size(mm)	10	15	30	30
Number of Parts	391	3	18	412
Number of Nodes	904,442	818,935	80,076	1,790,729
Number of Elements	885,012	805,934	88,718	1,771,305

Table 3.12 mentions the summary of mesh quality in the case of the tare-weight bus model. The numbers of quadrilateral and triangular elements are 1,757,153(99.2%) and 14,149(0.799%), respectively.

Table 3.12: Summary of shell element quality report for the tare-weight bus model

Criteria	***Allowable(threshold) value***
Min side length(mm)	3
Max side length(mm)	30
Aspect ratio	10
Warpage	10
Min quad. angle (deg)	45
Max quad. angle (deg)	135
Min tria. angle (deg)	30
Max tria. angle (deg)	120
Taper	0.7
Skew(deg)	45
Jacobian	0.6
#Quads (%): 1,757,153 (99.2%), *#Trias (%):* 14,149 (0.799%)	

The material model used for all structural frames and seat rail is executed by using PIECEWISE_LINEAR_PLASTICITY (MAT_24) material definition [4], [15], [68], [73]. In most rollover impacts, the chassis parts are in motion but not directly affected by the crashes[81]. Hence, the chassis, tilt table, and ground are developed by the material model of Rigid (MAT_20). A Null (MAT_09) material is used as a symbolic representation for occupant space (see Table 3.13)[82].

Table 3.13: Definition of material models for rollover simulation

Components	***Material Model***
Bus structure, seat frame, and seat-rail	Piecewise Linear Plasticity (MAT_24)
Chassis, tilt table, and ground	Rigid (MAT_20)
Residual Space	Null (MAT_09)

In the rollover simulation, 'ELEMENT_MASS_NODE_SET' is used to lump the mass of passengers, luggage, battery, and engine[28], [83], [84]. Figure 3.31 describes the mass element of the passengers assigned on the node of the seat frame. Moreover, the mass of luggage, battery, fuel tank, engine, and other miscellaneous parts are equally distributed on the chassis and structural components of the bus.

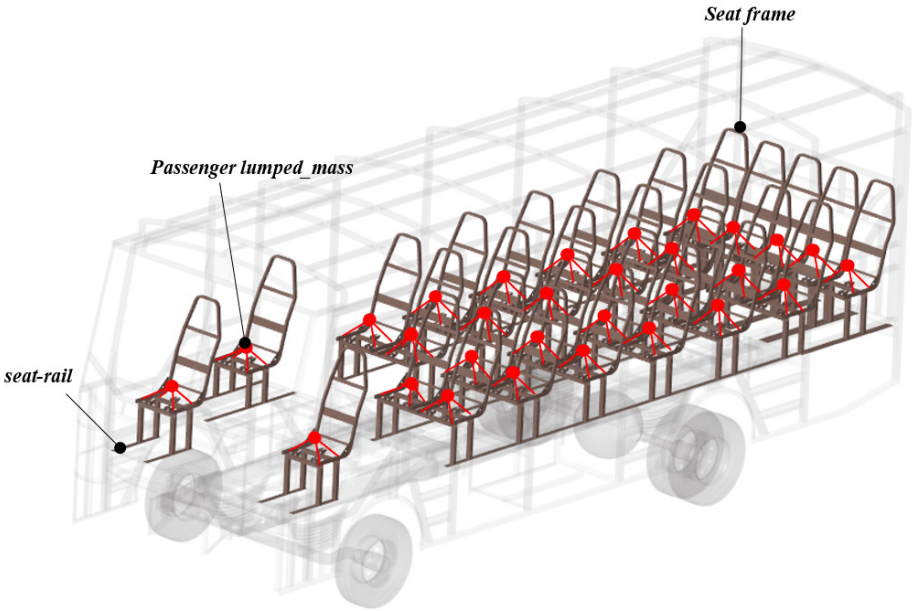

Figure 3.31: Arrangement of seat and seat rails with passenger mass

3.3.5.1.1 Initial and Loading conditions

During the rollover simulation, the complete vehicle is initially tilted in an unstable (equilibrium) position and a ditch of 800 mm[35]. The angle of the tilt table shall be greater than 35° and the trial & error simulation is needed to obtain the minimum tilt table angle that is used to trigger the vehicle to tip over[72], [85]. Hence, the minimum angle of the tilt table is 49° in unstable equilibrium position. The bus's initial angular velocity should not exceed 0.0875 rad/sec (5 deg/sec)[35]. Furthermore, the card 'INITIAL_VELOCITY_GENERATION' defines the initial angular velocity of the bus[86]. The external load card 'LOAD_BODY_Z' is applied as the gravity of the bus[82].

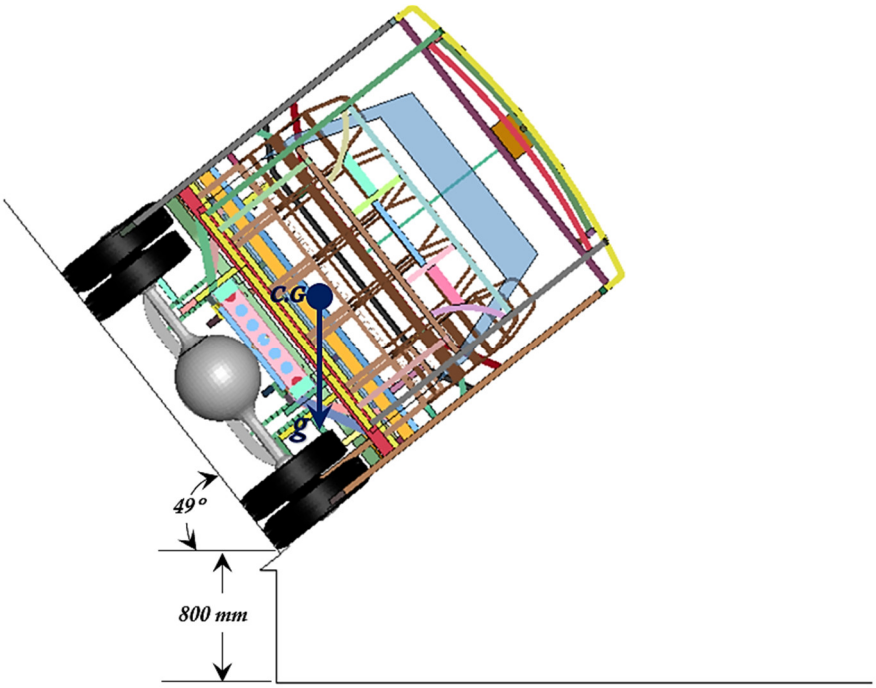

Figure 3.32: Initial conditions during rollover simulation

Figure 3.32 illustrates the unstable equilibrium position and initial loading conditions in the rollover case. However, the computational time of the simulation takes 2.25 seconds until the vehicle reaches motionless. The overall rollover simulation (Elapsed) time between 51 hr. to 86 hr., depending on the initial contact and finish time for each scenario., For accurate energy distribution with stable models during simulation, the option of mass-scaling was considered to regulate the time step (DT2MS) [29].

3.3.5.1.2 Description of contacts and Deformable to Rigid

The contact algorithm 'AUTOMATIC_ SURFACE_TO_SURFACE' defines the contact relationship between the structure & ground. And the coefficient of friction for steel-to-concrete contact is 0.65[68], [87]–[89]. The contact definition between tilt table & tires (rubber-to-steel) is developed using 'AUTOMATIC_NODE_TO_SURFACE'[59]. In this contact, the value of the coefficient of friction is 0.7[68]. The structural steel and ground (steel to steel) define using 'AUTOMATIC_SINGLE_TO_SURFACE' with its coefficient of friction is 0.15[68].

The Switch 'DEFORMABLE_TO_RIGID_AUTOMATIC' was highly recommended for flexible switch activation and easy use application. This switch is commonly used for a component to switch deformable and rigid automatically by the change of contact surface force or rigid wall force[89]–[91]. Hence, a vehicle's rollover simulation needs to change from deformable to rigid material or vice versa using a 'DEFORMABLE_TO_RIGID_AUTOMATIC' switch. The first switch is used to activate all parts of the model from deformable to rigid. The second switch

activates only the structure and seat with seat rail to deformable material. The two switches are paired and related to each other to automatically switch back and forth using a contact force.

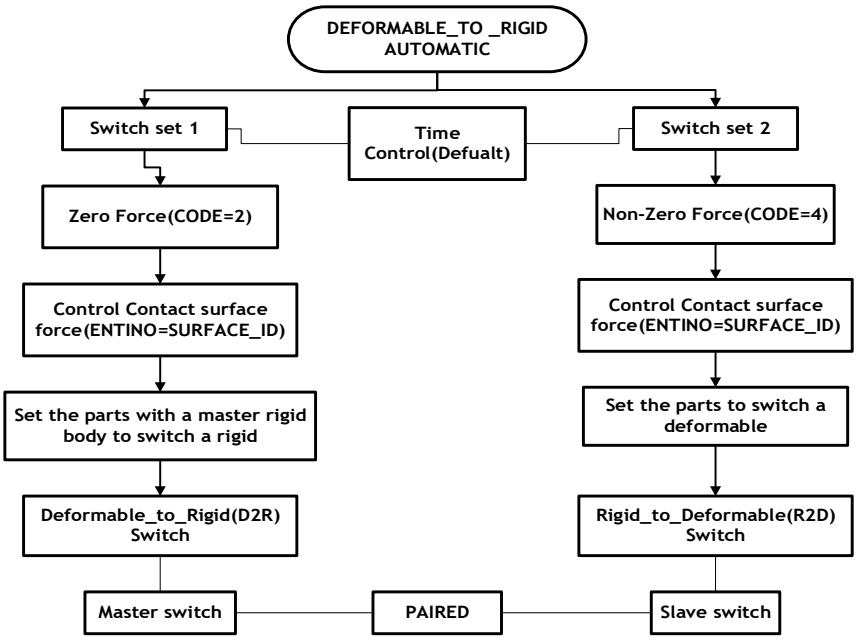

Figure 3.33: Activation of Automatic Deformable to Rigid switch in a rollover case

An illustration of activation of the switch during deformable to rigid or rigid deformable is shown in Figure 3.33. The rollover crash of the vehicle describes starting from the moment before the impact until the final impact using the three stages;

- ***Stage-I**: initial (unstable equilibrium) position. all parts of the model switches to a rigid definition(D2R) @ the time instant t=0.0 sec. (see Figure 3.34a).*
- ***Stage-II**: transition from rigid to deformable instantly before crash @ instant time $t=t_1$ (see Figure 3.34b).*
- ***Stage-III**: complete crash with ground @ $t=t_{final}$ (see Figure 3.34c).*

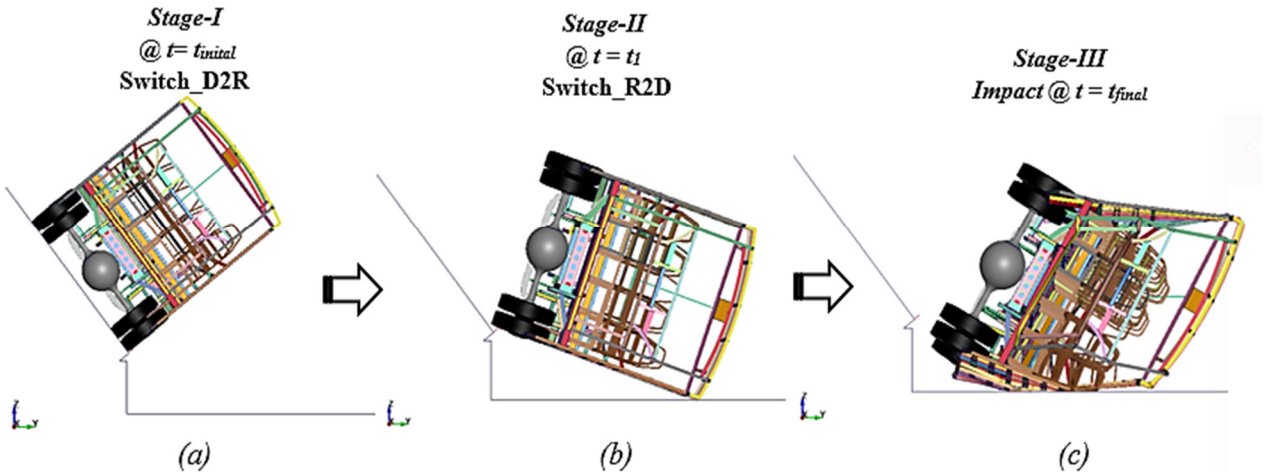

Figure 3.34: Stages of the rollover crash: a) Unstable equilibrium position, b) Instant before the impact, and c) Complete crash

In the switch of Deformable to Rigid, the maximum time step defines before the impact of the bus at the first and second stages of the rollover case. During the tare weight rollover case, the time step is reduced from $1.00e^{-5}$ to $1.00e^{-6}$ seconds between simulation time of 1.62 – 2.25 seconds. This rollover procedure is used to minimize the computational time[68]. The overall rollover simulation (Elapsed) time takes 51 hr. to 86 hr. (over three days), depending on all simulations' initial contact and finish time. For accurate energy distribution with stable models during simulation, the option of mass-scaling was considered to regulate the time step (DT2MS)[81].

3.4 Concept of Angular Deformation Index

Angular Deformation Index is a quantitative measure used to evaluate a margin of safety and a deformation extent in rollover simulation [28], [68]. During the actual case and simulation of the rollover, the angular index measures the strength of bus structural deformation, respectively[75].

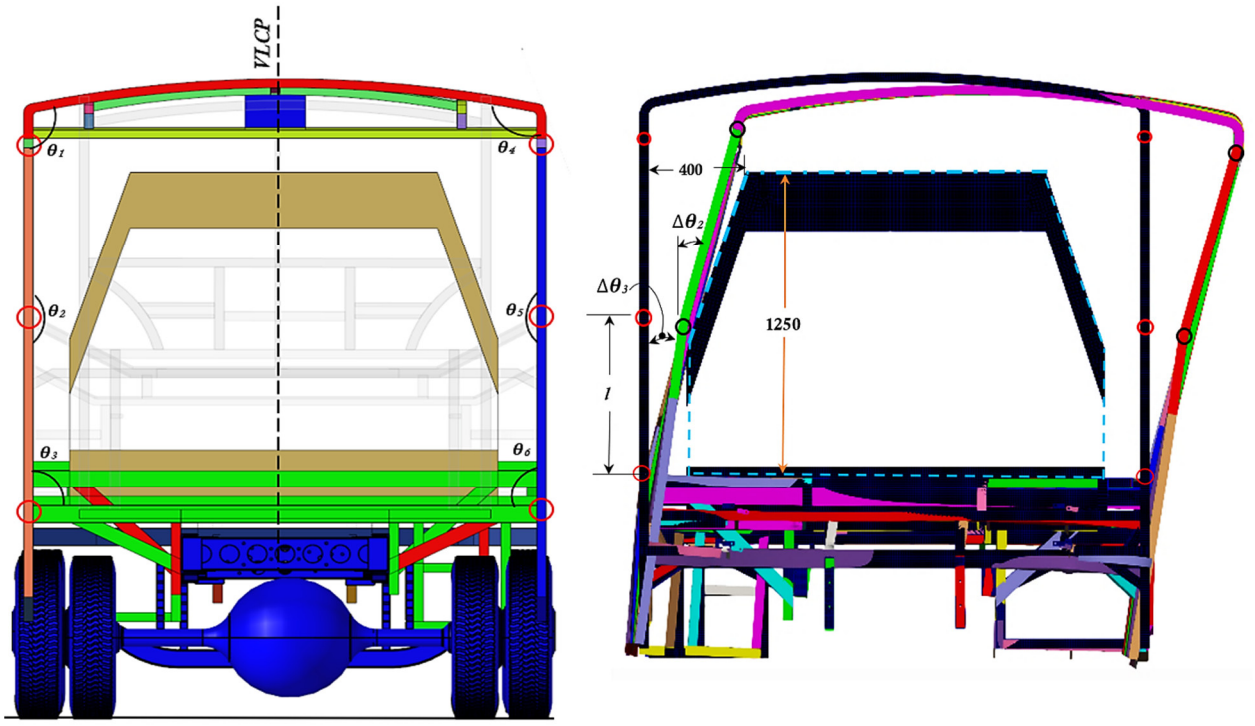

Figure 3.35: The concept of deformation angle and angular deformation index[28]

Figure 3.35 shows the angle between wall & floor (θ_3), angle of waist rails (θ_2) , and angle between roof & wall (θ_1) with a measured angular deformation. The Angular Deformation Index (DI_θ) can be determined as[28]:

$$DI_\theta = \frac{l}{400}\tan(\Delta\theta_3) + \frac{(1250 - l)}{400}\tan(\Delta\theta_2) \qquad 3.56$$

Where: $\Delta\theta_3$ - the angle changes between wall & floor, $\Delta\theta_2$ - the angle changes of waist rails and l - the distance from the floor to waist rails

According to Bojanowski 2009 [28], the deformation index is classified into five ranges to classify the structural strength by calculating using equation 3.56. First, When the DI is below 0.4, the structure assigns to a strong structure. Second, the intermediate strength of the structure is obtained within the interval $0.4 \le DI_\theta < 0.6$. Third, At the interval $0.6 \le DI_\theta < 0.8$, the structural strength is in an acceptable range. Next, the structure is considered as poor strength rating if the DI has the interval $0.8 \le DI_\theta < 1$. Lastly, If the DI is greater than or equal to 1, the strength rating of the structure is in an unacceptable range, which means the bus structure fails the rollover test as stated by the ECE R66. Overall, these index ranges were used to measure the residual space's structural crashworthiness capability and safety after rollover impact during this research.

3.5 Mesh Discretization and Verification of FE Models

The numerical simulation error assesses by the task of the model verification and discretization of the FE model[28]. In this research, the quasi-static FE analysis of structural connection was used to check whether the roof-side wall & floor-side wall connections withstand the quasi-static loading or not. Moreover, the mesh convergence study and the effect of welding types on the connection FE analysis are considered for all FE models. Moreover, Energy balance calculation conducts to verify the FE Models of all rollover simulations.

In the rollover simulation, checking the energy balance is the main factor in assessing the solution's errors. This verification guidelines presents the concept of energy conservation laws[28], [68], [92]. The applied total energy of the structure can be determined as stated by ECE R66[35]:

$$E_{Total} = 0.75Mg\Delta h \text{ Or } E_{Total} = 0.75Mg\left(\sqrt{\left(\frac{W}{2}\right)^2 + H_o^{\,2}} - \frac{W}{2H}\sqrt{H^2 - (800)^2} + \frac{(800 * H_o)}{H}\right) \quad 3.57$$

Where:

W - the overall width of the bus, H - the height of the bus, and

H_o - the height of the center of gravity

3.5.1 Quasi-static FE Analysis of structural connections

The Crashworthiness behavior of the bus structure in rollover accidents depends on its Floor-Wall (FW) and Roof-Wall (RW) connections[38], [39]. Figure 3.36 displays the floor-wall and roof-wall connections arrangement for quasi-static analysis based on the state of Florida (FL) standard. Both connection FE analyses evaluated the strength of floor-wall and roof-wall connections using a numerical approach. The floor parts are fixed during the FW connection, as shown in Figure 3.37(left). Impactor load is gradually applied to the wall section. Then, The absorbed energy was measured after the sidewall rotates about 16.7 °(deg.)[38]. However, the roof parts are fixed in the

RW connection (see Figure 3.37(right). Impactor load is gradually applied to the wall section, and the absorbed energy was measured after the sidewall rotates about 23 °(deg.)[38]. Lastly, the results were compared to the required threshold energy per meter as stated by the Florida standard.

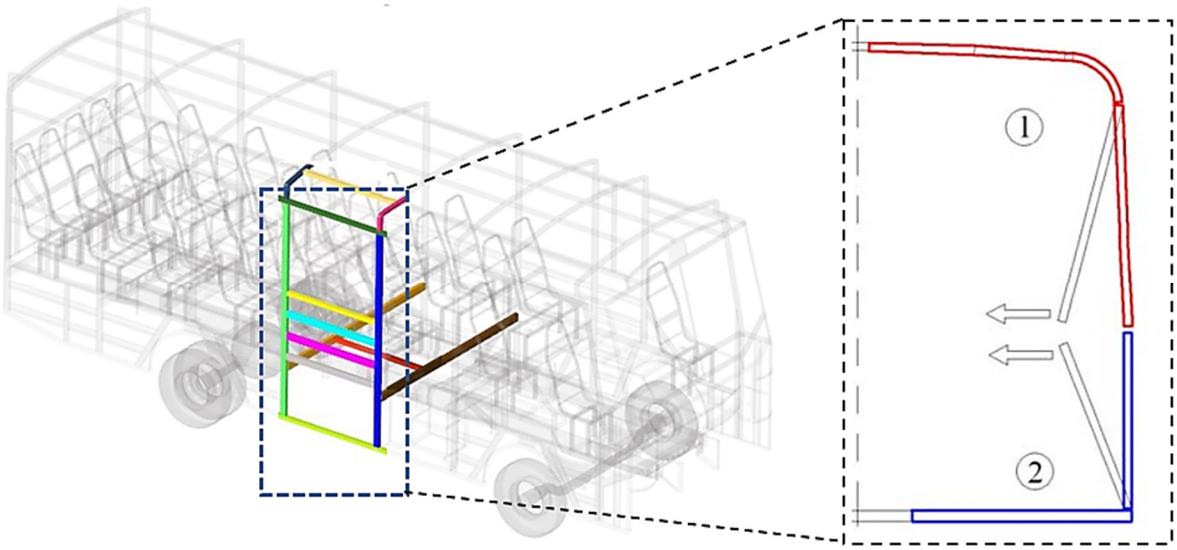

Figure 3.36: Arrangement for quasi-static FE analysis of RW and FW connections

3.5.1.1 FEA Procedures for structural connections analysis

The simulation procedures have been done as stated by Florida Standard using explicit dynamics in the LS-DYNA R11.0. The FE procedures of the structural connection analysis are similar to the quasi-static simulation of structure that was previously done. However, the main differences between the mesh density and effects of weld type analysis are the geometry, assembly, and FE discretization techniques in the FE Procedure.

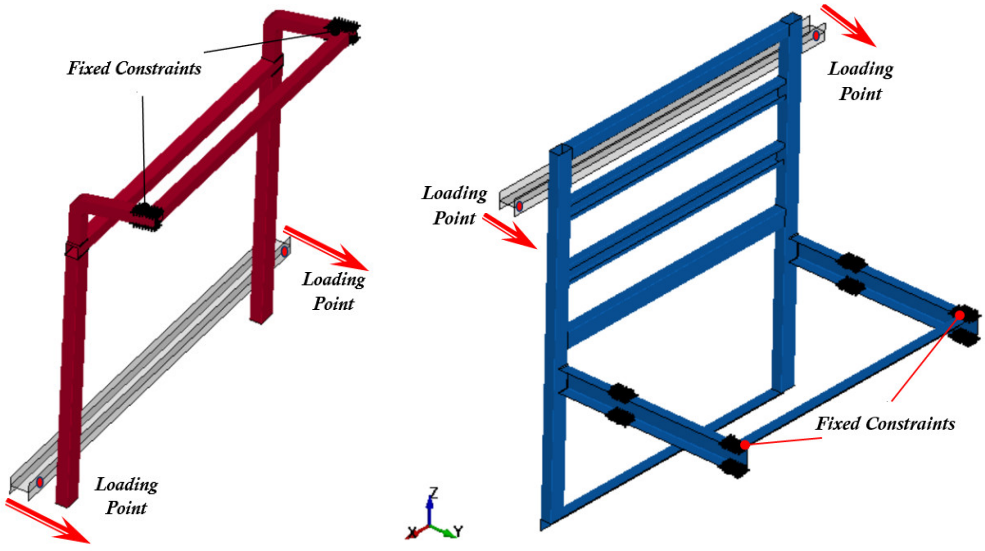

a) b)

Figure 3.37: FE Model setup of the structural connection: a) RW connection & b) FW connection

Additionally, Figure 3.37 illustrates the loading and boundary condition of the quasi-static connection as stated by Florida Standard. A quasi-static loading applies by the impactor displacement of 300 mm within the loading duration of 2 seconds using the 'PRESCRIBED _MOTION_RIGID_LOCAL' keyword.

3.5.1.1.1 Effects of Weld type on the quasi-static connection analysis

As mentioned earlier, the welding types are not considered during the manufacturing of the locally built midi-bus. In the welding process, the weld type and its size should be considered in the design of a weld joint[93]. However, most local bus manufacturers have used the two types of Shielded Metal Arc Welding (SMAW). These are:

a) ***Full arc weld*** – the full lengthen(continuous) welds (butt & fillet type) are modeled at connection edges of the frames
b) ***Spot arc weld*** – the solid spot welds (butt & fillet type) are formed at the corner of the frames, and the weld is formed without a hole[94].

This section studies the full and spot arc welds to compare the energy absorbing capacity during a quasi-static connection analysis using the Finite Element Method. According to a local midi-bus manufacturer, Electrode E6011, E6013, and E7018 are the most frequently used in structural welding members of the bus. These electrodes are primarily applicable for pressure vessels, piping, and structural members[95]. This study selects the E7018 type of weld electrode to study the effects of welding types with its size in the quasi-static connection FE Analysis. The weld defects and other factors that influence the welding quality are not considered in this study. However, the spot weld is equally located at the corner of the frames as spot weld pitch, shown in Figures 3.38 and 3.39. Moreover, the geometry of welds within their dimension in the RW and FW connection using the millimeter unit (mm) are mentioned in Appendix D (Figure D1-D2).

The weld behavior quasi-static connection FE Models consisted of the Roof-wall and Floor-wall connection. These connections describe the behavior of welding during the quasi-static loading test. The floor, roof, and wall frames, impactor, and welds (full and spot arc weld) are the parts of the connections FE model as shown in Figures 3.38 and 3.39. The entire quasi-static connections FE Model contains the maximum and minimum element size of 10 mm & 1.5 mm, respectively.

The FW connection comprises 26,806 elements with 30,869 nodes in the seventeen (17) parts and 22,148 elements with 24,021 nodes in the twenty-three (23) parts for full and spots arc weld FE models, respectively. Next, the RW connection consists of 18,236 elements with 22,657 nodes in the fifteen (15) parts and 12,776 elements with 14,417 nodes in the twenty-three (23) number of parts for full and spot arc weld FE models, respectively.

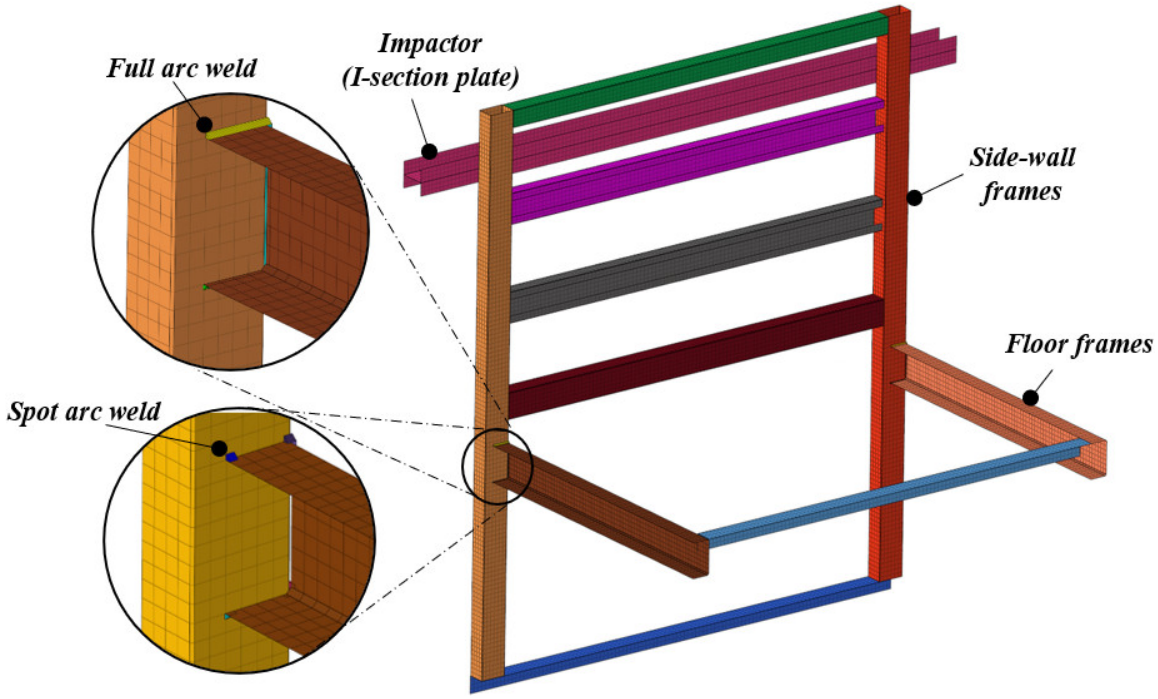

Figure 3.38: Main components in the FE Model of FW Connection

The plastic hinge of the two connections (roof-wall and floor-wall) connects using full and spot arc weld. The other part's connection is modeled as spot welds (rigid nodes) using the 'CONSTRAINED_SPOTWELD' card are presented.

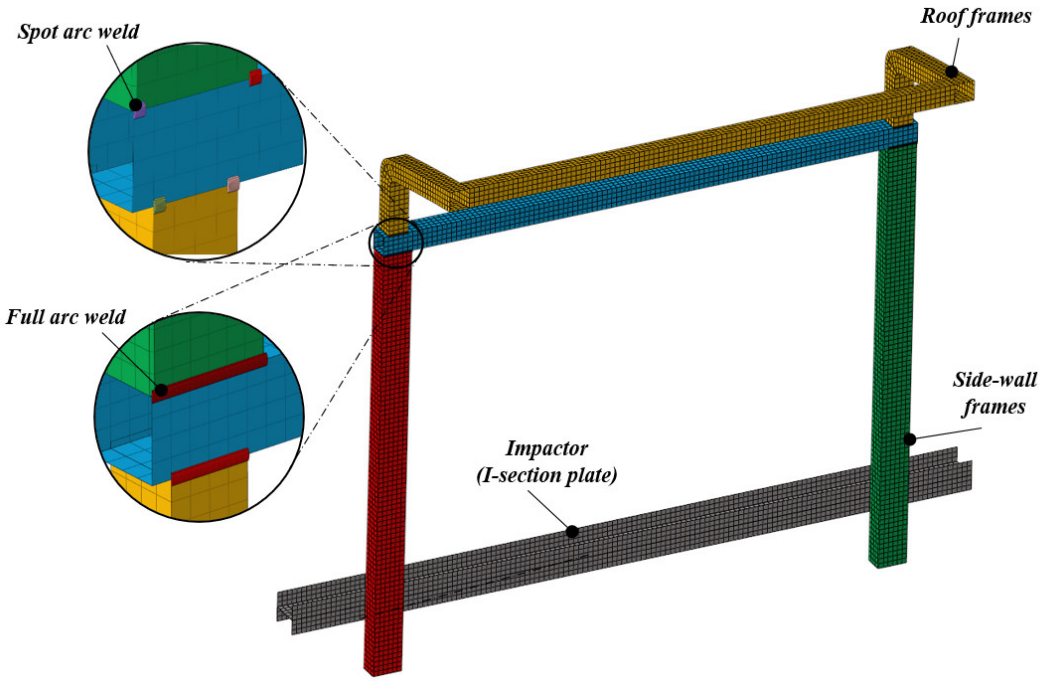

Figure 3.39: Main components in the FE Model of RW Connection

As depicted in Table 3.14, all parts and FE model statistics of the two welds on the quasi-static connection analysis.

Table 3.14: Statistics for FE Model of two welds on both connections

Parameters	***Full arc weld***		***Spot arc weld***	
	RW connection	*FW connection*	*RW connection*	*FW connection*
Min. Element Size(mm)	1.5		1.5	
Max. Element Size(mm)	10		10	
Number of Parts	15	17	23	23
Number of Nodes	22,657	30,869	12,776	24,021
Number of Elements	18,236	26,806	14,417	22,148

The welds are developed using solid elements, and the other components are shell elements. As mentioned before, the weld material property directly with the weld electrode E7018(E48018) & weld current (90 Ampere(A)) was taken from the tension test data, shown in Table 3.15[96].

The material used for all parts of roof-wall and floor-wall frames is conventional structural steel. The PIECEWISE_LINEAR_PLASTICITY (MAT_24) material definition was implemented for most steel materials [68]. The weld material and an impactor (I-section plate) are modeled using SPOTWELD(MAT_100) and RIGID (MAT_20), respectively. Moreover, the contacts of all frame parts define by using the 'AUTOMATIC_SINGLE_SURFACE' card. In addition, a contact card 'TIED_NODES_TO_SURFACE' is used to describe the contact between weld bead and frames[89]. Finally, the 'AUTOMATIC_SURFACE_TO_SURFACE' contact is used to define contact between an impactor and wall frames. The coefficient of friction for all contacted parts as a steel-to-steel material contact is 0.15[68].

Table 3.15: Material property of welds[96]

Property	***Weld material (E7018)***
Density ρ (kg/mm^3)	7850
Yield Strength σ_y (MPa)	390
Ultimate Tensile Strength σ_{ut} (MPa)	567
Young's Modulus E (GPa)	210
Poisson's Ratio v	0.3

3.5.1.1.2 Mesh Convergence study for all FE Models

Element discretization was used to minimize the numerical errors for all FE models through various mesh sizes. This section concerns discretizing the FE models of the original RW and FW connection. Thus, both the connection models are discretizing in 6 mm, 10 mm & 18 mm shown in Figure 3.40.

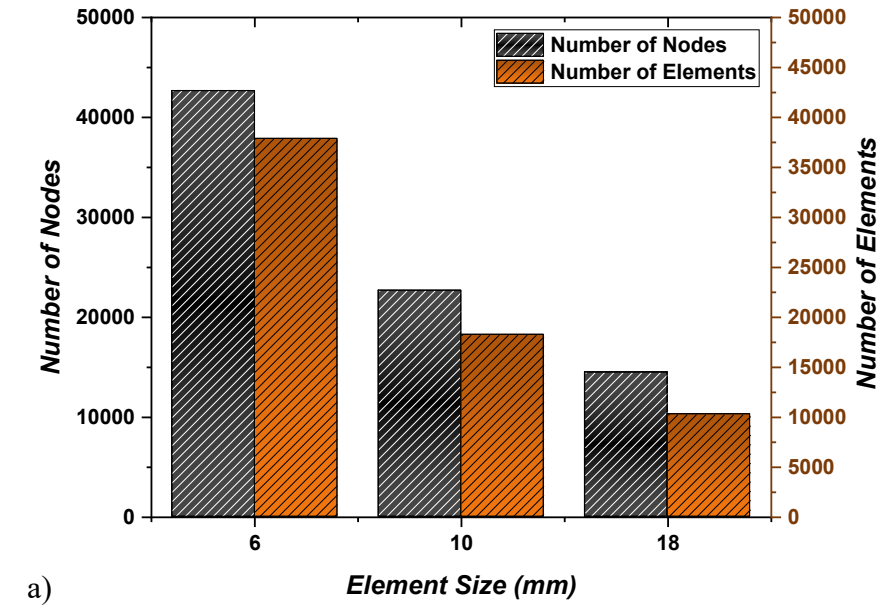

a)

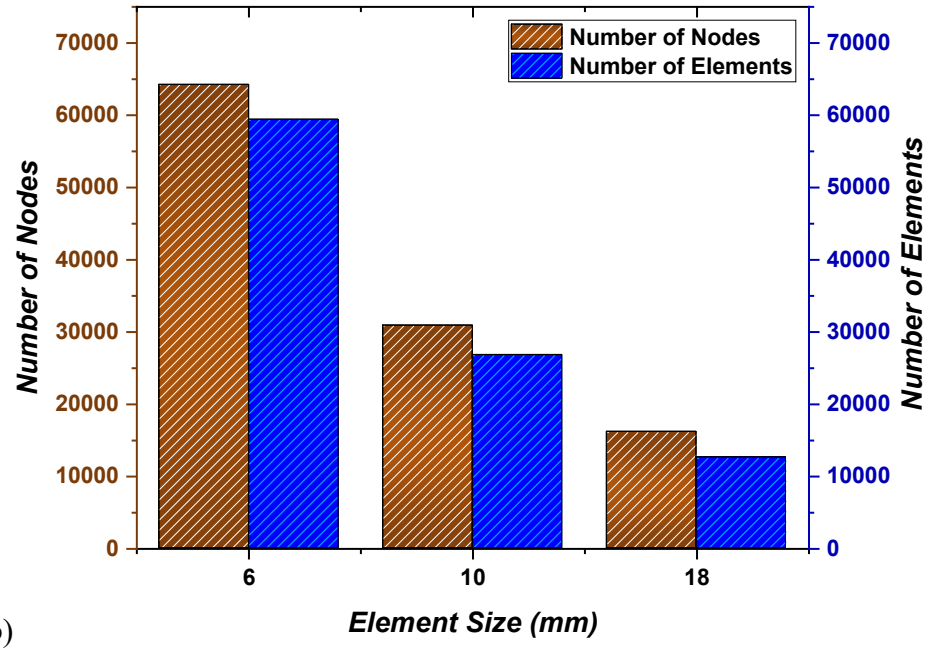

b)

Figure 3.40: Statistics of FE Models for the mesh convergence study: a) RW connection and b) FW connection

The FE Procedures of the mesh convergence study are similar to the effects of weld type on the connection quasi-static FE analysis. However, the only difference is the mesh density. Moreover, the weld formulation between all frame parts except the plastic hinge of the two connections is modeled as spot welds (rigid nodes) using the 'CONSTRAINED_SPOTWELD' card. However, the full arc welding joined the plastic hinge of the roof wall and the floor-wall connection.

Chapter Four

Structural Design and Optimization of a Midi – Bus Structure

4.1 Introduction

Optimization develops objective functions with constraints to maximize or minimize the desired value [97]. In the computer-based optimization process, the simulation requires a high number of iterations, the performance of computers, and large numbers of design parameters [28]. However, the reinforcement of the vehicle body is one of the optimization techniques to strengthen the vehicle's body [98]. In this study, the main goal is to specify the three alternative design solutions. However, this process was done by use of reinforcement and numerical optimization techniques using Response surface Optimization (RSO) in DesignXplorer (model – II_{stat}) and Successive Response Surface Method (SRSM) in LS-OPT (model – II_{roll}) and combined design approach by combing and modifying the model – II_{stat} and model – II_{roll} into a final model (model – III) for static and dynamic(rollover) conditions.

4.1.1 Locally built (original) midi-bus structure: Problem statement

As shown in Figure 4.1, most local bus bodybuilders used the wall support(U-channel) to support the wall and cover the skin of the bus from vibration. However, the weight of the bus structure increases due to the high numbers of wall support. Moreover, these components are not designed to connect (support) windows and waist rail. The other design defects from the manufacturer's side, At the end of the chassis, the rear portion of the bus extends around 500 – 700 mm to obtain more seats in the rear section. This design consideration eliminates the connection between of chassis body and floor section.

Table 4.1: Components with its mass of selected configuration

Component name	***Cross-section type***	***Qty.***	***Mass (kg)***
Front inclined pillar	L-angle	2	2.26
Roof arc member	SHS	8	36.06
Wall support member	U – channel	44	77.11

Furthermore, the dynamic(rollover) analysis shows that the roof arc and front inclined pillar have low energy absorption and maximum deformation from dynamic (rollover) analysis. This result

shows that the cross-section of the members affects the structural strength of the members. Moreover, the addition of support in the connection of the bus section is another manufacturer's problem. Table 4.1 describes cross-sections types and masses of the components of enhanced configurations.

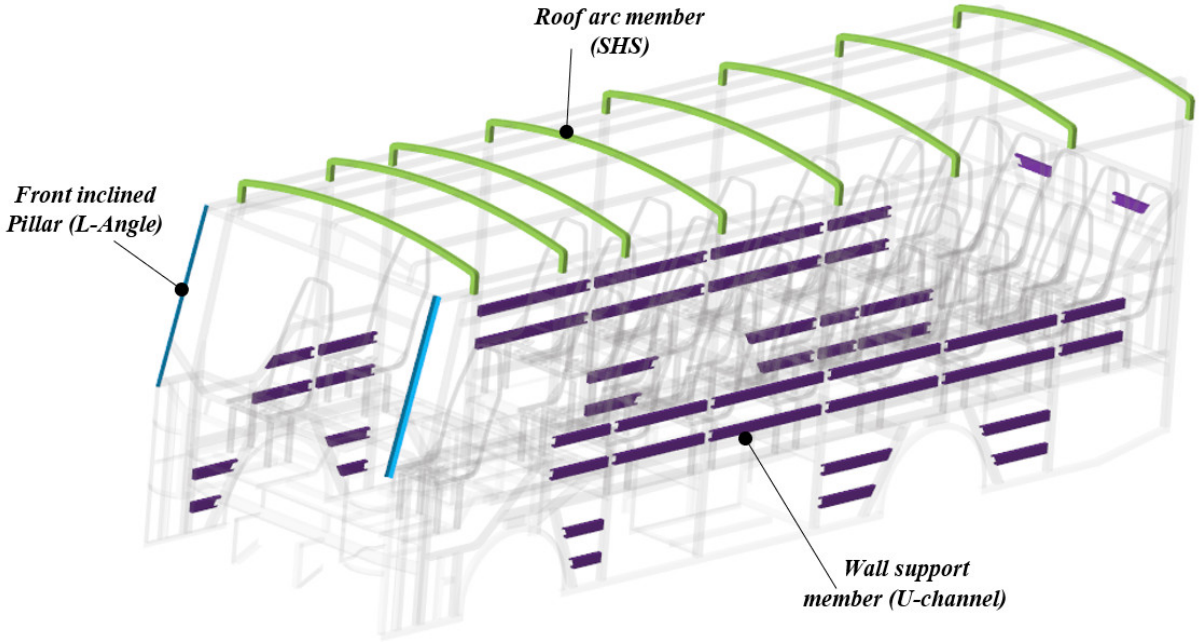

Figure 4.1: Selected Configurations to improve the original design

4.2 Reinforced design using Reinforcement Approach

This study applies structural reinforcement optimization consistent with engineering practice and knowledge for the existing bus structure. Most local bus manufacturer experiences the design of the structure's construction through try and error methods, this approach outcomes in low structural strength and safety of the passengers during accidents. The existing bus structure needs a structural design analysis and improvement to maximize the stiffness and minimize the structure's weight. The bus's weight is reduced by changing the frame of a bus structure for a lightweight design[41].

The main aim of the optimization method is to redesign and improve the bus structure within its mechanical behaviors. First, the existing bus structure examines carefully through the manufacturer constraint and the static and dynamic simulation using FE Method to select the components that might be modified. When this selected element leads to a high structural deformation, the substitution and modification of the structural components were considered. Figure 4.2 shows the process of optimization via reinforcement techniques for the existing bus structure.

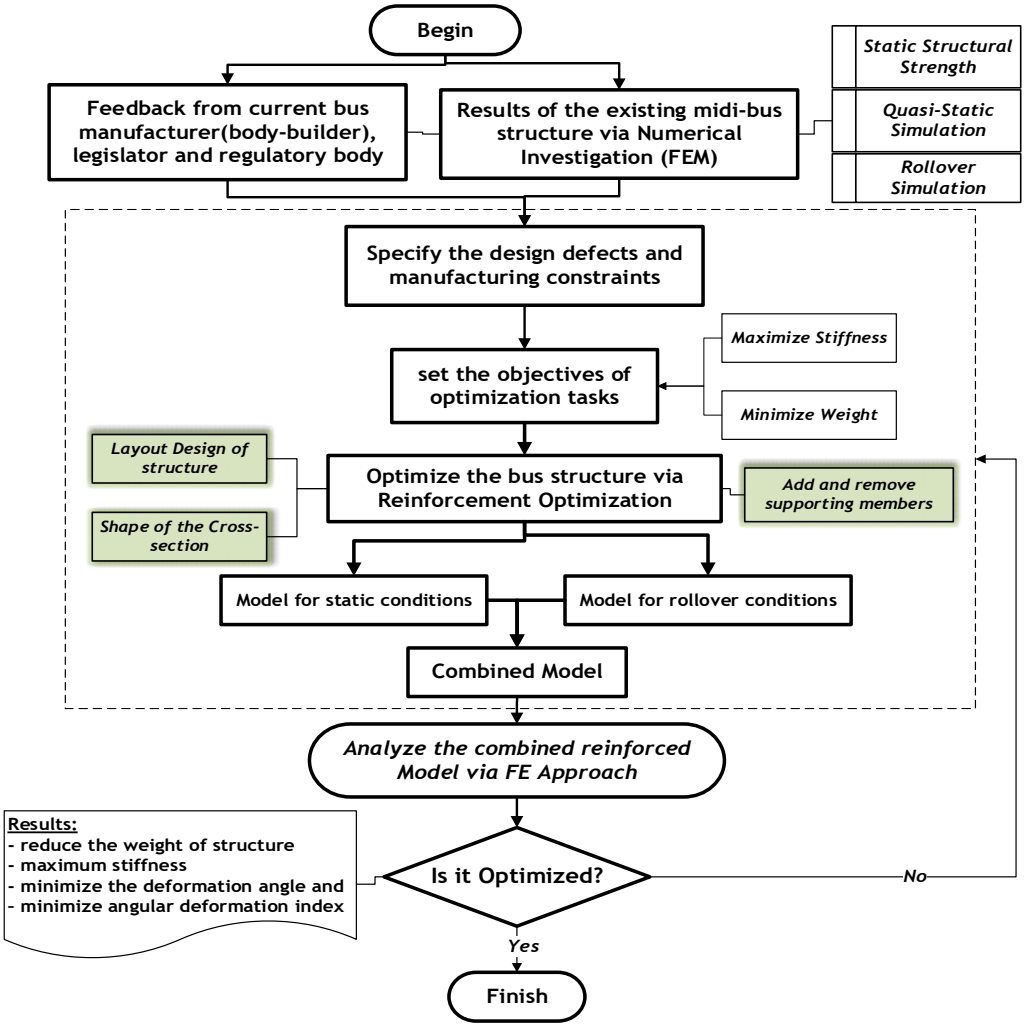

Figure 4.2: Procedure for the reinforced design of bus structure

4.2.1 Reinforcement Approach for all cases of FE analysis

In this study, the design modification(reinforcement) conducts the addition and replacement of the structural parts. The first approach concerns the layout of the structure and the shape of the cross-section in the structural parts. Next, the addition of supports was considered to assemble the section of the structure. The rectangular (lying orientation) profile has a much higher energy absorption for oblique impact load directions than the square cross-section [88]. The other important consideration for the rollover case is the strength of the floor-wall connection. Hence, the supporting member attaches at the corner of the floor and sidewall section on the front, medium, and rear portions to reduce the structural deformation. The connecting elements on both sides section constructs using inclined square cross-sections. This construction used to stiff the connection of vertical pillars, windows & waist rails. After simulation of quasi-static and rollover simulation original(baseline) structure, the front L-shaped (L-Angle steel) pillar experiences a high structural deformation. Later, the L-shaped pillar is substituted by a square cross-section. The dimensions of both selected and enhanced structure configurations are described, as shown in Table 4.2.

Table 4.2: Dimensions of replaced and reinforced configurations

Cross-section	***Dimensions*** *(HxBxT) or (HxBxTxh) mm*	
	Original Design	*Reinforced Design*
SHS tubes	*40x40x1.5*	*40x40x1.5*
L-Angle	*40x40x1.5*	*40x40x3*
U-channel	*70x40x1.5x16.5*	-
RHS tubes	-	*60x40x1.5*

The original structure contains maximum deformation at the end of the roof and floor section from the results of static strength analysis. The leading causes of this preliminary design are the extension of seats and poor assembly of the rear to roof and wall to rear connection. However, the above design defects improve through additional support members using square and L-shaped cross-sections shown in Figure 4.3. Therefore, the reinforced midi-bus structure has been considered the following structural design modifications:

- Roof arc members to strengthen the roof -parts using rectangular cross-section (RHS)
- Inclined connecting elements (Supporting members - #1) at the left & right section of frames
- Supporting members from #2 to #4 developed to build a connection between roof and sides pillars with rear pillars, Support for extended floor section & chassis, and Support for connection side walls and floor during the rollover, respectively
- Inclined front(A) pillar at the front section of the structure (square cross-section (SHS)) to strengthen the front pillar

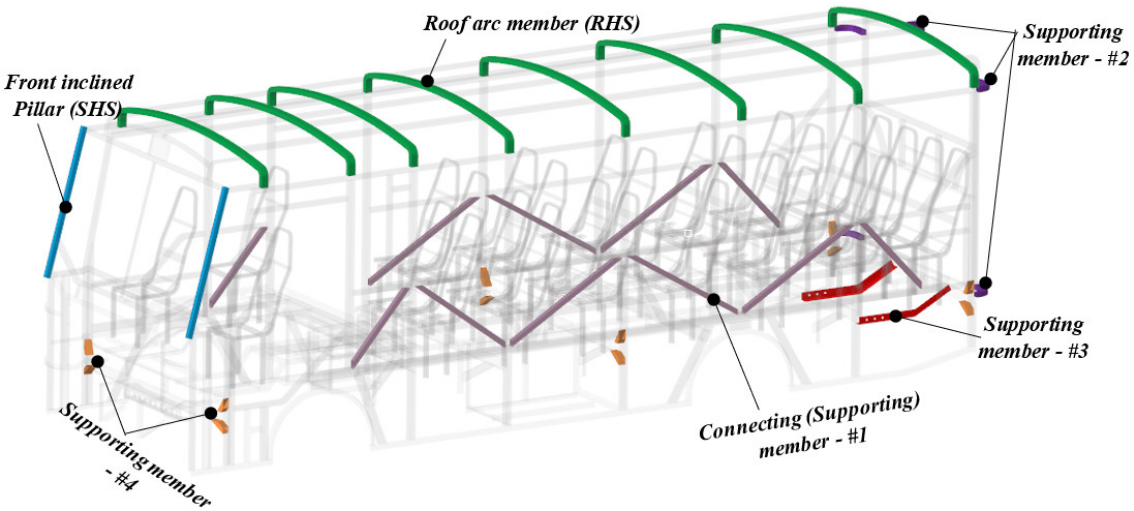

Figure 4.3: Illustrates the enhanced configurations of the reinforced design

Table 4.3 describes cross-sections types and masses of the components of enhanced configurations. In sum, this model decreases its weight by 29.98 kg compared to the original model. In addition, the 3D geometry illustration of the reinforced structure is described in appendix C (see Figure C4).

Table 4.3: Components with its mass of enhanced configuration

Component name	*Cross-section type*	*Qty.*	*Mass (kg)*
Front inclined pillar	SHS	2	4.53
Roof arc member	RHS	8	44.74
Supporting member - #1	SHS	11	19.7
Supporting member - #2	SHS	5	2.58
Supporting member - #3	L-Angle	2	7.86
Supporting member - #4	RHS	12	6.12

4.3 Optimization Method via Response Surface Optimization (RSO) in Static Case

Parametric optimization can be used to help designers determine the optimal sizes and shape of a structure using independent design variables (thickness, length, and coordinates) [99], [100]. Response Surface Optimization (RSO) methods were done to increase the bending stiffness and weight reduction of the structure in case of pure bending, as shown in Figure 4.4.

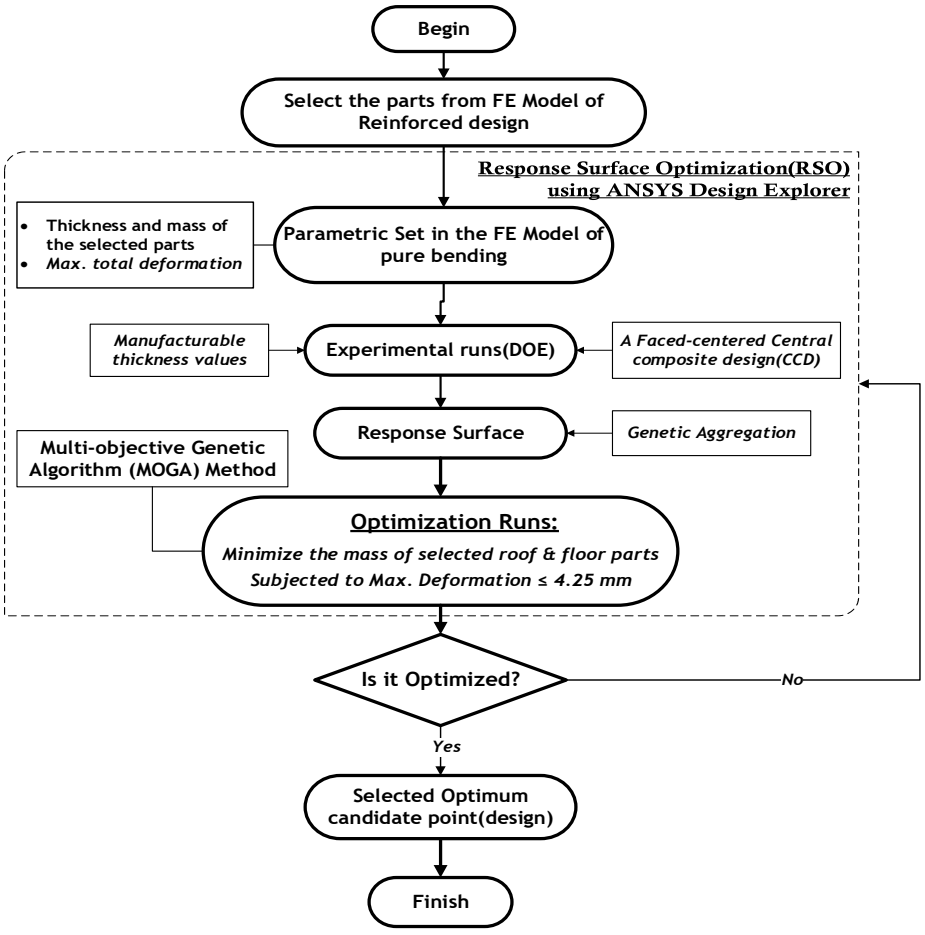

Figure 4.4: Response Surface Optimization process via ANSYS Design Explorer

During optimization, the changing thickness can minimize the weight although filling the constrained torsional and bending values simultaneously[101]. First, the reinforced design of the structure parametrizes by the thickness, mass, and total deformation of the selected nine parts of the roof and floor section. Next, the ANSYS Design Explorer develops the one hundred-thirteen (113) experimental runs with five manufacturable thickness values using a faced-centered Central Composite Design. Moreover, in this research, the Response Surface Optimization (RSO) facilitates the Multi-Objectives Genetic Algorithm (MOGA) to maximize the bending stiffness and minimize the mass of the selected parts during pure bending loading conditions.

4.3.1 Design of Experiments (DOE)

Design of experiments(DOE) is a method used to suit the simulated response data with experimental data or mathematical equations in design optimization[99]. An appropriate choice of components of structure bound by optimization is vital to declare rational optimization analysis [101]. During the static strength FE Analysis of the reinforced structure, the maximum total deformation occurs at the roof sections of four parts (T6 – T9). Moreover, the minimum deformation occurred at the floor section (T1 – T5) in all loading cases. These parts are only selected to optimize the reinforced structural design because multiple variables with many levels require many simulations runs in numerical optimization. As depicted in Figure 4.5, the geometrical illustration of nine selected parts of the reinforced structure.

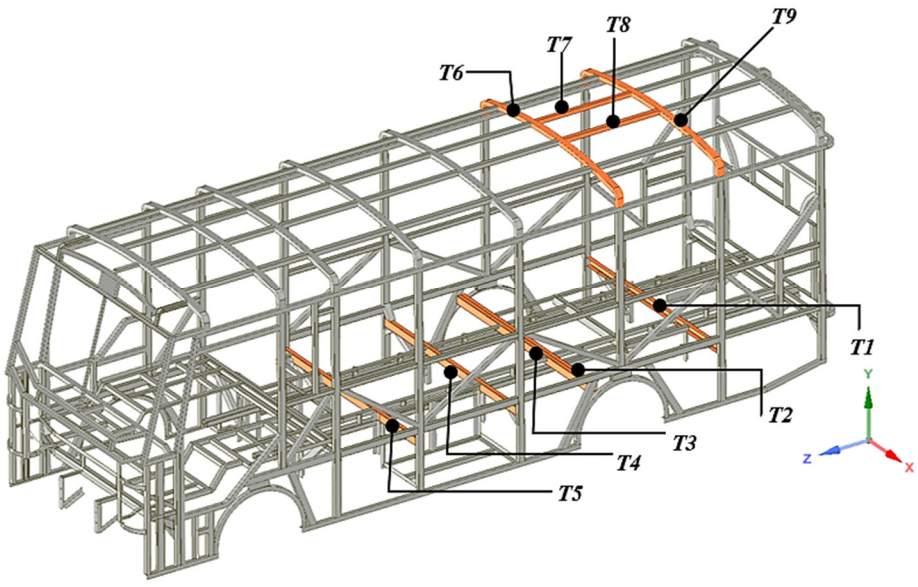

Figure 4.5: selected parts of the reinforced structure

Table 4.4: Cross-section and levels of thickness of Selected parts

Sections	*Parts*	*Cross-section*	*Thickness(mm)*	*Ranges of mfg. values(mm)*
Floor	T1 - T5	C – Channel	3	1,1.5,2,2.5,3
Roof	T6 - T9	SHS	1.5	1,1.5,2,2.5,3

Table 4.4 describes the cross-section types with the thickness of the selected parts with specified ranges of manufacturable values.

In this research, nine input variables (T1- T9) at five manufacturable levels (1, 1.5, 2, 2.5 & 3 mm) needs 113 design points (experimental runs), as shown in Figure 4.6. A faced-centered Central Composite Design (CCD) is a typical design of experiment type due to its efficiency when providing much information within a minimum number of experiments[99]. The one hundred-thirteen (113) DOE points take more than five days of computing time to obtain the outputs parameters (mass and total deformation).

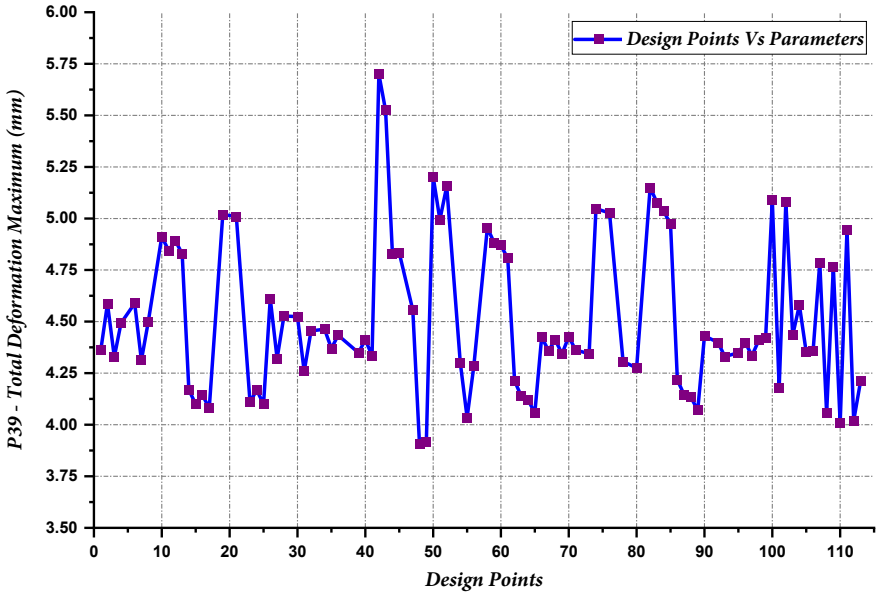

Figure 4.6: Total deformation(maximum) parameter at each design point

4.3.2 Response Surface

After the experimental runs, the responses (maximum deformation and mass results) are obtained through the FE simulation for design scenarios.

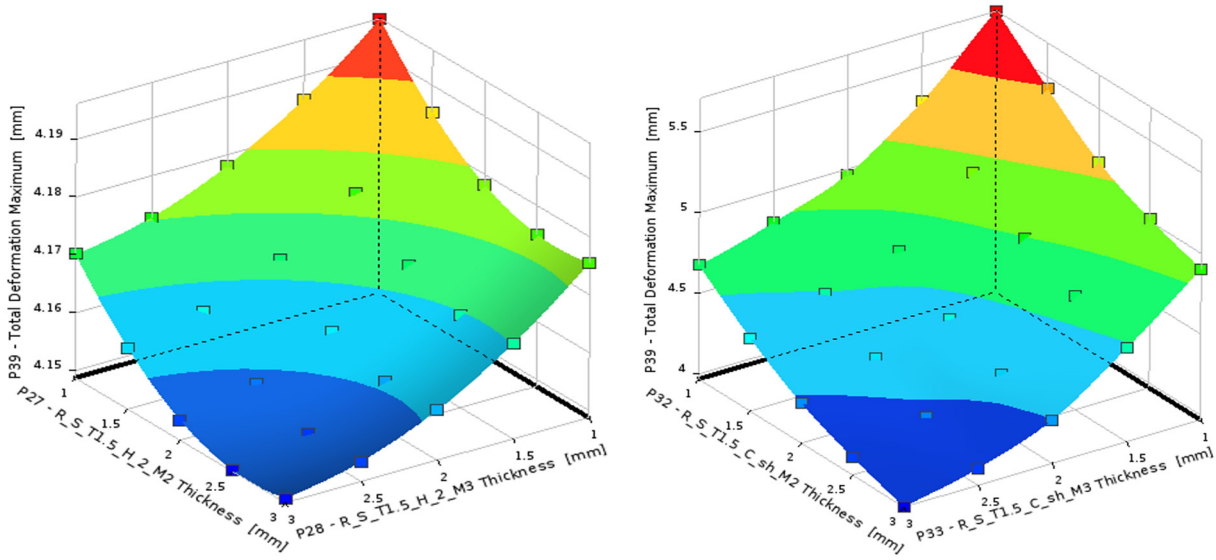

Figure 4.7: Representation of 3D response surface for four input variables

Each scenario dataset is used to fit perfectly the models of the response surface correctly. As depicted in Figure 4.7, these response surface models provide various responses about design variables (thickness of the parts). Moreover, in the case of two variables (P27 and P28) with thickness gives the maximum deformation response of 4.15 – 4.2 mm, as shown in Figure 4.7(left). However, Figure 4.7(right) displays that the response deformation of 4 – 5.75 mm can be obtained from the two-thickness variable (P32 & P33).

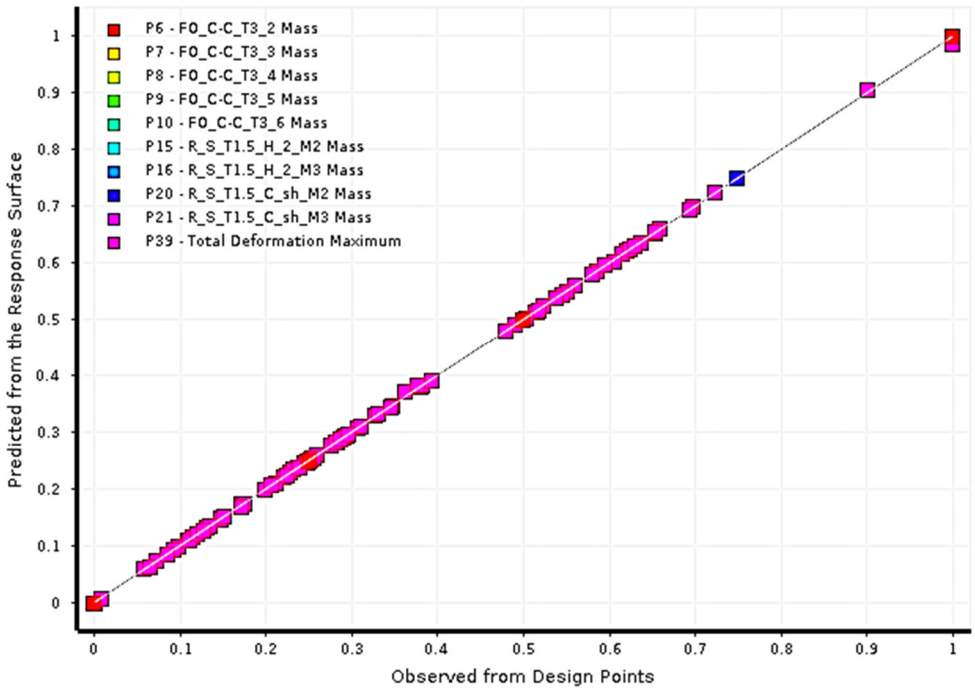

Figure 4.8: Illustration of the goodness of fit for observed and predicted results

The goodness of fit (correlation matrix) is calculated for the design of experiment points to check the accuracy of the response surface. As shown in Figure 4.8, most points are fallen on the lines, which means the response surface can predict values for most of the design points within its ranges. Accordingly, it is likely to conclude that the predictable response surface fits the observed design points.

4.3.3 Optimization Method

Multi-Objective Genetic Algorithm (MOGA) is an optimization method that supports many objectives and constraints at the comprehensive optimum finding[102]. The interactive approach considers the constraint approach with two functions (objective and constraint) to identify a single best compromise solution as a form of [97]:

$$\begin{aligned} &\text{minimize } f_1(t) \\ &\text{subject to } f_2(t) \le c \\ &\text{and } t \in \Omega \end{aligned} \qquad 4.1$$

Where: Ω – sets of the lower and the upper bounds on inputs variable ($t_L \le t \le t_U$)

c –the bounds of the outputs ($c_{min} \le c \le c_{max}$).

The genetic algorithm (GA) is broadly used in structural optimization due to the advantage of simple operation and accurate optimal solution with fast convergence speed[103]–[105]. As mentioned from design points curves, the various lowest value of total deformation occurred below 4.25 mm. and also, it is possible to reduce the total deformation below 4.25 mm, compared to the reinforced model. Thus, it is decided that the constraint of deformation is less than or equal to 4.25 mm. In this section, the design objective and constraints are sets-up using a Multi-Objective Genetic Algorithm (MOGA) in the response surface optimization. These are:

i. Minimize the mass of selected parts
ii. Subjected to total deformation ≤ 4.25 mm

The optimization task initially produces 9000 samples, assigns 1800 samples (per iteration) and 20 iterations to acquire three candidate points. The optimization also converged after 10,591 evaluations. The most significant candidate design point is obtained by searching for the best objective function value over the vast feasible region of the design spaces[99], [106]. After optimization runs, the three (3) design candidates are determined, as shown in Table 4.5. Thus, A candidate point 1(CP - #1) is selected as an optimal design candidate due to reduced mass and deformation with possible thickness values(manufacturable).

Table 4.5: Candidate points (CP) obtained from optimization

Parameters	**CP – #1 (Selected)**	**CP – #2**	**CP – #3**
T_1 (P1), mm	2.5	1	2
T_2 (P2), mm	1.5	3	1.5
T_3 (P3), mm	1	1	1
T_4 (P4), mm	1	1	1.5
T_5 (P5), mm	1	1	1
T_6 (P27), mm	1	1	1
T_7 (P28), mm	1	1	1
T_8 (P32), mm	2.5	2.5	2.5
T_9 (P33), mm	2.5	3	3
Total mass of the parts (P6-10,15,16,20, 21), kg	39.08	40.94	40.94
Maximum Total Deformation (P39), mm	4.19	4.23	4.11

Figure 4.9 describes the sensitivities of the outputs with input thickness. These sensitivities imply that all thickness parts are positively correlated with direct impacts for mass outputs (instead of

deformation). Moreover, only three thickness parameters (P-1,32 & 33) negatively correlate with the maximum total deformation. They also have some amounts of influence but inversely.

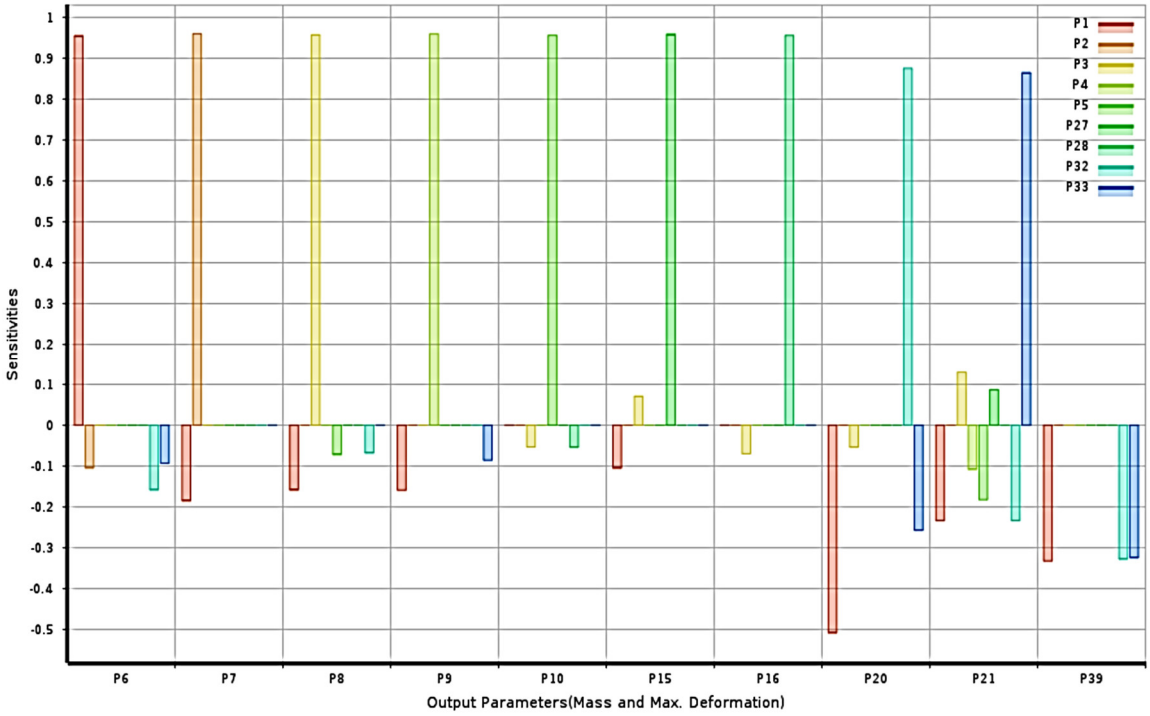

Figure 4.9: Output parameters sensitivities with inputs variables

4.4 Optimization Method via Successive Response Surface Method (SRSM) for quasi-static analysis

Optimization methods using Response Surface Method (SRSM) are commonly used in design optimization of crashworthiness[15], [68], [107], [108]. Moreover, the main aim of this optimization is to maximize the reinforced structure's strength within a maintained level of weight during the rollover case. However, the analysis was carried out using LS – DYNA and LS-OPT (successive response surface method (SRSM)). Furthermore, the optimization task was done to identify the significance of the section of the reinforced structure in response to the loading experienced in ECE - R66 quasi-static testing procedures.

Figure 4.10 displays the selected parts of the structure for optimization tasks. In the design of experiments (DOE), The design variables are the thickness of the parts. These parts are grouped into three groups based on their assembly section. From equation 5.53, the minimum requirement of absorbed energy of the reinforced design (model – I) was equal to 4.86 kJ. Moreover, it is a fact that the highest value of energy absorption indicates the better strength of the structure.

Consequently, Multi-objective optimization was done by reducing the total mass of the selected parts (objective function) and keeping the structure's energy absorption above 4.86 kJ (constraint). The energy absorption response was specified on the output of history by integrating the reaction force vs. displacement of the structure. Similar to equation 4.1, the only difference was that the

upper bound constraint of this optimization is absorbed energy response. Furthermore, it can be expressed as:

Minimize the mass of selected parts

Subjected to: Absorbed Energy (E_{st}) ≥ 4.86 kJ

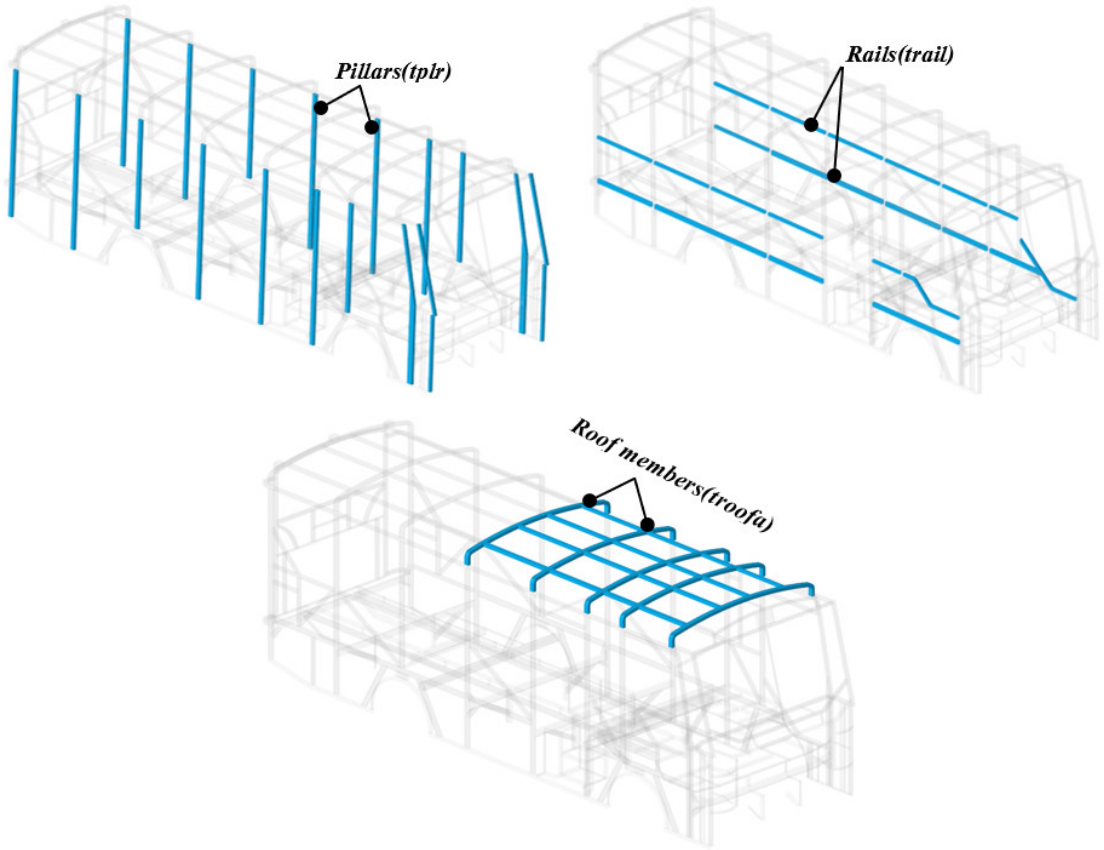

Figure 4.10: Selected parts of the reinforced structure for quasi-static case optimization

The initial thickness values for these parts and the manufacturable lower and upper bounds(ranges) in the design of the experiment are listed, as shown in Table 4.6.

Table 4.6: The selected parts thickness and its range of values from reinforced structure

Sections	***symbols***	***Cross-section***	***Initial thickness(mm)***	***Ranges of mfg. values(mm)***
Roof	troof	RHS & SHS	1.5	1,1.5,2,2.5,3
Rails	trail	SHS	1.5	1,1.5,2,2.5,3
Pillars	tplr	RHS	1.5	1,1.5,2,2.5,3

Figure 4.11 displays the optimization process to minimize the total mass of the structural member in the three thickness parameters (trail, troofa, and tplr) using LS-OPT. First, the three parameters are assigned for all selected parts in the FE Model of quasi-static using LS – DYNA. Moreover, it is imported to the optimization tool of LS-OPT. Then, linear ordered polynomial sampling is selected to identify the seven simulation points using D – optimal selection using LS-OPT. Next, the response of mass parts, internal energy, reaction force, and absorbed energy of the structure

was formulated. Moreover, the output history of reaction force, displacement, and Force vs. displacement plot were defined. Lastly, the objective and constraint of the optimization process was developed using a Genetic Algorithm for two iterations.

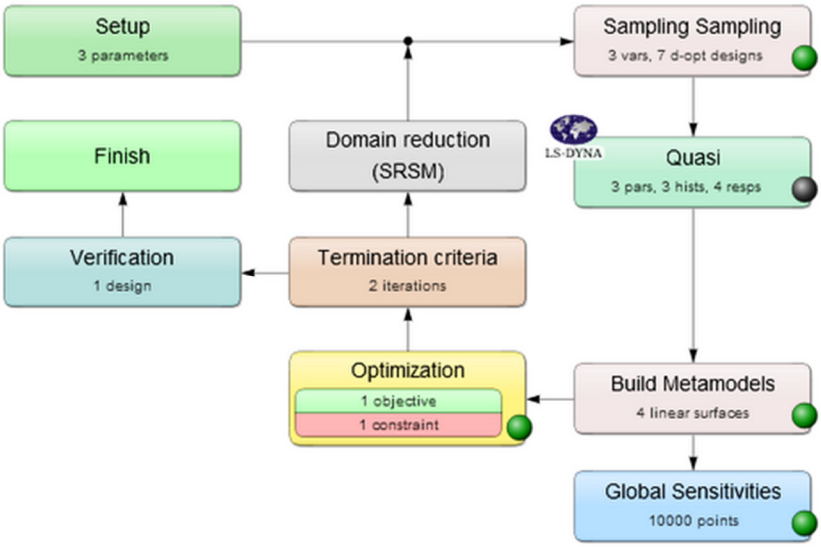

Figure 4.11 Flow chart of the structural optimization of the reinforced structure in quasi-static simulation via LS-OPT

4.4.1 Study of Sensitivity via ANOVA and Global (GSA/Sobol)

Figure 4.12 to Figure 4.13 show sensitivity analysis results for the total mass of the parts and responses absorbed energy by Global Sensitivity Analysis (GSA) with Sobol's and Analysis of Variance (ANOVA) approach. The trails and troofa are the minor influence variables for the mass parts. However, the thickness of the vertical pillars(tplr) is the essential variable, and it has a 95% confidence interval of the response function. Moreover, the roof members also do not influence the response of absorbed energy, as shown in Figure 4.13.

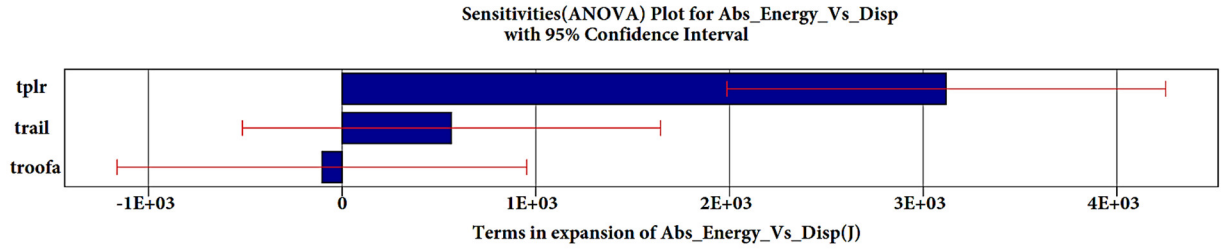

Iteration 1

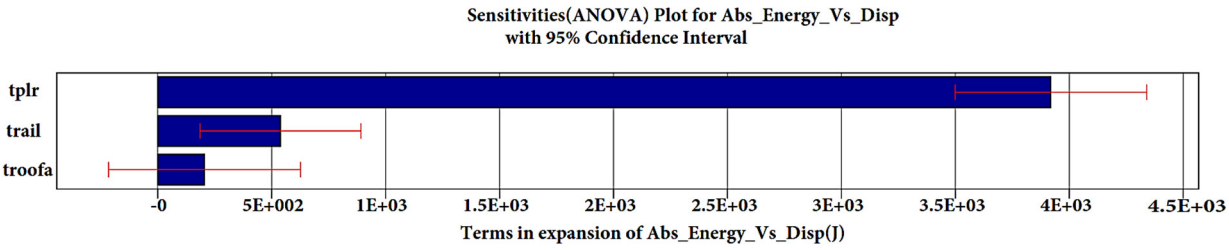

Iteration 2

Figure 4.12: Sensitivity (ANOVA) plot for the absorbed energy for all iterations

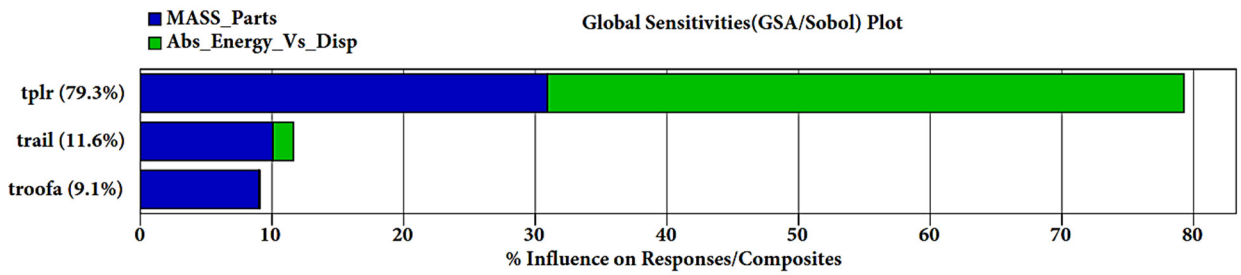

Iteration 1

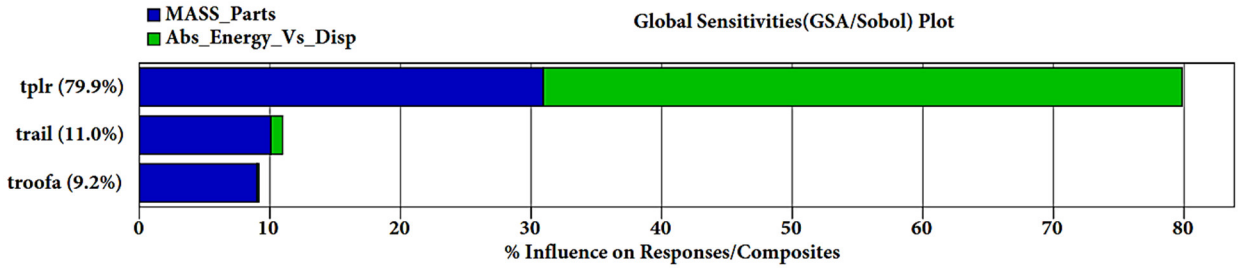

Iteration 2

Figure 4.13: Global Sensitivity (GSA/Sobol) plot for the mass of the parts and absorbed energy for all iterations

4.4.2 Optimization history using Linear Response Surface

In this section, the overall optimization iteration was performed within the linear response surface approximation. These approaches requested seven jobs per iteration. This means the optimization runs 14+1 jobs for all quasi-static simulations. Thus, using successive response surface methods, the optimization approach took over ten days (238 hours) for all simulations.

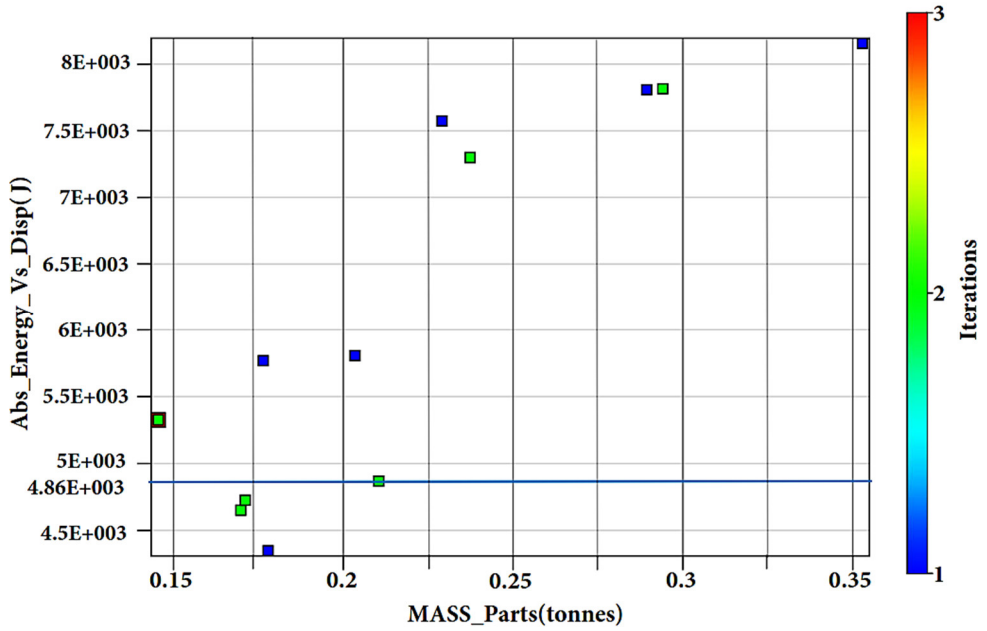

Figure 4.14: The response of absorbed energy vs mass of the parts at the design variables

Figure 4.14 displays the tradeoff between the absorbed and total mass of the selected parts in all iterations. As shown in the 1st (first) iteration of the design space, responses and design points have resulted in a most extensive and widely spread. Furthermore, more focused design points are identified to obtain a new optimum result. The force vs displacement plots history of all simulations is presented, as depicted in Figure 4.15. However, the output histories of force-displacement curves are obtained by the cross plots of force and displacement in LS – OPT[109]. From response history, the minimum and maximum reaction forces are 13.7 kN and 25 kN, respectively. It occurred at the first iteration.

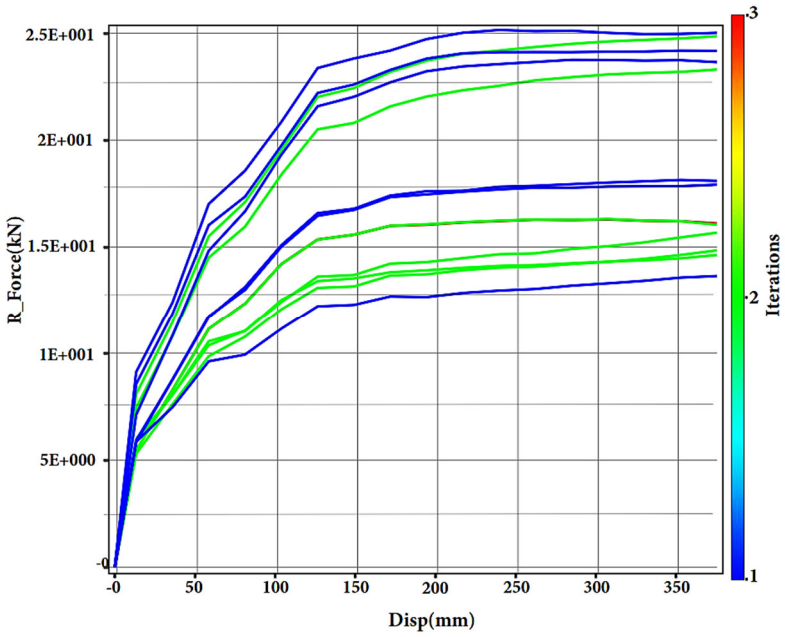

Figure 4.15: The history of force vs displacement in all iterations

The metamodel adequacy for the linear-based response surface function of absorbed energy in all iterations is displayed in Figure 4.16 and Figure 4.17.

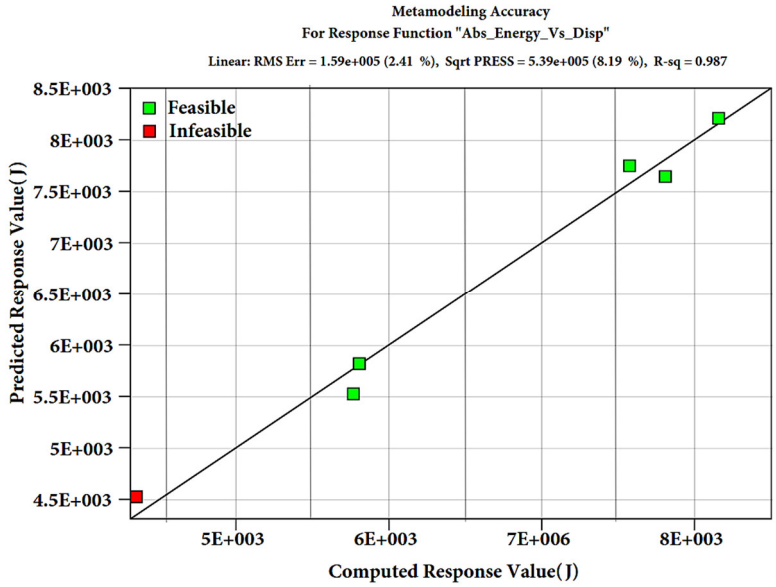

Figure 4.16: Metamodeling adequacy for a response of absorbed energy in the first iteration

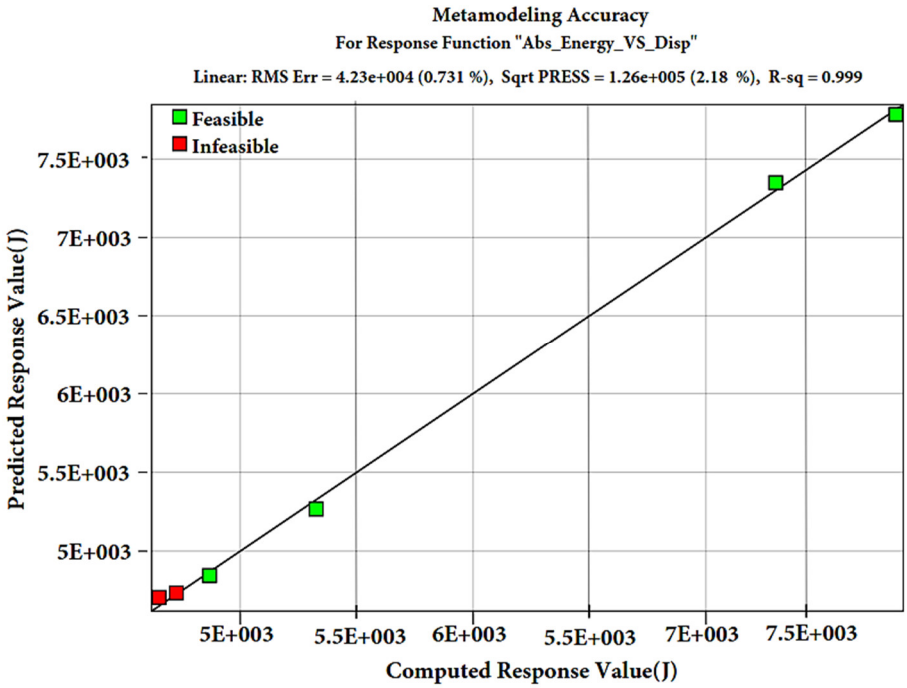

Figure 4.17: Metamodeling adequacy for the response of absorbed energy in the second iteration

To determine the best quality of the fit during metamodel adequacy for responses, the error of root mean square (RMS) and the square (R^2) should be small and higher, respectively[28], [109]. Thus, the perfect fit (R^2 =1) was found in both iterations for the mass parts response. However, the R^2 of the absorbed energy response in the first and second iterations equals 0.987 and 0.999, respectively. This result denotes an almost perfect fit for all iteration.

Table 4.7 illustrates the metamodeling errors in the linear response approximation for all responses of iterations.

Table 4.7: Metamodeling errors in linear metamodel for two responses

Response	***Metamodel type***	***RMS error(ε_{RMS}), (%)***	***Sqrt_press(ε_{Max}), (%)***	***R-sq(R^2)***
total mass_parts	Linear – iter- 1	4.88e-8	1.69e-7	1
total mass_parts	Linear – iter- 2	6.44e-8	2.01e-7	1
Absorbed energy	Linear – iter- 1	2.41	8.19	0.987
Absorbed energy	Linear – iter- 2	0.731	2.18	0.999

Figure 4.18 a) to c) displays the parts' thickness variable in design optimization history (red color). The blue color plots also represent the bounds of variables as per manufacturable in each number of iterations. In optimization history, both variables, the thickness of the rails (trail) and roof (troofa) section was decreasing to reduce the mass of parts (see Figure 4.18 b) & c)). However, the optimization history for the thickness of pillars(tplr) is constant, which means the thickness of the

pillars is restricted to fulfill the constraint value of the response of absorbed energy within a lightweight.

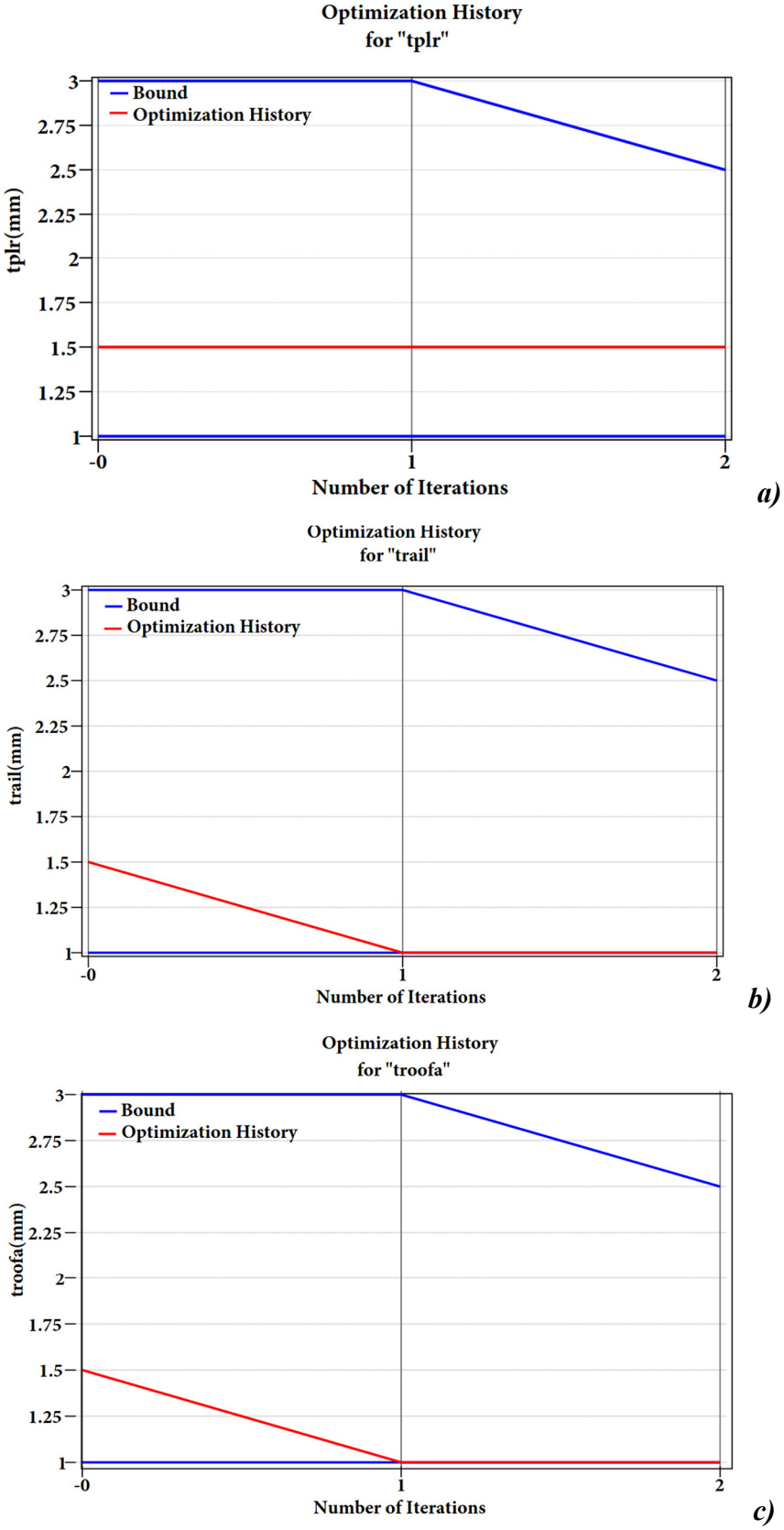

Figure 4.18: Optimization history and bound for all variables; a) Pillars (tplr), b) Rails(trail) and c) Roof(troofa)

In Figures 4.19 & 4.20, the history of optimization presents the response of mass parts and absorbed energy. The decreasing rail and roof thickness reduced the mass of all parts from 0.176 tons (176 kg) to 0.145 tons (145 kg), equal to 17.6 %. At the same time, the increase of the thickness in the vertical pillars (*tplr*) increases the value of absorbed energy. Moreover, it improves the energy absorbing capacity of the bus structure (energy requirement of ECE R66 Standard).

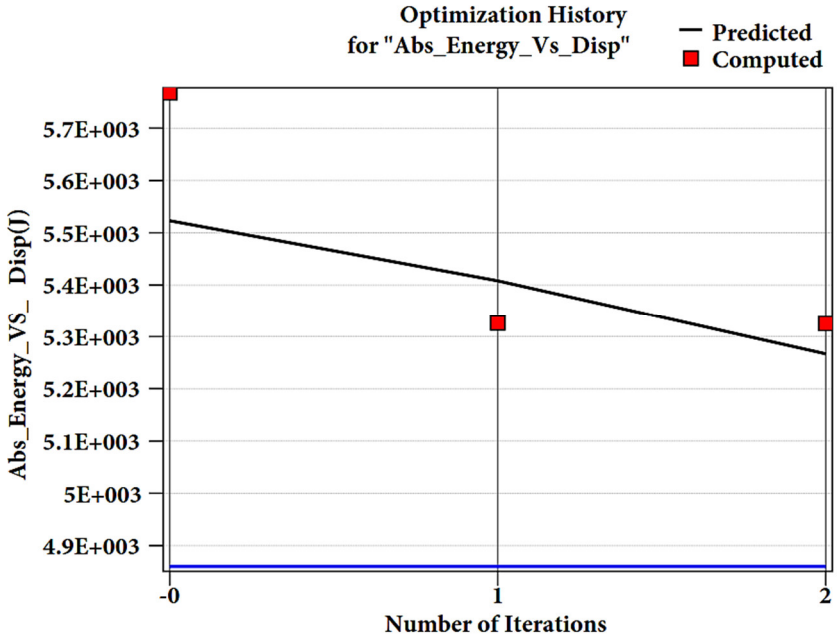

Figure 4.19: Optimization history for the absorbed energy of the models

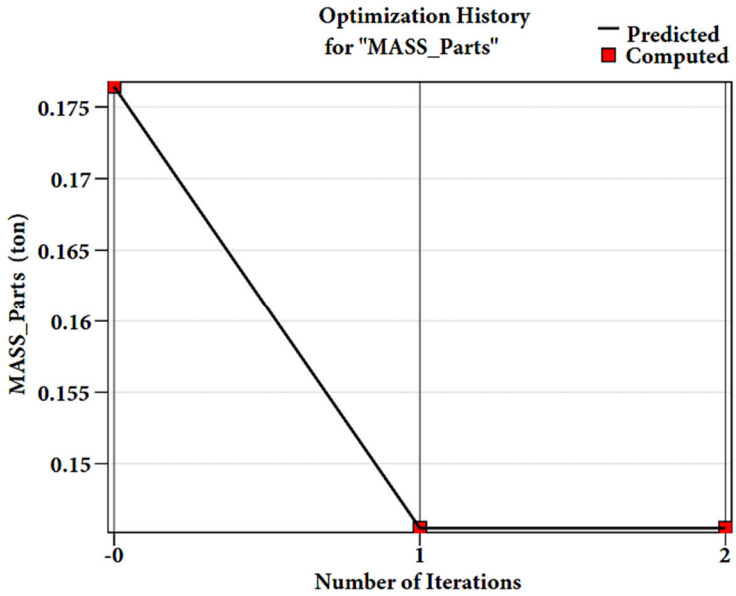

Figure 4.20: Optimization history for the mass of the parts

4.5 Combined Design for Static and Rollover analysis

Combining models using a manual approach is crucial to improve the stiffness of the bus structure[101]. As mentioned earlier, the two numerically optimized models (model – II_{stat} (RSO) and model - II_{roll} (SRSM)) were determined due to the variation of FE analysis in the static and

rollover case. However, the midi-bus structure should have a single model to satisfy the strength in both analysis cases. Furthermore, in this study, the new model can be modified manually to improve statical stiffness and crashworthiness capability for static and rollover cases. This model can be the final model presenting maximized strength within a level of weight.

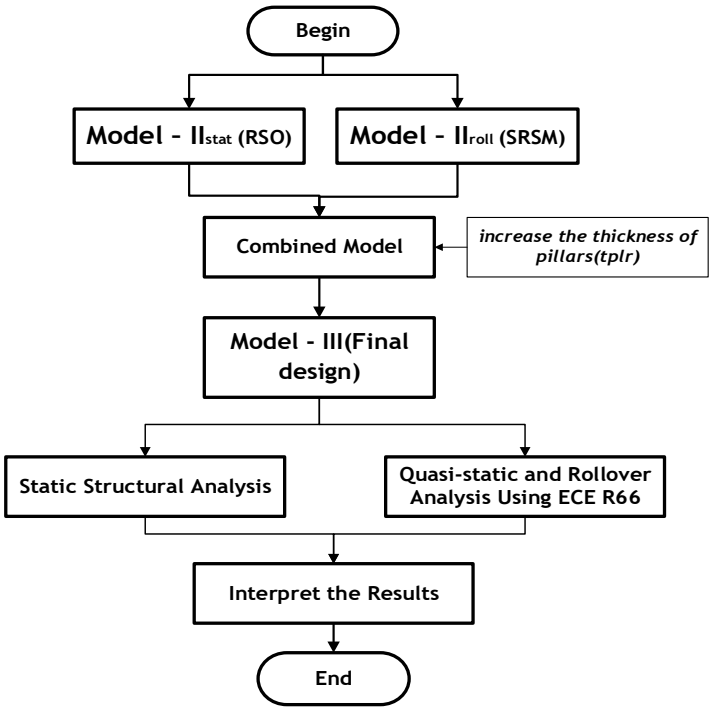

Figure 4.21: Process of the combined design approach for both static and rollover analysis

During this combined design approach, both models (model – II_{stat} (dark blue color) and model – II_{roll}(red color)) structural configurations are merged to find the better structural strength of the bus during static and rollover cases, as shown in Figure 4.22. This combination takes place by manually substituting the thickness of the parts obtained from both models.

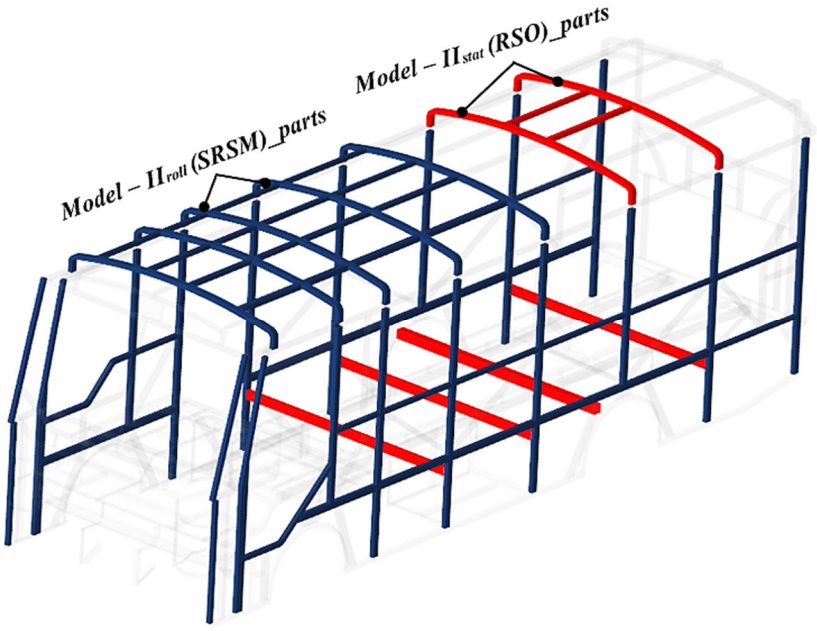

Figure 4.22: Combined configuration of the model – II_{stat} and model – II_{roll}

From quasi- static optimization results mentioned earlier, the thickness of vertical pillars increases, the strength of the structure also increases during rollover case. At that moment, the thickness of vertical pillars(tplr) increases from 1.5 mm to 2.5 mm. Lastly, the final model (model - III) can be modeled for all FE analysis cases.

Generally, the total mass of the structure's combined design (model – III) was equal to 563.9 kg, and this means the mass of model – III was reduced by 2.33 %, compared to a baseline model. However, the weight of the reinforced model (model – I (RD)) is less than the combined model (model – III) by 3.06 %.

Chapter Five

Results and Discussion

5.1 Static Strength Analysis Results

During the statical strength analysis, the output parameters (total deformation, stress, stiffness, and weight) of the baseline and the threes design optimizations of the midi-bus structure are presented and discussed based on the loading cases.

5.1.1 Pure Bending (Vertical Bending) Case

In the pure bending load mode, the minimum deformation was located at the frontal parts, passenger compartment parts, and frontal-side part of the structure, as shown in Figure 5.1. The baseline model of the bus structure has the most considerable deformation (6.2 - 6.5 mm) located at the location of luggage on roof parts due to the weight of roof luggage (see Figure 5.1 a).

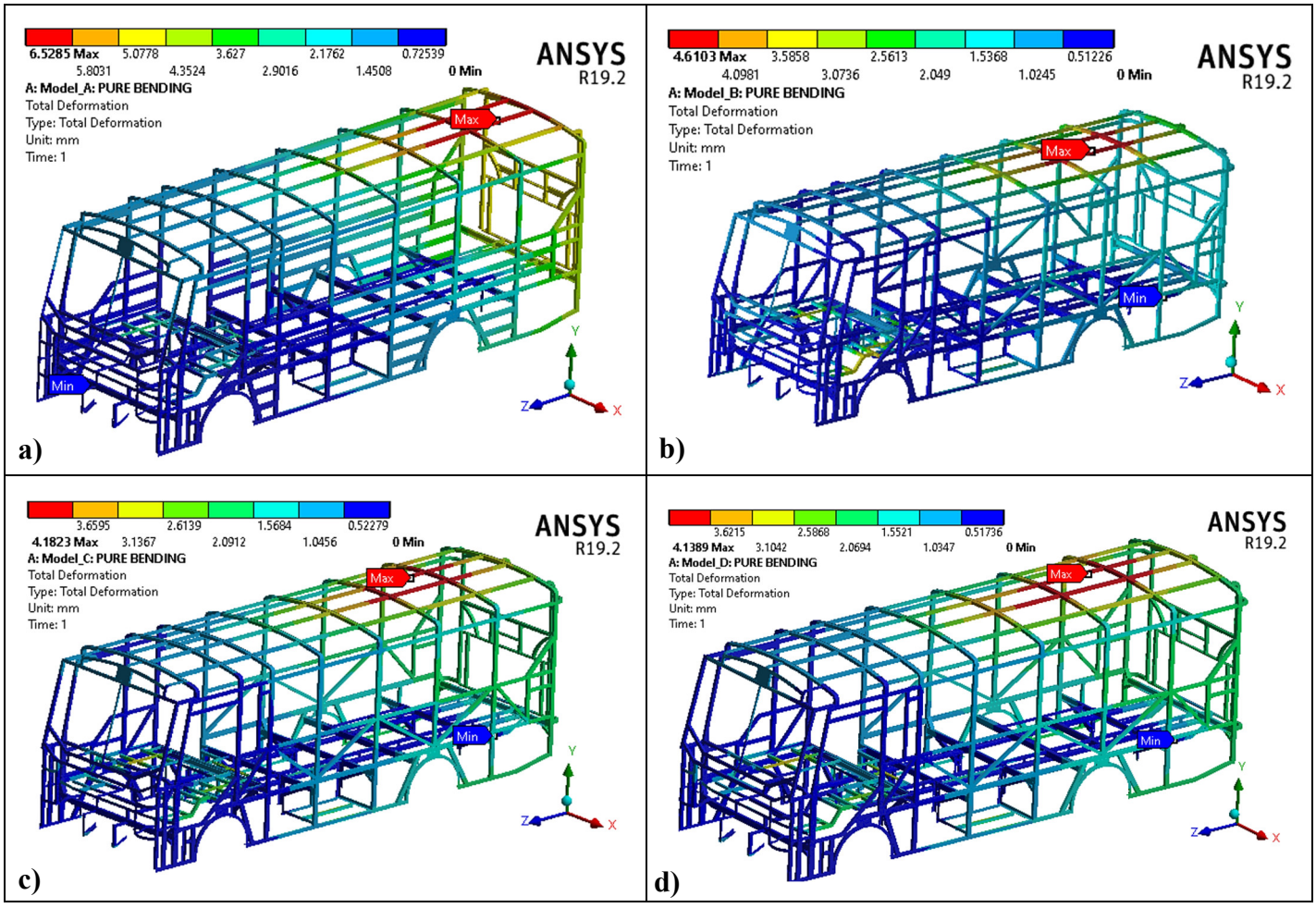

Figure 5.1: Total deformation in pure bending: (a) Baseline model; (b) Model – I(RD); (c) Model – II(RSO) and (d) Model – III

The total deformation of the reinforced model in pure bending decreased by 29.4 %. In addition, MOGA optimization techniques also reduced the deformation of the reinforced model by 9.11 %. Moreover, Model - III has a lower deformation than other models, shown in Figure 5.1 d).

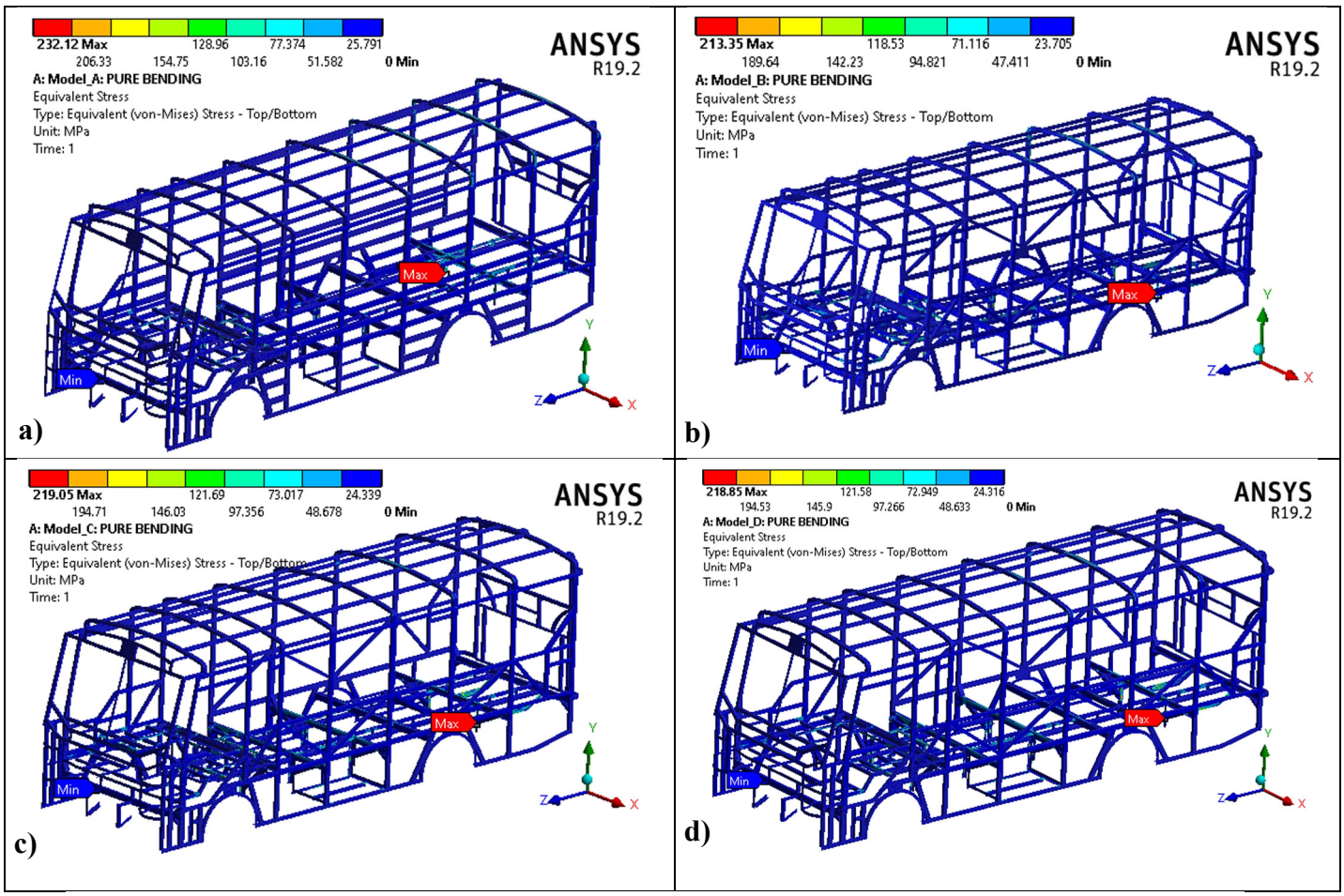

Figure 5.2: Equivalent stress in pure bending: (a) Baseline model; (b) Model – I(RD); (c) Model – II(RSO) and (d) Model – III

In the pure loading case, the equivalent stress of bus structure is decreased from 232 MPa to 213.35 MPa by reinforcement design, as shown in Figure 5.2 (a) - d)). Moreover, the equivalent stress of Model – II(RSO) and Model - III equals 219 MPa and 218.85 MPa, respectively. The maximum equivalent stress is located at the floor supports (hole of bolted parts).

5.1.2 Pure Torsion (Longitudinal Torsion) Case

Figure 5.3 depicts that the most considerable deformation of four the baseline (original) model is 6.32 mm, which is still located on the roof luggage of the bus structure. Furthermore, the maximum deformation of the reinforced model is 5.6 mm and occurs at the frontal structure. However, MOGA optimization techniques also reduced the deformation of the reinforced model by 3.57 %. Model – III has the same deformation as Model – II(RSO) in this loading case.

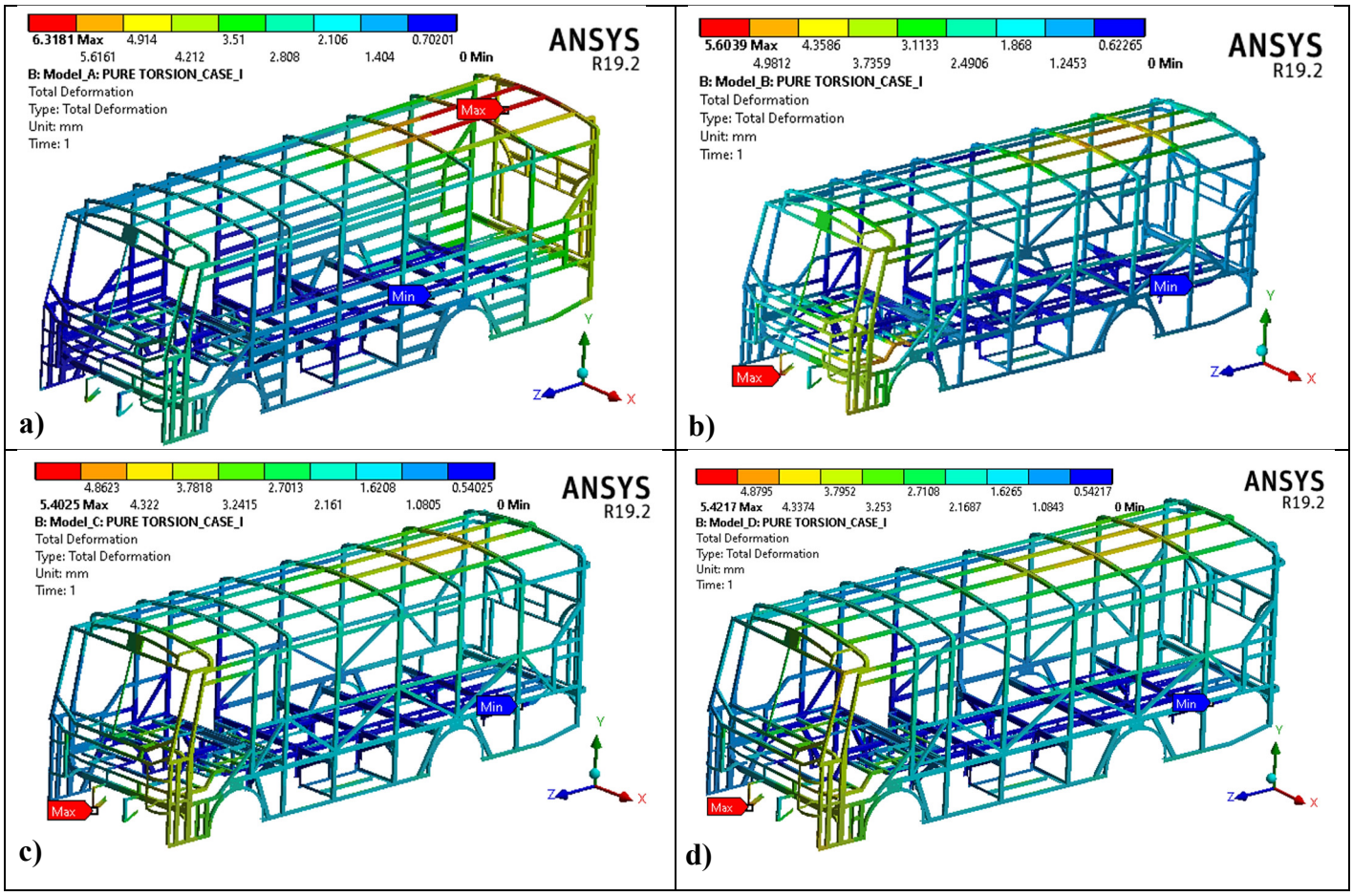

Figure 5.3: Total deformation in pure torsion: (a) Baseline model; (b) Model – I(RD); (c) Model – II(RSO) and (d) Model – III

The most considerable equivalent stresses of the baseline model, Model – I, Model – II, and Model – III are 230 MPa, 221.62 MPa, 229 MPa, and 228.8 MPa, respectively, as shown in Figure 5.4. The maximum equivalent stresses are located at floor parts and bolted parts (hole of L-shaped frame) for all models. Moreover, the reinforced model has less equivalent stress in the torsional load case than the other models.

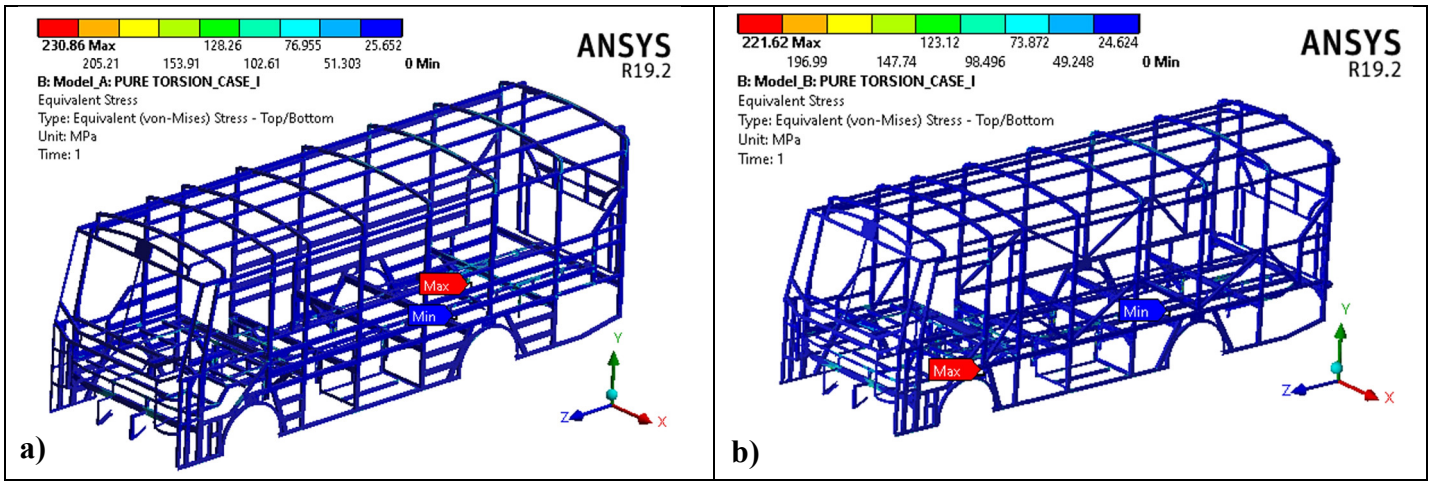

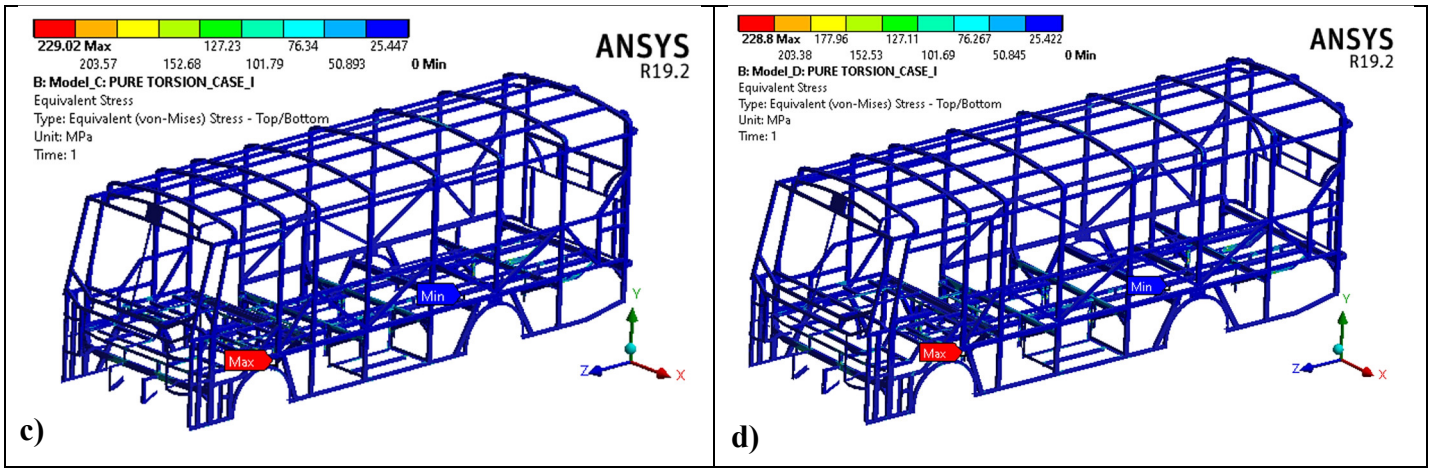

Figure 5.4: Equivalent stress in pure torsion: (a) Baseline model; (b) Model – I(RD); (c) Model – II(RSO) and (d) Model – III

5.1.3 Emergency Breaking (Longitudinal) Case

Figure 5.5 describes that the contour of deformation of four models during the breaking loading case. In this loading case, the total deformation of Model – I, Model – II, and Model – III decreased by 18.5 %, 26.13 %, and 26.62 %, compared to a baseline model.

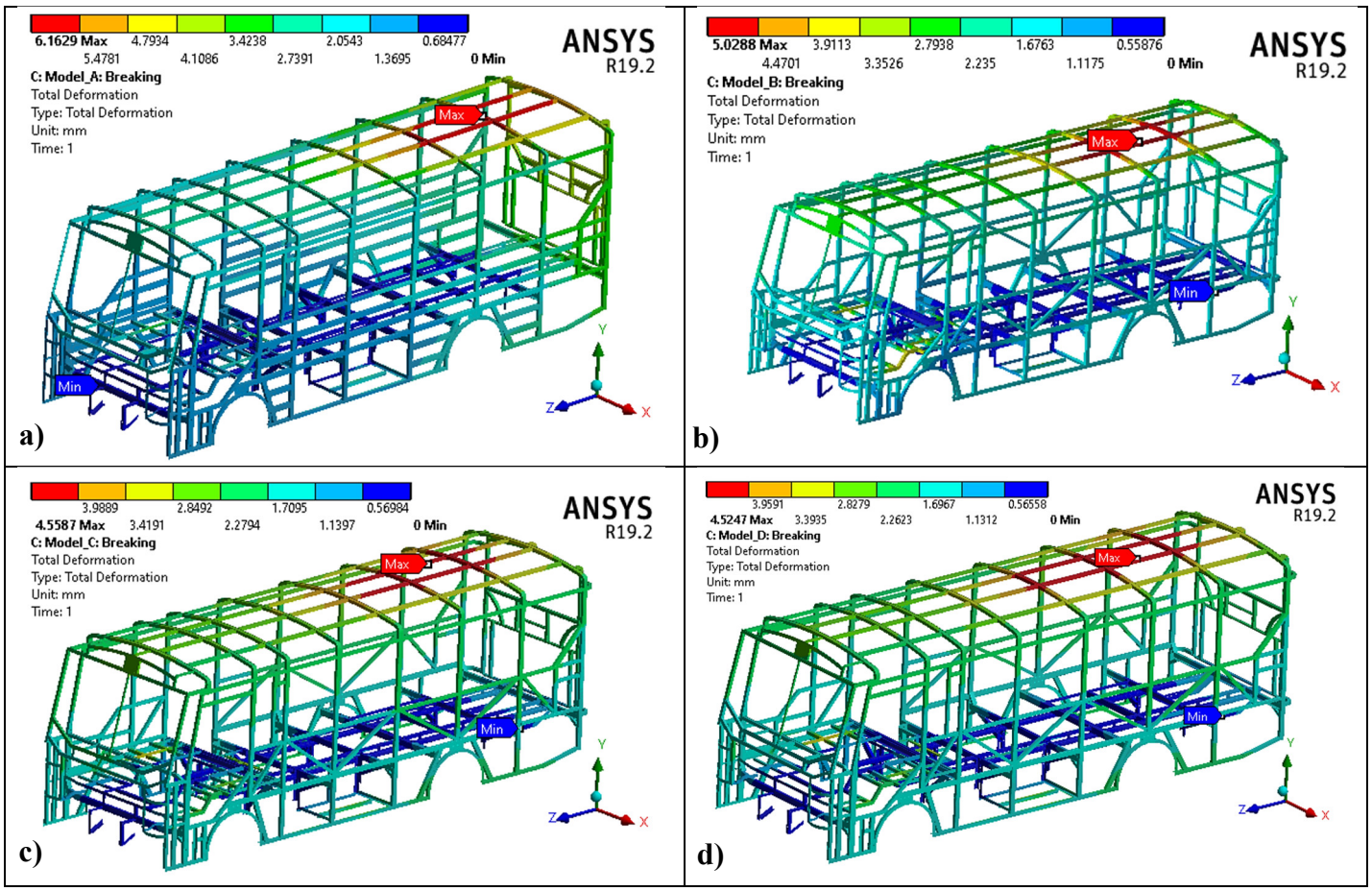

Figure 5.5: Total deformation in emergency breaking(longitudinal) case: (a) Baseline model; (b) Model – I(RD); (c) Model – II(RSO) and (d) Model – III

In this section, the equivalent stresses of the original and reinforced models are 223.75 MPa and 214 MPa, respectively, as shown in Figure 5.6 a) & b). Moreover, the equivalent stresses of the model – II and model – III models are 223.14 MPa and 219.4 MPa, respectively, as shown in Figure 5.6 c) & d). The maximum equivalent stresses are still located at floor parts and bolted parts (hole of L-shaped frame) for both models. However, maximum von Mises stress of the original and reinforced model is located at frontal-floor parts and rear-floor parts.

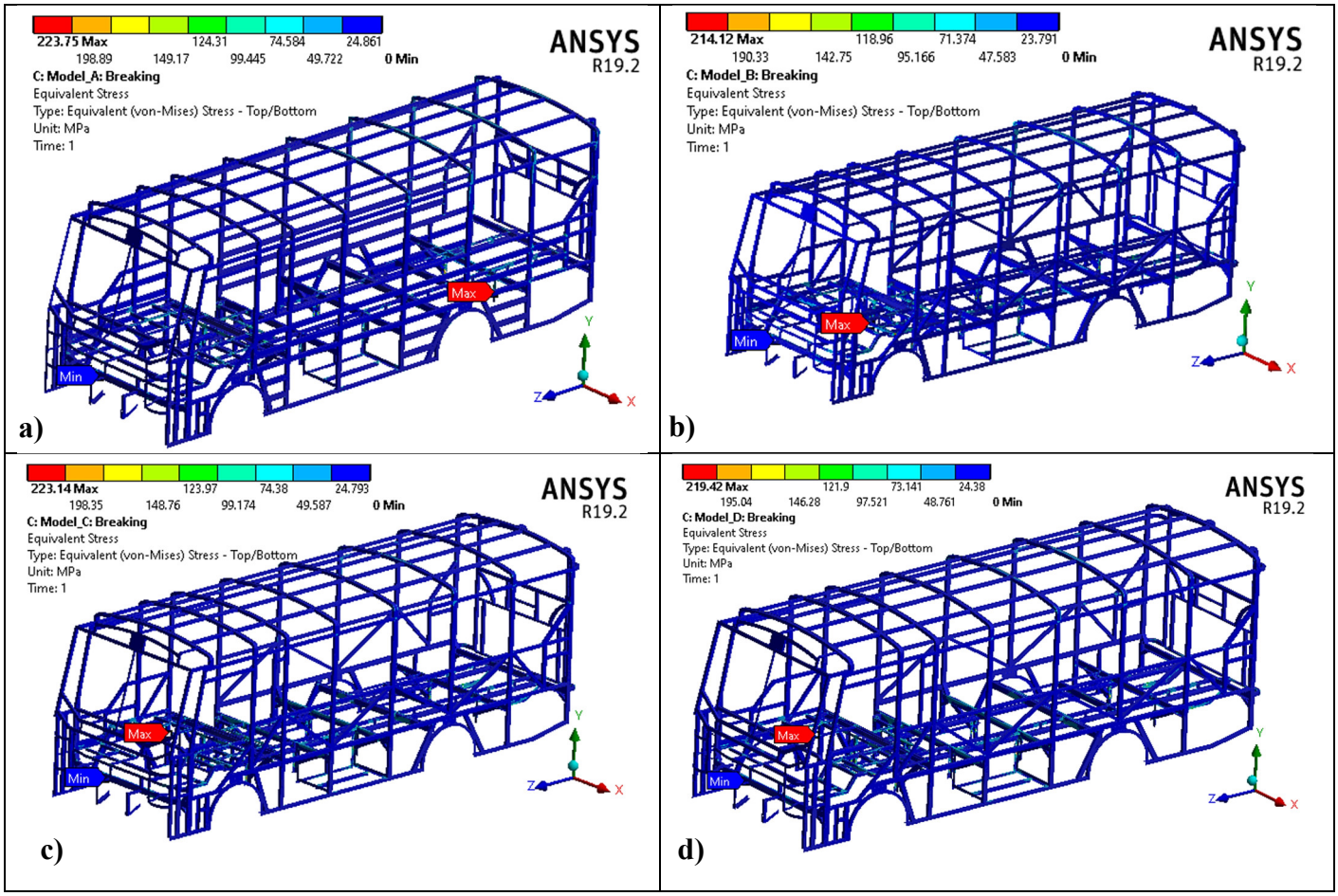

Figure 5.6: Equivalent stress in emergency breaking(longitudinal) case: (a) Baseline model; (b) Model – I(RD); (c) Model – II(RSO) and (d) Model – III

5.1.4 Lateral Bending (Cornering/Steering) Case

In the load case of emergency steering, the original model, model - II, and model - III of the bus structure have the most considerable deformation (10.04 - 12.78 mm) located at the location of luggage and rear frames on the roof parts due to both the weight of roof luggage and lateral gravitational load (see Figure 5.7 a, c & d). However, the maximum deformation of the reinforced model was 9.4 mm, only located luggage parts on the roof section (see Figure 5.7 b).

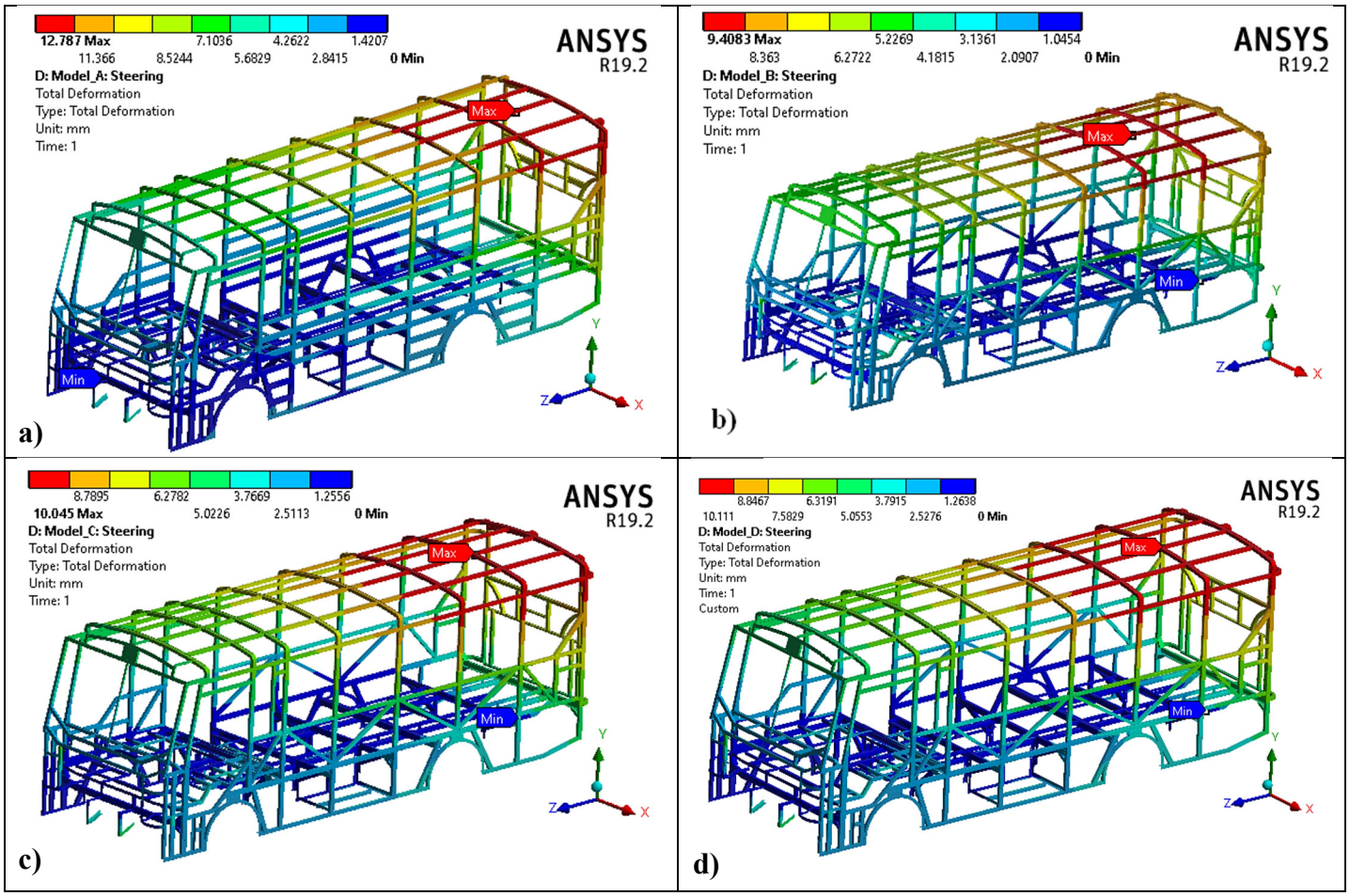

Figure 5.7: Total deformation in lateral bending(steering): (a) Baseline model; (b) Model – I(RD); (c) Model – II(RSO) and (d) Model – III

The original model, model - II, and model - III of the bus structure have the most considerable maximum equivalent stress (255 - 272 MPa) still located at the location floor parts and bolted parts (hole of L-shaped frame) (see Figure 5.8 a, c, & d). However, the maximum equivalent of the reinforced model was 238.75 MPa (see Figure 5.8 b).

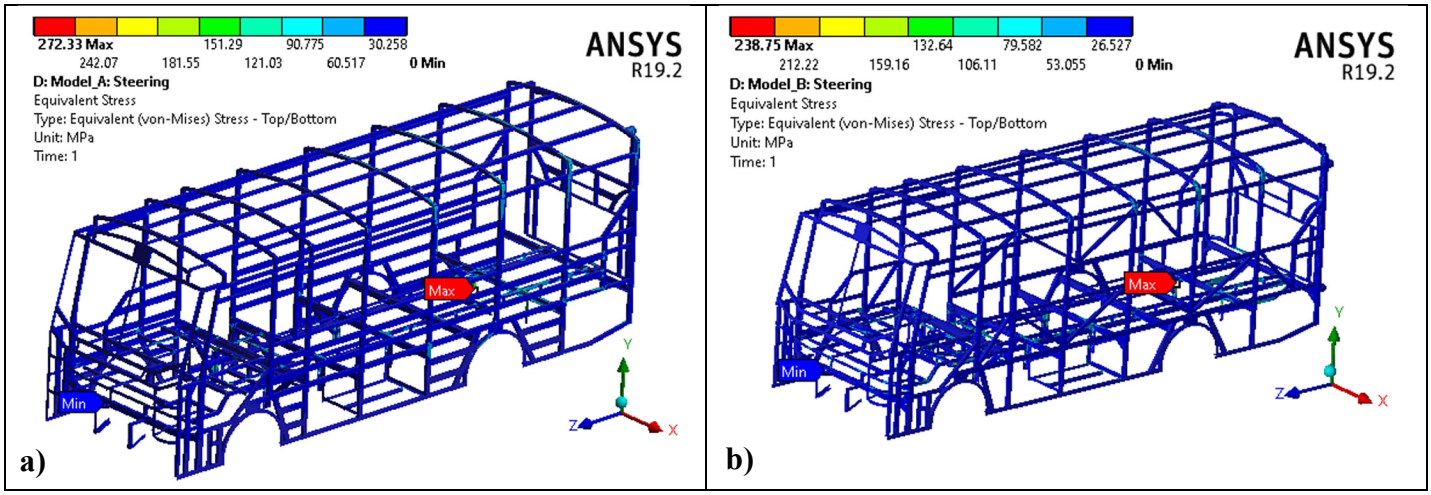

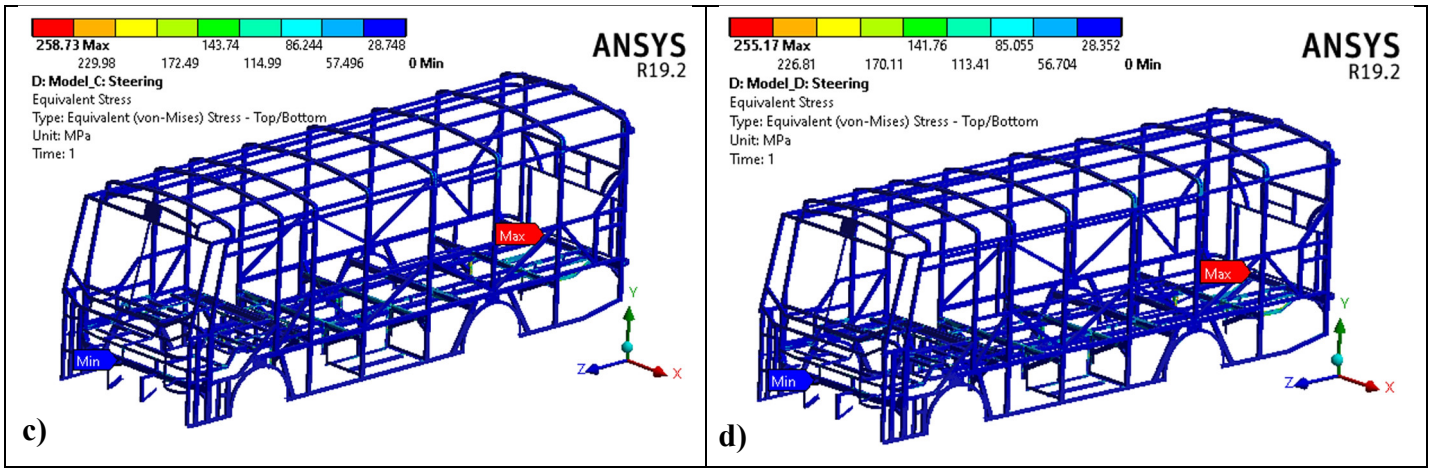

Figure 5.8: Equivalent stress in lateral bending(steering): (a) Baseline model; (b) Model – I(RD); (c) Model – II(RSO) and (d) Model – III

Generally, The maximum equivalent stress of the structure should not exceed the material's yield stress and meet the strength conditions [110]. Thus, all maximum stress of models was obtained below the yield strength of the material, as shown in Table 5.1.

Table 5.1: Comparison of baseline model & other alternative models in all loading case

Loading conditions		***Baseline Design***	***Model - I (RD)***	***Model – II$_{stat}$ (RSO)***	***Model – III***
Pure Bending	*Total Deformation(mm)*	6.53	4.61	4.19	4.13
	Equivalent Stress (MPa)	232.12	213.35	219.05	218.85
	Bending stiffness(N/mm)	4589.5	6500.9	7152.6	7256.5
Pure Torsion	*Total Deformation(mm)*	6.32	5.60	5.40	5.42
	Equivalent Stress (MPa)	230.86	221.62	229.02	228.8
	Torsional Stiffness (Nm/deg)	1379.93	1553.24	1604.31	1600.32
	Angle of Rotation(deg)	0.84	0.74	0.69	0.71
Emergency Breaking	*Total Deformation(mm)*	6.16	5.03	4.55	4.52
	Equivalent Stress (MPa)	223.75	214.02	223.14	219.42
Emergency Steering	*Total Deformation(mm)*	12.79	9.41	10.04	10.11
	Equivalent Stress (MPa)	272.33	238.75	258.73	255.17
Bus structure	*Total Mass(kg)*	577.35	547.15	532.70	563.90

Table 5.1 displays a summary of results under four loading conditions in the static strength analysis. First of all, the weight of a bus structure reduced from 577.35 Kg to 547.15 Kg by 5.23

% (see Table 5.1). This result indicates that removing the connecting member (U-channel) from the sides section and adding the inclined supports can effectively reduce the structure's weight. Furthermore, the MOGA Optimization was minimized the reinforced model from 547.15 kg to 532.70 kg by 2.64 % through-thickness variation of the roof and floor parts of the structure. However, the mass of baseline and Model – III has a difference of 2.32 %.

Figure 5.9 presents the result of the deformation of the four models in four loading conditions. The total deformation of the reinforced model in pure bending, pure torsion, steering, and breaking decreased by 29.4 %, 11.39 %, 18.34 %, and 26.42 %, respectively. Accordingly, the reduction of deformation showed that the reinforced design is stiffer than the original design. Moreover, MOGA optimization techniques also reduced the deformation of a reinforced model by 9.11 %, 3.57 %, and 9.54 % for all cases except the steering loading case. Furthermore, Model–III's deformation is similar to model – II(RSO) in all loading cases, as shown in Figure 5.9.

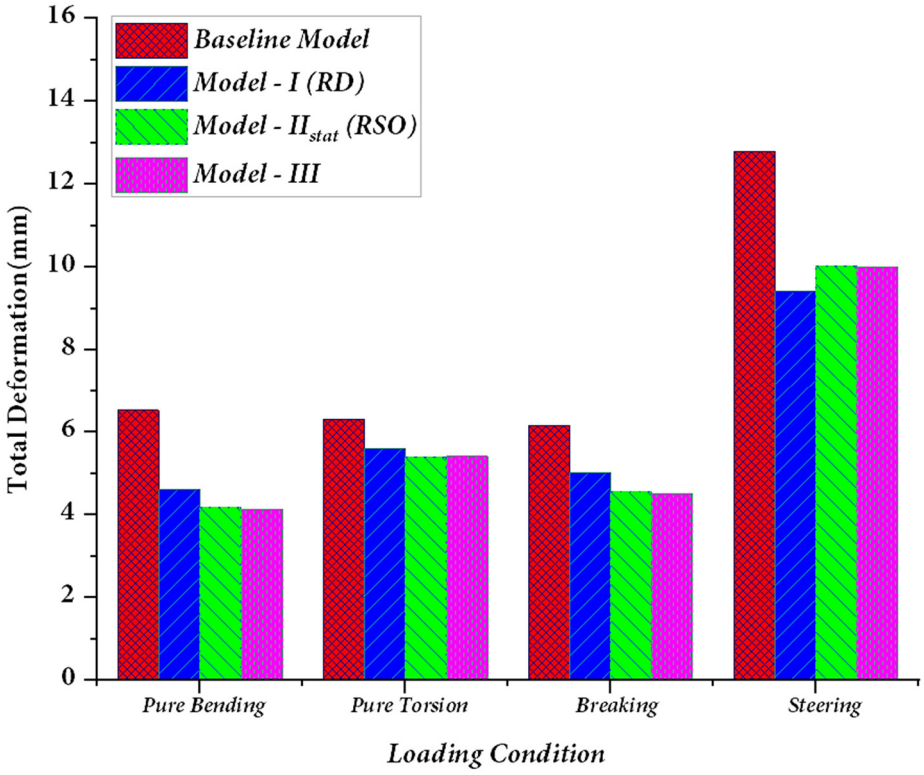

Figure 5.9: Comparison of deformation between four models

The frame strength and stiffness are indicators for the behavior of bus structures[111]. This section presented the maximum bending and torsional stiffness obtained in the cases of static analysis for original, reinforced (model – I), Model – II(RSO), and Model – III design (see Figure 5.10). The bending stiffness difference between original and reinforced is 41.65 %. Moreover, the bending stiffness of the optimized (RSO) model increases by 10.02 % compared to the reinforced model. However, the difference in bending stiffness among models – II & III is 1.45 %. This result implies that model -III is stiffer than a model – II_{stat} in the bending case.

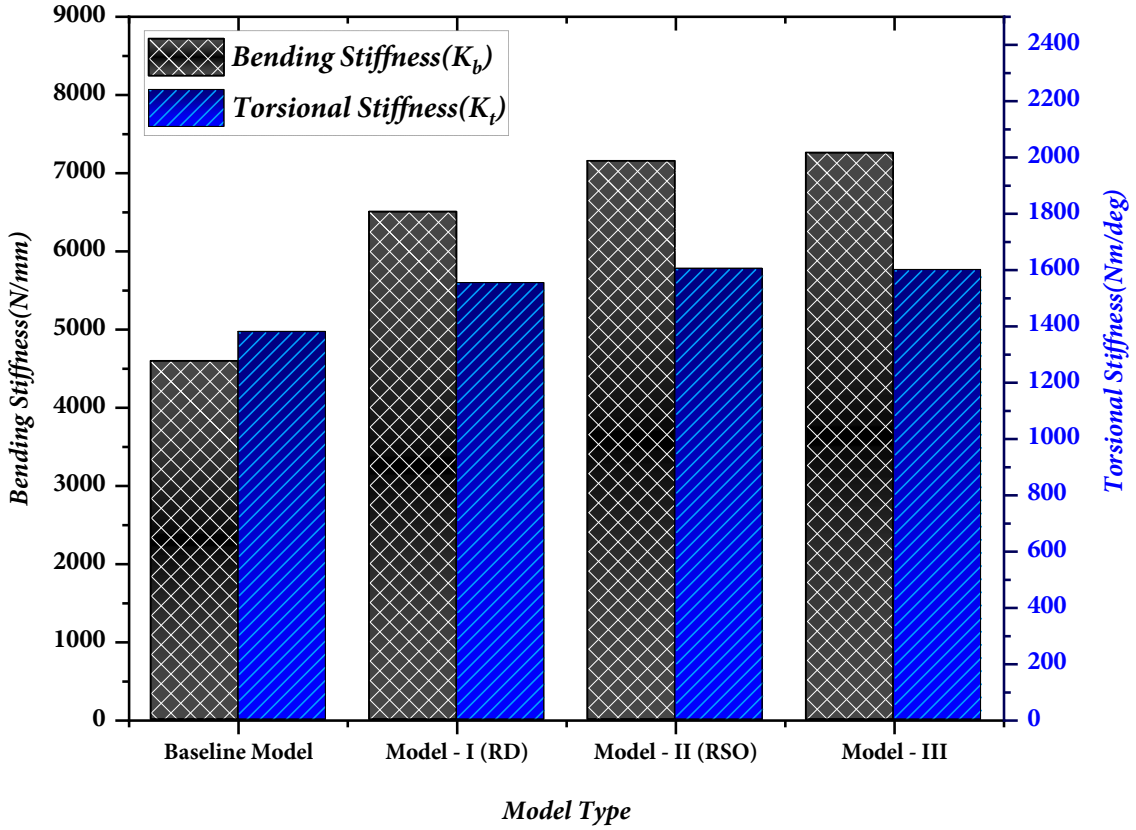

Figure 5.10: Comparison of stiffness among four models

In addition, a reinforced bus structure's torsional rigidity or stiffness increases from 1379.93 Nm/deg to 1553.24 Nm/deg. However, the difference in torsional stiffness among the reinforced vs. optimized models is 51.07 Nm/deg. The results indicate that the reinforced design with the Multi-objective Genetic Algorithm (MOGA) must be considered to obtain the stiffed structure during the static condition. Moreover, the difference in torsional stiffness between models – II & III is equal to 0.268 %.

Generally, the high stiffness within the reduced weight of the reinforced design can be obtained by changing the layout, crosse-section, and the addition of reinforcement of the baseline structure. Additionally, from both Response Surface Optimization and combined design approaches, it is possible to suggest that model – II(RSO) and model - III have a better-stiffed structure than others in both bending and torsional case.

5.2 Quasi-static Simulation Results

This study evaluates the reaction force and the absorbed energy parameters during a quasi-static simulation of the structure. The contour of stress specifies the maximum stress present at the contact area of impactor (rigid plate) loading, the joint areas of vertical pillar-roof, and the vertical pillar-floor section, as shown in Figure 5.11. A vertical pillar is highly intruded into residual space (RS) from the baseline simulation, as shown in Figure 5.11 b).

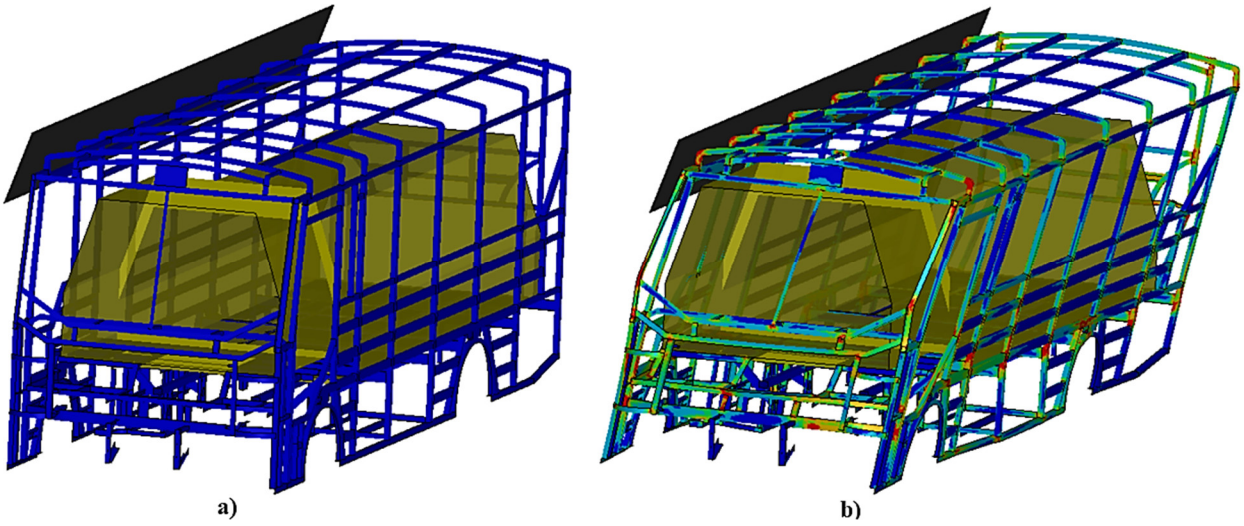

Figure 5.11: Stress distribution in baseline model of quasi-static simulation: a) initial stage and b) final deformed condition

During the quasi-static simulation, the impactor load gradually increased until it touched the residual space. Perhaps, At the displacement of 375 mm, the simulation was motionless. Although the peak reaction forces for each model changes differently based on the capacity of load resistance. Thus, Figure 5.12 displays the reaction force developed on the Baseline model, model – I, model – II, and model – III are 14.5 kN, 17.7 kN, 16.3 kN, and 20.2 kN. In addition, only the reinforced force converged after the displacement of 280 mm.

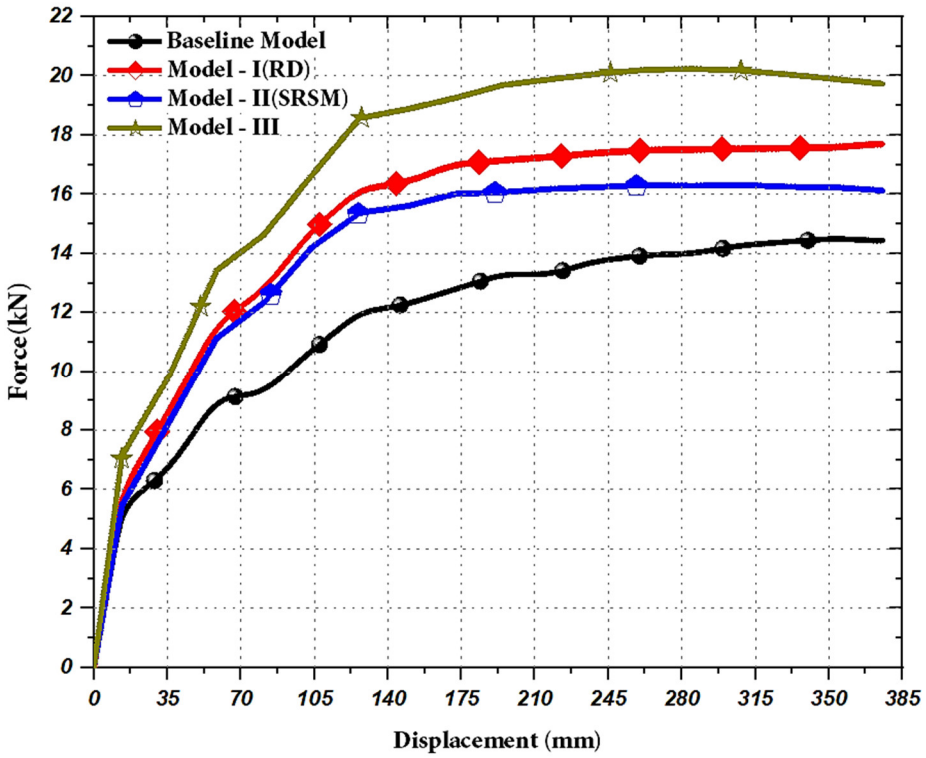

Figure 5.12: Force versus displacement graph for all models during quasi-static simulation

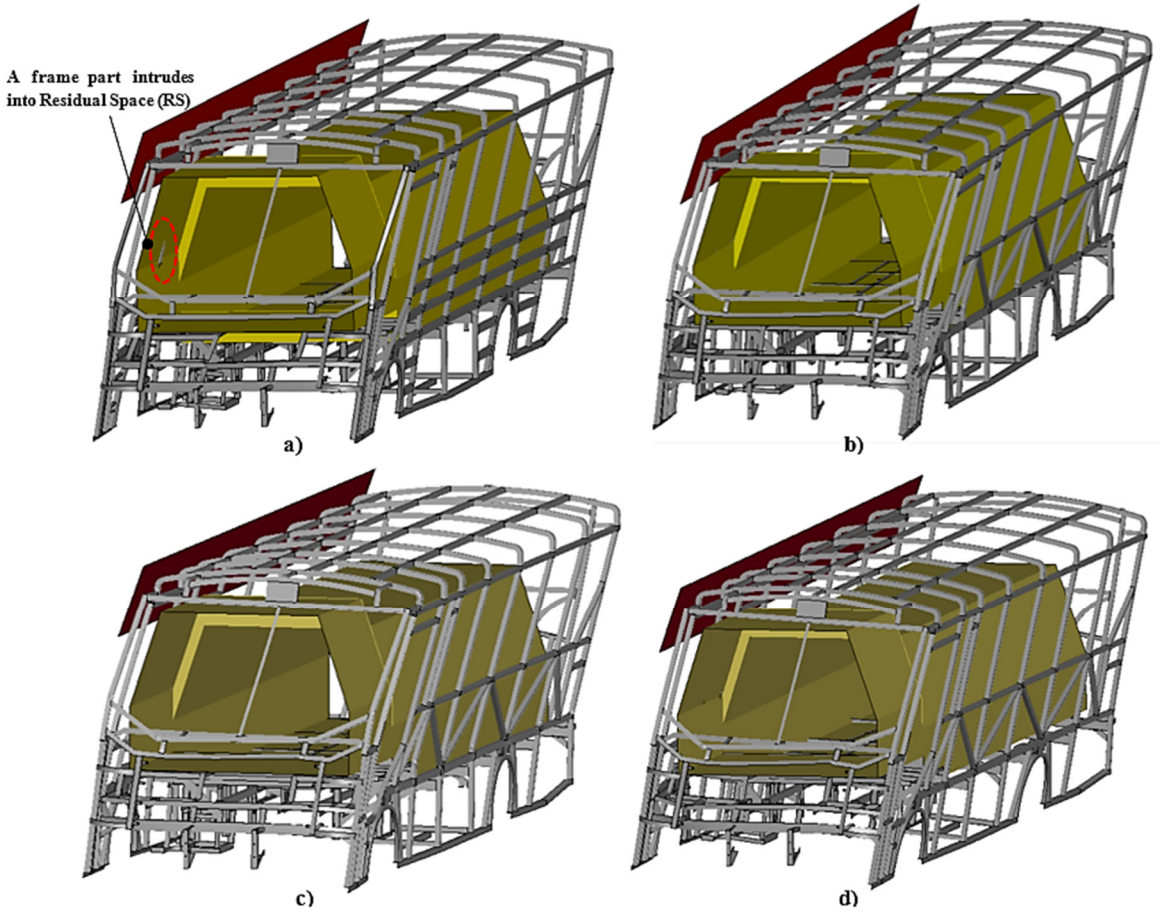

Figure 5.13: Final deformation of models at the quasi-static simulation: a) baseline model; b) model – I(RD); c) model – II(SRSM); and d) model – III

All the models for the quasi-static analysis, shown in Figure 5.13, follow the same deformation pattern when the cages' deformation is reached in a residual space. However, one of the baseline structural parts is intruded the residual space, shown in Figure 5.13 a).

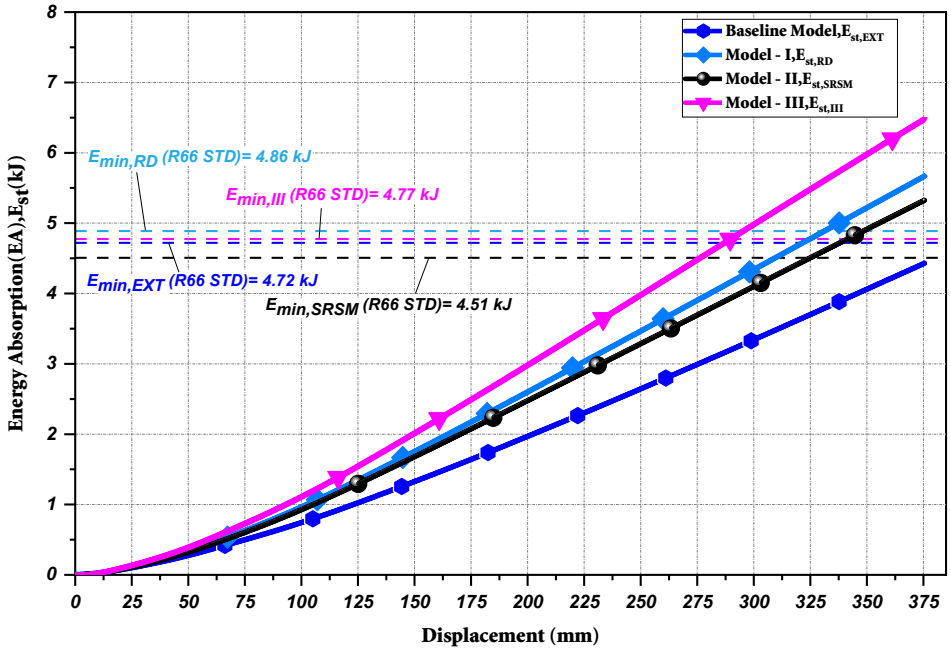

Figure 5.14: Comparison of energy absorption between baseline & alternative models

Figure 5.14 shows the minimum requirement of absorbed energies and energy absorbed by the structure (E_{st}) of the four structure models. The Absorbed energy of the baseline model, model – I(RD), model – II(SRSM), and model – III are 4.43 kJ and 5.67 kJ, 5.32 kJ, and 6.48 kJ, respectively. Accordingly, the energy-absorbing capability of bus structure ($E_{st,ext}$) is lower than the minimum value energy absorbed by the original bus structure ($E_{min,ext}$). This result also implies that the existing(original) bus structure fails the tests and causes one of the bays to touch the residual space, as shown in Figure 5.14. However, the reinforced energy absorption capacity ($E_{st,RD}$) is greater than the minimum requirement energy-absorbing structure ($E_{min,RD}$). Therefore, it was found that the reinforced structure passed the tests. Moreover, model - II(SRSM) and model – III also passed the requirement of the standard.

Notably, the reinforced (model – I) model is stronger than the baseline and model - II_{roll} (SRSM). However, model–III's absorbed energy increased by 14.3 %, compared to model – I(RD). This important finding is undoubtedly an equivalent method for the rollover test, as stated by UNECE R66.

5.3 Rollover Simulation Results

This study estimates the value of the internal energy of structure and seats in a baseline(original) tare – weight rollover case. Significantly, the internal energy of the structure's main components and bus sections compared to visualize their capacity throughout the simulation. During the tare–weight rollover case, the maximum deformation of the original structure was located at pillar A and bays (B1 – B3), as shown in Figure 5.15.

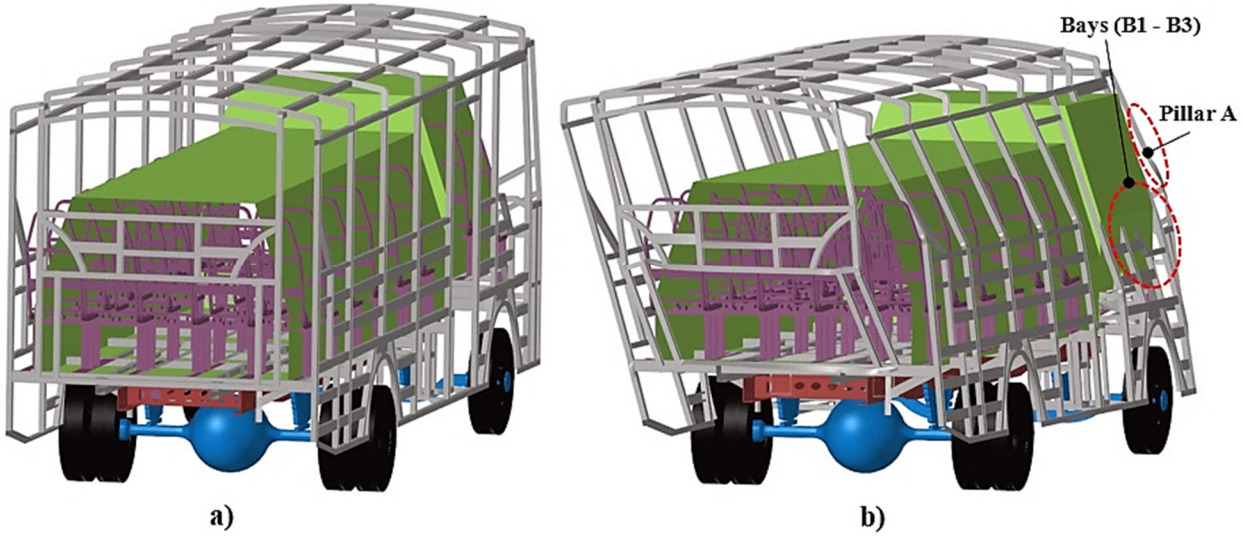

Figure 5.15: Deformation of original structure & seats frame in tare – weight rollover case: a) initial phase and b) maximum deformation

Additionally, the high deformation of seats presents at the first and second seats of the passenger. In the tare-weight rollover, the structure and seat's internal energies are 23.3 kJ and 0.85 kJ, respectively, as shown in Figure 5.16. In terms of percentage, the internal energy of the bus structure and seat represent 96.5 % and 3.5 % during a rollover crash.

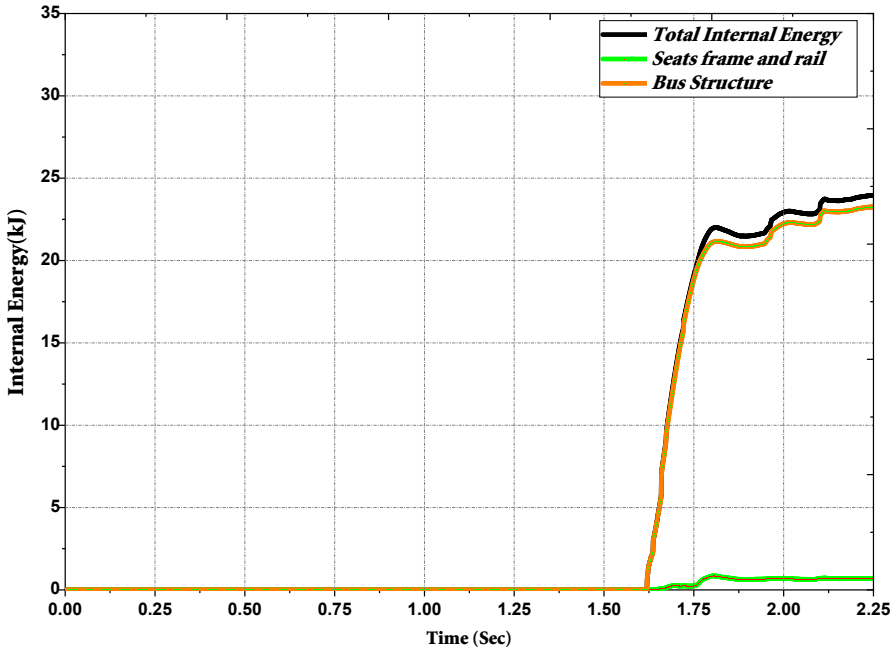

Figure 5.16: Internal energy of the bus structure and seats in tare-loading cases

The internal energy of the structure is higher than the internal energy of the seat frames. Moreover, this finding shows that when the absorbed energy of the frame is higher, the structural part of the midi-bus is the most significant for the strength of the rollover case. A similar conclusion was reached by (Cezary Bojanowski, 2009), [28], where the author has shown the effect of skin parts on the strength of bus in rollover crashes test. The screenshot of contour stress plots for the baseline model in the tare – weight rollover is shown in Appendix C (See Figure C1 – C3.) of this thesis.

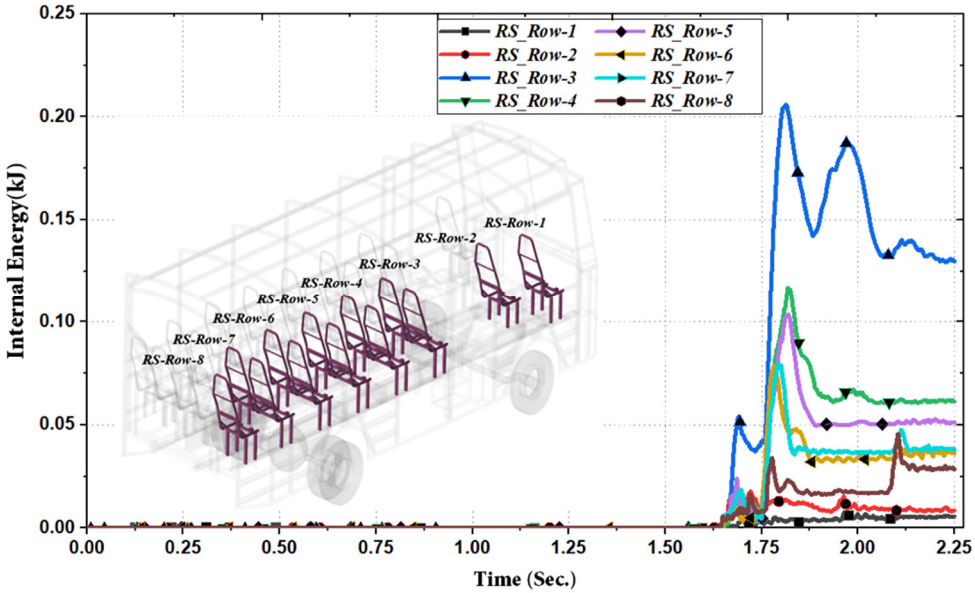

Figure 5.17: Internal energy of the right seat frame in original tare-loading cases

Figure 5.17 describes the energy absorbing capacity of the right seats' frames throughout rollover crashes. The maximum internal energies of the right seats from rows 1 to 8 are 0.01 kJ, 0.02 kJ, 0.21 kJ,0.12 kJ, 0.10 kJ, 0.08 kJ, 0.08 kJ and 0.05 kJ, respectively. This finding shows that the lower energy-absorbing occurs at the first and second seats of the passenger.

Although, the result of internal energy- time for six sections of the structure after the crash are plotted as shown in Figure 5.18. Accordingly, the minimum and maximum internal energy of 2.25 kJ and 6.56 kJ were obtained at the roof and right section of the bus structure because they are highly deformed until the rollover crash is stopped, leading to more energy absorption. Furthermore, the roof and front section have the lowest energy absorbing capacity because the rollover crash is not directly affected. Moreover, the convergence of the internal energy of bus sections starts at 0.4 seconds, except for the right and floor sections.

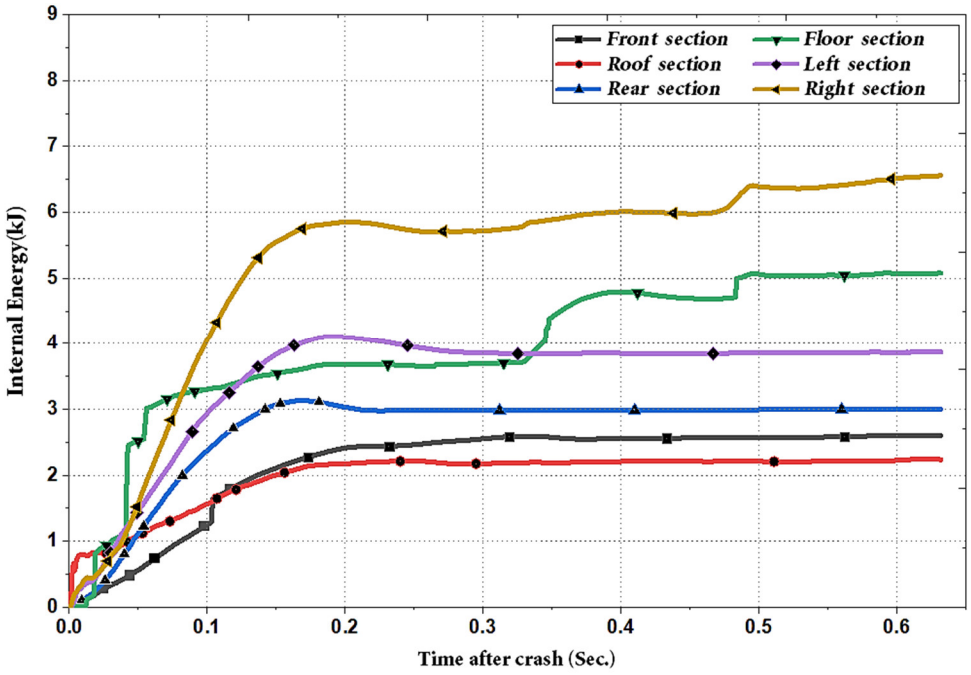

Figure 5.18: Internal energy of the bus structure sections in the original tare-loading case

The sum of each component's internal energy contributes to the overall energy capability of the structure after the crash. In addition, Figure 5.19. shows the internal energy of each component. The absorbed energy of the components differs depending on the deformation throughout the crash. Hence, the internal energy of the A & B pillar, roof arc member, vertical pillars, window-rail, waist rail, and skirt pillar are 1.42 kJ, 2.15 kJ, 1.90 kJ, 5.85 kJ, 0.15 kJ, 0.83 kJ, and 0.19 kJ, respectively. This result shows that the lowest and highest internal energy occurred at the window-rail and vertical pillar, respectively. Due to the high impact on the roof arc members and vertical pillar, the absorbed energy of these components is high compared to other components.

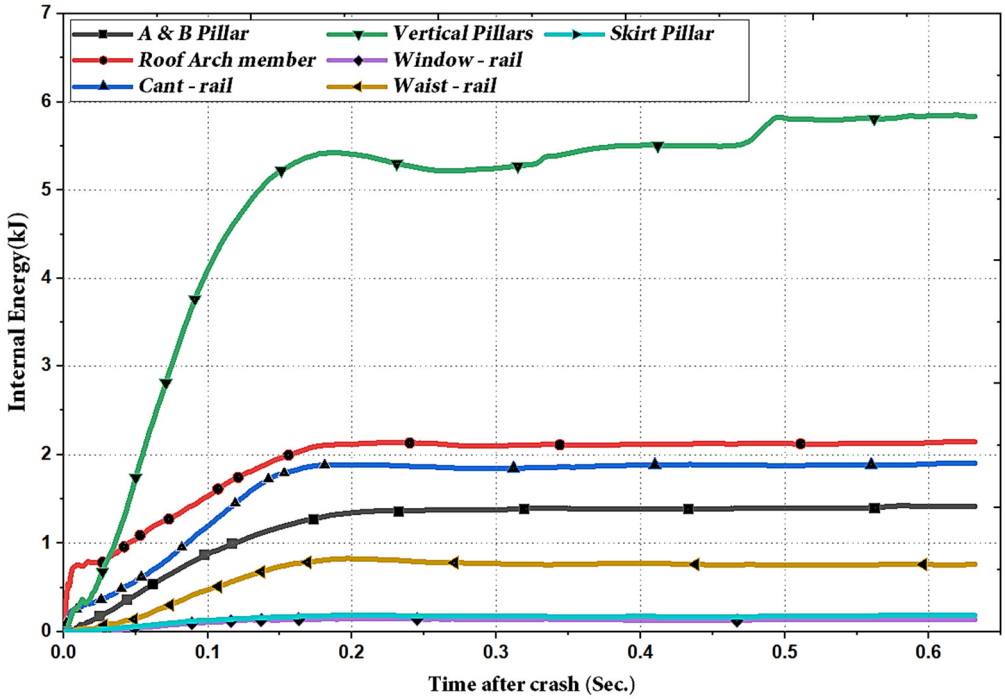

Figure 5.19: Internal energy of the components of the original model in tare-loading cases

5.3.1 Tare-weight of the bus with & without seat frame cases

Additionally, this work studies the effects of inertia and center of gravity (CG) on the tare-weight rollover crash. This section presented the rollover simulation results of tare weight for all tare-weight cases. Moreover, it was found that the internal and kinetic energy were determined to compare the structural strength of the two cases.

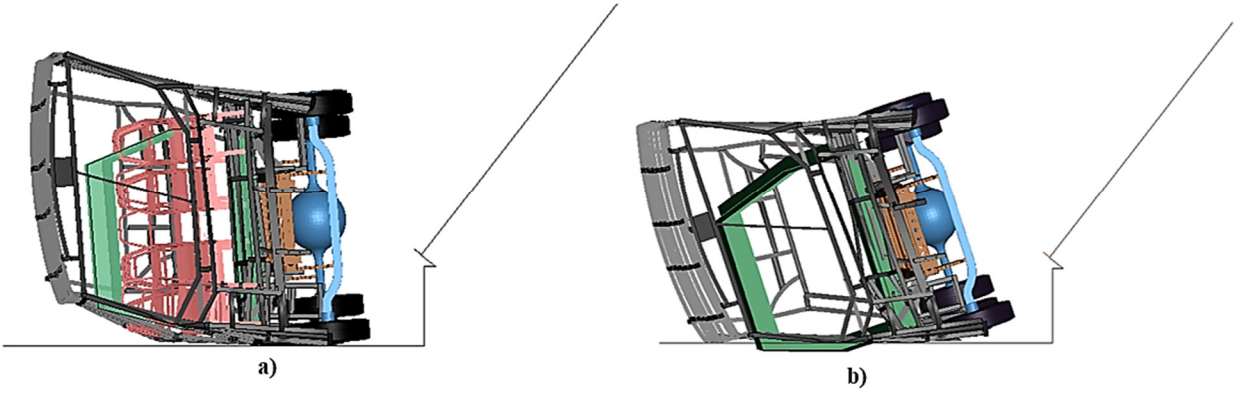

Figure 5.20: Comparison of deformation between all the two tare-weight cases: a) with seat frame (case – a) & b) without seat frame (case – b)

As described in Figure 5.20, the tare-weight deformation without seat frame (case - b) is greater than the tare- weight with the model of the seat frame (case - a). because of the distributed location of the mass of the seat frame, the center of gravity changes its positions in rollover crashes. Then, the center of gravity location occurs at the lower portion of the bus due to the distribution of seat mass on the floor. Moreover, the lower location of the center of gravity pushes down the tare-

weight without the seat frames model to practice the largest deformation after impacts. Also, the case b structural deformation increases until the structure passes away the residual space, shown in Figure 5.20 b).

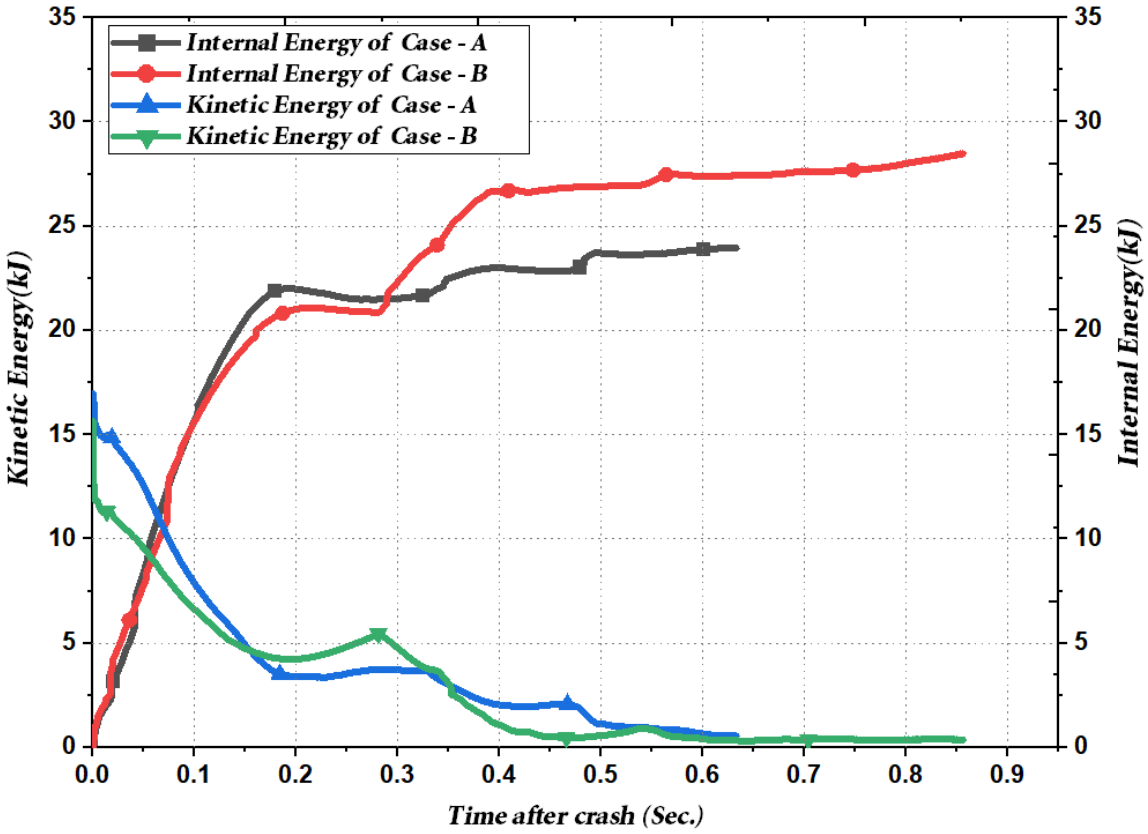

Figure 5.21: Internal energy for two cases of original tare-weight rollover simulation

Figure 5.21 illustrates that the absorbed energy in case a and b after impact are 23.94 kJ and 28.48 kJ, respectively. These two cases diverge due to the center of gravity (CG) location during the mass distribution of seats on the structure. The convergent of internal energy for cases a and b takes 0.5 and 0.6 seconds. The kinetic energy of case – a and b are 16.7 kJ and 15.6 kJ, respectively. However, the kinetic energy of case – b increases until it reaches from 0.2 sec to 0.3 sec, which means the center of gravity positions changes to push the bus down into the ground, shown in Figure 5.21. This result shows that case b is more deformed than case a throughout the rollover crash.

5.3.2 Rollover results at various loading Scenarios

As mentioned before, this study conducts a rollover simulation of the midi-bus for three loading cases. These scenarios measure the structural deformation and strength of the bus structure during different loading cases. In addition, the comparison of baseline and reinforced design evaluates according to deformation angle and angular deformation index parameters as mentioned in Figure 5.22.

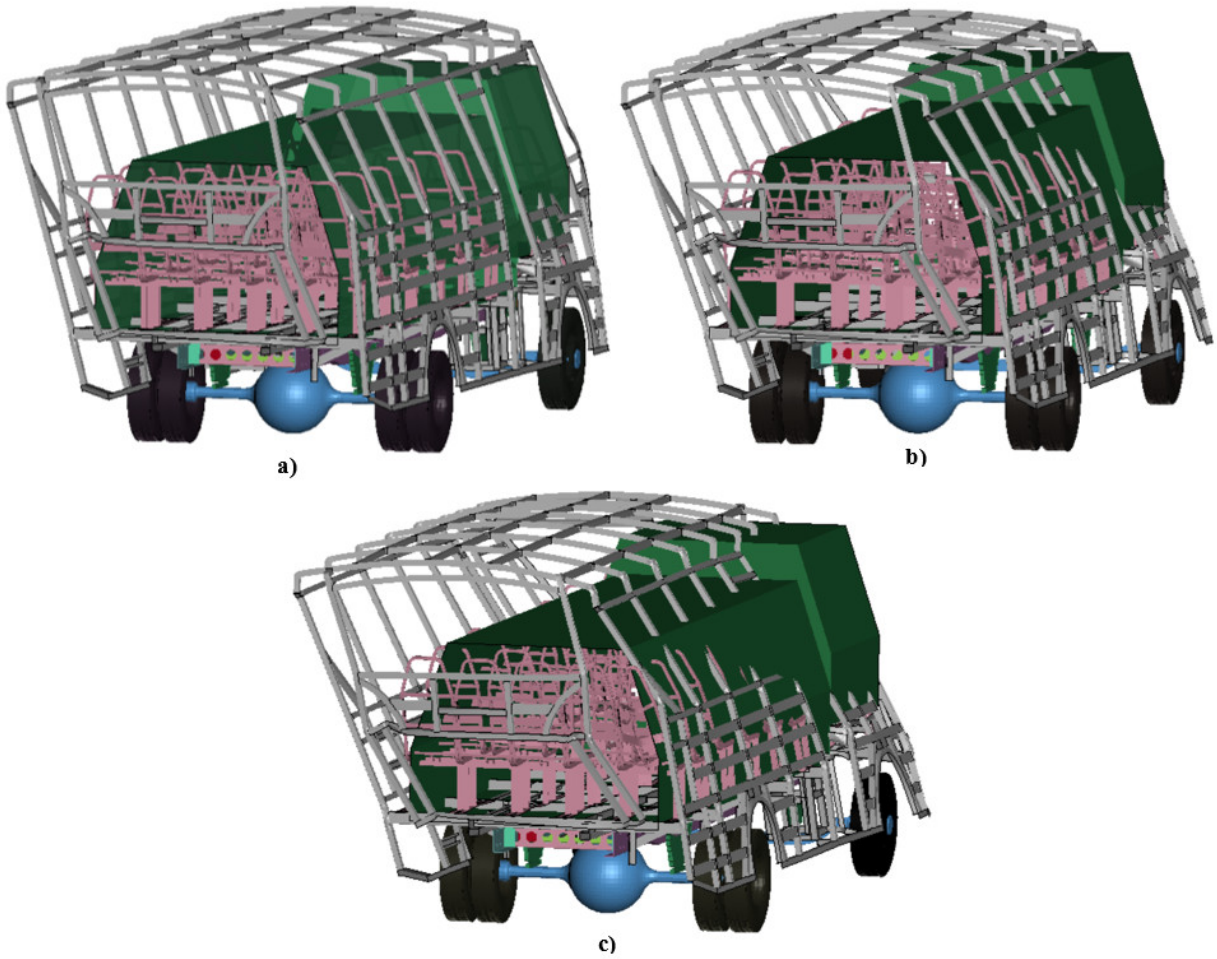

Figure 5.22: Deformation of the original model through rollover simulation cases: a) tare-weight scenario b) full-loading scenario, and c) over-loading scenario

When the value of loading increases, the structure deformation goes to high failure(severe) mode for a rollover crash. The result presented here provides three findings indicating the deformation with its location during all three scenarios of a rollover crash. First, the tare-weight case develops less deformation at pillar A and bays(B1-B3) than in other scenarios (see Figure 5.22 a). Second, in the case of full-loading, the high structural deformation develops at pillar A and bays from B1 to B4 compared to the tare-weight case (see Figure 5.22 b). Lastly, the excessive deformation also occurred from pillar A to bay 5(B5) (Figure 5.22 c).

After the crash for the baseline model in the case of tare-weight, full-load, and over-load, the maximum impact forces are 105.9 kN, 151.6 kN, and 195.9 kN, respectively (see Figure 5.24). This result implies that when the loading capacity of the bus increases, the impact crash force also increases after the rollover crash.

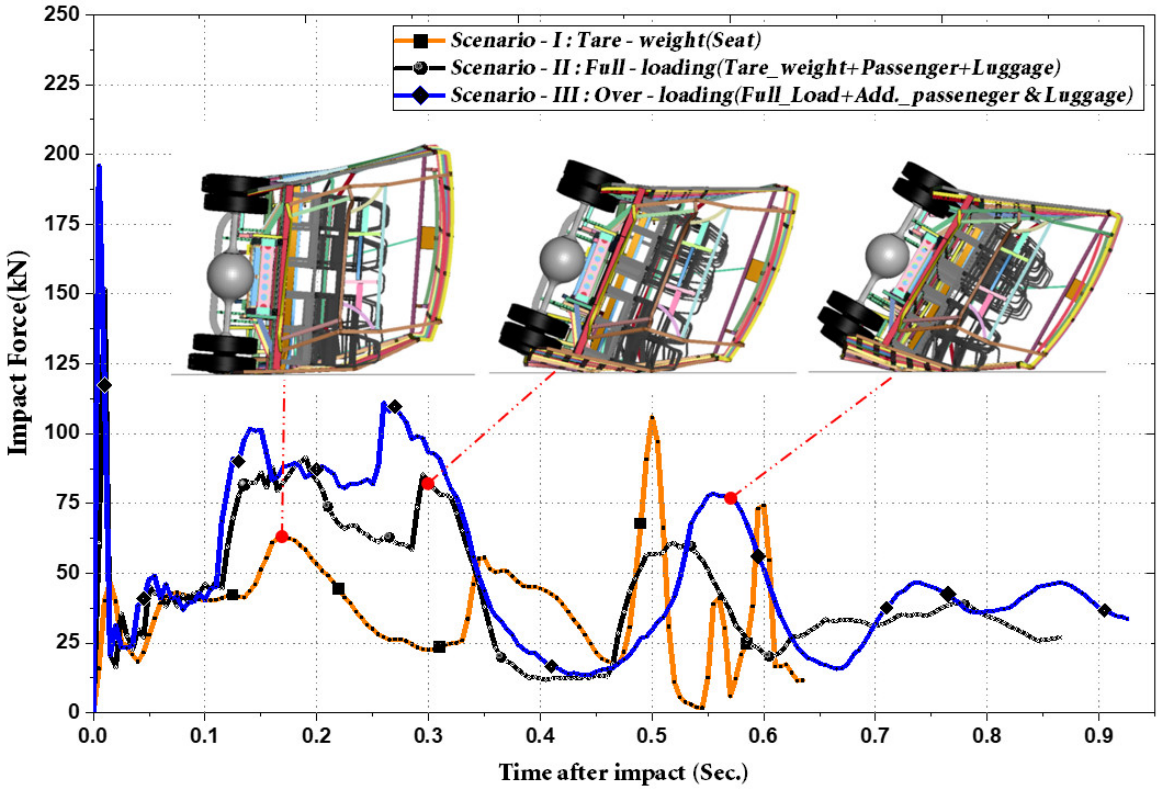

Figure 5.23: Plot of impact forces - time for all three scenarios of the original model.

Figures 5.24 and 5.25 describe the internal and kinetic energy for all three scenarios of the two models after the rollover crash. It is known that the value of internal and kinetic energy for both models increases when the loading(weight) capacity is high. For instance, the internal energy of scenarios – I, II & III are 23.9 kJ, 37.6 kJ, and 45.7 kJ, respectively.

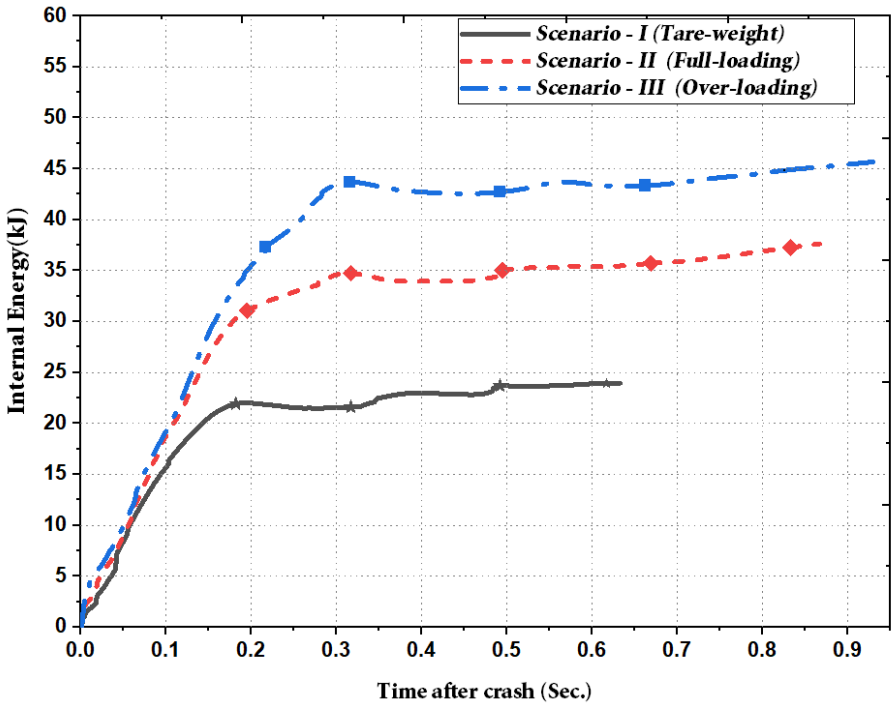

Figure 5.24: Internal energy for all three scenarios of a baseline model

The values of kinetic energy for all three scenarios are described, as shown in Figure 5.25. However, the difference in kinetic energy is obtained due to different amounts of mass in all scenarios.

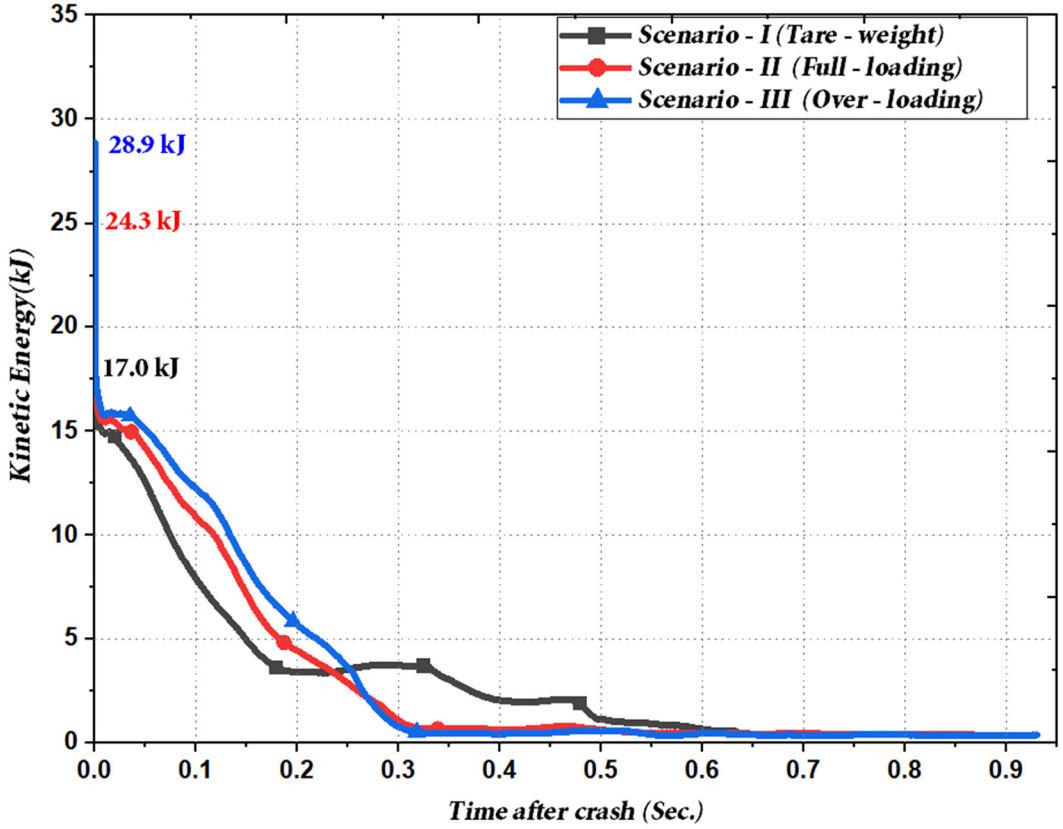

Figure 5.25: Kinetic energy for all three scenarios of a baseline model

5.3.3 Comparison of Baseline model and other Alternative solutions

As mentioned earlier, the alternative solutions are model – I(RD), model – II(SRSM), and model – III. In this section, angular deformation index and internal energy parameters are estimated to compare the crashworthiness capacity of the baseline model and alternative solutions during the tare-weight rollover scenario. The final deformations of these four models are displayed, as shown in Figure 5.26. First, a baseline model is intruded on the residual space and highly deformed (See Figure 5.26 a). Furthermore, model – II(SRSM) is less deformed as compared to a baseline model. However, a model – I(RD) is less deformed than baseline and model – II. Next, a model – III is less deformed than all models, and the residual space is far from the model's frame, as shown in Figure 5.26 d).

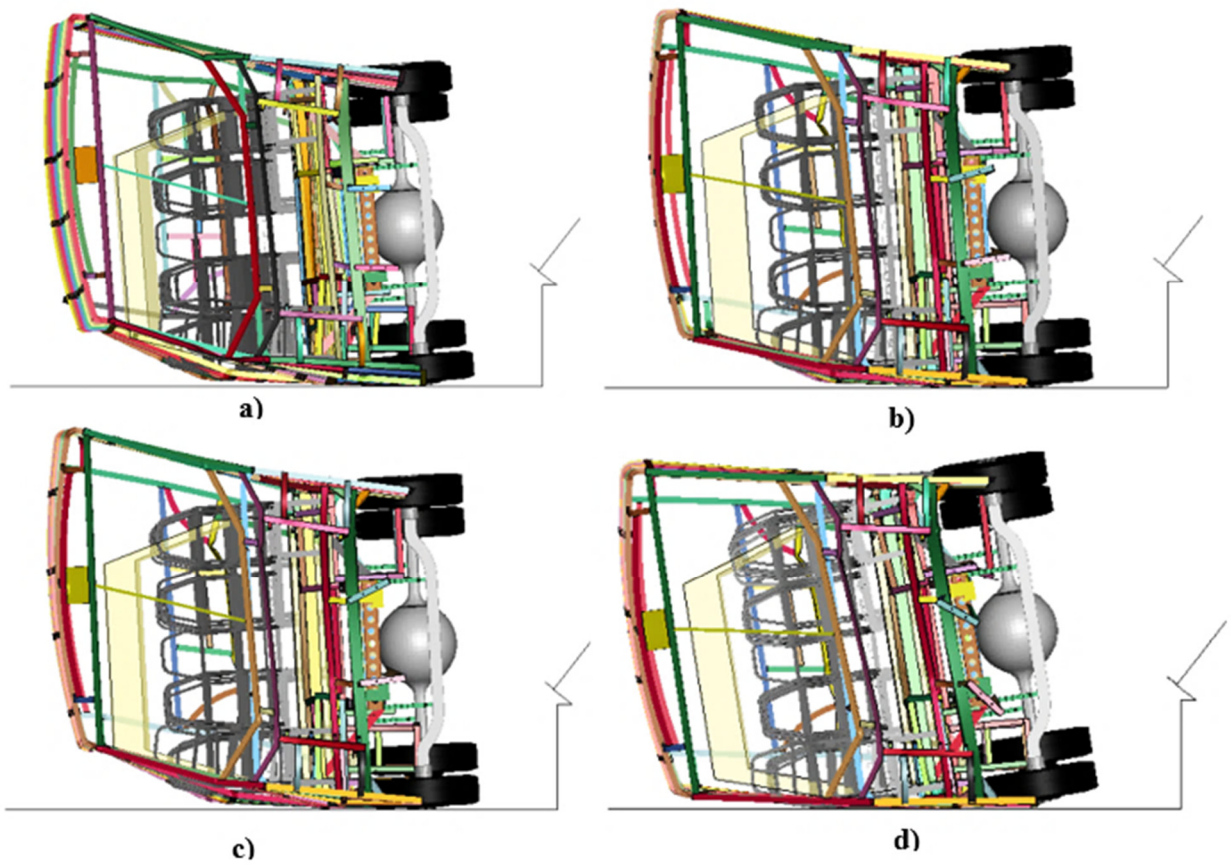

Figure 5.26: Comparison of deformation in the tare-weight rollover: (a) Baseline model; (b) Model – I(RD); (c) Model – II(SRSM) and (d) Model – III

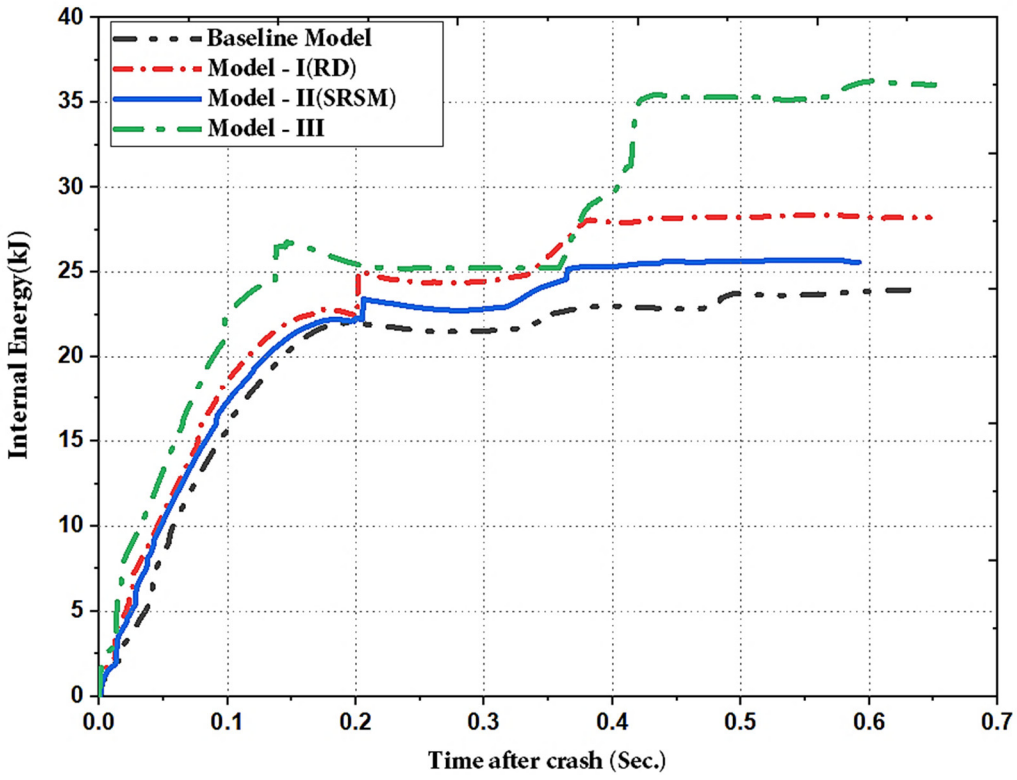

Figure 5.27: Comparison of Internal energy between four models

Figure 5.27 displays the internal energy of the baseline model and three alternative designs in the tare – weight scenario. Thus, the internal energy of baseline model, model – I, model – II, and model – III are 23.94 kJ, 28.3 kJ, 25.7 kJ, and 36.2 kJ, respectively. As shown in Figure 5.27, the internal energy of baseline model, model – I, and model – II are converged similarly from 0.0 – 0.2 sec. The results show that model – II(SRSM) has less weight with enough energy absorbing capacity than the baseline model by varying the thickness of pillars, windows, and waist rails. However, model – III has the highest crashworthiness capability than others due to a combination of model – II(RSO) and model – II (SRSM) and the change of the thickness of pillars.

The Angular deformation index (DI_θ) is another parameter to identify the crashworthiness capability of the structure during a rollover crash. Moreover, the angular deformation index of the structure response was measured based on angles between nodes with time in LS-DYNA. As mentioned before, the rating of the angular deformation index (DI_θ) indicates the strength of structure during structural deformation. Therefore, this section also evaluates the angular deformation index to compare the four models in tare-weight rollover scenarios.

Table 5.2: Comparison of deformation index among four models in tare-weight scenario

Change of angles (deg) & DI	***Pillar A & bays (B1 – B3)***				***Bays (B4 – B8)***			
	Baseline	***M-I***	***M-II***	***M-III***	***Baseline***	***M-I***	***M-II***	***M-III***
$\Delta\theta_1$	-32.9	-19.6	-22.7	-13.5	5.8	2.2	2.6	2.6
$\Delta\theta_2$	2.6	8.4	12.0	1.8	0.6	0.5	0.5	0.6
$\Delta\theta_3$	17.5	7.6	6.8	3.9	-17.8	-8.4	-10.7	-3.7
$\Delta\theta_4$	26.4	18.2	21.9	14.1	-18.8	-12.3	-20.4	-13.6
$\Delta\theta_5$	6.5	9.4	13.1	3.0	21.4	11.9	21.5	10.3
$\Delta\theta_6$	-10.9	-3.9	-2.8	-1.8	5.9	3.2	3.1	5.1
DI_θ	***1.07***	***0.70***	***0.78***	***0.27***	***0.69***	***0.40***	***0.59***	***0.42***

The maximum DI_θ of the baseline model, model – I, model – II, and model – III are 1.07, 0.70, 0.78, and 0.42, respectively, as shown in Tables 5.2. These maximum deformation indexes are located at pillar A with bays (B1 – B3) for all models in the tare-wight rollover scenario except a model – III (bays (B4 – B8)). As depicted in Table 5.2, the change of plastic hinge angles and the maximum angular deformation index at the pillar and bays of the structure are described in the tare-weight scenarios for all four models.

Figure 5.28 compares the deformation index vs time curves of the baseline model and alternative models in the tare -weight rollover case. In this scenario, the baseline structure has an unacceptable and poor rate of strength. This rate describes that the entire structure failed due to high deformation at pillar A and bays(B1-B3). These results imply that the total structural strength of the baseline model is weak to survive in this rollover crash case. Moreover, both model - I(RD) and model – II(SRSM) have sufficient(acceptable) strength in tare – weight cases.

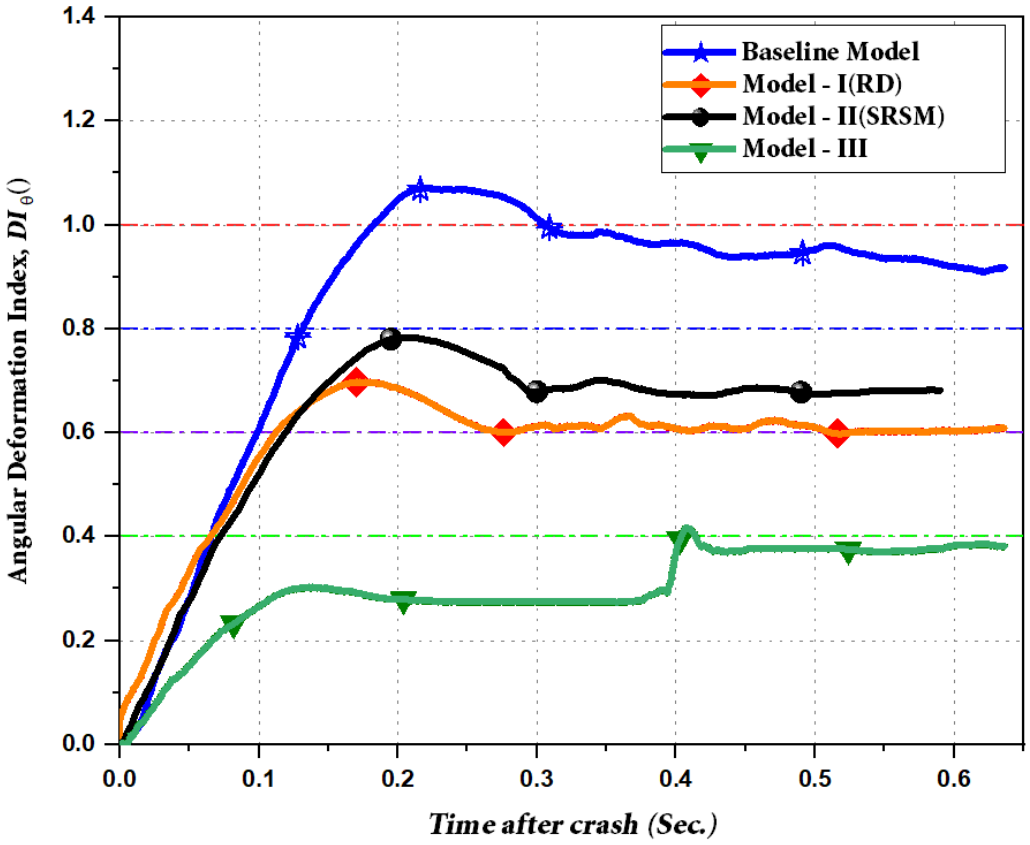

Figure 5.28: Comparison of deformation index among four models in tare - weight rollover scenario

However, the model – III (optimum) design occurred with the intermediate and strong strength during the tare–weight scenario. Thus, this indicates that the combined design of the structure is only in the safe rated condition compared to others.

5.3.4 FE Verification of Energy Balance in Rollover simulation

The LS-DYNA total energy(E_{Total}) is the sum of six components such as current internal energy(E_I), current kinetic energy(E_K), current sliding energy(E_{Sli}), current hourglass energy(E_{HG}), current system damping energy(E_D), and current stonewall/rigid wall energy(E_{RW}) and also must be equal with the sum of initial total energy(E_{Total_0}) & work done by external loads(W_{Ext}) [112], [113] :

$$E_{Total} = E_K + E_I + E_{Sli} + E_{RW} + E_{Damp} + E_{HG} = E_{Total_0} + W_{Ext} \quad 4.1$$

$$E_{Total_0} = E_{K_0} + E_{I_0} \quad 4.2$$

Where: E_{I_0} - the initial internal energy & E_{K_0} - the initial kinetic energy

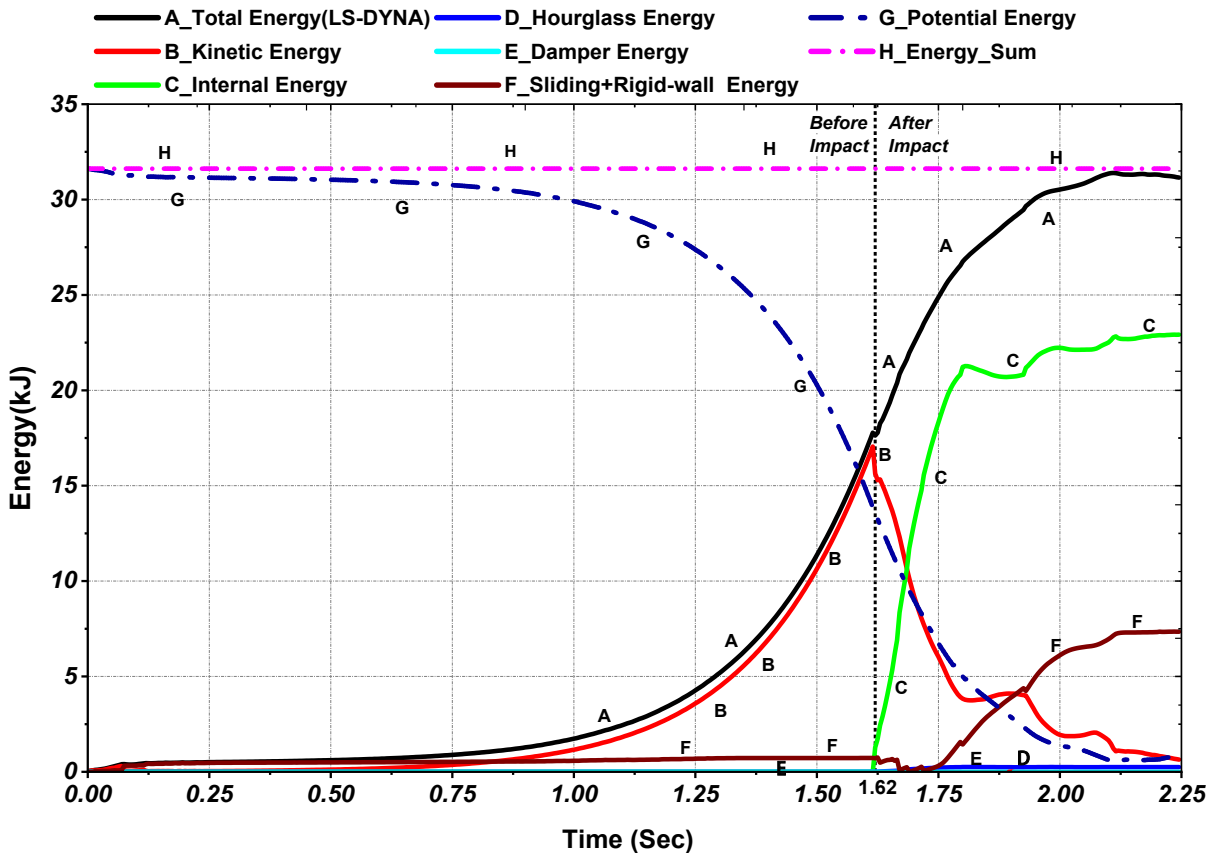

Figure 5.29: Energy balance in the original tare-weight rollover case

As described in equation 3.57, only 75 % of energy applies to the original structure and seat frame. The other 25 % of energy dissipates to the ground[85]. Figure 5.29 shows that the structures and seat frame sliding (contact) and rigid wall energy (Alphabet F) are equal to 7.35 kJ during rollover of the tare-weight scenario, containing 23.48 % of the total energy. Thus, the maximum hourglass energy of 0.25 kJ contained within 1.48 % of internal energy, still under the allowable limit of 10 %. Furthermore, the energy of damping finished as a zero level in the entire simulation.

The alphabet C (green line) represents the system's internal energy, as shown in Figure 5.29. the maximum internal energy of the system is equal to 23.94 kJ. The kinetic energy gains the peak value at 1.62 sec, equal to 17.05 kJ until the point of contact to the ground due to gravity acceleration. After that, it decreases to the value of 0.64 kJ at 2.25 seconds (final time) of rollover impact.

Another energy balance approach presents the energy ratio of the system throughout the rollover simulation using equation 4.3. In GLSTAT output, When the energy balance is accurate, the total energy and initial total energy ratio must be equal to 1.0. Additionally, the energy ratio accepts a range of ± 0.07 [112], [113]. The simulation energy ratio remained at the acceptable range(1 ± 0.07) through the tare-weight scenario, as shown in Figure 5.30. In addition, the remaining rollover simulation energy ratios are plotted in Appendix C (see Figure C5.).

$$e_{Ratio} = \frac{E_{Total}}{E_{Total_{,0}} + W_{Ext}} = 1 \pm 0.07 \qquad 4.3$$

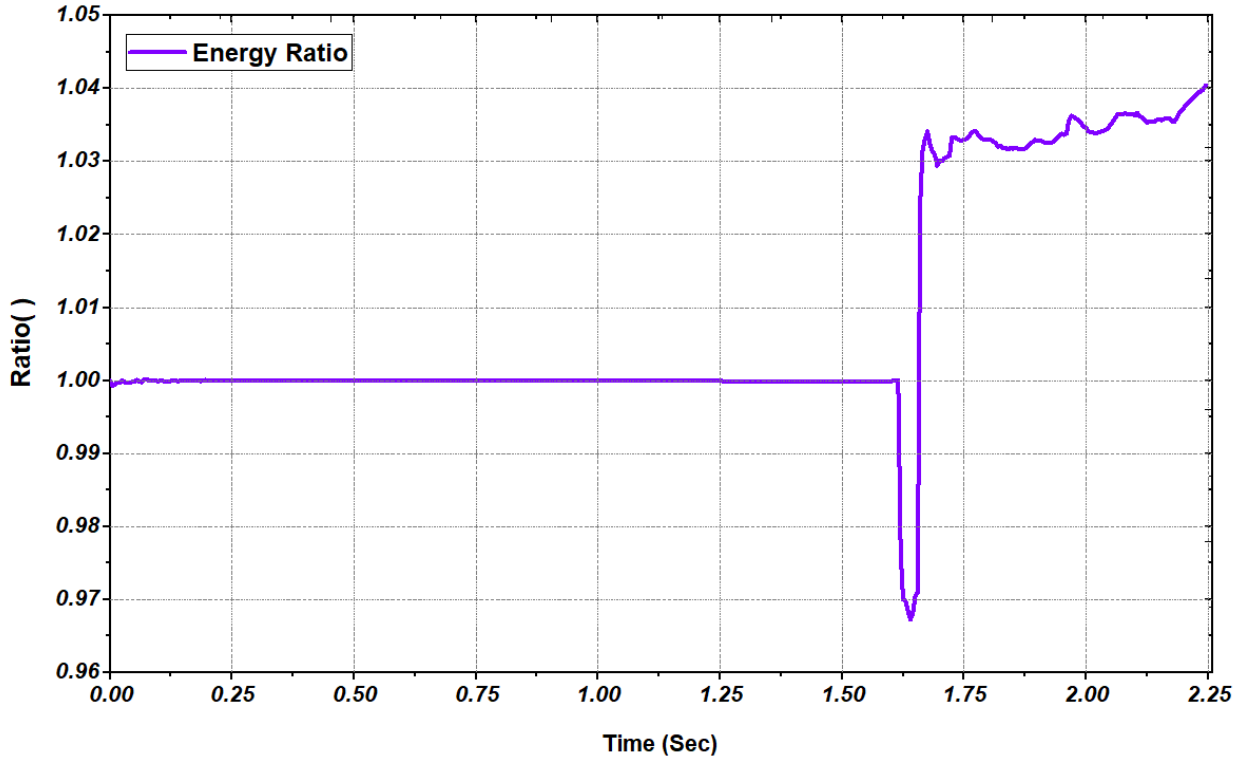

Figure 5.30: Energy ratio in the original tare-weight rollover case

5.4 Results of Mesh convergence study & Effects of weld types

5.4.1 Effects of weld types on the quasi-static connection analysis

As described in Figures 5.31 & 5.32, The RW and FW Connection simulation presents the stress contour for two welds at the equivalent stress of 260 MPa. The contour of maximum stress presents at roof bend area in full arc weld of the RW Connection shown in Figure 5.31 a). This result implies that the full arc weld is more strong in the quasi-static connection analysis.

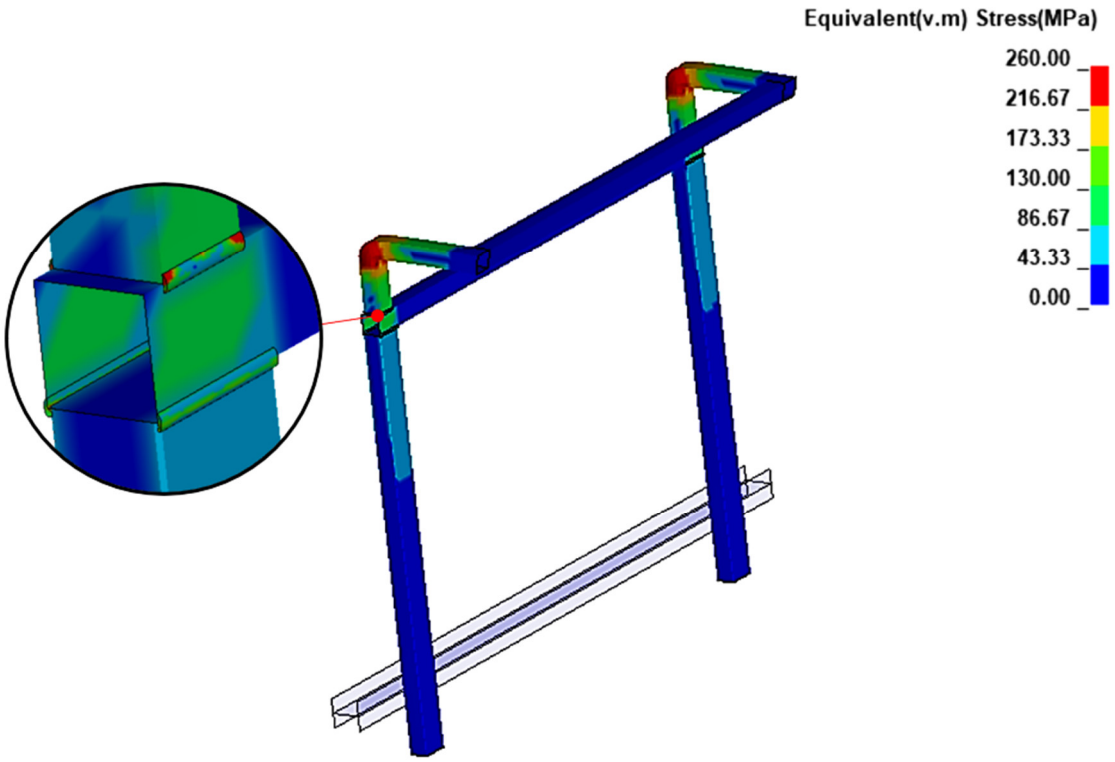

a)

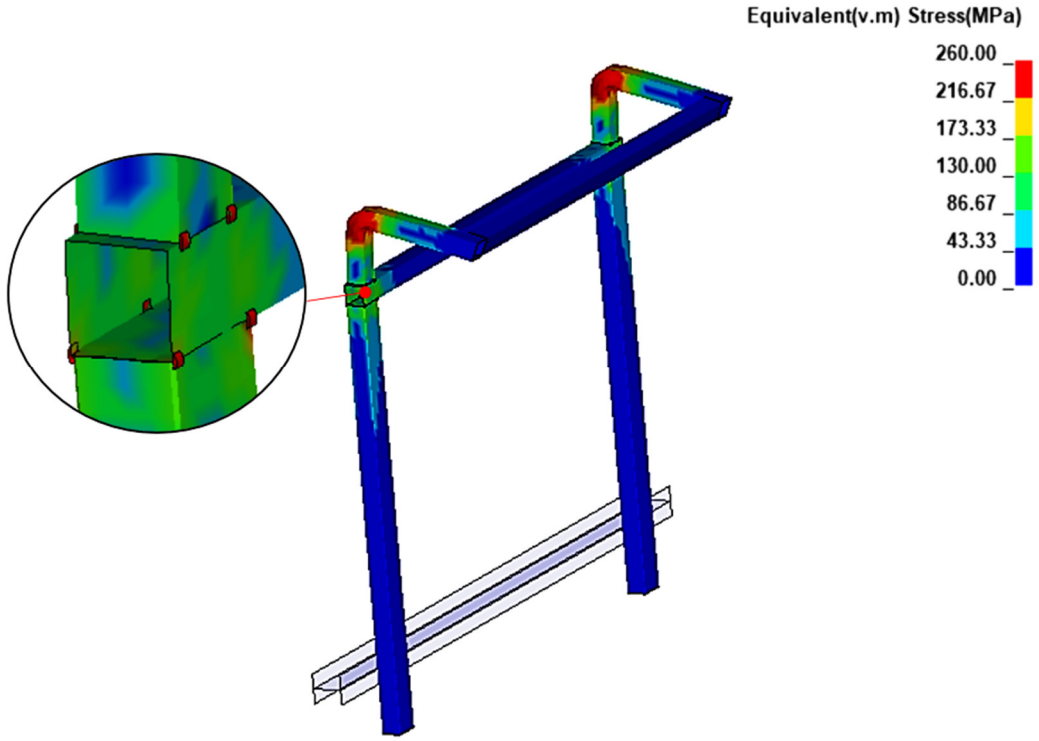

b)

Figure 5.31: Contour of stress for RW Connection: a) Full arc weld and b) Spot arc weld

On the other hand, maximum stress locates at the spot arc weld and roof bend areas (see Figure 5.31 b). Therefore, it is found that the full arc weld has less stress than the spot arc weld on the RW Connection analysis.

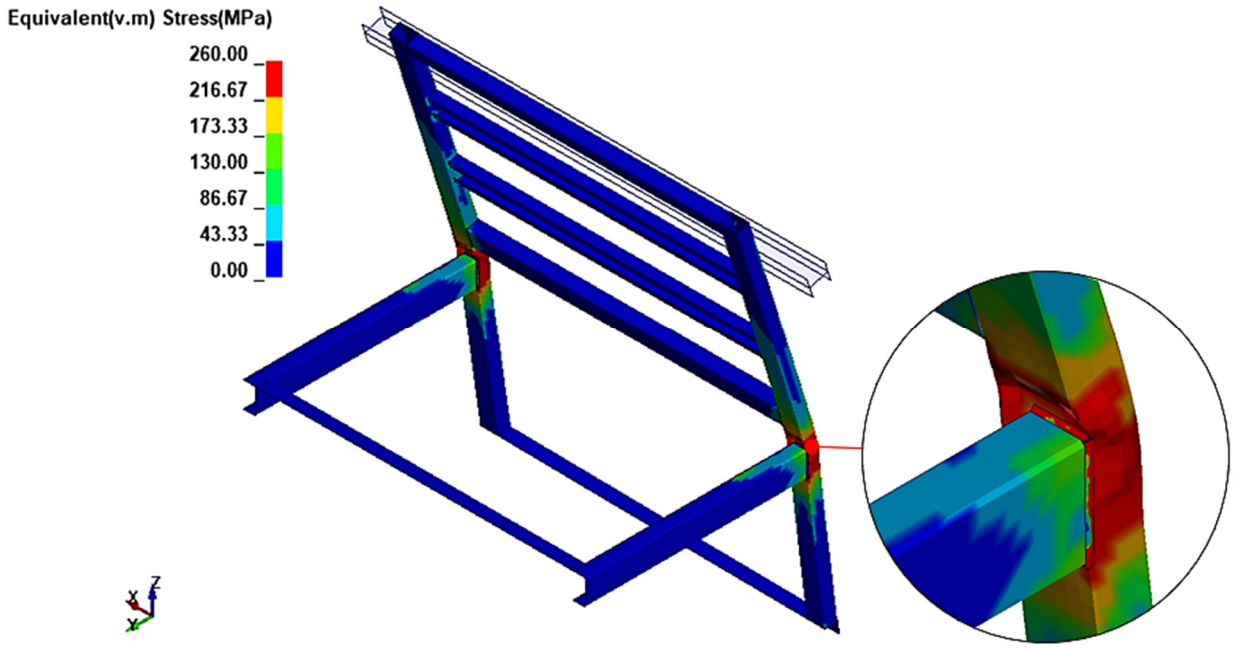

(a)

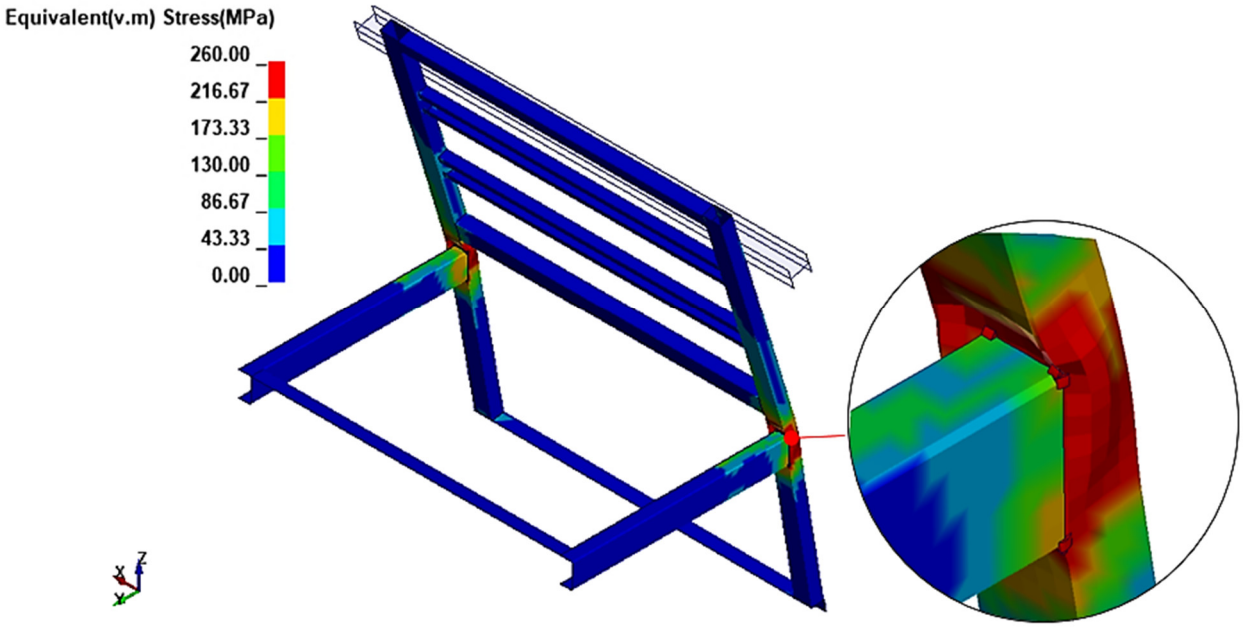

(b)

Figure 5.32: Contour of stress for FW Connection: a) Full arc weld and b) Spot arc weld

During the FW connection, the maximum stress presents at the joint area of the connection for two welds, as shown in Figure 5.32. Due to the location of their maximum stress being the same in both welds, it is not easy to compare the strength of the welds. Moreover, the equivalent stress can not be used as evaluation parameters in a quasi-static case. Instead, it is found that the energy absorption capacity evaluates the strength of the welds in both connections.

Figures 5.33 describe the moment vs rotation graphs of the two welds during all connection FE analyses. The difference of moment among both welds is 1.65 % within 24 deg rotation of RW connection. Moreover, In the FW connection, the moment difference of 9.1 % is contained within 18 deg of angular rotation.

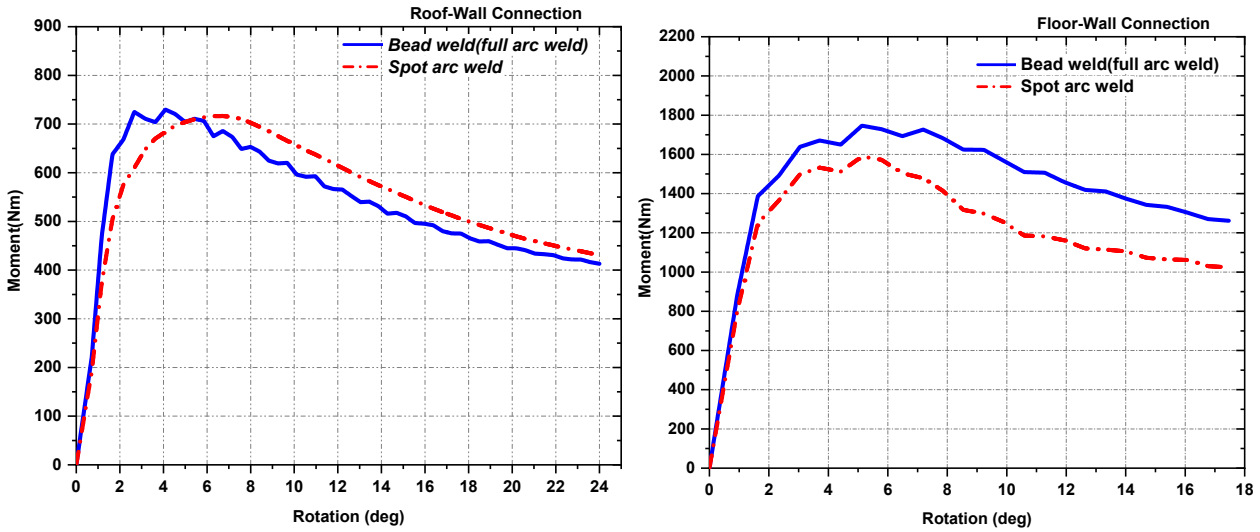

Figure 5.33: Moment-Rotation graph for RW connection(left) and FW connection(right)

The two welds failed the quasi-static analysis tests during the RW connection because they did not meet the Florida standards' threshold value, as shown in Figure 5.34. this result shows that the roof-wall connection of the original model contains a weak form of connection.

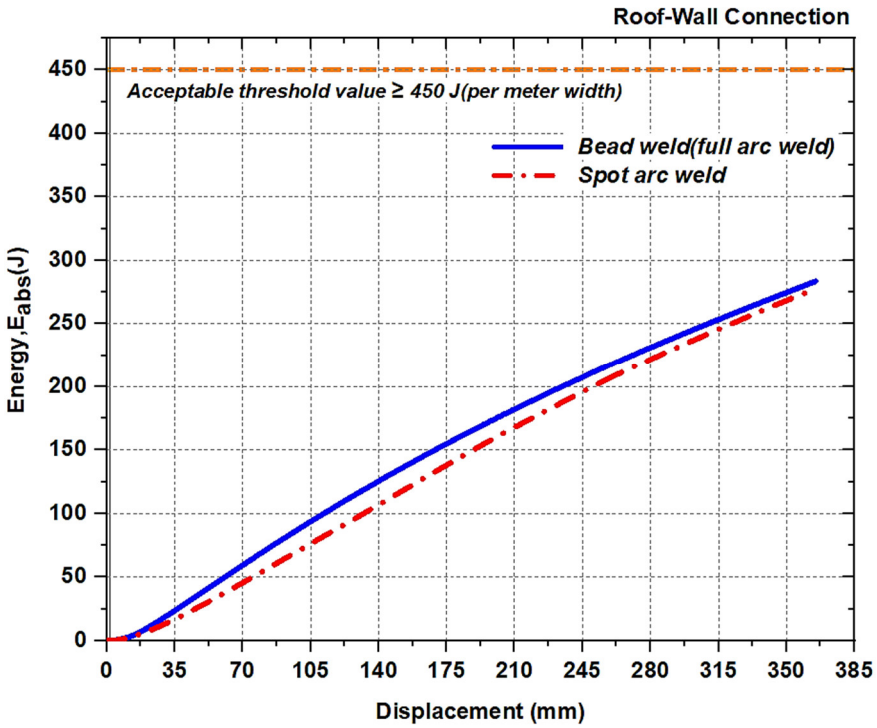

Figure 5.34: Comparison of energy absorption between two welds on RW connection

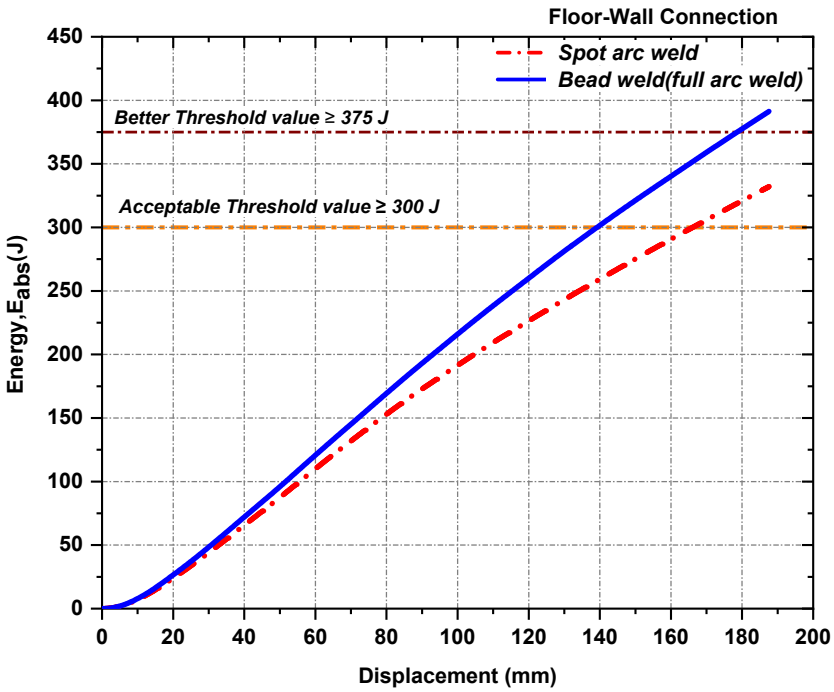

Figure 5.35: Comparison of energy absorption between two welds on FW connection

Figure 5.35 illustrates that the difference of absorbed energy between the two welds is 15.1 % within 190 mm displacement in the FW connection. In this connection simulation, both welding types pass Florida's (FL) threshold(required) value. However, the bead welded FW connection has a much better threshold value than spot welded.

Table 5.3: Results of moment and energy absorption for both welds

Weld types	***Roof-side wall connection***		***Floor-side wall connection***	
	Moment (Nm)	*Energy Absorbed (J)*	*Moment (Nm)*	*Energy Absorbed (J)*
Full arc weld	729	283	1750	391
Spot arc weld	717	277	1590	332
Difference (%)	1.65 %	2.12 %	9.14 %	15.08 %

Table 5.3 displays the summary of moment and energy absorption results for both weld analyses. However, the full arc weld has higher energy absorption than the spot arc weld in both connections.

This connection analysis result found that only the FW connection passes the Florida threshold value of energy absorption in both welding types. This finding indicates that the FW structural connection has well structural integrity than the RW connection. Lastly, the difference of the weld types on connections varies the energy absorbing capacity of connections, shown in Table 5.3. which means that the bead welded FW Connection experiences a better energy absorption capacity

than the spot-welded connection. Moreover, the absorbed energies of the two welds have a slight difference during the RW connection FE simulation. This result shows that the welding types have a few effects on the energy-absorbing capacity of the RW connection. Generally, the above findings suggest that the bead weld (full arc welding) type improves the quasi-static strength of the structural connections.

5.4.2 Mesh Convergence study

As depicted in Figure 5.36, the curves of moment vs rotation angle were obtained for three mesh densities of RW and FW connections. This study found that the element size of 18 mm is stiffer than the others in FW Connection. During the RW quasi-static connection simulation, all the mesh densities slightly differ on the result of the moment, as shown in Figure 5.36(left).

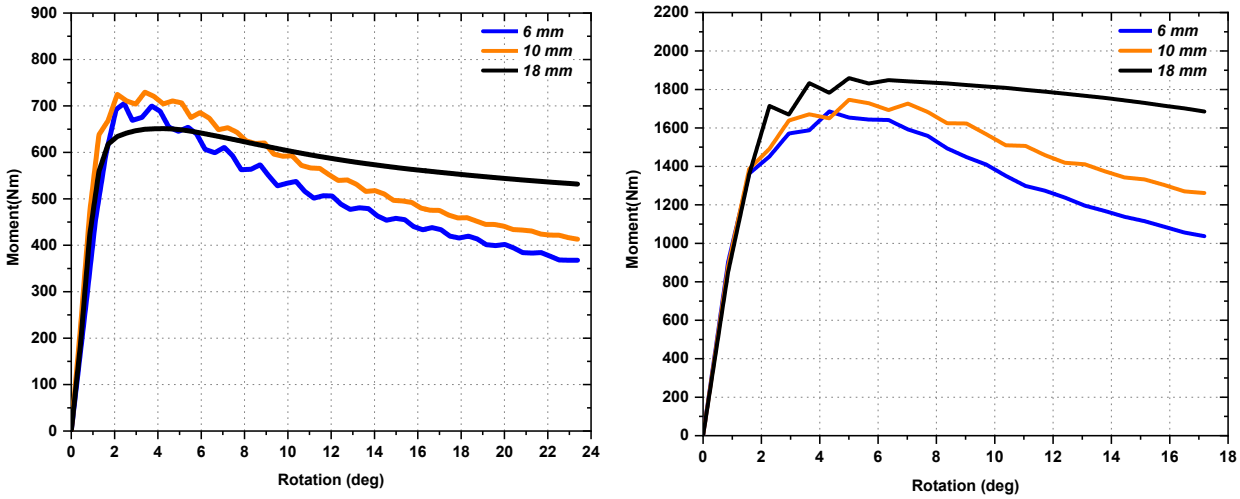

Figure 5.36: Moment - angle of rotation curves for RW connection(left) and FW connection(right)

Table 5.4: Summary of Mesh Convergence results for all connection

Mesh size *(mm)*	***Roof-side wall connection***			***Floor-side wall connection***		
	Energy (J)	*Moment (Nm)*	*Difference (%)*	Energy (J)	Moment (Nm)	*Difference (%)*
6	260.6	705	-	357.6	1690	-
10	283.4	729	3.40	391.2	1750	3.55
18	296.7	651	7.66	450.8	1860	10.06

As shown in Table 5.4, the results of 10 mm element size samples show a better agreement with the other elements. Hence, this conclusion shows that it is possible to possess the current mesh size (10 mm) for all developed FE models of midi-bus structures.

Chapter Six

Conclusion and Recommendation

5.1 Conclusion

This research uses numerical methods to facilitate a midi-bus structure's static, quasi-static, and rollover analysis (ANSYS/LS-DYNA). Moreover, this research also develops three alternative design solutions: reinforcement design, numerical optimization (Design Explorer/LS – OPT), and a combined design approach for all FE analyses. Furthermore, the preferable welding types on the original structural connections via quasi-static simulation.

The main output parameters include total deformation, stiffness, and equivalent stress estimates in the static strength analysis according to the pure bending, pure torsional, steering (cornering), & breaking loading conditions. Moreover, the shell thickness as a design parameter(variable) is defined in optimization tasks to reduce the structure's weight within better stiffed. and also, during reinforcement design, the design cross-section and layout of the frame with the addition of reinforcement are considered as design inputs for baseline structure. Consequently, the static strength analysis and optimization obtained results can be summarized as follows:

- In the baseline model, the maximum deformations occurred at roof luggage and the top of rear frames for all loading conditions except pure torsion case. Furthermore, the maximum equivalent stresses are located at floor parts & bolted support parts (hole of L-shaped frame) of the original structure for all loading conditions.
- The weight of the baseline model is optimized by decreasing from 577.35 kg to 547.15 kg and 532.70 kg using Reinforced design and Response surface Optimization approach, respectively. However, the combined approach is only reduced the baseline model by 2.33 %. Moreover, the bending and torsional stiffness of all the design alternatives are increased.

Overall, it can be concluded that from proposed design alternatives, Arrangements of the truss (supporting member -#1) and cross-section types of frames with the addition of reinforcements on the original(baseline) structure can be found the lightweight and stiffed the reinforced design (model – I), compared to a baseline model. Next, the response surface optimization design (model – II(RSO)) can also present the stiffed structure with reduced weight by variation of thickness of roof and floor parts of the reinforced model. Lastly, the combined design combines both the static and rollover models to experience a much better-stiffed structure in both analysis cases, almost the same as for static the result of a model – II(RSO).

Generally, it suggests that the combined model (model -III) increases the stiffness for all loading conditions. However, the Response surface Optimization with MOGA Approach also gives a lightweight structure with sufficient bending and torsional stiffness, compared to a baseline model.

This research paper also facilitates the rollover crashworthiness capability of the structure and seats frame at quasi-static loading and rollover scenarios. In addition, the three alternative designs for rollover were conducted using reinforcement design, optimization by successive response surface method using LS-OPT, and combined design approach for all static and rollover analysis. From both analysis and optimization results, the following conclusions are mentioned:

- The energy absorption of the original(baseline) model is less than the minimum requirement energy by ECE R66 in quasi-static simulation, which means the original bus structure fails the rollover tests due to one of the bays being touched the residual space. However, all design alternative solutions pass the test because of fulfilling the requirement of the standard.
- During the tare-weight rollover case, the entire structure failed due to high deformation at pillar A and bays(B1-B3). Moreover, the lowest and highest internal energy occurred at the skirt pillar and vertical pillar.
- The deformation of the tare-weight without seat frame (case - b) is highest than the tare-weight with the model of the seat frame (case - a) throughout the rollover due to the center of gravity (CG) position. Moreover, When the midi-bus loading capacity increases, structural deformation increases to high failure(severe) mode during three loading rollover scenarios. Significantly, the overloading of passenger and luggage loads leads to the baseline structure at the severe failure mode and fatalities and injuries of occupants during rollover crashes.
- As per the tare – weight rollover analysis and optimization results, the difference of internal energy among three alternatives (model – I(RD), model – II(SRSM), and model – III) and baseline model are 18.2 %, 7.35 %, and 51.2 %, respectively. Moreover, the maximum deformation index (DI_{θ}) of the baseline model, model – I, model – II, and model – III are 1.07, 0.70, 0.78, and 0.42, respectively.

Generally, it can be found that the baseline structure, model - I(RD) & model – II(SRSM), and model – III (optimum) design have unacceptable, acceptable, acceptable, and intermediate strengths, respectively. The first design approach is that the reinforced design experiences sufficient strength by adding the support and change of cross-section on the front pillars. Moreover, a model – II(SRSM) has less weight with adequate energy absorbing capacity than a reinforced model by varying the thickness of pillars, windows, and waist rails. Lastly, a combined

(model – III) structure design exhibits the safe rated condition and highest crashworthiness capability by a combination of the model – II(RSO) and model -II(SRSM) and the change of the thickness of pillars. Finally, it suggests that the combined design must be considered to obtain the safe occupant's space with a better rollover strength.

In addition, the effects of welding type (full and spot arc welds) on the roof-wall & floor-wall connection analysis were carried out in quasi-static loading simulation along with Florida Standard. As a result, the following summarized results can be concluded:

- The difference of absorbed energy among the two welds on the FW and RW connections is 15.1 % and 2.1 %, respectively, within 190 mm displacement. This result shows that the full arc(bead) weld type has better energy absorption than spot arc welding in both structural connections.

From the above analysis result, it can be achieved that only the FW connection passes the Florida threshold value of energy absorption in both welding types due to well structural integrity. This finding indicates that the FW Connection of the midi-bus has well structural integrity for the midi-bus structure during rollover crashes. On the other hand, both welded types of RW connections are failed due to lower energy absorption than a threshold value, which means the RW connection can experience insufficient structural strength during a rollover. Moreover, it can be concluded that the bead weld (full arc welding) type experiences slightly to better the energy absorbing capacity of the quasi-static structural connections.

5.2 Recommendation

After this paper, the following recommendation must be taken high consideration by a local manufacturer and legislator bodies (transport ministers):

- Through experimental tests, the legislator body and manufacturers can determine the center of gravity, mass distribution, and stability.
- Both manufacturers and legislator bodies are encouraged to use the full equivalent testing procedure of rollover stated by UNECE R66 & connection test stated by Florida standards.
- Recommended new model of structure can be considered and checked to practice the strength during manufacturing by a local manufacturer.
- Frontal pillars (Pillar A) and bays from B1 to B5 are the most significant components responsible for the rollover crashworthiness of the bus for all loading capacity.
- An experimental test of static strength and a compatibility test should be conducted to measure the strength of the bus before driving and launching to the community.
- The full arc(bead) welding should be implemented to join the floor-wall and roof-wall connections of the bus structure compared to spot arc welding.

5.3 Future Works

This research initiates the others to work further researches on the locally manufactured midi-bus. Due to the scope and limitation of this thesis work, the following future tasks via experimental & numerical approaches should be conducted:

- A full-bus rollover test with all components and dummy ballast (Experimental Method)
- Frontal Crash, Side impact test, and Rear Impact test
- Impact Hammer and side-wall panel test
- Strength test of passenger's seats according to UNECE R80
- Crash compatibility test

References

[1] Automotive Industry Standard - AIS-052, “Code of Practice for Bus Body Design and Approval -Revision 1,” vol. 052, no. 1. India, p. 102, 2008.

[2] J. Bai, G. Meng, and W. Zuo, “Rollover crashworthiness analysis and optimization of bus frame for conceptual design,” *J. Mech. Sci. Technol.*, vol. 33, no. 7, pp. 3363–3373, 2019.

[3] M. Bin Yusof, M. Amirul, and A. Bin, “Effect of Mass on Bus Superstructure Strength Having Rollover Crash,” *Int. Sci. Index*, vol. 6, no. 8, pp. 1443–1449, 2012.

[4] J. Karliński, M. Ptak, P. Działak, and E. Rusiński, “Strength analysis of bus superstructure according to Regulation No. 66 of UN/ECE,” *Arch. Civ. Mech. Eng.*, vol. 14, no. 3, pp. 342–353, 2014.

[5] G. S. Tulu, S. Washington, and M. J. King, “Characteristics of Police-reported Road Traffic Crashes in Ethiopia over a Six Year Period,” in *Proceedings of the 2013 Australasian Road Safety Research*, 2013, pp. 1–13.

[6] UNECE 2004, “Statistics about rollover accident of buses – VI,” Hungary, 2004.

[7] (UNECE 2020), “Road Safety Performance Review - Ethiopia,” United Nations Economic Commission for Africa & Europe, Geneva, 2020.

[8] T. W. Tech, I. Iturrioz, and A. D. De Meira Júnior, “Numerical simulation of bus rollover,” *SAE Tech. Pap.*, 2007.

[9] M. D. Iozsa, D. A. N. A. Micu, and G. Frățilă, “Influence of Crash Box on Automotive Crashworthiness,” *Recent Adv. Civ. Eng. Mech.*, pp. 49–54, 2014.

[10] C. C. Liang and L. G. Nam, “Comparative analysis of bus rollover protection under existing standards,” *WIT Trans. Built Environ.*, vol. 113, pp. 41–53, 2010.

[11] M. K. Rahman, “Body Section Analysis in Bus Rollover Simulation,” *J. East. Asia Soc. Transp. Stud.*, vol. 9, pp. 1967–1981, 2011.

[12] W. Zhou, A. Kuznectov, C. Q. Wu, and I. Telichev, “A comparative numerical study of motorcoach rollover resistance under ECE R66 and proposed NHTSA regulation conditions,” *Int. J. Crashworthiness*, vol. 25, no. 2, pp. 1–16, 2019.

[13] S. E. Chopade, R. S. Mahajan, S. Raju, S. Joshi, C. P. Mishra, and A. Chavare, “Certification of Buses as per AIS-031/ ECE-R66 Using CAE Methods,” *SAE Tech. Pap.*, pp. 1–8, 2009.

[14] V. Phadatare, P. Hujare, and C. Inamdar, “Techno-Societal 2016,” *Techno-Societal 2016*, 2018.

[15] C. C. Liang and G. N. Le, “Bus rollover crashworthiness under European standard: An optimal analysis of superstructure strength using successive response surface method,” *Int. J. Crashworthiness*, vol. 14, no. 6, pp. 623–639, 2009.

[16] D. Croccolo, M. De Agostinis, and N. Vincenzi, "Structural analysis of an articulated urban bus chassis via FEM: A methodology applied to a case study," *Stroj. Vestnik/Journal Mech. Eng.*, vol. 57, no. 11, pp. 799–809, 2011.

[17] S. Rooppakhun and J. Wichairahad, "The strength analysis of a bus superstructure based on the accuracy improvement of T-junction flexible joint stiffness," *Int. J. Eng. Technol.*, vol. 7, no. 3, pp. 62–67, 2018.

[18] C. Reyes-ruiz, O. R. Cervantes, A. O. Prado, and E. Ramirez, "Analysis and Optimization of a Passenger Bus Frame Through Finite Element Software," *2013 SIMULIA Community Conf.*, 2013.

[19] H. Wang, X. Jin, and Z. Lin, "FEM static and dynamic analysis of the body structure of SK6120 low floor city bus," *SAE Tech. Pap.*, 2002.

[20] F. Lan, J. Chen, and J. Lin, "Comparative analysis for bus side structures and lightweight optimization," *Proc. Inst. Mech. Eng. Part D J. Automob. Eng.*, vol. 218, no. 10, pp. 1067–1075, 2004.

[21] M. J. L. B. and B. L. B. A. Gauchia, V. Diaz, "Torsional stiffness and weight optimization of a real bus structure," *Int. J. Automot. Technol.*, vol. 11, no. 1, pp. 41–47, 2010.

[22] W. Zhong, R. Su, L. Gui, and Z. Fan, "Multi-objective topology and sizing optimization of bus body frame," *Struct. Multidiscip. Optim.*, vol. 54, no. 3, pp. 701–714, 2016.

[23] A. Y. Ismail, G. Na, and B. Koo, "Topology and response surface optimization of a bicycle crank arm with multiple load cases," *Appl. Sci.*, vol. 10, no. 6, 2020.

[24] C. Bojanowski and R. F. Kulak, "Multi-objective optimisation and sensitivity analysis of a paratransit bus structure for rollover and side impact tests," *Int. J. Crashworthiness*, vol. 16, no. 6, pp. 665–673, 2011.

[25] T. W. Tech and I. Iturrioz, "Structural optimization of a bus in rollover conditions," *SAE Tech. Pap.*, 2009.

[26] L. Kwa, J. W. Wekezer, B. Gepner, and J. Siervogel, "Development of simplified safety assessment procedure for paratransit buses," *Comput. Methods Mech.*, no. 028818, 2011.

[27] Y. Li, F. Lan, and J. Chen, "Experimental and Numerical Study of Rollover Crashworthiness of a Coach Body Section," *SAE Int.*, 2018.

[28] C. Bojanowski, "Verification , Validation and Optimization of Finite Element Model of Bus Structure for Rollover Test," Florida State University, 2009.

[29] Ö. K. Mertcan Kaptanoğlu, "(TEZ) Rollover crashworthiness of a multipurpose coach," in *OTEKON 2014, Otomotiv Teknolojileri Kongresi*, 2015, p. 223.

[30] M. S. Sidhu, "Rollover of Bus," *SML ISUZU Ltd.*, vol. 144 533, pp. 1–13, 2012.

[31] S. Kumar, "Rollover Analysis of Bus Body Structure as Per AIS 031/ECE R66," *Simul.*

Driven Innov., pp. 1–7, 2012.

[32] H. Hu, C. L. Yang, and J. Wang, "Development and validation of finite element model for the welded structure of transit bus," *Int. J. Heavy Veh. Syst.*, vol. 19, no. 4, pp. 371–388, 2012.

[33] C. and I. A. L. 2009, "Florida Standard for Crashworthiness and Safety Evaluation of Paratransit Buses," *Transit Off. Florida Dep. Transp.*, pp. 1–14, 2009.

[34] N. A. S. I. Series and N. Base, *Crashworthiness of Transportation Systems: Structural Impact and Occupant Protection*. 1997.

[35] UNECE R66, "Uniform technical prescriptions concerning the approval of large passenger vehicles with regard to the strength of their superstructure," Geneva, 2006.

[36] S. No and R. M. This, "Federal motor vehicle safety standards," *Fed. Regist.*, vol. 70, no. 186, pp. 56425–56426, 2005.

[37] Federal Motor Vehicle Safety Standard, "FVMSS NO. 216; Roof Crush Resistance," 1997.

[38] L. Staes, J. Godfrey, and others, "FTA Standards Development Program: Crashworthiness/Crash Energy Management for Transit Bus," 2020.

[39] Florida Department of Transportation(FDOT), "Crash and Safety Testing Standard for Paratransit Buses, Revision 2.01," Florida, 2007.

[40] S. Lapapong, N. Pitaksapsin, S. Sucharitpwatkul, T. Tantanawat, R. Naewngerndee, and A. Phuchamnong, "Stress analysis and validation of superstructure of 15-meter long bus under normal operation," in *SAE Technical Papers*, 2013, vol. 1, pp. 69–74.

[41] Z. Yang, B. Deng, M. Deng, and G. Sun, "A study on finite element analysis of electric bus frame for lightweight design," in *MATEC Web of Conferences*, 2018, vol. 175, pp. 1–4.

[42] D. A. Micu, D. Iozsa, and C. Stan, "Quasi-static simulation approaches on rollover impact of a bus structure," *WSEAS, ACMOS*, pp. 81–86, 2014.

[43] I. Nurhadi and R. Zain, "Development of computer based procedure for quantitative evaluation of bus superstructure in type approval," *J. KONES*, vol. 17, no. 2, pp. 371–378, 2010.

[44] M. K. Mohd Nor and M. Z. Dol Baharin, "Rollover analysis of heavy vehicle bus," *Appl. Mech. Mater.*, vol. 660, pp. 633–636, 2014.

[45] V. D. Phadatare, "Performance Improvement of Bus Structure for Rollover Analysis Using FEA and Validation of Roll Bar," *IOSR J. Mech. Civ. Eng.*, vol. 17, no. 10, pp. 16–19, 2017.

[46] A. Thosare and S. B. Patil, "Rollover Analysis of Bus Body to Meet AIS-052 regulations and Optimization of the Body," *Int. Eng. Res. J.*, 2017.

[47] Rogov Petr Sergeevich and Orlov Lev Nikolaevich, "Verification of Computer Simulation Results of Bus Body Section Rollover," *J. Traffic Transp. Eng.*, vol. 3, no. 2, pp. 118–127,

2015.

[48] L. Yang and S. Deng, "Structural local analysis and optimization of bus body skeleton," *5th Int. Conf. Civ. Eng. Transp.*, no. Iccet, pp. 1975–1979, 2015.

[49] S. Wang, Y. Pan, G. Zhang, and H. Cui, "Analysis of the Rollover Crash Worthiness of the Bus Body Structure Based on ECE R66 Regulation," *J. Highw. Transp. Res. Dev. (English Ed.*, vol. 9, no. 4, pp. 99–101, 2015.

[50] J. Na, T. Wang, and Z. Xu, "Research on a one-step fast simulation algorithm for bus rollover collision based on total strain theory," *Int. J. Crashworthiness*, vol. 19, no. 3, pp. 275–287, 2014.

[51] J. Korta and T. Uhl, "Multi-Material Design Optimization," *J. KONES Powertrain Transp.*, vol. 20, no. 1, 2013.

[52] M. Bin Yusof and M. A. A. bin Afripin, "Effect of beam profile size on bus superstructure strength having rollover crash," *Appl. Mech. Mater.*, vol. 372, pp. 620–629, 2013.

[53] Y. Li, F. Lan, and J. Chen, "Experimental and numerical study of rollover crashworthiness of a coach body section," *SAE Int.*, vol. 8, 2012.

[54] R. Su, L. Gui, and Z. Fan, "Multi-objective optimization for bus body with strength and rollover safety constraints based on surrogate models," *Struct. Multidiscip. Optim.*, vol. 44, no. 3, pp. 431–441, 2011.

[55] R. S. Mahajan, P. N. Daphal, and S. M. Athavale, "Study and Analysis of Rollover Resistance of Bus Body Structure by Non-Linear FEM Technique and Experimental Method," *SAE Tech. Pap.*, pp. 205–209, 2003.

[56] M. Matolcsy, "The severity of bus rollover accidents," *Crashworthiness Transp. Syst.*, p. 07, 1997.

[57] K. Friedman, J. Hutchinson, E. Weerth, and D. Mihora, "Implementation of composite roof structures in transit buses to increase rollover roof strength and reduce the likelihood of rollover," *Int. J. Crashworthiness*, vol. 11, no. 6, pp. 593–596, 2006.

[58] Y. C. Lin and H. C. Nian, "Structural design optimization of the body section using the finite element method," *SAE Tech. Pap.*, 2006.

[59] S. J. Park, W. S. Yoo, and Y. J. Kwon, "Rollover analysis of a bus using beam and nonlinear spring elements," *WSEAS Trans. Math.*, vol. 5, no. 5, pp. 526–531, 2006.

[60] A. Subic and J. He, "Improving bus rollover design through modal analysis," *Int. J. Crashworthiness*, vol. 2, no. 2, pp. 139–152, 1997.

[61] C. Bojanowski, B. Gepner, L. Kwasniewski, C. Rawl, and J. Wekezer, "Roof Crush Resistance and Rollover Strength of a Paratransit Bus," *8th Eur. LS-DYNA® Users Conf.*, vol. 66, no. May 2011, pp. 1–13, 2011.

[62] D. Valladares, R. Miralbes, and L. Castejon, "Development of a numerical technique for bus rollover test simulation by the F.E.M.," *WCE 2010 - World Congr. Eng. 2010*, vol. 2, pp. 1361–1365, 2010.

[63] B. Schofield, "Vehicle Dynamics Control for Rollover Prevention," Lund University, Lund, 2006.

[64] H. F. Chen and D. A. Guenther, "Modeling of rollover sequences," *SAE Tech. Pap.*, 1993.

[65] Z. Jin, B. Li, and J. Li, "Dynamic Stability and Control of Tripped and Untripped Vehicle Rollover," *Synth. Lect. Adv. Automot. Technol.*, vol. 3, no. 2, pp. 1–120, 2019.

[66] Y. Guizhen, L. Honggang, W. Pengcheng, W. Xinkai, and W. Yunpeng, "Real-time bus rollover prediction algorithm with road bank angle estimation," *Chaos, Solitons and Fractals*, vol. 89, pp. 270–283, 2016.

[67] J. Gertsch and T. Shim, "Interpretation of roll plane stability models," *Int. J. Veh. Des.*, vol. 46, no. 1, pp. 72–93, 2008.

[68] B. D. Gepner, "Rollover Procedures for Crashworthiness Assessment of Paratransit Bus Structures," Florida State University, 2014.

[69] Y. Liu, "ANSYS and LS-DYNA used for structural analysis," *Int. J. Comput. Aided Eng. Technol.*, vol. 1, no. 1, pp. 31–44, 2008.

[70] A. Gauchia, B. L. Boada, M. J. L. Boada, and V. Diaz, "Integration of MATLAB and ANSYS for Advanced Analysis of Vehicle Structures," in *MATLAB Applications for the Practical Engineer*, no. August 2017, 2014.

[71] Y. Li, F. Lan, and J. Chen, "Experimental and numerical study of rollover crashworthiness of a coach body section," *SAE Int.*, vol. 8, 2012.

[72] J. W. Wekezer and K. Cichocki, "Structural response of paratransit buses in rollover accidents," *Int. J. Crashworthiness*, vol. 12, no. 3, pp. 217–225, 2007.

[73] M. A. Guler, K. Elitok, B. Bayram, and U. Stelzmann, "The influence of seat structure and passenger weight on the rollover crashworthiness of an intercity coach," *Int. J. Crashworthiness*, vol. 12, no. 6, pp. 567–580, 2007.

[74] S. Wicaksono, M. Rizka Faisal Rahman, S. Mihradi, and I. Nurhadi, "Finite element analysis of bus rollover test in accordance with UN ECE R66 standard," *J. Eng. Technol. Sci.*, vol. 49, no. 6, pp. 799–810, 2017.

[75] I. Abdul Hamid and Q. M. Li, "New definitions of deformation index for the measurement of bus survival space in crash," *Proc. Inst. Mech. Eng. Part D J. Automob. Eng.*, vol. 233, no. 8, pp. 2108–2119, 2019.

[76] Isuzu Motors Limited, "Isuzu N-Series Body Builders Guide," 2014.

[77] General Motors Isuzu Commercial Truck and American Isuzu motors Inc., "Isuzu Body

Builder's Guide." 2003.

[78] Isuzu Motors Inc., "Isuzu N-Series Body Builder Guides." 2016. [Online]. Available: www.isuzutruckservice.com%0ADownload

[79] J. Bitzenbauer, U. Franz, and K. Schweizerhof, "Deformable Rigid Bodies in LS-DYNA with Applications – Merits and Limits," 2005.

[80] LSTC 2021, "Hourglass-Welcome to the LS-DYNA support site," *Livermore Software Technology Corporation (LSTC)*. https://www.dynasupport.com/howtos/element/hourglass (accessed May 19, 2021).

[81] M. Seyedi, S. Jung, and J. Wekezer, "A comprehensive assessment of bus rollover crashes : integration of multibody dynamic and finite element simulation methods," *Int. J. Crashworthiness*, vol. 0, no. 0, pp. 1–16, 2020.

[82] Q. Wang, W. Zhou, I. Telichev, and C. Q. Wu, "Load Transfer Analysis of a Bus Bay Section Under Standard Rollover Test Using U*M Index," *Int. J. Automot. Technol.*, vol. 19, no. 4, pp. 705–716, 2018.

[83] S. M. Elseufy, N. M. Mawsouf, and A. Ahmad, "Safety Evaluation of Buses During Rollover," *J. Manag. Eng. Integr.*, vol. 6, no. March, pp. 102–108, 2013.

[84] E. C. Chirwa, H. Li, and P. Qian, "Modelling a 32-seat bus and virtual testing for R66 compliance," *Int. J. Crashworthiness*, vol. 20, no. 2, pp. 200–209, 2015.

[85] L. Kwasniewski, C. Bojanowski, J. Siervogel, J. W. Wekezer, and K. Cichocki, "Crash and safety assessment program for paratransit buses," *Int. J. Impact Eng.*, vol. 36, no. 2, pp. 235–242, 2009.

[86] Livermore Software Technology Corporation, *Keyword User ' S Manual Vol II*, vol. I, no. May. 2007.

[87] R. B. G. and R. H. G., "Friction Coefficient of Steel on Concrete or Grout," *J. Struct. Eng.*, vol. 111, no. 3, pp. 505–515, Mar. 1985.

[88] M. Gleba, "Effect of Friction on Vehicle Crashworthiness during Rollover," Florida State University Libraries, 2015.

[89] W. Zhou, A. Kuznectov, C. Q. Wu, and I. Telichev, "A comparative numerical study of motorcoach rollover resistance under ECE R66 and proposed NHTSA regulation conditions," *Int. J. Crashworthiness*, vol. 25, no. 2, pp. 131–146, 2020.

[90] L. Zhu, "Development of Guidelines for Deformable and Rigid Switch in Ls-Dyna Simulation," University of Nebraska, 2009.

[91] W. Zhou, A. Kuznetcov, I. Telichev, and C. Wu, "Deformable-Rigid Switch in Computational Simulation of Bus Rollover Test," *Int. Union Theor. Appl. Mech.*, no. August, pp. 3–4, 2016.

[92] I. A. Hamid, K. A. Kamarudin, M. R. Osman, A. N. S. Z. Abidin, and Z. H. Zulkipli, "Finite Element Bus Rollover Test Verification," *J. Soc. Automot. Eng. Malaysia*, vol. 3, no. 4, pp. 57–63, 2019.

[93] J. G. Hicks, *Welded design : theory and practice*, 1st ed. Cambridge England: Woodhead Publishing, 2000. [Online]. Available: www.woodhead-publishing.com%0AFirst

[94] A. N. Standard, "AWS D1.3/D1.3M:2008 An American National Standard : Structural Welding Code - Steel," American Welding Society (AWS), 1980.

[95] A. E. Technician, *Shielded Metal Arc Welding (SMAW) - Part A*, 1st ed. Province of Alberta, Canada: Minster of Advanced Education and Technology, 2011.

[96] D. Sumardiyanto and S. E. Susilowati, "Effect of Welding Parameters on Mechanical Properties of Low Carbon Steel API 5L Shielded Metal Arc Welds," *Am. J. Mater. Sci. 2019*, vol. 9, no. 1, pp. 15–21, 2019.

[97] A. D. Belegundu and T. R. Chandrupatla, *Optimization Concepts and Applications in Engineering*, 3rd ed. Cambridge University Press, 2019.

[98] G. N. Vanderplaats, "Structural optimization for statics, dynamics and beyond," *J. Brazilian Soc. Mech. Sci. Eng.*, vol. 28, no. 3, pp. 316–322, 2006.

[99] X. Chen and Y. Liu, *Finite element modeling and simulation with ANSYS Workbench*. CRC press, 2018.

[100] G. Liu, L. Guo, X. Wang, and Q. Wu, "Topology and parametric optimization based lightweight design of a space reflective mirror," *Opt. Eng.*, vol. 57, no. 07, p. 1, 2018.

[101] T. Kim, "Study on the stiffness improvement of bus structure," in *SAE Technical Papers*, 1993, no. 412.

[102] ANSYS 2020 R1, "DesignXplorer User ' s Guide," *ANSYS, Inc.*, no. January, 2020.

[103] G. Lai, J. Liu, and F. Zeng, "Application of multi-objective genetic algorithm in ship shafting alignment optimization," in *Proceedings - 2017 10th International Symposium on Computational Intelligence and Design, ISCID 2017*, 2018, vol. 2, pp. 275–278.

[104] W. Feng and W. hai Yong, "Optimization design of a bus body frame," in *Advanced Materials Research*, 2013, vol. 605–607, pp. 600–603.

[105] B. L. Boada, A. Gauchia, M. J. L. Boada, and V. Diaz, "A genetic-based optimization of a bus structure as a design methodology," *12th IFToMM World Congr. Besancon*, pp. 18–21, 2007.

[106] G. Grebenişan and N. Salem, "The multi-objective genetic algorithm optimization, of a superplastic forming process, using ansys®," in *MATEC Web of Conferences*, 2017, vol. 126.

[107] H. Kurtaran, A. Eskandarian, D. Marzougui, and N. E. Bedewi, "Crashworthiness design

optimization using successive response surface approximations," *Comput. Mech.*, vol. 29, no. 4–5, pp. 409–421, 2002.

[108] S. S. Esfahlani, H. Shirvani, S. Nwaubani, A. Shirvani, and H. Mebrahtu, "Comparative study of honeycomb optimization using Kriging and radial basis function," *Theor. Appl. Mech. Lett.*, vol. 3, no. 3, p. 031002, 2013.

[109] N. Stander, W. Roux, T. Goel, T. Eggleston, and K. Craig, "LS - OPT User' s Manual: A Design Optimization and Probabilistic Analysis Tool," *Livermore Softw. Technol. Corp.*, no. February, 2012.

[110] Y. hui Wang, C. Zhang, Y. qiang Su, L. yang Shang, and T. Zhang, "Structure optimization of the frame based on response surface method," *Int. J. Struct. Integr.*, vol. 11, no. 3, pp. 411–425, 2020.

[111] T. Pravilonis, E. Sokolovskij, A. Kilikevičius, J. Matijošius, and K. Kilikevičiene, "The usage of alternative materials to optimize bus frame structure," *Symmetry (Basel).*, vol. 12, no. 6, 2020.

[112] LSTC 2021, "Total energy-Welcome to the LS-DYNA support site," *Livermore Software Technology Corporation (LSTC)*. https://www.dynasupport.com/howtos/general/total-energy (accessed May 19, 2021).

[113] LSTC 2021, "Energy data-Welcome to the LS-DYNA support site," *Livermore Software Technology Corporation (LSTC)*. https://www.dynasupport.com/tutorial/ls-dyna-users-guide/energy-data (accessed May 19, 2021).

Appendices

Appendix A: Mass of the midi-bus, length of bay & mass distribution of the bay

Table A1: Masses of the midi-bus

Masses(kg)	
Model	***Chassis NPR 71K***
unladen kerb mass of the vehicle, M_k	4500
mass of the front axle, M_f	1150
mass of the rear axle, M_r	3350
mass of left-side of the vehicle, M_L	2150
mass of right-side the vehicle, M_R	2350

Table A2: Results of the length of the bay

Length of the bay (W_{i-k})***,*** *mm*					
W_{1-3}	W_{2-4}	W_{3-5}	W_{4-6}	W_{5-7}	W_{6-8}
730	695	970	1110	1110	1110

Table A3: Distributed Mass of the Bays (Rings) of the original bus

Bay (Ring)	***Masses on the bottom (m_1^j), right-side (m_2^j), roof (m_3^j) & left-side (m_4^j)***				**Total sum** (kg)
	m_1^j *(kg)*	m_2^j *(kg)*	m_3^j *(kg)*	m_4^j *(kg)*	
B1	357	49	33	55	494
B2	878	53	29	61	1021
B3	321	47	34	41	443
B4	291	35	33	39	398
B5	308	47	41	54	450
B6	543	39	49	35	666
B7	355	47	56	45	503
B8	364	51	53	55	523
Unladen Kerb Mass					**4498**

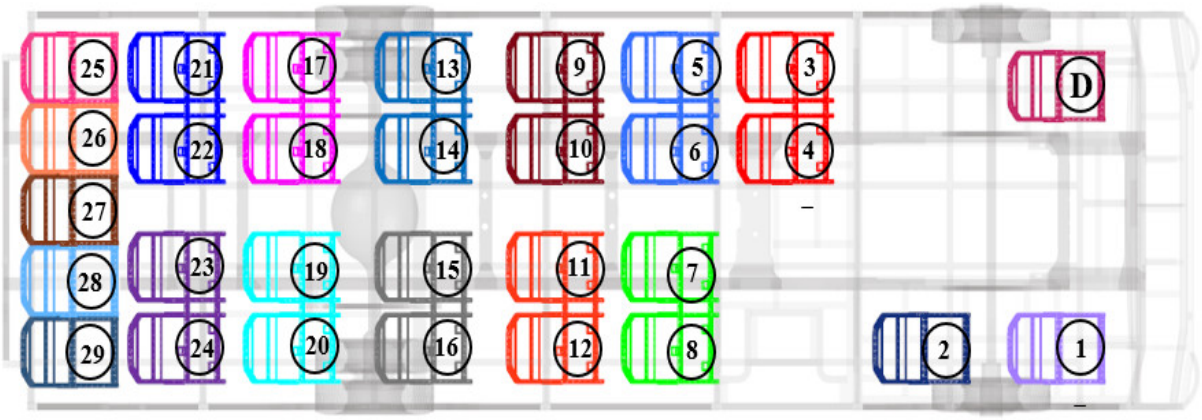

Figure A1: Arrangement of seats for NPR71K chassis model

Appendix B: Graphs and Snapshots from the quasi-static simulation

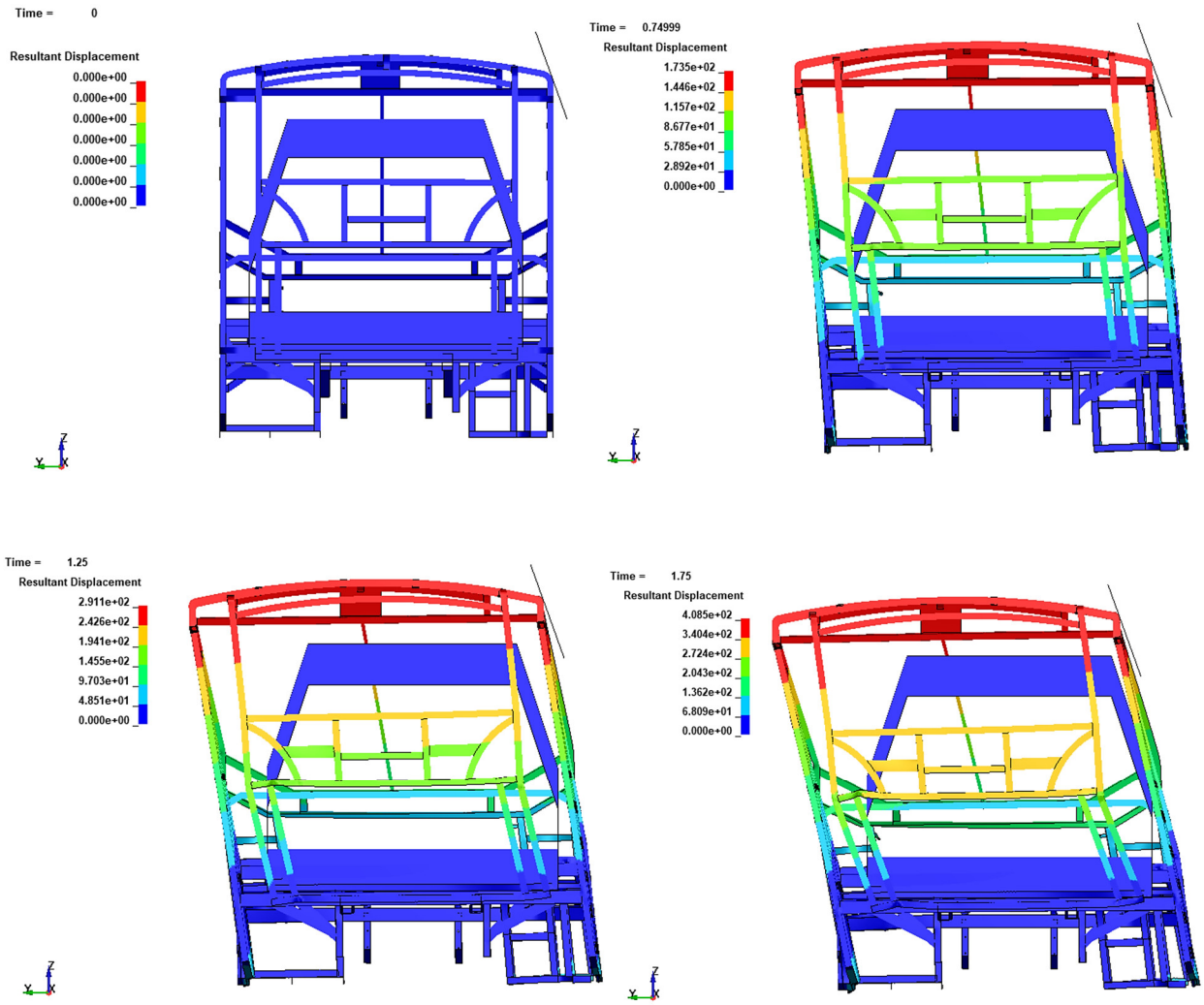

Figure B1: Deformation of the original model in quasi-static simulation from 0 - 1.75 sec.

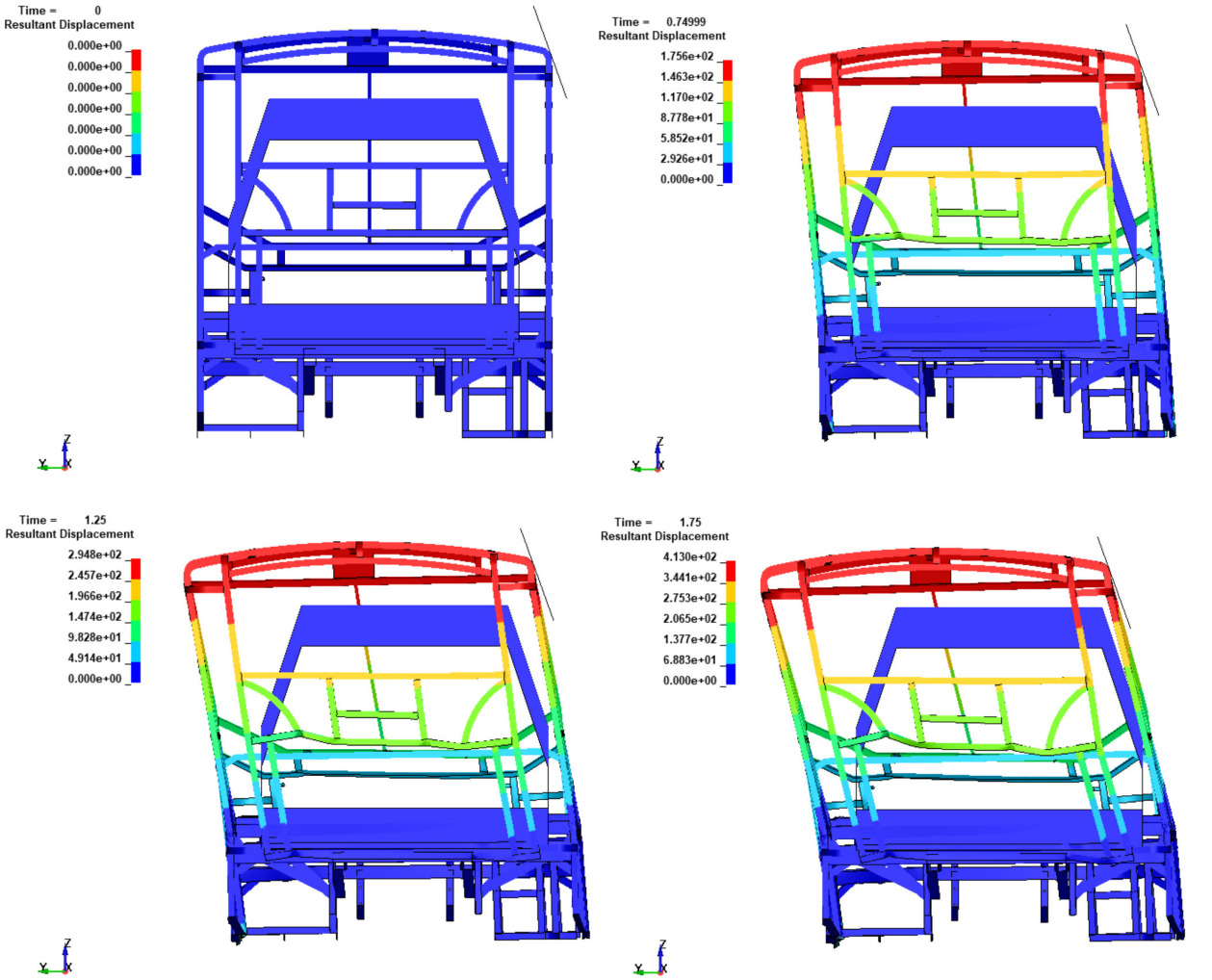

Figure B2: Deformation of reinforced model in quasi-static simulation from 0 - 1.75 sec.

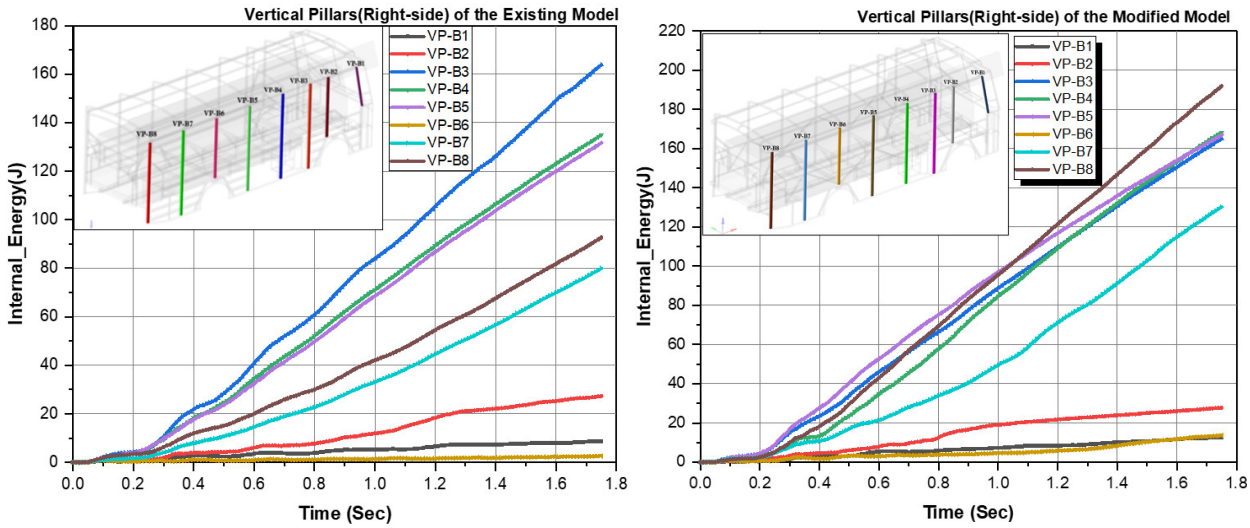

Figure B3: The internal energy of vertical pillars in the original and reinforced model

Appendix C: Geometry of reinforced model, Graphs and Snapshots from the rollover simulation

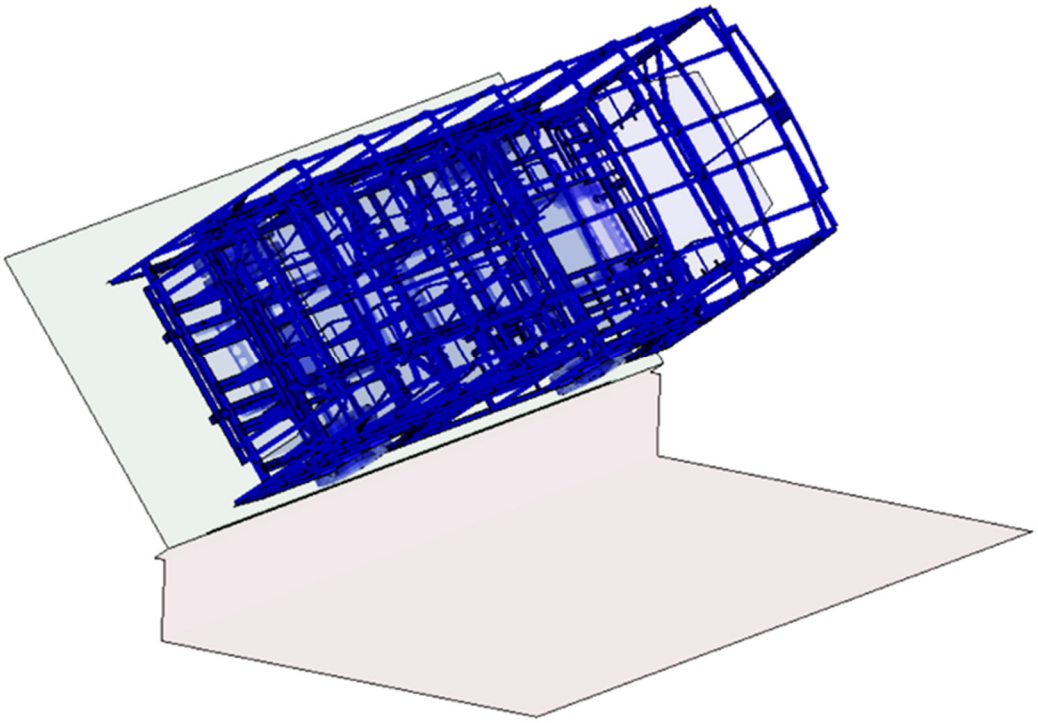

Figure C1: Baseline midi-bus in tare – weight rollover simulation @ t = 0.0 sec

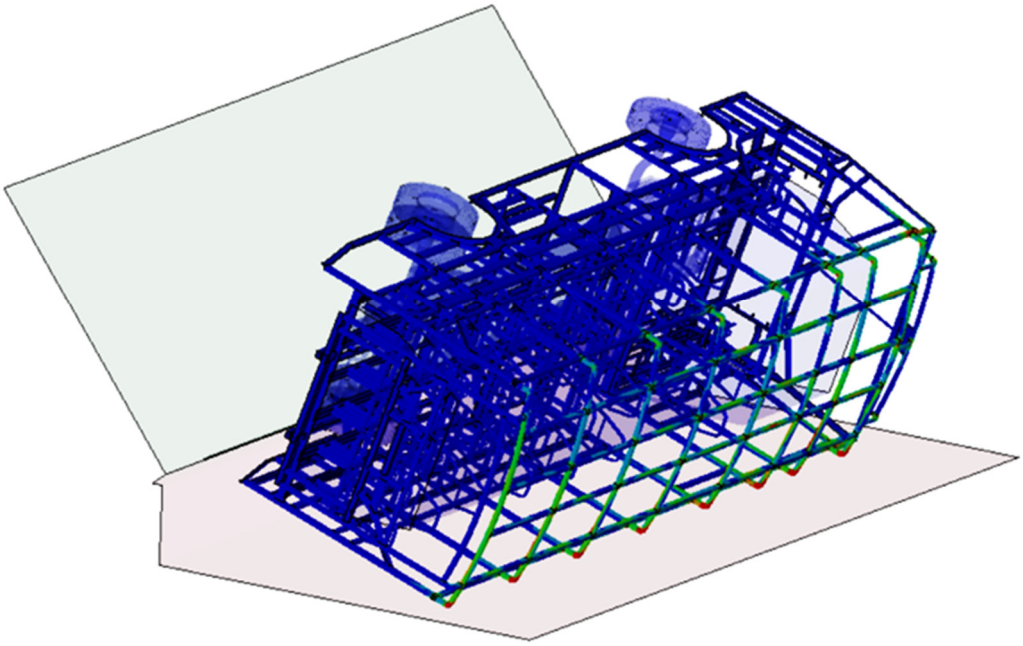

Figure C2: Baseline midi-bus in tare – weight rollover simulation @ t = 1.61 sec

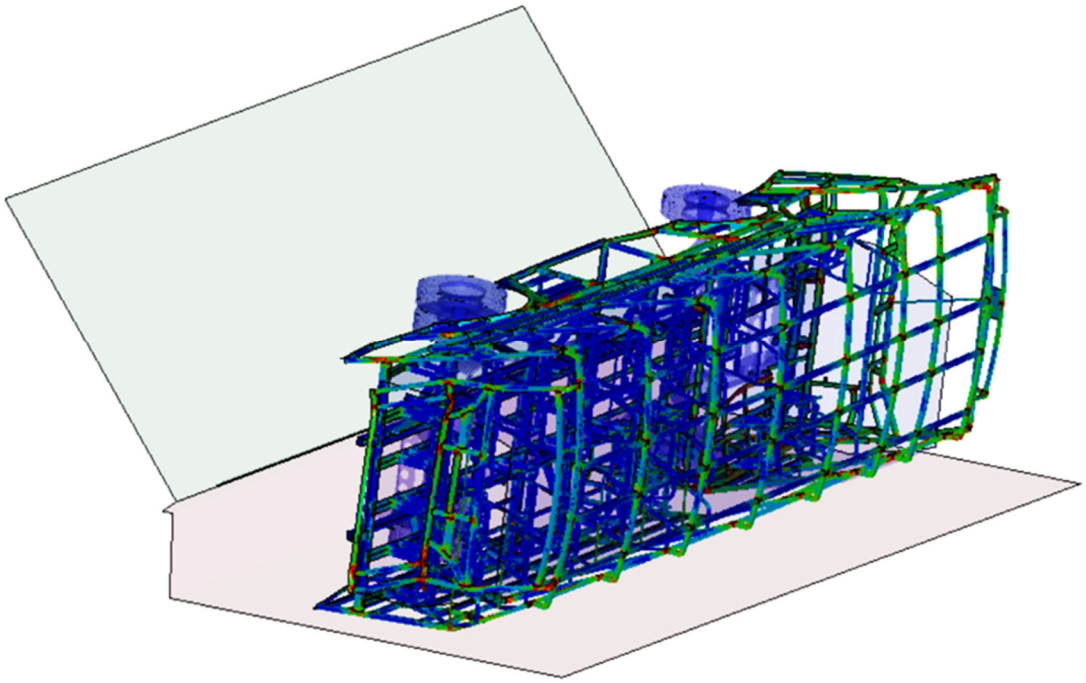

Figure C3: Baseline midi-bus in tare – weight rollover simulation @ t = 2.25 sec

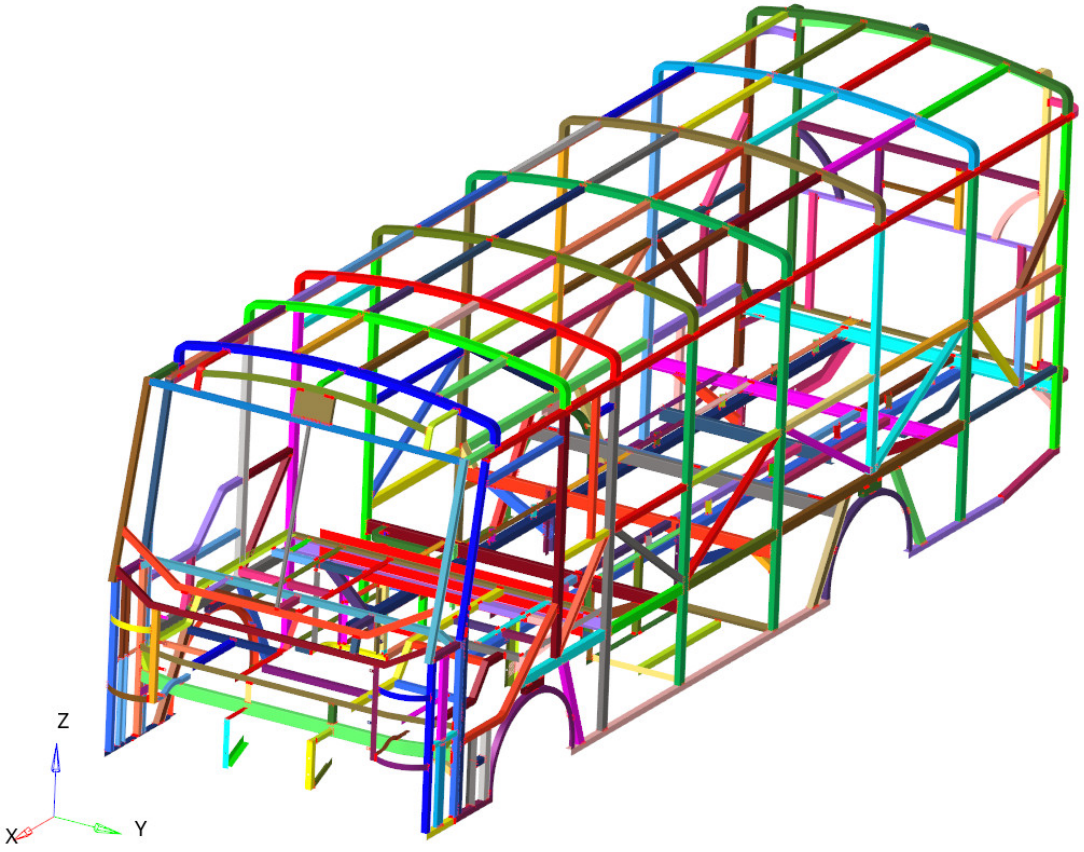

Figure C4: The geometry of the reinforced structure (Model – I)

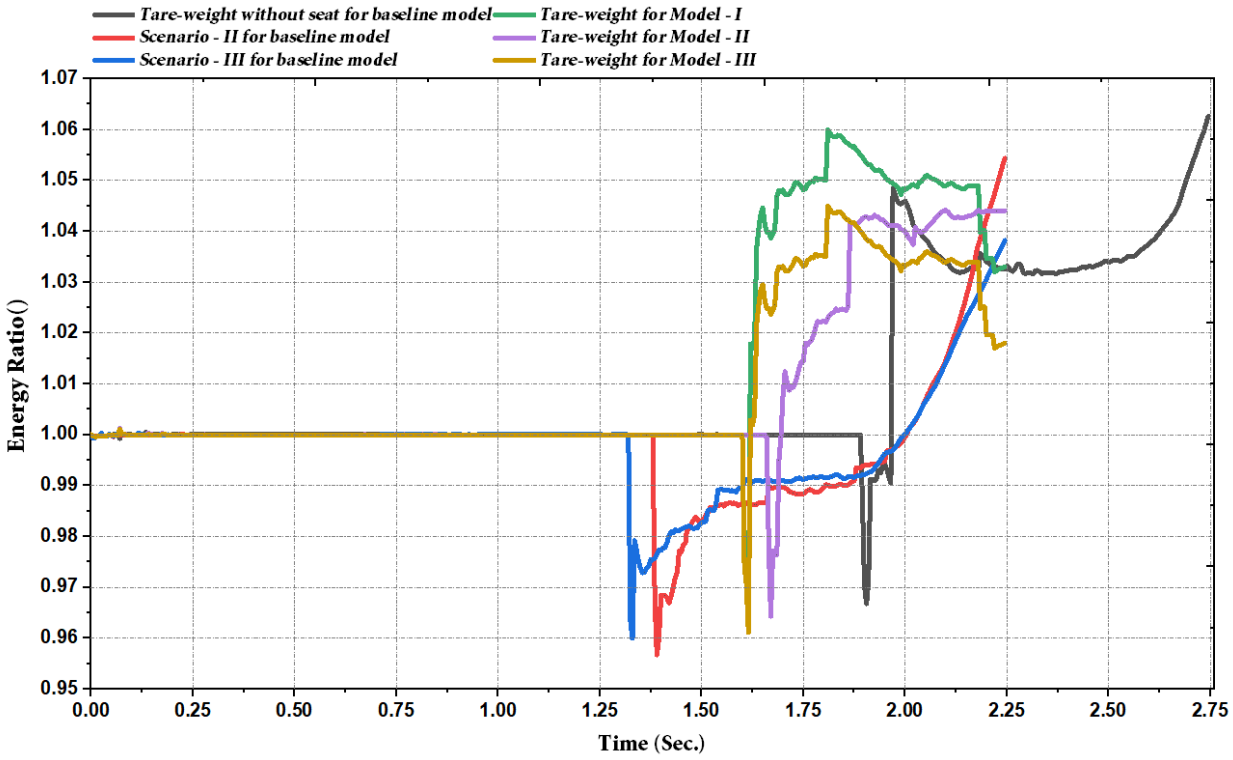

Figure C5: The plot of energy ratio for all remaining FE models

Appendix D: Geometry and Dimension of welds on the structural connections

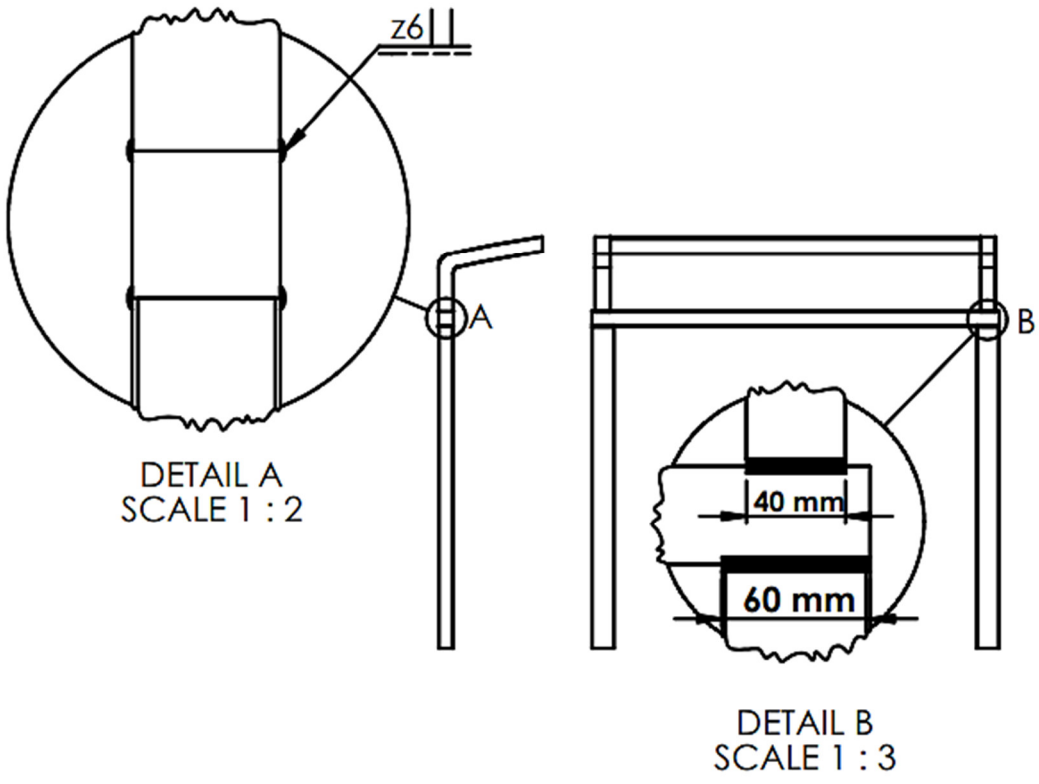

a)

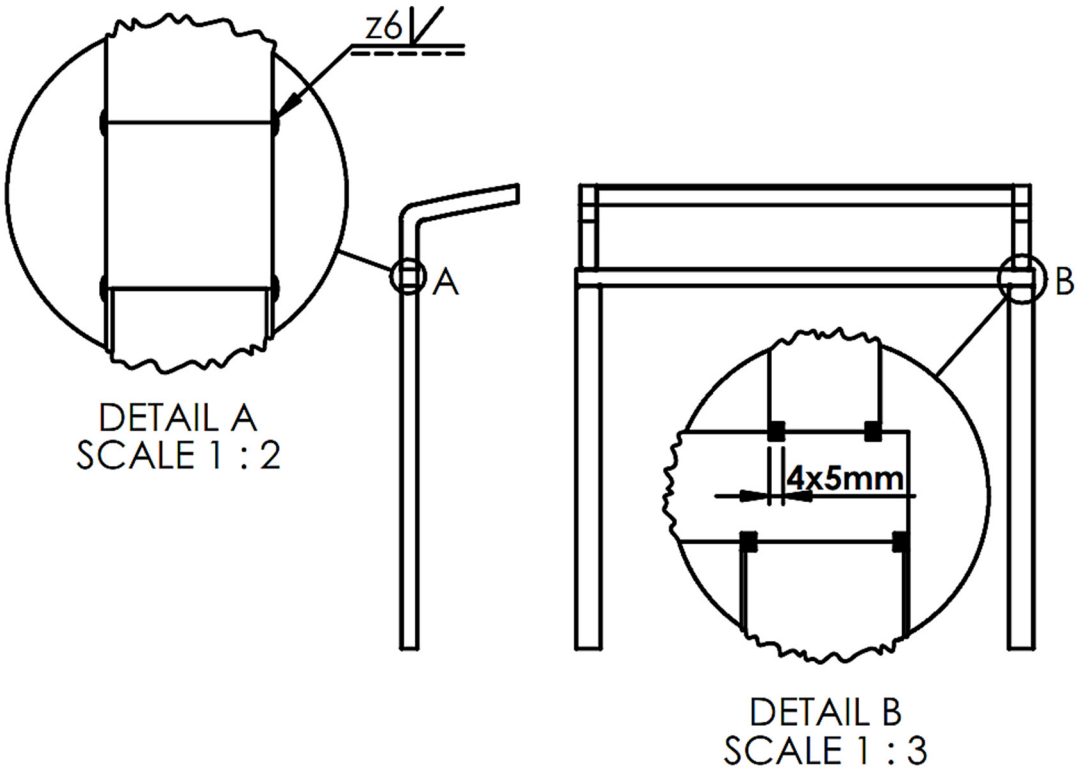

b)

Figure D1: Geometry of welds in the RW connection: a) full arc weld & b) spot arc weld

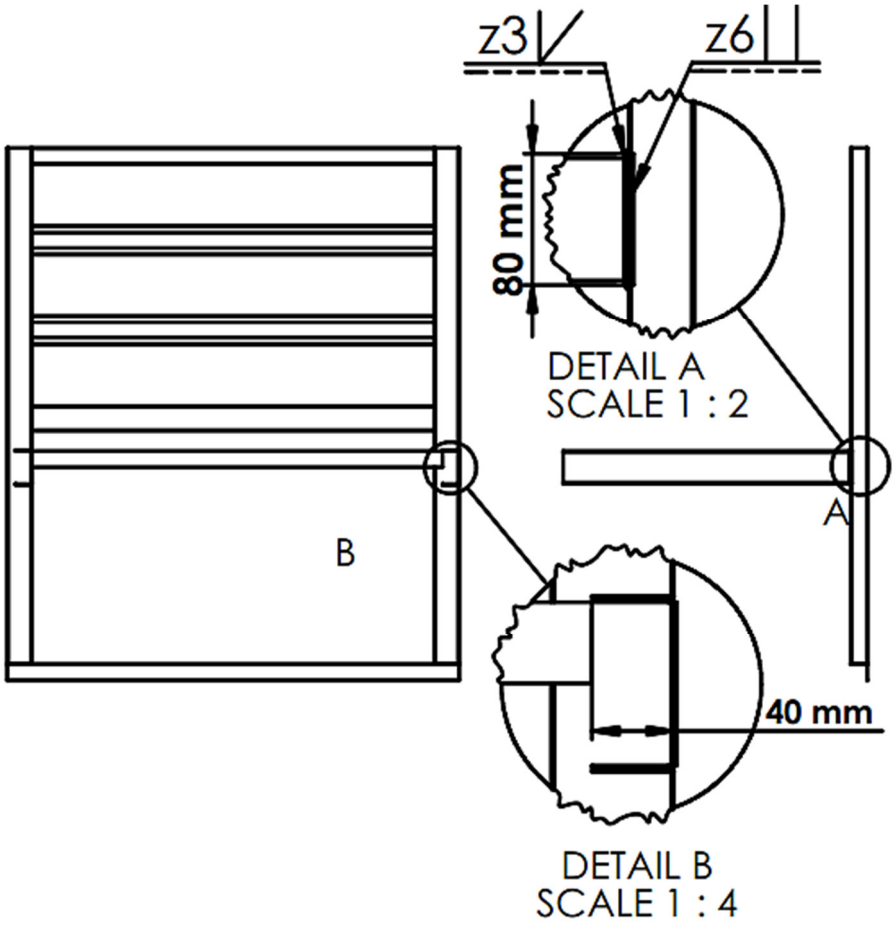

a)

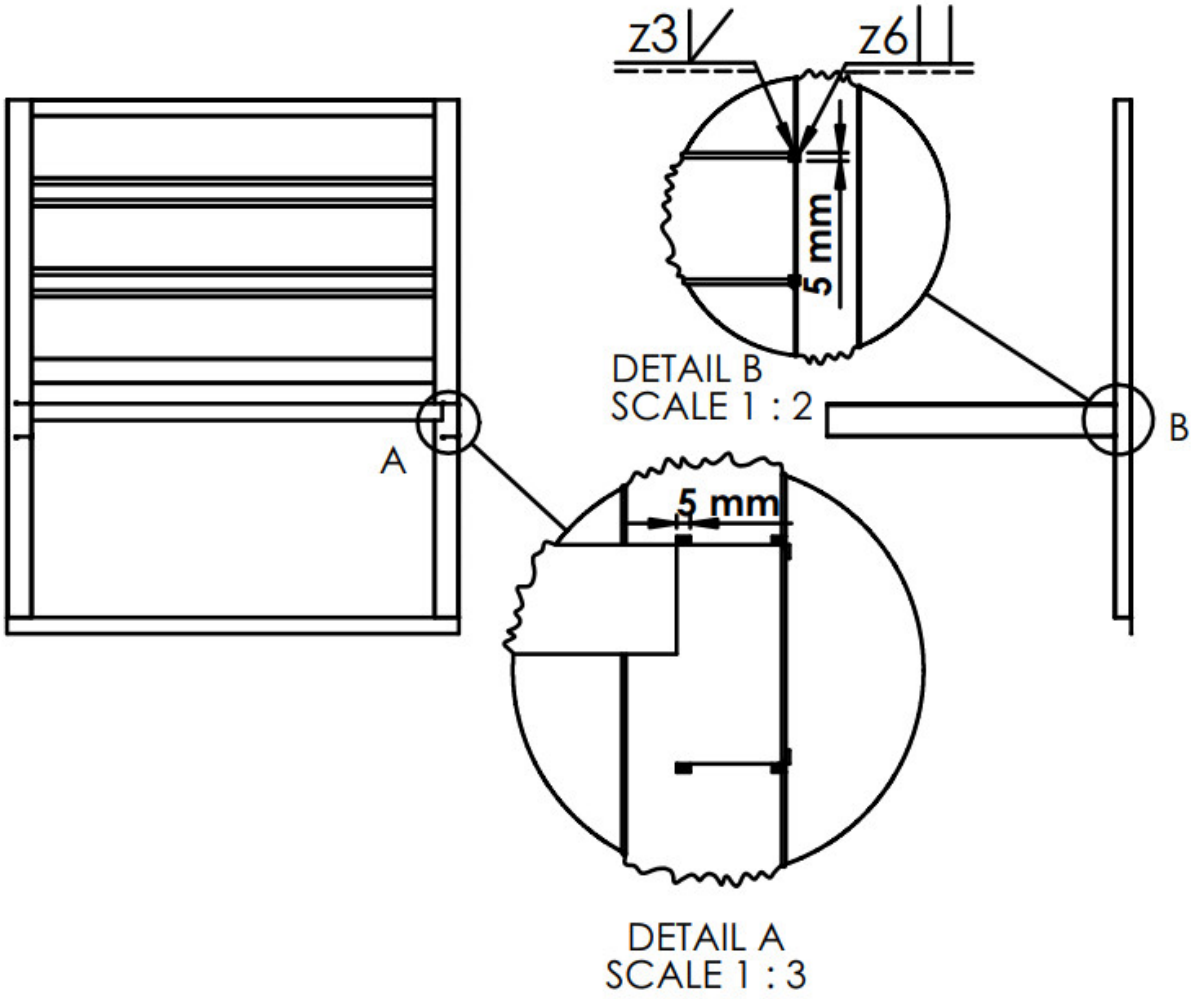

b)

Figure D2: Geometry of welds in the FW connection: a) full arc weld & b) spot arc weld